

Emergent Properties of *in silico* Synaptic Transmission in a Model of the Rat Neocortical Column

THÈSE N° 5208 (2011)

PRÉSENTÉE LE 6 DÉCEMBRE 2011
À LA FACULTÉ SCIENCES DE LA VIE
LABORATOIRE DE NEUROSCIENCE DES MICROCIRCUITS
PROGRAMME DOCTORAL EN NEUROSCIENCES

ÉCOLE POLYTECHNIQUE FÉDÉRALE DE LAUSANNE

POUR L'OBTENTION DU GRADE DE DOCTEUR ÈS SCIENCES

PAR

Srikanth RAMASWAMY

acceptée sur proposition du jury:

Prof. H. Lashuel, président du jury
Prof. H. Markram, Dr S. L. Hill, directeurs de thèse
Prof. C. Petersen, rapporteur
Prof. I. Segev, rapporteur
Prof. G. Silberberg, rapporteur



ÉCOLE POLYTECHNIQUE
FÉDÉRALE DE LAUSANNE

Suisse
2011

स॒ह ना॑ववतु । सह नौ॑ भुनक्तु । sa॒ha na॑vavatu | sa॒ha nau॑ bhunaktu |
स॒ह वी॒र्यं॑ करवावहे । sa॒ha vī॒ryam॑ karavāvahai |
ते॒ज॒स्विना॑वर्ध॒तमस्तु॑ मा वि॒द्विष॑वहे ॥ te॒ja॒s॒vinā॑vadhī॒tamastu॑ mā vi॒dviṣ॑avahai ॥
ॐ शान्तिः॑ शान्तिः॑ शान्तिः॑ ॥ om śāntiḥ॑ śāntiḥ॑ śāntiḥ॑ ॥

May He protect us; May He nourish us;

May we work conjointly with great energy,

May our knowledge be resplendent;

May we not mutually dispute;

Let there be Peace in me;

Let there be Peace in my environment;

Let there be Peace in the forces that act on me.

- *Taittiriya Upanishad 2.2.2*

To Amma, Appa, Pati and Suma

“Do not go where the path may lead, go instead where there is no path and leave a trail.”

— Ralph Waldo Emerson

Chez les mammifères, le cortex cérébral occupe approximativement 80% du volume total et est considéré comme étant responsable des fonctions cognitives les plus élevées, telles que la mémoire, l'attention, ou encore la perception par les sens. Le néocortex est la partie la plus récente dans l'histoire de l'évolution du cortex et mérite sans doute le titre de région cérébrale la plus complexe jamais étudiée. Le "microcircuit néocortical" est un écosystème du néocortex composé d'un assortiment riche et varié de neurones, divers tant sur le plan de leurs propriétés morphologiques que de leurs propriétés électriques. Dans ces microcircuits néocorticaux, les neurones sont arrangés en feuillets, que l'on appelle "couches". On suppose que l'unité fonctionnelle fondamentale du néocortex est la colonne néocorticale (CNC). Une seule colonne corticale consiste en plusieurs milliers de neurones arrangés de manière verticale sur l'ensemble des six couches. La structure du néocortex dans son ensemble émerge de la répétition organisée et stéréotypée de plusieurs milliers de ces colonnes corticales, au sein desquelles les neurones communiquent les uns avec les autres par des points spécialisés dans le transfert d'information appelés "synapses". La dynamique des transmissions synaptiques peut être aussi variée que les neurones impliqués dans cette transmission eux-mêmes et contribue de manière cruciale aux propriétés fonctionnelles du microcircuit.

Le Blue Brain Project ("projet cerveau bleu" – BBP) constitue la première tentative élaborée visant à construire un modèle unifié de la CNC par l'intégration systématique des données et au moyen de simulations biologiquement détaillées. Ces 5 dernières années, le BBP a développé une infrastructure permettant une modélisation respectant les contraintes issues des données expérimentales et intégrant l'information biologique à des niveaux de complexité multiples. Suivant des principes premiers dérivés de l'expérimentation biologique, la chaîne d'outils a subi un processus constant de raffinement, afin de faciliter la construction fréquente de modèles détaillés de CNC.

Le sujet central de cette thèse est la caractérisation des propriétés fonctionnelles des transmissions synaptiques *in silico* via l'incorporation des principes de communication synaptique dérivés des expériences biologiques. Afin d'étudier la transmission synaptique *in silico*, il est impératif de comprendre quels sont les acteurs principaux influençant la manière dont les signaux synaptiques sont traités dans les microcircuits néocorticaux – canaux ioniques et profils de distribution, modèles de neurones individuels et dynamique des voies synaptiques.

Premièrement, grâce à un examen exhaustif de la littérature existante, j'ai identifié les propriétés cinétiques des différents canaux ainsi que leurs profils de distribution sur les neurones néocorticaux, afin de pouvoir construire des modèles *in silico* de canaux ioniques.

J'ai ensuite développé un prototype d'infrastructure pour pouvoir analyser les caractéristiques somatiques et dendritiques de modèles de neurones individuels répondant aux contraintes dictées par la cinétique des canaux ioniques. Enfin, au sein d'un environnement de simulation intégrant les canaux ioniques, les modèles de neurones individuels et la dynamique propre à la transmission synaptique, j'ai répliqué des protocoles expérimentaux *in silico*, ce afin de caractériser les propriétés de transmission des connexions monosynaptiques. Ces connexions synaptiques, issues de la superposition axo-dendritique d'arbres neuronaux, proviennent de plusieurs versions du modèle de CNC construites au préalable grâce à l'environnement de simulation du BBP.

Dans cette thèse, je montre que lorsque les principes de la transmission synaptique dérivés d'expériences *in vitro* sont incorporés à des modèles informatiques de connexions synaptiques, l'anatomie et le comportement physiologique de ces connexions modélisées à partir de règles biologiques élémentaires correspondent bien aux données récoltées *in vitro*. Cette thèse démontre que les propriétés de réponse synaptique moyenne *in silico* résistent bien aux perturbations des propriétés anatomiques et physiologiques des connexions modélisées au sein du circuit néocortical local. Une découverte fondamentale de cette thèse concerne la fonction de ce microcircuit néocortical. Par l'examen de l'effet de la diversité morphologique des neurones sur la transmission synaptique *in silico*, je démontre en effet que, dans le microcircuit néocortical, cette diversité morphologique intrinsèque confère une invariance à la réponse synaptique moyenne, appelée "robustesse et invariance au niveau du microcircuit".

Mots-clefs: colonne néocorticale, *in silico*, *in vitro*, calibration, validation, modèles de canaux ioniques, modèles de neurones individuels, modèle synaptique probabiliste, voies synaptiques, connexions excitatrices et inhibitrices

ABSTRACT

The cerebral cortex occupies nearly 80% of the entire volume of the mammalian brain and is thought to subservise higher cognitive functions like memory, attention and sensory perception. The neocortex is the newest part in the evolution of the cerebral cortex and is perhaps the most intricate brain region ever studied. The neocortical microcircuit is the smallest 'ecosystem' of the neocortex that consists of a rich assortment of neurons, which are diverse in both their morphological and electrical properties. In the neocortical microcircuit, neurons are horizontally arranged in 6 distinct sheets called layers. The fundamental operating unit of the neocortical microcircuit is believed to be the Neocortical Column (NCC). Functionally, a single NCC is an arrangement of thousands of neurons in a vertical fashion spanning across all the 6 layers. The structure of the entire neocortex arises from a repeated and stereotypical arrangement of several thousands of such columns, where neurons transmit information to each other through specialized points of information transfer called synapses. The dynamics of synaptic transmission can be as diverse as the neurons defining a connection and are crucial to foster the functional properties of the neocortical microcircuit.

The Blue Brain Project (BBP) is the first comprehensive endeavour to build a unifying model of the NCC by systematic data integration and biologically detailed simulations. Through the past 5 years, the BBP has built a facility for a data-constraint driven approach towards modelling and integrating biological information across multiple levels of complexity. Guided by fundamental principles derived from biological experiments, the BBP simulation toolchain has undergone a process of continuous refinement to facilitate the frequent construction of detailed *in silico* models of the NCC.

The focus of this thesis lies in characterizing the functional properties of *in silico* synaptic transmission by incorporating principles of synaptic communication derived through biological experiments. In order to study *in silico* synaptic transmission it is crucial to gain an understanding of the key players influencing the manner in which synaptic signals are processed in the neocortical microcircuit - ion channel kinetics and distribution profiles, single neuron models and dynamics of synaptic pathways.

First, by means of exhaustive literature survey, I identified ion channel kinetics and their distribution profiles on neocortical neurons to build *in silico* ion channel models. Thereafter, I developed a prototype framework to analyze the somatic and dendritic features of single neuron models constrained by ion channel kinetics. Finally, within a simulation framework integrating the ion channels, single neuron models and dynamics of synaptic transmission, I replicated *in vitro* experimental protocols *in silico*, to characterize the transmission properties of monosynaptic

connections. These synaptic connections, arising from the axo-dendritic apposition of neuronal arbours were sampled across many instances of *in silico* NCC models constructed *a priori* through the BBP simulation toolchain.

In this thesis, I show that when principles of synaptic transmission derived from *in vitro* experiments are incorporated to model *in silico* synaptic connections, the resulting anatomy and physiology of synaptic connections modelled from elementary biological rules closely match *in vitro* data. This thesis work demonstrates that the average synaptic response properties *in silico* are robust to perturbations in the anatomical and physiological properties of modelled connections in the local neocortical microcircuit. A fundamental discovery through this thesis is an insight into the function of the local neocortical microcircuit by examining the effect of morphological diversity on *in silico* synaptic transmission. I demonstrate here that intrinsic morphological diversity confers an invariance to the average synaptic response properties *in silico* in the local neocortical microcircuit, termed "microcircuit level robustness and invariance".

Keywords: Neocortical column, *in silico*, *in vitro*, calibration, validation, ion channel models, single neuron models, synaptic transmission, probabilistic synapse model, synaptic pathways, excitatory and inhibitory connections

ACKNOWLEDGEMENTS

परुषमपि गुरुणां बुद्धिबोधार्थमुक्तं वचनमनुसरन्त्याति शिष्यो महत्त्वम्।
खनितलगतरत्नं श्रेष्ठमप्यत्र शाणो- त्कषणमधिगतं तद्भ्राति मौलौ नृपाणाम्।

puruShamapi gurUNAM buddhibodhArthamuktaM
vachanamanusaranyAti shiShyo mahattvam|
khanitalagataratnaM shreShThamapyatra shANo -
tkaShaNamadhigataM tadbhAti maulau nRupANAM|

"A disciple attains prominence by carrying out the orders of his preceptors, given with the intention of illuminating his intellect, however harsh they might be. Even though a gem found in a mine might be precious, it needs to undergo the rigours of a grindstone, before it adorns the crown of monarchs."

It has been a remarkable journey in 'building' the brain with the Blue Brain Project. I am indebted to Prof. Dr. Henry Markram for accepting me as a PhD. student, for his faith, advice, criticism, ceaseless demand for excellence, insight and encouragement. I pay my greatest reverence to Henry for making people believe in what Ayn Rand said in Atlas Shrugged "God will keep stepping on you mercilessly until you lift up his foot". Thanks Henry, for making me think and breathe layer 5 pyramidal cells and synapses!

I am very grateful to Dr. Felix Schürmann for teaching me a thing or two about meticulousness and precision, criticism, attention to detail and most importantly drilling into me the "art of scrutiny". I have learnt a huge deal from Felix on being a thoughtful scientist and an effective team player.

My deep gratitude goes to Dr. Sean Hill for patiently bearing with my innumerable mistakes, always encouraging and teaching me something I would never have thought of through our day to day interactions. Sean's attention to detail has had a huge influence on me. It has been a great learning experience with Sean.

My heartfelt thanks go to Prof. Idan Segev for being a luminary and ceaseless source of inspiration. I am truly fortunate to have known a scientist and fatherly figure like Idan and honoured to have him as part of my jury committee. I am also very thankful to Prof. Carl Petersen for his incredible passion for neuroscience, teaching me how to see through a paper, mentorship, great words of encouragement and agreeing to be part of my jury committee. I am grateful to Prof. Gilad Silberberg, for his discussions on Martinotti cells and graciously agreeing to be part of my jury committee. My deepest thanks also go to Prof. Hilal Lashuel for being

the President of my jury and Ms. Michele Bonnard Giacobino for her support, kindness and organizational abilities.

I owe a lot to the late Prof. Phil Goodman who left behind a legacy with unconditional words of advice, pleasing demeanour and passion for science.

My gratitude goes to Prof. Pramod Rastogi for his ready advice, enthusiasm, delightful discussions and yeoman efforts in ensuring that the Indian tricolour always flies aloft in its entire grandeur.

I am eternally grateful to Profs. Pablo Varona Martinez & Gonzalo Garcia de Polavieja, my mentors at the Universidad Autonoma de Madrid and Instituto Cajal, CSIC Madrid for leading me through my baby steps in neuroscience and their legendary generosity and motivation. A big hug to Dr. Sara Arganda Carreras for teaching me electrophysiology, how to work with leeches, her friendship and bubbly spirit.

Having been with Blue Brain almost from its inception, I have had the great fortune of collaborating with and learning from several inspiring people. If it weren't for these giants, then I wouldn't have been able to see further. All of these people have left an indelible impression on me - Rajnish *Ranjo* Ranjan for his role in teaching me the art of programming, support and 'never say die' attitude, James *Jojo* King for his criticism, programming skills, patience and 'dial Jim for help' service, Imad *Le Capitaine* Riachi for his knowledge, several discussions, insight and advice, Martin *Everything about something* Telefont for his great camaraderie, advice and rants about everything under the sun at 7 AM everyday, Eilif *Nice guy* Mueller for his prudence, most inspiring mentorship, amazing insight and home brew, Sebastian *Seb* Lasserre for all his help, discussions and support, Georges *GK* Khazen for his constant support, kindness and help with statistics, Juan *Whisky dyc* Hernando for his computer science knowledge, Konstantinos *Kostas* Sfyarakis for his unassuming nature, John *JLK* Kenyon for his programming skills, Daniel *Dan* Keller for his encyclopaedic neuroscience knowledge and constant encouragement, Michael *Wolf* Reimann for his Matlab expertise and gallons of beer, Shruti *Shruta* Muralidhar for all the quizzes and interneurons, Rodrigo *12 patch* Perin for his knowledge and precision, Luca *Gamba* Gambazzi for his OS X lessons, Thomas *Layer 6* Berger for his overwhelming neuroscience knowledge and personality, Werner *Pillow* van Geit for his kindness and neuron modelling skills, Vincent *MEA* Delattre for countless discussions, Dr. Michele Giugliano for his words of advice and kindness, Dr. Yun Wang for critically reading my manuscripts, and Dr. Marc-Oliver Gewaltig for his knowledge, reading through this thesis, words of advice and rounds of beer!

I have also learnt a lot from our collaboration with Prof. Idan Segev's students at the Hebrew University, my deepest gratitude goes to Shaul Druckmann, Albert Gidon, Etay Hay and Yoav Bannitt for their friendship and sharing knowledge.

I am very thankful to Matt Perich, Adrian Cachinero Vasiljevic, Pieter Dermont, Henri Saab, Ruben Moor, Nikolai Chapochnikov, Alvaro Rodriguez, Aurelien Mace, Miha Pelko, Garik Suess, Jie Bao, Thomas McColgan, Thomas Tränkler, Guilherme Testa Silva, Sundeep Teki, Shadi Akiki,

Anirudh Vij, Adnan Abid, Bruno Magalhaes, Anna Traussnig, Nenad Buncic, Fabien Delalondre, Joe Graham, Jeff Mueller, Carlos Aguado Sanchez, Bathelemy von Haller and Renuad Richardet for their friendship and support.

I salute Christiane Debono for her amazing efficiency, problem solving abilities, humour and extreme kindness. It has been a great delight to know someone like Christiane. I am grateful to Richard Walker for his many enlightening lessons on how to craft words for effective scientific communication.

The largesse of Mme. Elisabeth Riedweg, the late Mme. Elsa Siegrist and Mr. Henri Riedweg in housing me for the past 5 years speaks oodles about the Vaudois attitude in accepting foreigners and rightfully introducing them to Switzerland. I bow down in respect to the late Mme. Elsa Siegrist and Mr. Henri Riedweg for their zest towards life and for showing me how to live and let live.

Mere words cannot do justice to thank my dearest friends Harsha Kasi, Kamesh Mahadevan, Prashanth Purushottam & Urmila Prakash for making life outside research so much more easier and bearable. Thanks for being there and allowing me to be myself around you!

I am not a self made person, and what I am is a true reflection of the upbringing, faith, belief and support of my incredible parents, Padma and Ramaswamy Iyengar for instilling in their only child how to strive to be a good human being no matter what. I shudder to imagine what I would have been if not for their way of life of determination and pursuit of truth against all odds. What I am today is a standing tribute to my grandparents, Andamma and P.B Srinivasan who eternally moulded and shaped my values and beliefs, taught me to persevere, never give up and sowed the seeds for an outlook towards journalism. I am also indebted to my role model - my uncle K.V Sridhar whose wisdom, attitude towards life, passion for fact-finding and globe-trotting always inspired me to do better.

Indeed, behind every successful man there is a woman - I am grateful to beloved Suma for coming into my life, her constant encouragement, support, laughter and for always being there for me.

“A man is but the product of his thoughts what he thinks, he becomes.”

- Mahatma Gandhi

CONTENTS

I INTRODUCTION	1
1 INTRODUCTION	3
1.1 The Neocortical column in the mammalian brain	5
1.2 Reconstructing the NCC in silico - The Blue Brain Project	9
1.3 Thesis outline and description of results	12
II PROBLEM DEFINITION	15
2 INCORPORATING PRINCIPLES OF NEOCORTICAL SYNAPTIC TRANSMISSION: FROM IN VITRO TO IN SILICO	17
2.1 Setting the field for synaptic transmission in silico - who are the players?	17
2.2 Player 1: Ion channels in the neocortical microcircuit	19
2.2.1 Biological knowledge	19
2.2.2 Building models of ion channel kinetics	21
2.3 Player 2: The morphological and electrical diversity of neocortical neurons	24
2.3.1 Biological knowledge	24
2.3.2 Building single neuron models	28
2.4 Player 3: Principles of synaptic communication in the neocortical microcircuit	30
2.4.1 Biological knowledge	30
2.4.2 Biophysical models of synaptic transmission	37
2.5 Summary	38
III MAIN RESULTS	39
3 THE TTL5 SYNAPTIC PATHWAY IN SILICO	41
4 INTRA- AND INTER-LAMINAR PYRAMIDAL PATHWAYS IN SILICO	79
4.1 Abstract	83
4.2 Introduction	83
4.3 Methods	84
4.3.1 3D anatomical reconstruction of PC morphologies	84
4.3.2 Morphology repair	84
4.3.3 Constructing inter- and intra-laminar PC microcircuits	85
4.3.4 Stochastic synapse model	85
4.3.5 Biophysical pyramidal cell model	86
4.3.6 <i>In silico</i> stimulation and recording	86
4.3.7 Data analysis	87

4.4	Results	87
4.4.1	Intra-laminar connections	88
4.4.2	Inter-laminar connections	91
4.5	Discussion	92
4.6	Author contributions	93
5	INHIBITORY AND EXCITATORY PATHWAYS IN SILICO	99
5.1	Abstract	103
5.2	Introduction	103
5.3	Methods	103
5.3.1	3D Reconstruction	103
5.3.2	Morphology Repair	104
5.3.3	Circuit Building	104
5.3.4	Touch detection	104
5.3.5	Functionalizing structural appositions	104
5.3.6	Dynamics and parameters of synaptic transmission	105
5.3.7	Mapping rules for synaptic transmission	105
5.3.8	Biophysical single neuron models	105
5.3.9	<i>In silico</i> stimulation and recording	105
5.3.10	Data analysis	106
5.4	Results	106
5.4.1	Anatomy of in silico Inhibitory-Excitatory and Excitatory-Inhibitory connections	106
5.4.2	Physiology of in silico Inhibitory-Excitatory connections	107
5.4.3	Physiology of in silico Excitatory-Inhibitory connections	109
5.5	Discussion	111
5.6	Author contributions	112
IV	CONCLUSIONS AND PERSPECTIVES ON FUTURE WORK	131
6	CONCLUSIONS AND PERSPECTIVES ON FUTURE WORK	133
V	BIBLIOGRAPHY	135
7	BIBLIOGRAPHY	137
	References	137
VI	APPENDIX	153
8	THE THICK-TUFTED LAYER 5 PYRAMIDAL NEURON	155
9	CHANNELPEDIA	201
10	SINGLE NEURON STATUS REPORT	223

LIST OF FIGURES

- Figure 1.1 Reconstruction of a thick-tufted layer 5 pyramidal neuron with depiction of different neuronal compartments. Dendrites shown in red and the axonal arbour in blue. Green arrowheads illustrate segments randomly selected for spine reconstruction (taken from [Romand et al. 2011]) 7
- Figure 1.2 An illustration of the localization of ion channels on the neuronal membrane and their influence on synaptic transmission and AP output. Nav channels are found in the axon initial segment (AIS), nodes of Ranvier and presynaptic terminals. Voltage-gated potassium Kv1 channels are found in adult myelinated axons and presynaptic terminals. Canonically, EPSPs and IPSPs from the somatodendritic region spread passively to the AIS where APs are generated by depolarization, and travel to the presynaptic nerve terminals to activate voltage-gated calcium (Cav) channels that increase intracellular Ca²⁺ levels, thereby triggering neurotransmitter release. HCN channels have a gradient distribution that increases in density from the soma to the distal dendrites (dark blue shading). Kv2.1 channels are found in clusters on the soma and proximal dendrites (light yellow ovals). Kv3 channels are found throughout the dendrite. Kv4.2 channels are located more prominently on distal dendrites (light blue shading). Kv channels in the dendrites contribute to controlling back propagation. Strong enough inputs in the dendritic region can generate dendritic APs. Dendritic Cav channels increase in density toward the proximal dendrites and the soma (taken from [Lai and Jan 2006]) 8
- Figure 1.3 Elementary building blocks of neural microcircuits. The scheme shows the minimal essential building blocks required to reconstruct a neural microcircuit (taken from [Markram 2006]) 10
- Figure 2.1 Different inward and outward currents and the ion channels that underlie ionic current. Scale bars, 20 mV and 200 ms. (taken from [Toledo-Rodriguez et al. 2005a]) 20
- Figure 2.2 The ion channel database: containing ion channel kinetics and dendritic distributions modelled from published literature 22

- Figure 2.3 Morphological diversity in the neocortex: **a**, Bipolar cell. **b**, Chandelier cell. **c**, Layer 4 pyramidal cell. **d**, Layer 4 star pyramidal cell. **e**, Martinotti cell. **f**, Layer 6 cortico-cortical cell. **g**, Layer 6 cortico-thalamic cell. **h**, Nest basket cell. **i**, Small basket cell. **j**, Double bouquet cell. **k**, Layer 2/3 pyramidal cell. **l**, Large basket cell. **m**, Layer 4 spiny stellate cell. Drawings are not to scale (taken from [Anwar et al. 2010]) 24
- Figure 2.4 Electrical diversity in the neocortex: neuron types classified according to the Petilla convention. The membrane potentials correspond to responses to intra-somatic step current injections in the rat neocortex (taken from [Ascoli et al. 2008]) 25
- Figure 2.5 An illustration of chemical synaptic transmission (taken from "Alzheimer's Disease" - Unraveling the Mystery, National Institute on Aging, US National Institutes of Health) 31
- Figure 2.6 The neocortical microcircuit – major cell types and synaptic connections. Excitatory neurons are in red, inhibitory neurons are in blue, excitatory synapses are shown as V-shapes, inhibitory synapses are shown as circles, and electrical synapses are shown as a black zigzag. Dashed circles depict afferent and efferent extracortical brain regions. Inhibitory synapses onto pyramidal neurons (PC) are displayed according to the target domains: axonal inhibition is provided by chandelier cells (ChC), somatic inhibition by basket cells (BC), and dendritic inhibition by double-bouquet cells (DBC), bipolar cells (BP), neurogliaform cells (NGC), Martinotti cells (MC) and Cajal-Retzius cells (CRC). PCs projecting to different brain areas reside in different layers: layer 5 is the main projection layer, with PCs projecting to subcortical regions such as the brainstem (Bs), spinal cord (SC), superior colliculus, basal ganglia (BG) and thalamus (TH). Layer 6 PCs project mainly to the thalamus, and PCs in superficial layers project to other cortical targets, such as neighbouring columns and the contralateral cortical hemisphere (CL). The representation of the different interneurons also changes across layers, with NGCs and DBCs mainly located in superficial layers, and MCs dominating the deep layers. BCs of different types constitute 50% of interneurons in layers 2–6. Interneurons display diverse interlaminar targeting preferences: DBCs target dendrites that are typically located deeper than the soma, and MCs mainly target dendrites in the more superficial layers. BCs, NGCs, BPs and CRCs innervate neurons mainly within the same layer, although BC axons also spread laterally and innervate neurons from neighbouring cortical columns. Additional abbreviations: WM, white matter (taken from [Grillner et al. 2005]) 33

- Figure 2.7 Differential synaptic facilitation and depression via the same axon innervating two different targets. **A**, a light microscopic pseudocolor image of three biocytin-filled neurons. The pyramidal neuron on the left innervated the pyramidal neuron on the right and the bipolar interneuron on the right. **B**, single trial responses (30 Hz) to same AP train (taken from [Markram et al. 1998]) 34
- Figure 2.8 Simultaneous whole-cell recordings from a triplet (schematically shown on top) in which a pyramidal cell (P) innervated a bitufted (B) and a multipolar cell (M) (taken from [Reyes et al. 1998]) 35
- Figure 2.9 Phenomenological model of frequency dependent synaptic transmission. Each incoming AP utilizes U a fraction of the available/recovered synaptic efficacy R . When an AP arrives, U is increased by an amplitude of U_f and becomes a variable, U_1 . U_f is the running value of U . Depressing synapses can be simulated either by making U very large or by making τ_{facil} (facilitation time constant F) very small (taken from [Markram et al. 1998]). 38
- Figure 4.1 The *in silico* mean latency to EPSP onset, 20 - 80% rise time, amplitude, decay time constant, transmission failures and CV of EPSP amplitude compared against *in vitro* data for L2/3PC connections. The bars in red are the mean *in vitro* measurements, corresponding mean *in silico* measurements are shown in blue. The error bar indicates the S.D. Statistical significance was tested using Fisher's exact two sample test, ** $P < 0.01$, $\alpha = 0.01$. 94
- Figure 4.2 The *in silico* mean latency to EPSP onset, 20 - 80% rise time, amplitude, decay time constant, transmission failures and CV of EPSP amplitude compared against *in vitro* data for L4PC connections. The bars in red are the mean *in vitro* measurements, corresponding mean *in silico* measurements are shown in blue. The error bar indicates the S.D. Statistical significance was tested using Fisher's exact two sample test, ** $P < 0.01$, $\alpha = 0.01$. 95
- Figure 4.3 The *in silico* mean latency to EPSP onset, 20 - 80% rise time, amplitude, decay time constant, transmission failures and CV of EPSP amplitude compared against *in vitro* data for L5STPC connections. The bars in red are the mean *in vitro* measurements, corresponding mean *in silico* measurements are shown in blue. The error bar indicates the S.D. Statistical significance was tested using Fisher's exact two sample test, ** $P < 0.01$, $\alpha = 0.01$. 96

Figure 4.4	The <i>in silico</i> mean latency to EPSP onset, 20 - 80% rise time, amplitude, decay time constant, transmission failures and CV of EPSP amplitude compared against <i>in vitro</i> data for L4SS - L2/3PC connections. The bars in red are the mean <i>in vitro</i> measurements, corresponding mean <i>in silico</i> measurements are shown in blue. The error bar indicates the S.D. Statistical significance was tested using Fisher's exact two sample test, ** P < 0.01, α = 0.01.	97
Figure 5.1	Mean number of synaptic contacts per connection for <i>in silico</i> Inhibitory-Excitatory and Excitatory-Inhibitory connections compared against <i>in vitro</i> data. Bars in red and blue respectively show the mean number of synaptic contacts per connection for <i>in vitro</i> and <i>in silico</i> pathways. The variability in terms of standard deviation is shown by vertical error bars.	114
Figure 5.2	Mean <i>in silico</i> IPSP amplitudes from BP to PCs	115
Figure 5.3	Mean IPSP amplitudes from BTC to PC	116
Figure 5.4	Mean IPSP amplitudes from ChC to PC	117
Figure 5.5	Mean IPSP amplitudes from DBC to PC	118
Figure 5.6	Mean IPSP amplitudes from LBC to PC	119
Figure 5.7	Mean IPSP amplitudes from MC to PC	120
Figure 5.8	Mean IPSP amplitudes from NBC to PC	121
Figure 5.9	Mean IPSP amplitudes from SBC to PC	122
Figure 5.10	Mean EPSP amplitudes from L2PC to IN	123
Figure 5.11	Mean EPSP amplitudes from L3PC to IN	124
Figure 5.12	Mean EPSP amplitudes from L4PC to IN	125
Figure 5.13	Mean EPSP amplitudes from L4SS to IN	126
Figure 5.14	Mean EPSP amplitudes from L5STPC to IN	127
Figure 5.15	Mean EPSP amplitudes from L5TTPC to IN	128
Figure 5.16	Mean EPSP amplitudes from L6CCPC to IN	129
Figure 5.17	Mean EPSP amplitudes from L6CTPC to IN	130

LIST OF TABLES

Table 4.1	No. of synaptic contacts for <i>in silico</i> PC-PC connections (mean \pm S.D.). For every entry, the italicised values in parentheses indicate the <i>in vitro</i> mean \pm S.D.	98
-----------	---	----

Table 4.2	<i>In silico</i> synaptic transmission properties of PC-PC connections. For every entry, the italicised values in parentheses indicate the <i>in vitro</i> mean \pm S.D., where available. In case of a significant mismatch with <i>in vitro</i> data the corresponding <i>in silico</i> values are highlighted in red (Fisher's exact two sample test, $P < 0.01$, $\alpha = 0.01$). 98
Table 5.1	Dynamics and parameters for <i>in silico</i> synaptic transmission in the NCC model. The parameters were mainly obtained from [Markram et al. 1997a; 1998, Gupta et al. 2000, Wang et al. 2006, Silberberg and Markram 2007] 105
Table 5.2	Mapping rules for synaptic dynamics. For every given Morpho-Electrical (ME) type in the NCC model, the synapse type onto PCs and from PCs is indicated. Connections from INs to INs are of the type I2 (inhibitory, depressing). The rules were mainly obtained from [Markram et al. 1997a; 1998, Gupta et al. 2000, Markram et al. 2004, Wang et al. 2006]. For an explanation of the ME types, see 4. 113

GLOSSARY OF TERMS

NCC	Neocortical column
BBP	Blue brain project
3D	Three dimensional
PC	Pyramidal cell
IN	Interneuron
ME-type	MorphoElectrical-type
TTL ₅	Thick-tufted layer 5
SSC	Spiny stellate cell
SBC	Small basket cell
NBC	Nest basket cell
LBC	Large basket cell
MC	Martinotti cell

ChC	Chandelier cell
DBC	Double bouquet cell
BP	Bipolar cell
NGC	Neurogliaform cell
c	continuous
b	bursting
d	delayed
IS	Irregular bursting
AC	Accelerating
AD	Accommodating
NA	Non-accommodating
RS	Regular spiking
IB	Intrinsically bursting
ST	Stuttering
PV	Parvalbumin
SOM	Somatostatin
CCK	Cholecystokinin
NPY	Neuropeptide-Y
CB	Calbindin
CR	Calretinin
VIP	Vasoactive intestinal polypeptide
PIC	Persistent inward currents
I _h	Hyperpolarization activated cation current
LTP	Long term potentiation
LTP	Long term potentiation
STDP	Spike-timing dependent plasticity
AMPA	alpha-amino-3-hydroxy-5-methyl-4-isoxazolepropionic acid

NMDA N-Methyl-D-aspartate

GABA gamma-Aminobutyric acid

Part I

INTRODUCTION

INTRODUCTION

“To know the brain ... is equivalent to ascertaining the material course of thought and will, to discovering the intimate history of life in its perpetual duel with external forces.”

Santiago Ramón y Cajal

— *Recuerdos de mi Vida*, 1937

The thesis work presented here was conducted as part of the Blue brain project (BBP) [Markram 2006]. The BBP is the first comprehensive endeavour to build a unifying *in silico* model of the mammalian neocortical column (NCC) through *in vitro* data acquired from the somatosensory cortex S1 of juvenile rats, by systematic data integration and biologically detailed simulations.

As the common operating unit in the mammalian cerebral cortex, the NCC contains a puzzling plethora of neurons, which are distinct both in terms of morphology and electrical behaviour [Mountcastle 1997]. Neurons communicate. Neuronal communication occurs at specialised points of information transfer called synapses. A myriad of ion channels distributed on the neuronal membrane control the firing properties of these neurons and the manner in which they integrate synaptic signals. [Hille 1992, Lai and Jan 2006, Toledo-Rodriguez et al. 2005a]. The organizing principles for synaptic dynamics in the neocortical microcircuit is extremely diverse [Gupta et al. 2000, Thomson and Lamy 2007].

This thesis work has focussed on setting the stage to characterize the properties of *in silico* synaptic transmission by incorporating principles of synaptic communication derived through biological experiments. Towards this end, it is important to develop an elementary understanding of the major players impacting the processing of synaptic signals in the local neocortical microcircuit - ion channel kinetics and distribution profiles, single neuron models and dynamics of synaptic pathways.

As part of this thesis, I initially worked on modelling ion channel kinetics in neocortical neurons and identifying distribution profiles on dendrites and programming a prototype report on the electrical properties of single neuron models that were constrained with the modelled ion channel behaviour and distributions. Thereafter as part the BBP simulation toolchain, these single neuron models were assembled to reverse-engineer an *in silico* model of the NCC in a bottom-up manner guided by biological rules. The kinetic parameters for synaptic communication between neurons that were derived from biological experiments were incorporated for *in silico* synaptic

transmission, by modelling stochastic neurotransmitter release, quantal conductances, time constants for recovery from depression and facilitation and axonal delays. I then replicated *in vitro* experimental protocols *in silico* to simulate thousands of virtual whole cell experiments (current clamp/voltage clamp) in order to characterize the emergent dynamics of monosynaptic connections between several known pre and postsynaptic neuron combinations.

In order to reverse-engineer the NCC to build a biologically detailed *in silico* model consisting of several thousand multi-compartmental neuron models, ion channel kinetics and stochastic synaptic transmission with diverse rules for synaptic mapping, it is imperative that the underlying pieces of the neocortical microcircuit (as described above) are modelled from and validated against biological data. The BBP has established a facility for simulation based neuroscience research by consolidating a treasure trove of *in vitro* data within a biologically detailed *in silico* model. By means of an automated and iterative work flow process, the *in silico* model is undergoing a process of continuous refinement, guided by existing experimental knowledge on the one hand and driving the design of experiments to procure newer data on the other.

1.1 THE NEOCORTICAL COLUMN IN THE MAMMALIAN BRAIN

The neocortex is the seat for most of the higher order brain functions such as sensory integration, perception, memory storage, cognition, consciousness, and personality [Kandel et al. 2000]. It is considered to be the most recently evolved brain structure. The mammalian neocortex is a continuous assembly of cells forming six distinct layers (labeled from I to VI, with I being the outermost and VI being the innermost).

The appearance of the neocortex is quite smooth in rodents, and other small mammals, whereas in primates and other larger mammals it has deep grooves (*sulci*) and wrinkles (*gyri*). The *sulci* and *gyri* considerably increase the surface area of the neocortex without taking up too much volume, endowing higher order primates, particularly humans with enhanced cognitive abilities. The neocortex occupies as much as 80% of the volume of the mammalian brain.

The general functional unit of the neocortical microcircuit, the so-called neocortical column (NCC) is believed to occur across different cortical regions [Mountcastle 1997]. NCCs are spatially restricted arrangements of neurons, spanning across all cortical layers. Neurons within a column show similar response properties to external stimuli and are densely interconnected, thereby displaying stereotypical microcircuitry across columns (reviewed by [Silberberg et al. 2002]). The emergence of mammalian intelligence could be attributed the modularity of the NCC, which exhibit a dramatic increase in number from mouse to man. Therefore, the study of the mammalian neocortical microcircuit of model organisms like rodents continues to provide fundamental insights into the microcircuitry. However, the ultimate goal is to utilize this knowledge to unravel the working principles of the human neocortex, perhaps through pathbreaking initiatives like The Human Brain Project (www.humanbrainproject.eu).

Preliminary evidence for columnar organization of the neocortex was revealed through single unit electrophysiological recordings [Mountcastle 1957, Powell and Mountcastle 1959, Mountcastle 1997], where marked transitions in electrical signals were observed from one block of neural tissue to other adjacent blocks. Following the pioneering work of Hubel & Wiesel on orientation selectivity in cat visual cortex [Hubel and Wiesel 1959], the NCC has been the focus of several studies across different cortical areas. A typical NCC can vary from 300 - 600µm in diameter across mammals and the prevalent stereotypical structure of anatomical organization is rather debatable. A widely held view, which favours a defined anatomical substrate points that a single NCC consists of anywhere between 60 - 100 minicolumns bound together by short range horizontal connections [Jones 2000]. However, the view of the NCC as an ensemble of minicolumns still remains an open ended question [Purves et al. 1992, Swindale 1998, Markram 2008].

In the rodent barrel cortex, columns are known to occur as somatotopically defined structures [Petersen 2007]. However, elsewhere in the neocortex, like the somatosensory or prefrontal cortices, they can overlap either partially or completely, thus introducing a clear challenge to fix the dimensions of clearly defined columns [Markram 2008].

If the NCC can be regarded as the functional unit of the neocortex, then perhaps a neuron can be rightfully regarded as the functional unit of the NCC. A single neuron in the neocortical microcircuit consists of a unique morphology, with a cell body (soma), axonal and intricate dendritic arbours, possibly divided into basal, apical, oblique and tuft dendritic branches (see Figure 1.1)

Ion channels, which are macromolecular pores in cell membranes, regulate the electrical behaviour of neurons. In addition to being localised on the soma, ion channels are also present in varying densities on dendrites of a neuron, having roles in the integration of synaptic inputs received by dendrites of a neuron (see Figure 1.2). Several neuronal disorders, for instance epilepsy, schizophrenia among others result from dysfunctions of voltage gated ion channels. These abnormalities can cause communication defects in the neocortical microcircuit. It is therefore important to understand the function and distribution of ion channels in the neocortical microcircuit [Toledo-Rodriguez et al. 2005a, Migliore and Shepherd 2002].

"I communicate, therefore I am." Different neurons in the neocortical microcircuit connect to each other through synapses. Depending on the presynaptic neuron, a synapse can either be excitatory or inhibitory. Pyramidal cells, which form the principal class of excitatory neurons, establish excitatory synapses with postsynaptic neurons, whereas interneurons mainly form inhibitory synapses. The functions performed by different microcircuits depend on the anatomical and physiological properties of the various synaptic pathways connecting neurons. The neocortical microcircuit consists of monosynaptic and polysynaptic pathways, where two or more neurons could be connected to one another. These synaptic connections give rise to dynamics and functional properties of a synaptic pathway. Dynamic interactions between neurons lead to emergent states in synaptic pathways. A study of synaptic pathways is therefore important as their function maintains the critical balance of excitation and inhibition during cortical activity and dictates the emergent dynamics of the neocortical microcircuit.

In order to study the properties of synaptic transmission in an *in silico* model of the NCC, it is critical to build faithful models of the various composite pieces that constitute the NCC. But, how is a model of the NCC built at the first place? The following section briefly reviews the state of the art of the Blue Brain Project in reconstructing a model of the NCC *in silico*.

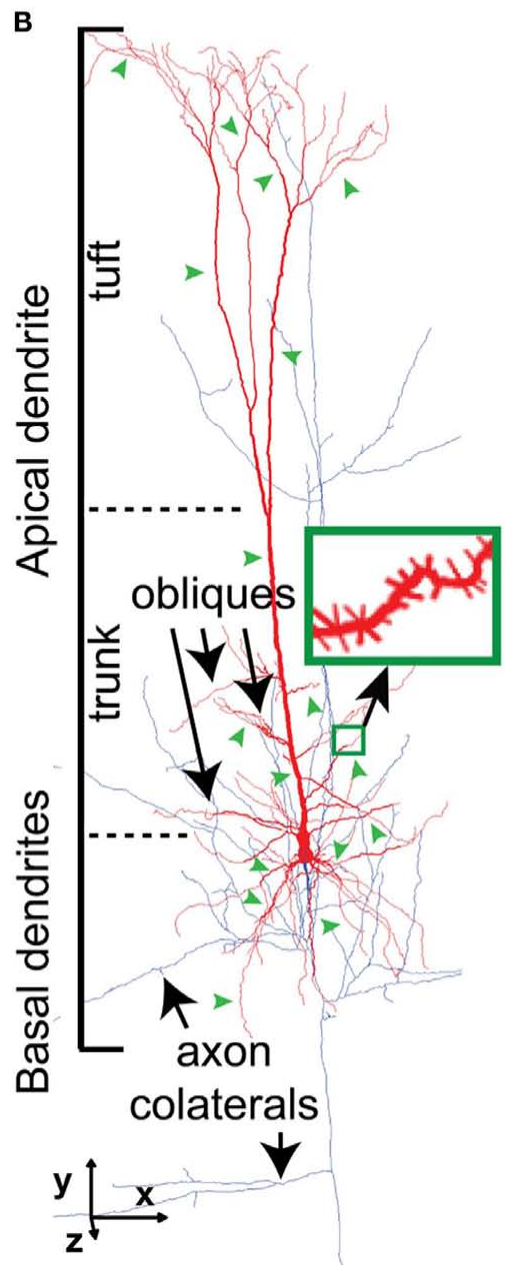


Figure 1.1: Reconstruction of a thick-tufted layer 5 pyramidal neuron with depiction of different neuronal compartments. Dendrites shown in red and the axonal arbour in blue. Green arrowheads illustrate segments randomly selected for spine reconstruction (taken from [Romand et al. 2011])

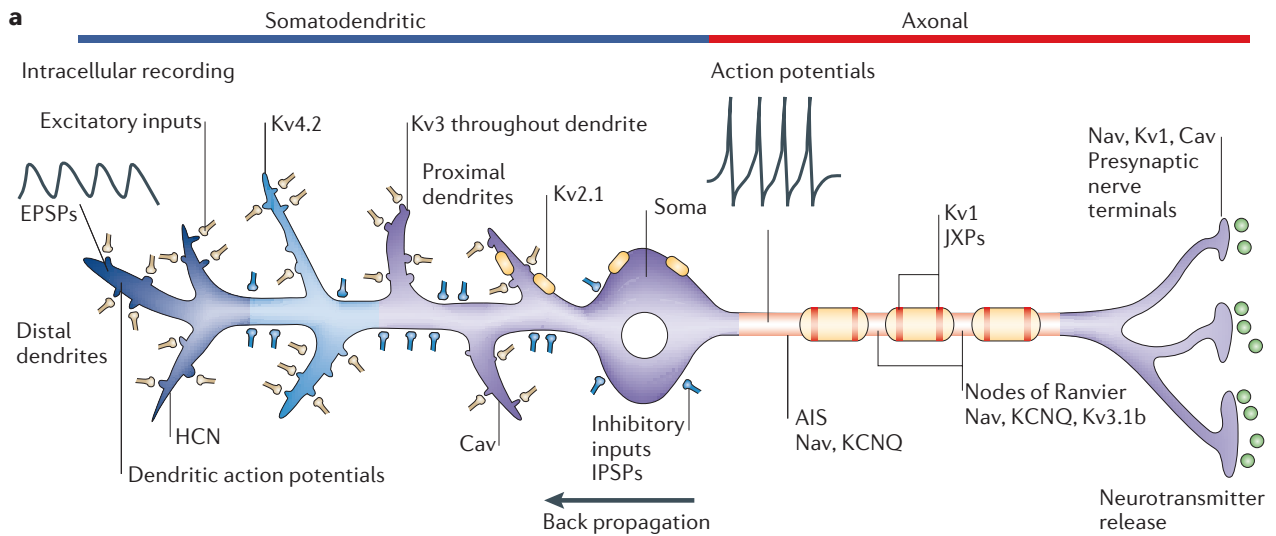


Figure 1.2: An illustration of the localization of ion channels on the neuronal membrane and their influence on synaptic transmission and AP output. Nav channels are found in the axon initial segment (AIS), nodes of Ranvier and presynaptic terminals. Voltage-gated potassium Kv1 channels are found in adult myelinated axons and presynaptic terminals. Canonically, EPSPs and IPSPs from the somatodendritic region spread passively to the AIS where APs are generated by depolarization, and travel to the presynaptic nerve terminals to activate voltage-gated calcium (Cav) channels that increase intracellular Ca^{2+} levels, thereby triggering neurotransmitter release. HCN channels have a gradient distribution that increases in density from the soma to the distal dendrites (dark blue shading). Kv2.1 channels are found in clusters on the soma and proximal dendrites (light yellow ovals). Kv3 channels are found throughout the dendrite. Kv4.2 channels are located more prominently on distal dendrites (light blue shading). Kv channels in the dendrites contribute to controlling back propagation. Strong enough inputs in the dendritic region can generate dendritic APs. Dendritic Cav channels increase in density toward the proximal dendrites and the soma (taken from [Lai and Jan 2006])

1.2 RECONSTRUCTING THE NCC IN SILICO - THE BLUE BRAIN PROJECT

Launched in July 2005, the goal of the BBP is to understand neocortical function and dysfunction through biologically detailed *in silico* models and simulations of the NCC. By the end of 2007, the BBP had reached its first milestone by demonstrating a proof of principle for constructing biologically detailed *in silico* models of the NCC, consisting of ~10,000 multi-compartment neuron models, ion channel kinetics and stochastic synaptic transmission.

With a spectrum of mental disorders believed to affect more than 1 billion people annually, a simulation driven research platform like the BBP would enable the identification of vulnerabilities to reveal candidates to study cortical dysfunction and generate predictions to design targeted therapeutic treatment [Markram 2006]. To this end, a biologically detailed model is most imperative. Therefore, the BBP is principally a data driven approach to simulation based research, integrating data procured through years of biological experiments. Indeed, neuroscience has witnessed several initiatives in the past towards realizing large scale cortical models ranging from recursive arrangement of "ball and stick" like neurons to model network activity [Traub et al. 1992, Bush and Sejnowski 1996] to using biophysical neuron models to simulate supragranular cortical layers [Djurfeldt et al. 2008]. However, the fundamental difference is that the BBP is not merely an attempt to build a model of the NCC, but to build a simulation based research facility where experimental data can be continuously integrated and consolidated.

The past couple of decades have witnessed tremendous growth of biological data due to advances in experimental techniques. A platform like the BBP can serve to integrate all this data in a biologically detailed model of neocortical function. The biological refinement of the *in silico* NCC model is carried out by means of a bottom-up calibration process, which aligns the models across multiple levels - from ion channel kinetics to emergent network dynamics. Large scale simulations with the NCC model are visualized through a dedicated supercomputer in order to realize short turn-around times.

I briefly review the BBP production workflow used to construct *in silico* models of the NCC with the elementary building blocks (see Figure 1.3). A more detailed description is given in an earlier article by H. Markram (2006) [Markram 2006]. The *in silico* NCC model is composed of 3D morphological reconstructions that serve a two fold purpose a) to build detailed multicompartmental single neuron models with active dendrites b) to derive the locations of putative synaptic contacts at incidental loci of axo-dendritic apposition. At first, the reconstructed morphologies are repaired, where they are corrected for slicing artefacts to re-grow severed axonal and dendritic arbours [Anwar et al. 2010]. Following their repair, the morphologies are used by an evolutionary search algorithm to obtain an optimized representation of experimentally measured somatic responses to prolonged injections of supra-threshold current. The free parameters in the algorithm are the maximal conductances of somatic and dendritic ion channels, modelled in the Hodgkin-Huxley (H-H) formalism. The

3D neurons are then imported into a circuit building application, which loads the neurons into their layers according to a 'recipe' of neuron numbers and proportions. A "collision-detection" algorithm is run to determine the structural locations of all axo-dendritic touches (putative synapses) to match the experimentally derived statistics of structural touches. The execution of this algorithm requires a Blue Gene/P supercomputer to partition the work load [Allen et al. 2001]. Probabilities of connectivity between different neuron types are used to convert the structural touches into functional synaptic connections. The manner in which the axons map onto the dendrites between specific anatomical classes and the distribution of synapses received by a class of neurons are used to verify and fine-tune the biological accuracy of the synaptic mapping between neurons [Markram 2006].

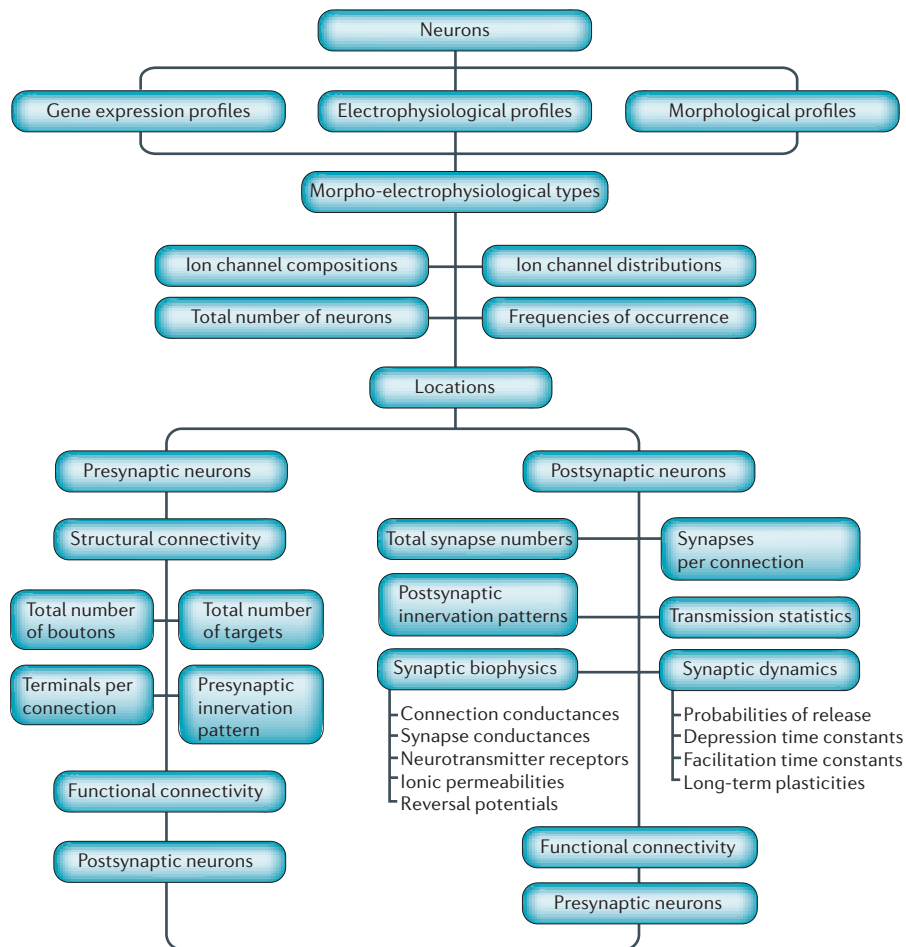


Figure 1.3: Elementary building blocks of neural microcircuits. The scheme shows the minimal essential building blocks required to reconstruct a neural microcircuit (taken from [Markram 2006])

The synapses are functionalized according to the synaptic parameters for different connection classes within statistical variations of each class, biophysical synapse models with stochastic neurotransmitter release and experimentally derived dynamic parameters are used to simulate synaptic transmission with the axonal delay being computed as the distance from the cell body to each synapse. This circuit configuration is then read by a subroutine in the NEURON

simulator [Hines and Carnevale 2000] (www.neuron.yale.edu) that calls up each model neuron and inserts the location and functional properties of every synapse on the axon, soma and dendrites. Effectively, individual processors of the Blue Gene/P supercomputer are converted into model neurons — therefore, the entire Blue Gene/P is converted into an *in silico* replica of the NCC for further network level simulations.

1.3 THESIS OUTLINE AND DESCRIPTION OF RESULTS

This thesis work focusses on characterizing, calibrating and validating the functional properties of *in silico* synaptic transmission by incorporating synaptic communication principles derived through biological experiments. Towards this end, I undertook the following within the framework of the BBP —

1. Building ion channel models and identifying distribution profiles from literature for single neuron modelling in collaboration with Prof. Idan Segev's lab (at the Hebrew University in Jerusalem)
2. Evaluating the goodness of fit for the generalization of somatic and dendritic features of single neuron models across different morphological types in the *in silico* NCC model
3. Modelling the dynamics of *in silico* monosynaptic excitatory & inhibitory connections in the NCC model from principles of synaptic transmission known through *in vitro* experiments
4. Measuring, comparing and validating the emergent *in silico* synaptic properties in the NCC model against *in vitro* data

Chapter 2 formulates the problem definition for this thesis, where I describe the principal players that foster the emergence of synaptic response properties. I also discuss how these principal players are modelled within the BBP framework to set the stage to study *in silico* synaptic transmission.

A major portion of the work undertaken here focussed on replicating *in vitro* experiments to study the emergent properties of *in silico* synaptic connections in the NCC model. The main results are presented in Chapters 3, 4, and 5.

Chapter 3 (*manuscript submitted to The Journal of Physiology*) presents a study of the emergent properties of *in silico* synaptic transmission in monosynaptic connections between thick-tufted layer 5 (TTL5) pyramidal neurons in the NCC model. I implemented a probabilistic model of synaptic transmission with AMPA and NMDA kinetics and replicated *in vitro* stimulation protocols to study the anatomical and physiological properties of *in silico* TTL5 connections and compared them against *in vitro* data. This study reveals for the first time that at the level of the local neocortical microcircuit, the average synaptic response properties (latency of EPSP onset, rise time, amplitude and decay time constant) are robust to perturbations in anatomical and physiological properties and their variability decreases due to an increase in the intrinsic diversity of TTL5 morphologies.

Chapter 4 (*manuscript in preparation*) demonstrates the emergent anatomy and physiology of inter- and intra-laminar excitatory *in silico* synaptic connections in layers 2/3, 4, 5 and 6. This work revealed that *in silico* synaptic properties (latency of EPSP onset, rise time, amplitude and decay time constant, transmission failures and coefficient of variation of EPSP amplitude) emerged due to the axo-dendritic overlap of 3D reconstructed neuron morphologies across

different neocortical layers, closely matching the *in vitro* data. Furthermore, this work also complements the discovery of robustness and invariance due to morphological diversity in the local TTL5 microcircuit (see 3) and suggests that the previously described circuit level robustness and invariance are perhaps fundamental principles governing the function of the local neocortical microcircuit.

Chapter 5 (*manuscript in preparation*) investigates the emergent *in silico* synaptic properties of Excitatory-Inhibitory, Inhibitory-Excitatory monosynaptic connections. Pairs of synaptically connected neurons were sampled within typical inter-somatic distances measured from *in vitro* experiments to characterize the emergent *in silico* synaptic properties by replicating *in vitro* stimulation protocols. Synaptic contacts from inhibitory interneurons onto PCs occur at specific regions of target PCs, showing a high level of innervation domain specificity. The structural arrangement of 3D reconstructed neurons gave rise to *in silico* innervation patterns that were comparable to *in vitro* measurements. Synaptic transmission was simulated at functional synaptic contacts through a probabilistic model of GABA_a kinetics and the emergent *in silico* synaptic response properties were not significantly different from the *in vitro* observations.

In Chapter 6, I discuss avenues for future research directions emanating from this work.

As part of this thesis work, I also had the privilege to review the axonal, dendritic, synaptic and microcircuit properties of the TTL5 neuron based on published literature spanning almost 2 decades of research on the anatomy and physiology of this hallmark neuron. The review is presented in Chapter 8 (*manuscript in preparation for The Journal of Physiology*).

My initial contribution towards modelling almost 12 fundamental ion channel kinetics and distribution profiles through extensive literature survey set the stage to create an elementary prototype of an ion channel knowledgebase in a Wikipedia like fashion. The knowledgebase was later developed to the present version of *Channelpedia* by Rajnish Ranjan [Ranjan 2011], discussed in Chapter 9 (*manuscript submitted to Frontiers in Neuroinformatics*).

Chapter 10 presents a prototype that I designed and implemented in Matlab to generate automated feature based reports on the status of single neuron models. These reports provide a preview into the basic active and passive properties of single neuron models that go into building the NCC model. The prototype report was later ported into the Python programming language by Ruben J. Moor as part of his Master's thesis [Moor 2010] and James G. King of the BBP.

Part II

PROBLEM DEFINITION

INCORPORATING PRINCIPLES OF NEOCORTICAL SYNAPTIC TRANSMISSION: FROM IN VITRO TO IN SILICO

“Swiftly the brain becomes an enchanted loom, where millions of flashing shuttles weave a dissolving pattern — always a meaningful pattern — though never an abiding one.”

Charles Scott Sherrington

2.1 SETTING THE FIELD FOR SYNAPTIC TRANSMISSION IN SILICO - WHO ARE THE PLAYERS?

The role of 3 principal players is critical to set the field for studying the emergent properties of *in silico* synaptic transmission in a biologically detailed model of the NCC -

- Models of ion channel kinetics and distribution profiles on dendrites
- The rich electrical repertoire of neocortical neurons through single neuron models with active dendrites
- Principles of synaptic communication derived through *in vitro* paired recordings in neocortical neurons

Towards this end, I first identified and built models of ion channel kinetics and distribution profiles from literature, which are used to constrain single neuron models by a long-standing collaboration with Prof. Idan Segev’s laboratory at the Hebrew University, Israel. A single neuron model in the BBP terminology is referred to as an "ME-type", which refers to a combination of a morphological (M) type with an electrical (E) type to capture a particular electrical firing pattern.

Once these single neuron models are built, they are tested for their generalization across the diversity of neocortical morphological classes before being integrated into the BBP simulation workflow. I developed an automated prototype status report of the somatic and dendritic properties of single neuron models in order to validate their generalization.

Finally, after these single neuron models are validated, they are then imported into a circuit building application, which loads the neurons into their layers according to a ME-type "recipe" of neuron numbers and proportions. A "collision-detection" algorithm then determines the structural positioning of all axo-dendritic touches, and neurons are jittered and spun until the structural touches match experimentally derived statistics. The structural circuit

encompasses all possible physical locations of axo-dendritic overlap, leading to the identification of a potential synapse at each such incidental location. Indeed, in reality only a fraction of these touches are actually retained as functional synapses, therefore, a structural to functional conversion that takes into account the probability of connection on a per pathway basis filters the structural touches into functional synapses. The synapse mapping rules derived from *in vitro* experiments are assigned to a pathway depending on the type of the pre and post-synaptic model neurons. Probabilistic models of synaptic transmission based on the phenomenological Tsodyks-Markram model are created at the physical location of each functional synapse, parametrized by experimentally derived values for the release probability, times constants for depression and facilitation, quantal conductances and axonal delays.

The model circuit constructed in this manner now constitutes the basic representation of a single NCC and is exported as a format readable by the NEURON simulator for *in silico* synaptic transmission experiments. In order to examine and validate the emergent synaptic properties in terms of the somatic PSP onset latency, 20 - 80% rise time, amplitude, and decay time constant *in vitro* experimental protocols are replicated to simulate virtual paired recording experiments *in silico*.

In the following sections, I briefly introduce the 3 principal players who set the stage for studying *in silico* synaptic transmission.

2.2 PLAYER 1: ION CHANNELS IN THE NEOCORTICAL MICROCIRCUIT

2.2.1 *Biological knowledge*

Neocortical neurons express a rich diversity of ion channels composed of particular combinations of pore-forming and auxiliary subunits [Toledo-Rodriguez et al. 2005a]. Furthermore, the functional characteristics of these channels are defined by their voltage sensitivity and gating kinetics (transitions between open and closed states). The melange of ion channels expressed by a particular type of neuron lays the stage for its function (see Figure 2.1). Slow conductances, such as the persistent inward currents (PIC), the hyperpolarization-activated cation current (I_h), voltage-activated K^+ currents and Ca^{2+} -dependent K^+ currents, further the time window for synaptic integration beyond the membrane time constant of the postsynaptic neuron. PIC can also support spontaneous repetitive firing [Häusser 2004]. Voltage dependence and kinetics of ionic currents provide mechanisms to discriminate particular input patterns and condition the postsynaptic response [Schoppa and Westbrook 1999]. Neurons with low voltage activated Ca^{2+} channels are tuned to sudden depolarization from hyperpolarized membrane potentials, whereas neurons with slowly activating Ca^{2+} channels respond differentially to sustained depolarization [Perrier et al. 2002].

The presence of various voltage-dependent channels, and particularly Ca^{2+} channels, in dendrites provides a mechanism for feedback of input integration onto synaptic transmission. An action potential (AP) generated at the soma in neocortical neurons can back-propagate into dendrites and induce local increases in intracellular Ca^{2+} concentration, leading to changes in strength of subsequent synaptic signals. Associated presynaptic and postsynaptic action potentials can lead to either long-term potentiation (LTP) or long-term depression (LTD) of synaptic transmission, depending on their order and timing [Sjöström et al. 2001]. Dendritic Ca^{2+} channels have also been found to participate in homeostatic plasticity mechanisms. The dual role of Ca^{2+} as a carrier of current through membranes and intracellular messenger provides a link between long-range electrical integration in dendrites and short-range biochemical processing, greatly enhancing the processing capacity of neocortical neurons [Toledo-Rodriguez et al. 2005a].

The most significant intrinsic factor determining the frequency of firing in neurons is the late afterhyperpolarization (AHP) following each action potential (see Figure 2.1). Prolonged, deep AHPs characterize neurons with low regular firing, whereas small AHPs favour high firing rates. The AHP is attributed to Ca^{2+} -dependent K^+ channels (KCa), activated by the Ca^{2+} entering the cell through voltage gated Ca^{2+} channels during the AP.

Several classes of voltage gated K^+ channels have been characterized through biophysical, pharmacological and molecular techniques. Most of these channels, belonging to the Kv1, Kv2 and Kv4 subfamilies, are activated at membrane potentials below the spike threshold (low voltage activated, delayed and delayed rectifying channels). Channels belonging to the delayed-rectifying Kv3 subfamily activate only at membrane potentials well above the spike

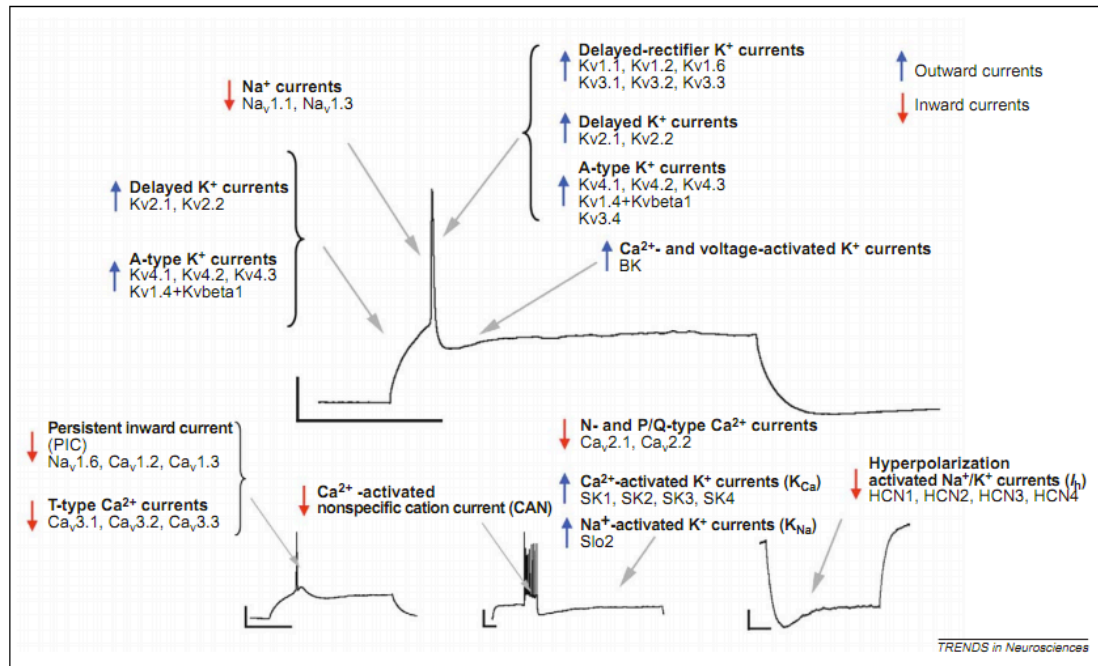


Figure 2.1: Different inward and outward currents and the ion channels that underlie ionic current. Scale bars, 20 mV and 200 ms. (taken from [Toledo-Rodriguez et al. 2005a])

threshold (see Figure 2.1). Furthermore, there are other types of K^+ channels that are activated by intracellular Ca^{2+} (SK family channels), a combination of voltage and Ca^{2+} (BK channels), or Na^+ . Several studies have endeavored to correlate the expression of one or several K^+ channels with the electrical behaviour of particular neurons [Lien and Jonas 2003, Toledo-Rodriguez et al. 2004]. Fast-spiking neocortical interneurons express the delayed-rectifier K^+ channels $Kv3.1$ and $Kv3.2$. Other correlations have looked at the expression of the A-type K^+ channel $Kv4.2$ with delayed firing onset and accommodation, and expression of the delayed-rectifier K^+ channel $Kv1.1$ with stuttering and irregular spiking behaviour [reviewed in Toledo Rodriguez 2004]. It has been suggested that the high-frequency firing of GABAergic interneurons enables constant release of neurotransmitter, leading to decreased excitability of the microcircuit. The firing frequency of these inhibitory neurons can be modulated by targeting $Kv3$ channels. In principal neocortical neurons, K^+ channels have been to be distributed as a decreasing gradient along the somato-dendritic axis [Korngreen and Sakmann 2000, Bekkers 2000a;b].

The voltage-dependent fast inactivating current through Na^+ channels is the principal current responsible for the depolarizing phase of the AP and thus is the essential current for neuronal excitation in general. Consequently, it can also be considered to be indispensable for the generation of epileptiform activity. The fast inward current provided by Na^+ channels dramatically increases the excitability of dendrites allowing for the generation and propagation of action potentials as well as shaping of synaptic potentials. Na^+ currents have rapid activation and inactivation kinetics. Na^+ currents are believed to play a crucial role in EPSP amplification, AP propagation, dendritic spike initiation and frequency dependence of AP back-propagation

[Stuart et al. 2007]. The distribution of Na channels in principal neocortical cells has been shown to be fairly uniform along the somato-dendritic axis [Stuart and Sakmann 1994].

High levels of I_h have been found in the dendrites of neocortical pyramidal neurons [Kole et al. 2006a]. Patch-clamp recordings in TTL5 neurons reveal a gradient of dendritic I_h , with current density increasing with increasing distance from the soma [Kole et al. 2006a]. Dendritic I_h is thought to be important in shaping the voltage response to excitatory synaptic inputs (for review see [Robinson and Siegelbaum 2003]). The importance of I_h in the normalization of EPSP time course was demonstrated by the finding that inorganic or organic I_h antagonists caused a preferential slowing of distal EPSPs relative to proximal EPSPs [Nicoll et al. 1993, Williams and Stuart 2002]. The presence of I_h in the distal dendrites is thought to modify the EPSP time course by enhancing the local resting membrane conductance, thereby providing a leakage path for current flow that decreases the local membrane time constant and hence speeds the decay of the distal EPSP. When activated, the inward I_h current depolarizes a neuron towards the threshold of voltage gated Ca^{2+} channel activation, which in turn leads to firing of an AP [Craven and Zagotta 2006].

2.2.2 Building models of ion channel kinetics

How are ion channel kinetics modelled and integrated into single neuron models as part of the BBP simulation framework? Currently, the single neuron models used in the simulation framework, built in collaboration with researchers at the Hebrew University consist of about 12 principal classes of ion channels. Using these generic ion channel models and distribution profiles on a neuronal morphology, it is possible to replicate known electrical phenomena including the modulation of the time course of postsynaptic potentials, back-propagating APs and somatic firing patterns to recreate the electrical diversity of neocortical neurons. The ion channel kinetics and time constants were identified through extensive literature survey and modelled based on the Hodgkin-Huxley (H-H) formalism through custom built tools in Matlab and NEURON [Ranjan 2011].

Based on the H-H formalism [Hodgkin and Huxley 1952], the general functional form for the current generated at an ion channel c is thus

$$I_c = g_c(V, t) * (V(t) - E_c(t))$$

where the "driving force", $V - E_c$, is the difference between the voltage across the membrane and the reversal potential for the ion channel in question, E_c . The time and voltage-dependent conductance $g_c(V, t)$ conductance is modelled as the product of activation, m , and inactivation, h , terms that are essentially sigmoid nonlinearities.

Through literature survey, I identified the activation and inactivation kinetics (m_∞, h_∞), time constants (m_τ, h_τ) and dendritic distribution profiles for principal ion channel classes expressed in neocortical neurons. The following ion channel kinetics were identified -

1. Na⁺ (transient and persistent)
2. Ca²⁺ (T, P and Q types)
3. K⁺ (slow, fast, delayed rectifier and muscarinic currents)
4. Hyperpolarization activated cation channels (I_h)
5. Big and small conductance Ca²⁺ dependent K⁺ channels (*BK* & *SK*)

The ion channel models based on the H-H formalism were automatically generated as ".mod" files using NMODL, a high level language implemented for the NEURON simulation environment. The dendritic distribution profiles were also identified and converted into a machine readable format. This automated process facilitated the construction and storage of several ion channel models in a custom built database (see Figure 2.2).

SELECT	USE INDEX	CHANNEL NAME	SEGMENT	CELL TYPE	ANIMAL
<input type="checkbox"/>	50	BK	soma	Cerebral Purkinje	Mouse
<input type="checkbox"/>	60	Ca	dend	Neocortical L5PC	rat
<input type="checkbox"/>	40	HHK	Axon	giant Axon	Squid
<input type="checkbox"/>	40	HHNa	Axon	giant Axon	Squid
<input type="checkbox"/>	60	Ih	dendrite	Neocortical L5PC	rat
<input type="checkbox"/>	50	KCa1	N.A	Muscle	rat
<input type="checkbox"/>	50	KCa2	N.A	soma	Leech
<input type="checkbox"/>	50	KCa3	N.A	soma	NA
<input type="checkbox"/>	20	Kfast	dendrite	Neocortical L5PC	rat
<input type="checkbox"/>	20	Kslow	dendrite	Neocortical L5PC	rat
<input type="checkbox"/>	100	Kv1.1	CellBody	Oocyte	rat
<input type="checkbox"/>	100	Kv1.2	CellBody	Oocyte	rat
<input type="checkbox"/>	100	Kv1.3	CellBody	Oocyte	rat
<input type="checkbox"/>	150	Kv1.4	CellBody	Oocyte	rat
<input type="checkbox"/>	150	Kv1.5	CellBody	Oocyte	Human
<input type="checkbox"/>	51	Kv1.6	CellBody	oocyte	Xenopus

Figure 2.2: The ion channel database: containing ion channel kinetics and dendritic distributions modelled from published literature

Following an important step to validate the modelled ion channel kinetics, the models were then used by our collaborators at the Hebrew University to construct single neuron

models through a multi-objective optimization algorithm developed by [Druckmann et al. 2007]. The optimization algorithm performed a search for initial conductances using electrical features extracted from responses to somatic step and ramp current injections through *in vitro* experiments, which formed the primary set of constraints [Druckmann et al. 2007; 2008, Hay et al. 2011].

The following section describes the importance of neuronal diversity in influencing the activity of the neocortical microcircuit and how these ion channel models fulfil their specific role in modelling the diverse electrical behaviour of neocortical neurons.

2.3 PLAYER 2: THE MORPHOLOGICAL AND ELECTRICAL DIVERSITY OF NEOCORTICAL NEURONS

2.3.1 *Biological knowledge*

The six layered neocortical microcircuit exhibits a rich diversity of neurons, classified according to a diversity of morphological, electrical, molecular and biochemical properties [Kawaguchi and Kubota 1997, Cauli et al. 1997, Somogyi et al. 1998, Gupta et al. 2000, Markram et al. 2004, Toledo-Rodriguez et al. 2005a] (see Figure 2.3). The morphological, electrical and biochemical diversity of neurons are critical building blocks that influence the activity patterns of the neocortical microcircuit.

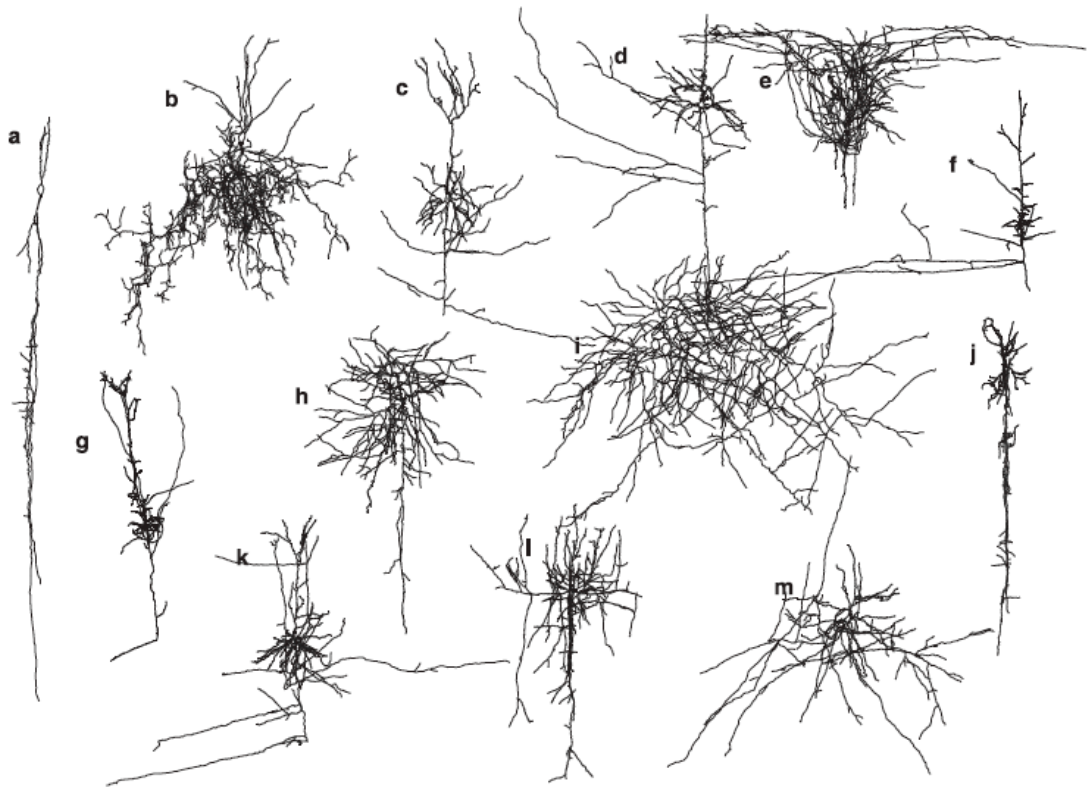


Figure 2.3: Morphological diversity in the neocortex: **a**, Bipolar cell. **b**, Chandelier cell. **c**, Layer 4 pyramidal cell. **d**, Layer 4 star pyramidal cell. **e**, Martinotti cell. **f**, Layer 6 cortico-cortical cell. **g**, Layer 6 cortico-thalamic cell. **h**, Nest basket cell. **i**, Small basket cell. **j**, Double bouquet cell. **k**, Layer 2/3 pyramidal cell. **l**, Large basket cell. **m**, Layer 4 spiny stellate cell. Drawings are not to scale (taken from [Anwar et al. 2010])

Unfortunately, there is no one-to-one mapping between the morphological, electrophysiological, molecular and biochemical properties of neurons, leading to decades of research on classification schemes [Lorente de No 1939, Connors and Gutnick 1990, Kawaguchi 1995, Kawaguchi and Kubota 1997, Cauli et al. 1997, Gupta et al. 2000, Markram et al. 2004, Helmstaedter et al. 2009]. By injecting a step current into the soma of a single neuron, the elicited response can be classified as fast-spiking (FS), regular spiking (RS), accommodating (AD), non-accommodating (NA), accelerating (AC), intrinsically-bursting (IB), and stuttering (ST) (see Figure 2.4).

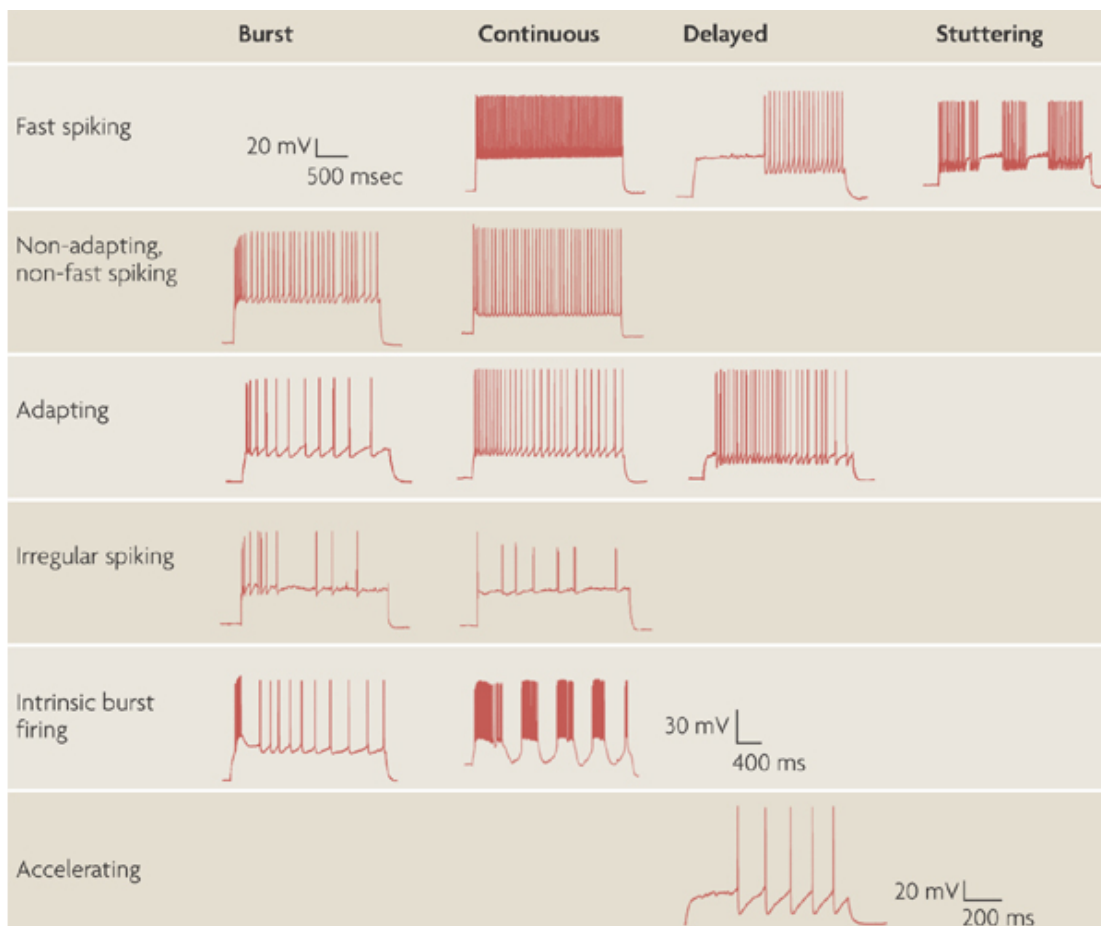


Figure 2.4: Electrical diversity in the neocortex: neuron types classified according to the Petilla convention. The membrane potentials correspond to responses to intra-somatic step current injections in the rat neocortex (taken from [Ascoli et al. 2008])

Morphologically, the postsynaptic innervation domain of the axon of a single neuron is perhaps the most rigorous classification. Soma and proximal-dendrite, dendrite, tufted dendrite, and axon-targeting cells can be distinguished [Markram et al. 2004], although certain classes of neurons usually do not restrict their innervation domain to a particular region of interest.

Biochemically, neurons have been investigated rather exhaustively for the expression of neuropeptides like somatostatin (SOM), cholecystokinin (CCK), neuropeptide Y (NPY) or vasoactive intestinal polypeptide (VIP), which mediate or modulate neuronal communication and calcium binding proteins like parvalbumin (PV), calretinin (CR) or calbindin (CB), which participate in Ca^{2+} cell signalling pathways by binding to Ca^{2+} . For certain types of neurons, the existence of electrical gap junctions has been also suggested as a classification scheme [Hestrin and Galarreta 2005]. Furthermore, neurons can be classified based on their activation profile *in vivo*, given the existence of some global reference like gamma oscillations in the hippocampus [Klausberger et al. 2003, Klausberger and Somogyi 2008].

The most general and fundamental discrimination can be made between projection neurons and local circuit neurons [Rakic 1975] according to the extent of the cell's axonal projections.

Projection neurons have axons that innervate regions which are located outside of the soma area, whereas local circuit neurons have an axonal arborization that is usually confined to their area of location (but see [Tomioka et al. 2005] for exceptions). Projection neurons are excitatory and almost exclusively pyramidal cells (PCs), whereas local circuit neurons, also called interneurons, are inhibitory with the exception of spiny stellate cells in layer 4 and some non-pyramidal neurons in layer 6. Pyramidal cells (PCs) are by far the most common neuronal cell types in the neocortex, comprising up to 80 % of all cortical neurons [DeFelipe and Fariñas 1992, Peters and Jones 1999, DeFelipe et al. 2002].

The Thick-tufted layer 5 (TTL5) PC in the primary somatosensory cortex has been investigated in exquisite detail and is regarded due to its experimental access as a paradigm projection neuron for studying synaptic dynamics, long term synaptic modifications, and active dendritic conductances [Stuart and Sakmann 1994, Markram and Sakmann 1994, Markram et al. 1995, Markram and Tsodyks 1996, Markram et al. 1997a,b, Schiller et al. 1997, Larkum et al. 1999b;a, Berger et al. 2001]. Regardless of the cortical area they are located in, TTL5 neurons are the main output neurons, projecting and transmitting information to subcortical structures.

Morphologically, several different types of PCs exist, which are specific to layers. Their somata has a pronounced pyramidal shape, and they feature a primary apical dendrite that is a thicker in diameter than the thinner basal dendrites. The apical dendrite is oriented towards the pia matter in a perpendicular fashion and usually reaches layer 1. Depending on the exact type, it evolves into a tufted dendrite. The basal dendrites extend radially from the soma and have an approximately uniform length. All dendrites are extensively covered with spines, almost doubling the membrane surface of the cell [Braitenberg et al. 1998]. The axon usually emerges directly from the soma at the opposite site of the apical dendrite, giving rise to a straight projection towards the white matter. On its way, the axon sends back multiple collaterals to its own layer and most others. Many PC types from all layers project to the contralateral hemisphere via the corpus callosum (callosal cells), whereas projections to extracortical brain areas are found only in infragranular layers 5 & 6.

Local circuit neurons or interneurons (IN) form about 15-20 % of neocortical neurons [White and Keller 1989]. These neurons lack the characteristic apical dendrite setting them apart from PCs. Their somata can have diverse shapes, even within the same subclass of interneurons, ranging from bipolar, bitufted, to multipolar, depending on the number, thickness and location of the primary dendrites [Markram et al. 2004]. These neurons have a dense local axonal arborization within the same or different layer of the soma location featuring thousands of boutons, hence these neurons are also referred to as local circuit neurons. Their axon usually does not spread across areal borders or to subcortical regions. The axonal arborization of INs has been a long standing criterion for classification, since it appears to be quite distinct between different cell groups. With the exception of the excitatory spiny stellate cells (SSC) in layer 4 and

the less well defined excitatory non-pyramidal cells in deep layer 6 [Andjelic et al. 2009], INs predominantly receive synapses on smooth aspiny dendrites (as opposed to PCs).

Basket cells (BCs) are a common group of INs present in all cortical layers except layer 1. BCs display a certain diversity in their morphological, electrophysiological and molecular properties. They form an extremely dense local axonal field around the somata of PCs. Several sub-classifications of BCs based on the morphometrics of axonal arborization have been put forth [Gupta et al. 2000, Wang et al. 2002]. The shape of their somata is quite diverse, ranging from multipolar to bitufted featuring a main dendrite, having relatively few or no spines. Electrophysiologically, they display a similar diversity, with NA, FS, and AD firing patterns. Although a matter of debate, most FS cells (with the exception of the rare Chandelier cells) that have been investigated but whose identity has not been morphologically confirmed are very likely to be BCs. Parvalbumin (PV) is the most important marker for BCs, but they can also contain, CB, NPY, and CCK as markers [Cauli et al. 1997]. Functionally, FS cells have been related to fast cortical network oscillations [Klausberger et al. 2003]. A finer subdivision of BCs into large, small and nest basket cells, based on morphological parameters was recently established [Gupta et al. 2000, Wang et al. 2002, Markram et al. 2004].

A widely studied group of INs are the Martinotti cells (MCs), named after Carlo Martinotti, their discoverer [Martinotti 1889]. MCs can be found in layers 2 – 6 in probably all mammalian species [Eccles 1983, Wahle 1993, Kawaguchi and Kubota 1997, Markram et al. 1998, Wang et al. 2004, Silberberg and Markram 2007]. Like BCs, the somata of MCs can have diverse shapes, but their axonal morphology is what makes them a very distinct class of INs. MCs display an ascending axon that bifurcates and ramifies extensively, reaching layer 1 [Marin-Padilla and Marin-Padilla 1982]. The lateral spread of axon collaterals can amount to several millimetres, giving the arborization a conspicuous "T- shape" appearance. MCs mainly display an accommodating firing pattern. MCs have also display a low spiking threshold, as well as a characteristic rebound spike following strong hyperpolarization [Kawaguchi and Kubota 1997, Goldberg et al. 2004]. All MCs stain positive for SOM [Wahle 1993, Wang et al. 2004, Toledo-Rodriguez et al. 2005b].

Chandelier cells (ChCs) are found across many mammalian species in all cortical layers except layer 1 and display a very conspicuous morphology [Somogyi 1977; 1979, Somogyi et al. 1982, Lewis and Lund 1990, Kawaguchi 1995, Kawaguchi and Kubota 1997, DeFelipe 1999, Szabadics et al. 2006, Woodruff et al. 2009; 2010]. Their somata and dendritic arbour are usually used as criteria for classification. However, the axonal arbour of ChCs is very unique. It densely ramifies in proximity to the soma, and builds chandelier-like ramifications of vertically arranged, bouton-rich strings. ChCs are axo-axonic cells, *i.e.* they selectively target the axonal initial segment of PCs, providing strategic and powerful inhibition to the neocortical network. ChCs are believed to play a crucial role in cortical function by preventing over-excitation, therefore the lack of ChCs has been attributed to temporal lobe epilepsy in the human neocortex [DeFelipe

1999]. Intriguingly, a recent electrophysiological study in human cortical slices has shown the opposite effect of ChCs contrary to their predominant function of inhibition, with excitatory effects on PCs (Szabadics et al., 2006). This is a clear-cut instance of the importance of not only the morphology but also the electrophysiological properties to fathom the function of specific neuronal classes. ChCs express PV and also CB [DeFelipe et al. 1989, Markram et al. 2004].

Double bouquet cells (DBC) are found in most mammals, mainly in supragranular layers [Jones 1975, Somogyi and Cowey 1981]. Like in other interneurons, their axonal arborization is their most prominent feature. Their axons form tight, horsetail-like, ascending and descending bundles that are confined to a very narrow area. The narrow axonal field seems to gradually decrease from primates to cats to rodents [DeFelipe et al. 2006], suggesting a relationship with the occurrence of minicolumns in primate visual cortex [DeFelipe et al. 1990, Vercelli et al. 2004]. They express CB and other markers with the exception of PV, SOM, and NPY [Markram et al. 2004].

Neurogliaform cells (NGCs) are small interneurons present in all cortical layers including layer 1 [Jones 1975, Valverde 1978, Kisvárdy et al. 1990, Hestrin and Armstrong 1996]. They have a very dense local axonal arborization that is mostly confined to the layer they originate in. NGCs also inhibit PCs with slow, long-lasting inhibition [Tamás et al. 2003].

2.3.2 Building single neuron models

The activity patterns of the neocortical microcircuit originate from the diverse electrical behaviour and synaptic interactions of constituent neurons. Electrical diversity ensures the relative contribution of intrinsic properties and synaptic potentials to neuronal output, which shapes the functional activity of the neocortical microcircuit. Recreating the electrical diversity of neurons in the *in silico* NCC model is therefore important.

I briefly review the general single neuron modelling strategy under the BBP simulation workflow. The majority of the single neuron modelling work is being carried out through an ongoing collaboration with Prof. Idan Segev's lab. in Israel, by Shaul Druckmann, Etay Hay and Albert Gidon. These single neuron models are then integrated into the BBP simulation workflow.

As an initial step, electrical features from experimental traces were extracted by step current injections into neurons through *in vitro* current clamp experiments. The set of electrical features used for single neuron modelling are elaborately described in [Druckmann et al. 2007; 2008, Hay et al. 2011].

Voltage-dependent ion channel kinetics and distribution profiles, identified from literature and populated in the ion channel database as described above were then inserted across neuron morphologies - at the soma for interneuron models and on the axon initial segment and dendrites for pyramidal neuron models. The value for the maximal conductance of each ion channel type was left as a free parameter to be fitted by the multi-objective optimizer algorithm.

The upper bound for the maximal conductance was selected based on estimates of reasonable biological bounds and later verified by checking that the acceptable solutions of the fitting are not affected by increasing the upper bound value.

Prototype single neuron models were constructed in the NEURON simulation environment [Druckmann et al. 2007; 2008, Hay et al. 2011]. Single models with somatic features were built to recreate the entire diversity of cAD, bFS, cFS, dFS, bST, cST, dST, bNA, cNA, dNA, bAD, bIS, and cIS ME-types (for an explanation of terms see Glossary of terms 4 on page xxii) . Furthermore, the dendrites of the electrical model for pyramidal neurons were made 'active' by distributing ion channels. This ensured to large extent that experimentally observed mechanisms of synaptic integration, attenuation of back-propagating APs and local generation of Ca^{2+} spikes in distal tuft dendrites were faithfully captured in pyramidal neuron models [Hay et al. 2011].

2.4 PLAYER 3: PRINCIPLES OF SYNAPTIC COMMUNICATION IN THE NEOCORTICAL MICROCIRCUIT

2.4.1 *Biological knowledge*

Charles Scott Sherrington coined the term "*synapse*", which is the point at which the neuronal impulse is transmitted from one neuron to another. The synapse is indeed the 'heart' of information transmission in the central nervous system. Generally speaking, synapses transmit information either chemically or electrically. Chemical synapses use a neurotransmitter for intercellular communication; the two most common types are the excitatory neurotransmitter Glutamate and the mainly inhibitory GABA. In addition, there is a myriad of other neurotransmitters and corresponding receptors present in the neocortical microcircuit. The other neurotransmitters mainly act as neuromodulators on a somewhat slower timescale (several seconds to minutes). Acetylcholine, glycine, norepinephrine, serotonin, dopamine and such modulators have been found to decisively alter the intrinsic properties of single neurons and microcircuits.

Chemical synapses are highly complicated biophysical devices with a vesicle release machinery in the presynaptic terminal and a dense protein complex in the postsynaptic site. How does synaptic transmission occur? In brief, an AP arriving at the presynaptic terminal leads to opening of voltage gated Ca^{2+} channels, elevating the local Ca^{2+} concentration, which in turn triggers the fusion of vesicles filled with neurotransmitter with the membrane in a highly non-linear manner [Katz and Miledi 1968]. When the neurotransmitter is released, it enters the synaptic cleft and binds to the postsynaptic receptors, which selectively open for specific ions, mediating the postsynaptic response by causing a membrane potential change in the postsynaptic compartment depending on the kind of neurotransmitter released (see Figure 2.5).

The postsynaptic site of glutamatergic synapses contain AMPA, NMDA and Kainate receptors. AMPA receptors show a linear relationship between the entering current and the postsynaptic membrane potential. NMDA receptors are more complicated and nonlinear, since they only open at relatively depolarized membrane potentials when a magnesium block is removed from the channel pore [Nowak et al. 1984, Jahr and Stevens 1990]. NMDA receptors are involved in synaptic plasticity and memory formation, mainly mediated by their high permeability of Ca^{2+} . Unfortunately, for the moment not much is known about the kinetics of kainate receptors in neocortical neurons.

GABAergic synapses are selective to chloride ions, whose reversal potential is close to the resting membrane potential of many neurons. Therefore, GABAergic synaptic events often appear as an increase in conductance without a visible change of the membrane potential of a neuron (shunting inhibition).

Neurotransmitter release is stochastic and quantal [Katz and Miledi 1968, Katz 1969, Korn and Faber 1991]. It only happens with a certain likelihood and in discrete events of unitary

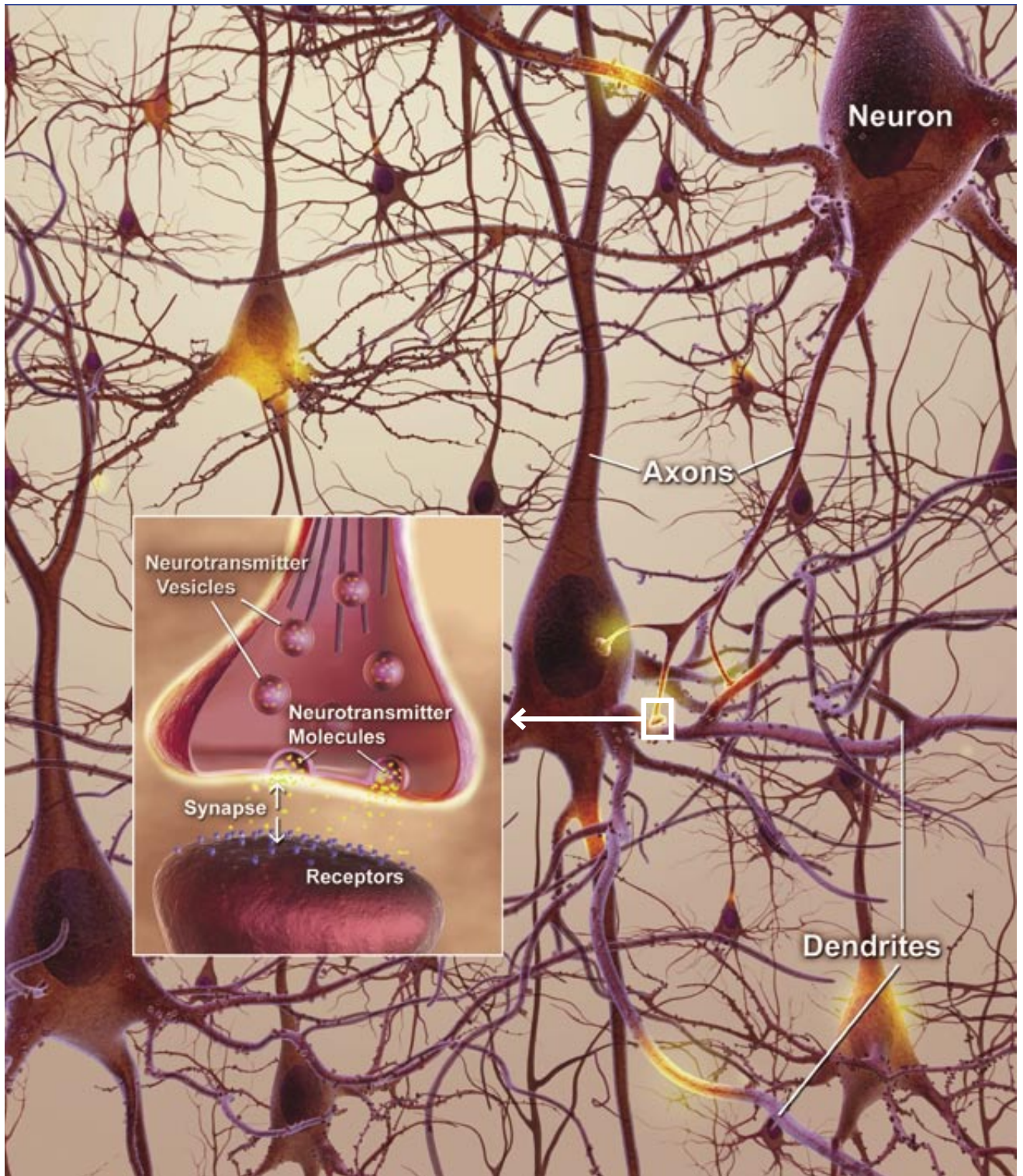


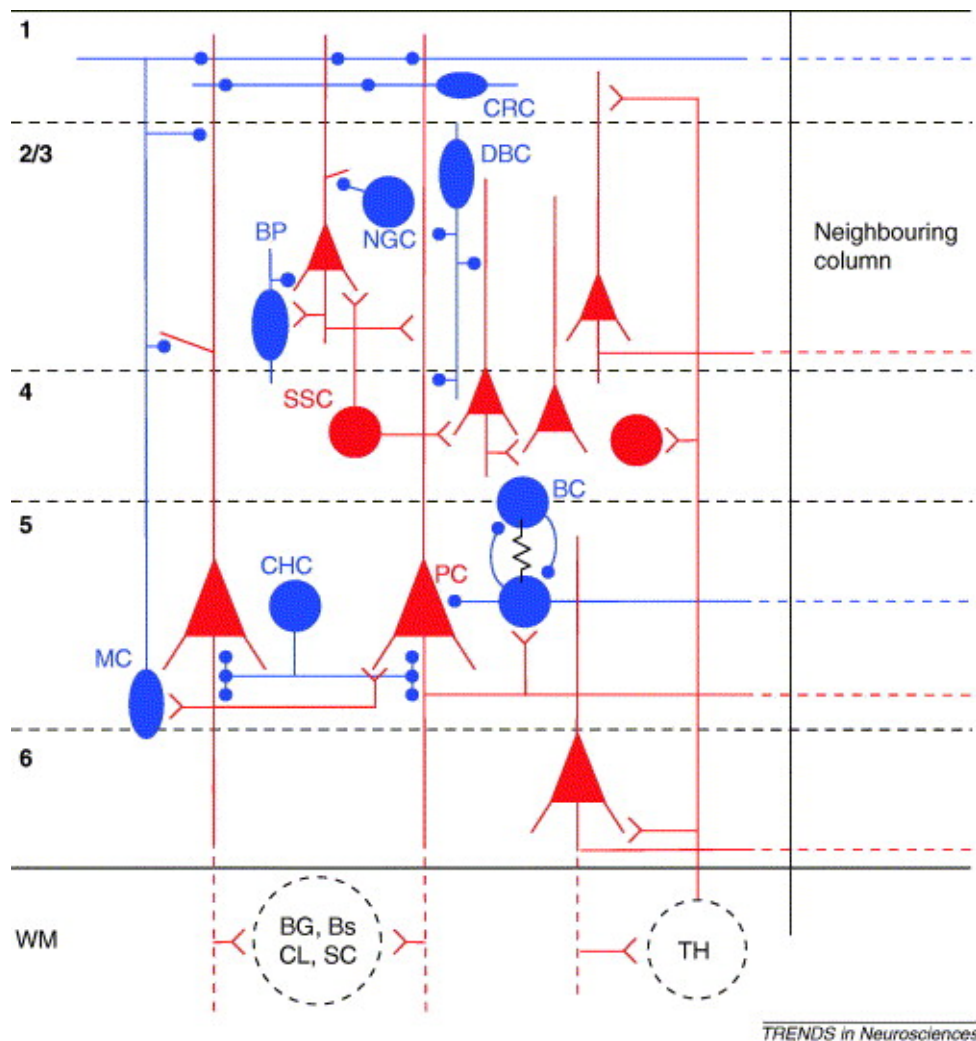
Figure 2.5: An illustration of chemical synaptic transmission (taken from "Alzheimer's Disease" - Unraveling the Mystery, National Institute on Aging, US National Institutes of Health)

size. A commonly used description for synaptic transmission is based on binomial statistics, using the parameters number of release sites (n), transmitter release probability (p), and quantal size (q) to characterize the efficacy of a connection (M). These parameters allow an accurate description of the response variability of synaptic transmission. In some large synapses in the CNS, the number of release sites can be observed and estimated ultra-structurally. The release probability is determined by changing the extracellular Ca^{2+} concentration, allowing a subsequent deduction of the quantal content of a single vesicle. However, connections between neocortical cells usually consist of multiple synaptic contacts [Markram 1997, Buhl et al. 1997, Markram et al. 1997a, Somogyi et al. 1998, Gupta et al. 2000, Markram et al. 2004, Koester and Johnston 2005], and their small physical size and small functional output compared to the noise level makes a quantal analysis of these synapses difficult (however, see [Koester and Johnston 2005]). Synaptic transmission is also a highly dynamic process, the strength of a synaptic response to a given AP is not constant but depends on the history of activity in that synapse [Eccles 1964, Thomson et al. 1993, Zucker and Regehr 2002]. Therefore, a synapse is not a device merely transmitting information about the instantaneous activity of a presynaptic neuron, but also relays information about the temporal context about an event, for example in the context of spike-timing dependent plasticity [Markram et al. 1997b, Bi and Poo 1998, Sjöström et al. 2001, Froemke and Dan 2002, Sjöström et al. 2007].

The functional properties of synaptic transmission foster dynamic interactions within the microcircuit and define the kinetics of the synaptic pathway. The dynamics of synaptic transmission between neocortical neurons is rather multifarious, adding to the complexity in the microcircuit [Gupta et al. 2000](see Figure 2.6).

An important principle of communication is the target specificity of synaptic connections [Markram et al. 1998, Reyes et al. 1998]. The temporal short term dynamics are not only determined by the presynaptic cell type, but also by the identity of the postsynaptic cell. A dramatic example of this differential signalling of a single axon is the TTL5 axon, establishing strongly depressing EPSPs with neighboring TTL5 neurons on the one hand, and strongly facilitating responses to MCs on the other (see Figures 2.7 , 2.8). Since the dynamics synaptic transmission are largely attributable to the synaptic vesicle release machinery (of presynaptic origin), it implies that the synapses of a given neuron are differentially built depending on the postsynaptic neuron type [Markram et al. 1998].

An important principle of neocortical synaptic transmission is the domain specificity of innervation, which is characteristic of IN-PC connections. Most INs have a preferential targeting location when they innervate a postsynaptic neuron. The most prominent example are ChCs that mainly innervate the axon initial segment of PCs. BCs selectively innervate somatic and peri-somatic targets of PCs [Somogyi et al. 1998, Brown and Hestrin 2009a], whereas DBCs, NGCs and MCs target dendrites of their postsynaptic partners. In particular, the MC is very unique in its target selectivity, since it strongly innervates the tufted dendrites of pyramidal



TRENDS in Neurosciences

Figure 2.6: The neocortical microcircuit – major cell types and synaptic connections. Excitatory neurons are in red, inhibitory neurons are in blue, excitatory synapses are shown as V-shapes, inhibitory synapses are shown as circles, and electrical synapses are shown as a black zigzag. Dashed circles depict afferent and efferent extracortical brain regions. Inhibitory synapses onto pyramidal neurons (PC) are displayed according to the target domains: axonal inhibition is provided by chandelier cells (ChC), somatic inhibition by basket cells (BC), and dendritic inhibition by double-bouquet cells (DBC), bipolar cells (BP), neurogliaform cells (NGC), Martinotti cells (MC) and Cajal-Retzius cells (CRC). PCs projecting to different brain areas reside in different layers: layer 5 is the main projection layer, with PCs projecting to subcortical regions such as the brainstem (Bs), spinal cord (SC), superior colliculus, basal ganglia (BG) and thalamus (TH). Layer 6 PCs project mainly to the thalamus, and PCs in superficial layers project to other cortical targets, such as neighbouring columns and the contralateral cortical hemisphere (CL). The representation of the different interneurons also changes across layers, with NGCs and DBCs mainly located in superficial layers, and MCs dominating the deep layers. BCs of different types constitute 50% of interneurons in layers 2–6. Interneurons display diverse interlaminar targeting preferences: DBCs target dendrites that are typically located deeper than the soma, and MCs mainly target dendrites in the more superficial layers. BCs, NGCs, BPs and CRCs innervate neurons mainly within the same layer, although BC axons also spread laterally and innervate neurons from neighbouring cortical columns. Additional abbreviations: WM, white matter (taken from [Grillner et al. 2005])

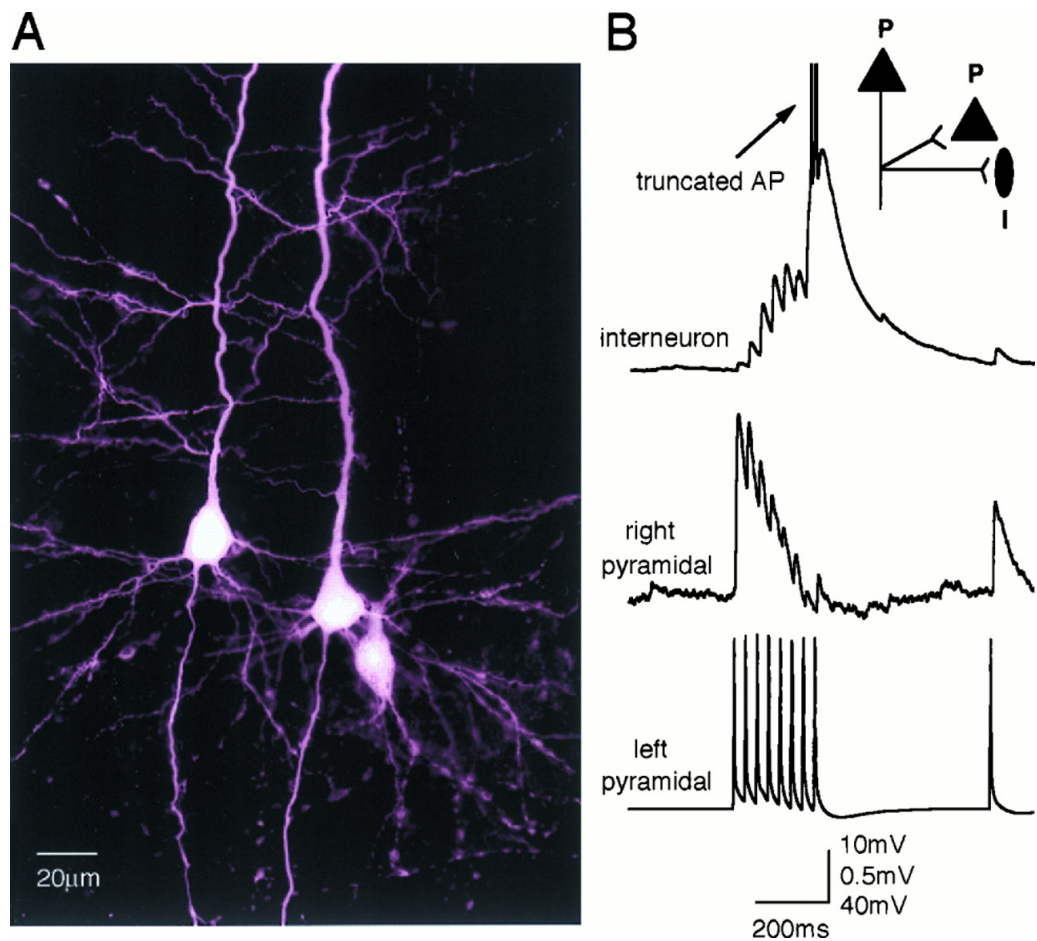


Figure 2.7: Differential synaptic facilitation and depression via the same axon innervating two different targets. **A**, a light microscopic pseudocolor image of three biocytin-filled neurons. The pyramidal neuron on the left innervated the pyramidal neuron on the right and the bipolar interneuron on the right. **B**, single trial responses (30 Hz) to same AP train (taken from [Markram et al. 1998])

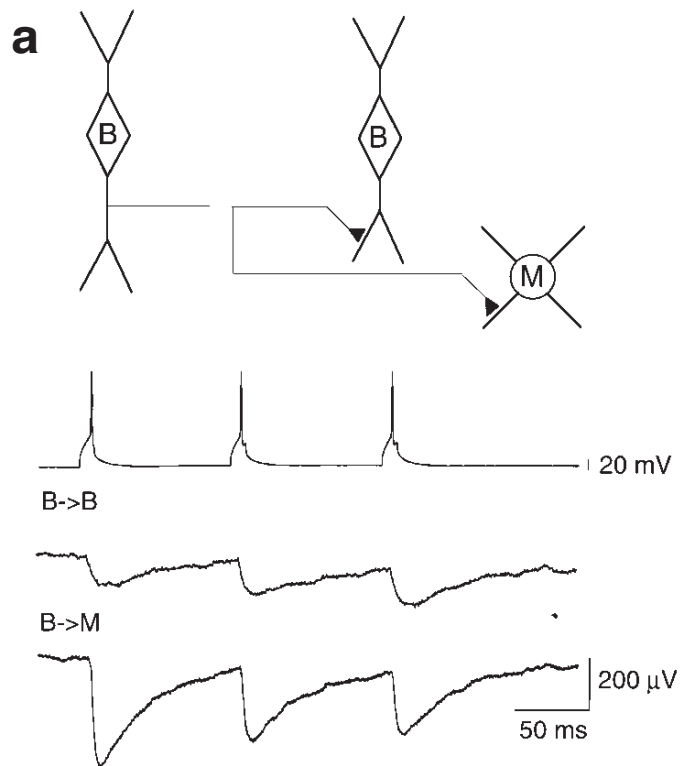


Figure 2.8: Simultaneous whole-cell recordings from a triplet (schematically shown on top) in which a pyramidal cell (P) innervated a bitufted (B) and a multipolar cell (M) (taken from [Reyes et al. 1998])

cells [Silberberg and Markram 2007]. Layer 2/3 PCs distribute their synapses more widely on basal, oblique, and apical dendrites, whereas synapses between TTL5 neurons are known to occur mostly on tertiary branches of basal dendrites. In general, PCs receive excitatory synapses onto spines, whereas inhibitory synapses are mainly formed on the dendritic shaft of the target neuron [Somogyi et al. 1998]. The location of preferential targeting dictates the efficacy of synaptic signalling. Due to electrotonic attenuation the impact of a strong synapse located on distal dendrites is not very efficacious in impacting the membrane potential at the soma. On the other hand, synapses located directly at the soma can exert a strong impact on the spike generating mechanism, acting as a gain control mechanism. Active dendritic conductances function to negate this tendency [Magee and Cook 2000, Häusser et al. 2000; 2001]. Target cell selectivity is another important principle of neocortical synaptic communication [Watts and Thomson 2005, Thomson and Lamy 2007]. A given presynaptic neuron is connected to another neuron with a particular likelihood. For example, TTL5 neurons connect to each other with a relatively low likelihood of about 10 – 15 % according to various studies [Markram et al. 1997a, Thomson et al. 2002, Song et al. 2005, Brown and Hestrin 2009b, Perin et al. 2011]. On the other hand, Layer 2/3 PCs connect to each other with a comparatively higher likelihood of about 15 – 30 % [Thomson et al. 2002, Holmgren et al. 2003]. In general, the likelihood of connectivity between PCs and INs and vice versa is rather high at about 20 – 50 % [Thomson et al. 2002, Holmgren et al. 2003, Silberberg and Markram 2007, Thomson and Lamy 2007]. Indeed, the likelihood of connectivity is heavily dependent on the proximity of neurons and previous studies have shown that the connection probability between pairs of TTL5 neurons falls drastically with an increase in the inter-somatic distance [Perin et al. 2011]. Although these data conclusively demonstrate a certain pattern of connection specificity between neocortical neurons, it has been suggested that the probability of two neighbouring neurons to connect is random [Braitenberg et al. 1998, Hellwig 2000, Kalisman et al. 2003; 2005]. Alan Peters put forth a rule, popularly known as "Peters' rule", which states that neurons interconnect in proportion to the contribution of their dendrites and axonal synaptic boutons to the neuropil [Peters and Feldman 1976]. This implies that connections are formed according to their geometrical constraints, forming synaptic connections due to accidental axo-dendritic overlap. This rule could explain non-random connectivity patterns like high reciprocity or specific connectivity motifs between TTL5 neurons [Markram et al. 1997a, Song et al. 2005, Perin et al. 2011]. Connection probabilities should, however, be interpreted with caution as connections could be potentially severed due to the brain slicing procedure used to estimate these ratios.

Several pioneering studies have unraveled the directed pathways of neocortical information flow. In general, there is good agreement within the research community that, at least in primary cortical areas, information flow from the thalamus to the cortex is rather stereotypical. Thalamic input arrives in layer 4, mainly on spiny stellate cells, which project to layer 2/3, which in turn innervates layer 5. In parallel, thalamus and layer 6 PCs form a direct loop of communication.

Layer 1 contains long-range axonal collaterals, conveyed information from “higher” associative cortical areas. Although these principal signalling pathways have been mainly investigated from anatomical tracing studies, multi-electrode recordings in the acute slice preparation have proven very useful, generating a treasure trove of information on synaptic communication [Lübke and Feldmeyer 2007a, Thomson and Lamy 2007, Lefort et al. 2009]. For instance, in the mouse somatosensory barrel cortex, separate pathways for lemniscal and paralemniscal projections including their cell- and even layer-specific targets could be revealed [Bureau et al. 2006]. It remains to be shown, however, if these findings hold true for other areas that do not display such a pronounced columnar organization.

2.4.2 Biophysical models of synaptic transmission

Synaptic connections give rise to dynamics and functional properties of a synaptic pathway. Dynamic interactions between neurons lead to emergent states in synaptic pathways. The PSP onset latency, rise time, amplitude and decay time constant as aggregates are important to determine the net impact of a presynaptic neuron on a population of postsynaptic neurons. It is therefore critical that the underlying biophysical models of synaptic transmission should mirror principles derived through *in vitro* experiments, bearing a direct influence on the emergent network dynamics of the model NCC.

Due to the overlap of several different time constants, arising from several molecular processes occurring mainly at the presynaptic terminal, a detailed biophysical description of activity dependent synaptic response to an arbitrary stimulation pattern is challenging. For neocortical synapses, especially for predominantly depressing synapses, a popular phenomenological model describing the dynamics of excitatory neocortical synapses has been developed [Tsodyks and Markram 1997]. The model captures several salient features of the observed frequency-dependence of synaptic transmission, using a relatively straight forward assumption that the “synaptic resources” (vesicles), can be in a recovered, active, or inactive state. Upon arrival of an action potential, a certain fraction (U , utilization of synaptic efficacy, analogous to neurotransmitter release probability) of the synaptic resources in the recovered state enters the active state, leading to the synaptic response. From the active state, synaptic resources rapidly enter the inactive state, from which they recover with a certain “recovery from depression” time constant D in order to enter again the recovered pool (see Figure 2.9). With this model, depressing synapses between TTL5 neurons have been accurately described. Furthermore, instead of using a fixed U , the model has been extended by using an activity-dependent utilization factor, incorporating a facilitation time constant F [Markram et al. 1998]. With this extension, facilitating synaptic responses can be described to a certain extent [Markram et al. 1998]. As a further modification, to include the trial-trial variability of the synaptic response based on the classical quantal model of synaptic transmission, the phenomenological model incorporates probabilistic neurotransmitter release [Fuhrmann et al. 2002].

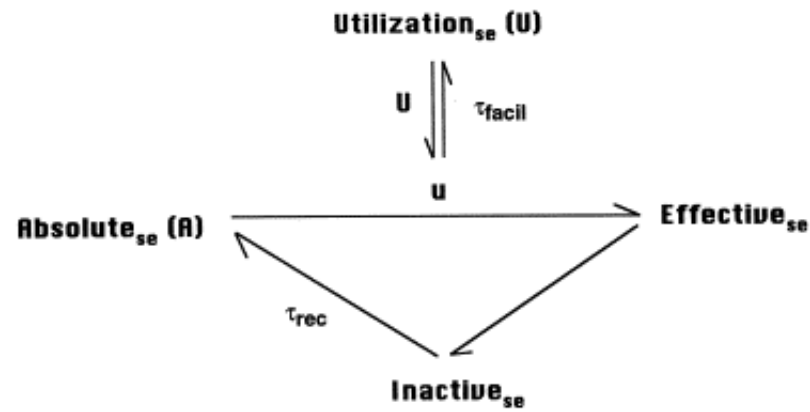


Figure 2.9: Phenomenological model of frequency dependent synaptic transmission. Each incoming AP utilizes U a fraction of the available/recovered synaptic efficacy R . When an AP arrives, U is increased by an amplitude of U_f and becomes a variable, U_1 . U_f is the running value of U . Depressing synapses can be simulated either by making U very large or by making τ_{facil} (facilitation time constant F) very small (taken from [Markram et al. 1998]).

2.5 SUMMARY

I have now elaborated on the principal players who set the field for studying *in silico* synaptic transmission - ion channel kinetics, diversity of neocortical neurons and principles of synaptic communication.

In the following part, I present the main results that were obtained by integrating the ion channel kinetics, single neuron models and rules of synaptic communication within the BBP simulation framework to study *in silico* synaptic transmission in the NCC model.

Part III

MAIN RESULTS

THE TTL₅ SYNAPTIC PATHWAY IN SILICO

*“Lulled in the countless chambers of the brain, our thoughts are linked by many
a hidden chain; awake but one, and in, what myriads rise!”*

Alexander Pope

MANUSCRIPT SUBMITTED TO THE JOURNAL OF PHYSIOLOGY

TITLE: Intrinsic Morphological Diversity of Thick-tufted Layer 5 Pyramidal Neurons Ensures Robust and Invariant Properties of *in silico* Synaptic Connections

AUTHORS: Srikanth Ramaswamy¹, Sean L. Hill¹, James G. King¹, Felix Schürmann¹, Yun Wang^{2,3} and Henry Markram¹

AUTHOR AFFILIATIONS: ¹ Brain Mind Institute, École Polytechnique Fédérale de Lausanne (EPFL), CH – 1015, Lausanne, Switzerland

² Caritas St. Elizabeth's Medical Center, Tufts University, Boston, MA 02135, USA

³ School of Optometry & Ophthalmology, Wenzhou Medical College, Wenzhou, Zhejiang, 325027, P.R.China

CORRESPONDING AUTHOR: Henry Markram, PhD,

Brain Mind Institute,

École Polytechnique Fédérale de Lausanne (EPFL),

CH – 1015, Lausanne, Switzerland

E-mail: henry.markram@epfl.ch

Ph. +41 21 693 9569

Fax. +41 21 693 5350

NUMBER OF FIGURES: 5, NUMBER OF TABLES: 2

KEYWORDS: Thick-tufted layer 5 pyramidal neuron, model, *in silico*, synaptic innervation pattern, synaptic transmission, synaptic properties, invariance, robustness

Abstract

The morphology of neocortical pyramidal neurons is not only highly characteristic but also displays an intrinsic diversity that renders each neuron morphologically unique. We investigated the significance of this intrinsic morphological diversity in networks composed of thick-tufted layer 5 (TTL5) pyramidal neurons, by comparing the *in vitro* and *in silico* properties of TTL5 synaptic connections. The synaptic locations of *in silico* connections were determined by placing 3D reconstructed TTL5 neurons randomly in a volume equivalent to that of layer 5 in the juvenile rat somatosensory cortex and using a “collision-detection” algorithm to identify the incidental loci of axo-dendritic overlap. The activation time of the modeled synapses and their biophysical properties were characterized based on experimental measurements. We found that the anatomical loci of synapses and the physiological properties of the somatically recorded EPSPs closely matched those recorded experimentally without the need for any fine-tuning. Furthermore, perturbations to both the physiological or anatomical parameters of the model did not alter the average physiological properties of the population of modeled synaptic connections. This microcircuit-level robust behavior was due to the intrinsic diversity of the morphology of pyramidal neurons in the microcircuit. We conclude that synaptic transmission in a network of TTL5 neurons is highly invariant across microcircuits suggesting that intrinsic diversity is a mechanism to ensure the same average synaptic properties in different animals of the same species. Finally, we show that the average physiological properties of the TTL5 microcircuit are surprisingly robust to anatomical and physiological perturbations also partly due to the intrinsic diversity of pyramidal neuron morphology.

Abbreviations AP, Action Potential; AMPAR, AMPA Receptor; CV, Coefficient of Variation; dt, simulation time step; K-S test, Kolmogorov-Smirnov test; NMDAR, NMDA Receptor; STDP, spike-timing dependent plasticity TTL5, Thick-tufted Layer 5.

Introduction

Thick-tufted layer 5 (TTL5) pyramidal neurons are the primary source of output from the neocortex to subcortical areas (Wang & McCormick, 1993; Kasper *et al.* 1994; for reviews

see DeFelipe & Fariñas, 1992; Spruston, 2008). The TTL5 neuron has a stereotypical axo-dendritic morphology (Peters, 1987; Larkman, 1991; for reviews see Markram, 1997; Spruston, 2008). The dendritic arbor characteristically comprises an apical trunk ascending from the apex of a pyramid-like soma, with oblique dendrites emanating at various angles from the trunk and terminal tufts in layer 1 and thin basal dendrites emanating from the base of the soma and radiating outward in all directions (for review see Spruston, 2008). The axon arborizes profusely within a distance of 300-500 μm to form local connections, giving rise to horizontal intra-cortical projections that connect neocortical columns and other brain regions, and also projects to subcortical areas (Gilbert & Wiesel, 1979; Thomson & Deuchars, 1994). Despite these highly stereotypical morphological features, each neuron is morphologically unique. Since a vast body of data has shown the importance of morphology for dendritic and synaptic integration, it would seem obvious that such intrinsic morphological diversity also generates diversity in the physiological properties of synaptic connections, and therefore, induce variability in the electrical behavior of neural microcircuits across different animals. One way to test the importance of morphological diversity for synaptic transmission is to construct a biologically accurate model of the TTL5 network with different instances of 3D reconstructed morphologies.

Synaptic transmission between TTL5 neurons is fundamental for local information processing within the cortical column as well as for information transfer to other cortical areas, serving as a paradigm for a spectrum of functional studies (Silva *et al.* 1991; Thomson *et al.* 1993; Yuste *et al.* 1994; Stuart & Sakmann, 1995; Markram *et al.* 1997; Larkum *et al.* 1999). The local dendritic and axonal arborization of TTL5 neurons is the most extensive and thus delineates the maximal dimensions of the local neocortical microcircuit. The expanse of the TTL5 axonal and dendritic arbors correspond roughly to the dimensions of functional neocortical columns that have been identified in cats and other higher species (Peters, 1987; Mountcastle, 1997). While rodents do not display such distinct functional compartmentalization of the neocortical sheet (with an exception of the barrel cortex) the same local microcircuits can be defined based on all the neurons that can be connected by the local axonal arborization of TTL5 neurons (Markram, 2008). Indeed, all neurons within this range are likely to be highly interconnected because of their overlapping axonal and

dendritic arbors (Le Bé & Markram, 2006). Such a cortical column can contain between 600-1300 TTL5 neurons, each of which is synaptically connected to around 40-60 neighboring TTL5 neurons within inter-somatic distances of about 100 μm (Markram *et al.* 1997; Song *et al.* 2005; Meyer *et al.* 2010). In the local neocortical microcircuit, the probability of a synaptic connection between two TTL5 neurons within an inter-somatic distance of 100 μm is approximately 10-15 % (Markram *et al.* 1997; Thomson *et al.* 2002; Song *et al.* 2005; Perin *et al.* 2011). Each connection involves an average of about 5.5 synaptic contacts (Markram *et al.* 1997; Kalisman *et al.* 2005). In juvenile rodents, the dynamics of these connections is characterized by a high initial probability of neurotransmitter release and short-term depression (Thomson *et al.* 1993; Tsodyks & Markram, 1997).

In the present study, we constructed an *in silico* model of synaptic connections between pairs of TTL5 neurons. The model used a set of experimentally reconstructed neuronal morphologies ($n = 33$) and was instantiated using *in vitro* data on axonal conduction delays, stochastic synaptic transmission, and quantal synaptic conductances. We also used a statistical cloning method to generate morphological variants of TTL5 neurons, based on their morphometric statistics. Importantly, we used an independently constructed biophysical model of the TTL5 neuron developed by Hay *et al.* (2011), which was not fine-tuned to obtain results of this study. A collision-detection algorithm between axons and dendrites, executed on a supercomputer, determined the locations of putative synapses in the model (Kozloski *et al.* 2008). The site of a potential synaptic contact was identified when an axon from a reconstructed neuron came within a given distance of a dendrite or soma of another neuron (see Methods). We then compared the *in silico* synaptic response properties recorded at the soma of the modeled neurons against *in vitro* measurements reported in Markram *et al.* (1997) as the biological benchmark (see Methods). To assess the impact of the anatomical and physiological factors determining the efficacy of model synaptic connections, we investigated the sensitivity of synaptic response properties to perturbations in a range of parameters, including axonal conduction delays, location and conductance of synaptic contacts, and the morphological diversity of TTL5 neurons.

Methods

Definition of terms

Synaptic connection: the set of synaptic contacts between the axon collaterals of a pre-synaptic neuron and the dendrites of a post-synaptic neuron.

Branch order: the number of bifurcations between an axonal or dendritic section and the soma. Branch order is denoted by $^{\circ}$. Thus, 1° refers to the first dendritic branch originating from the soma or the main apical dendrite.

Path distance: the distance between a given section and the soma, measured along the axon or the dendrite.

Synaptic innervation pattern: a histogram of the locations of synapses measured by branch order or path distance.

Synaptic response properties: properties describing the kinetics of TTL5 synaptic transmission, usually including the latency of EPSP onset at the soma, 20-80% rise time, amplitude and the decay time constant.

3D anatomical reconstruction of TTL5 morphologies

Biocytin stained morphologies ($n = 33$) were obtained from 300 μm thick sagittal brain slices from the somatosensory cortex of juvenile Wistar rats (aged 14-16 days). The methods used were compliant with Swiss national and institutional guidelines. Stained morphologies were reconstructed using the NeuroLucida system (MicroBrightField Inc., Colchester, VT, USA) and a brightfield light microscope (Olympus GmbH, Düsseldorf, Germany). The biocytin staining procedure led to $\sim 25\%$ shrinkage in terms of slice thickness and $\sim 10\%$ anisotropic shrinkage in terms of height and width. The reconstructed morphologies were corrected for shrinkage of thickness.

Morphology repair

The somata of TTL5 neurons recorded *in vitro* tend to be chosen $\sim 50\text{-}100\ \mu\text{m}$ beneath the surface of the slice. As a result, the slicing procedure severs about 20-40% of their axonal and dendritic arbors. To partially recover their anatomy, we re-grew cut portions using an

algorithm developed by Anwar *et al.* (2009). After compensating for measurement inaccuracies and tissue shrinkage, the algorithm repairs dendrites and axons separately, while maintaining the overall statistics of the neuron's morphology (Anwar *et al.* 2009).

The dendritic and axonal arbors were artificially cut and the algorithm attempted to regrow the cut arbor. We then compared the morphometric statistics of the regrown arbor to the intact portion of the *in vivo* reconstructed neuron through Sholl analysis and found a close statistical fit, which validated our repair process.

Constructing the TTL5 microcircuit

We loaded a 3D hexagonal volume ($500\ \mu\text{m} \times 500\ \mu\text{m} \times 370\ \mu\text{m}$) with randomly positioned model neurons derived from a diverse set of reconstructed TTL5 morphologies ($n = 33$). A hexagon allows close packing of columns and these dimensions were chosen such that the diameter of the hexagon accounted for the full extent of the dendritic arborization of TTL5 neurons. The thickness of the circuit was roughly equivalent to the thickness of layer 5 in the somatosensory cortex of juvenile rats and the density of neurons in the model circuit was in the ballpark of several previous estimates (about 30,000 - 50,000 TTL5 neurons/ mm^3 ; Peters, 1987; Garcia *et al.* 2006; Meyer *et al.* 2010). We repeated this procedure 10 times, thus creating 10 potential TTL5 microcircuits. In each case, synaptic contacts were identified using a collision-detection algorithm implemented on the BlueGene/P supercomputer. The algorithm detected all appositions between axonal arbors of pre-synaptic neurons and the dendrites of neighboring neurons. To account for bouton swelling and spine extension, we tried several different distances of axo-dendritic apposition to define a potential synaptic and chose a distance of $3\ \mu\text{m}$ (Peters' rule; Peters, 1979; Stepanyants *et al.* 2002; Shepherd *et al.* 2005; for review see Stepanyants & Chklovskii, 2005). The set of contacts found in this way represented the locations where it was physically possible to form a synapse without major structural changes in the axon or dendrite (Stepanyants *et al.* 2002). The set of contacts included connections between virtually all pairs of neurons with intersomatic distances within $\sim 100\ \mu\text{m}$ (*tabula rasa*-like connectivity; Kalisman *et al.* 2005). The potential synaptic contacts in each connection were then converted into functional synapses through an algorithm, constrained with the *in vitro* connection probability of 10%

measured for pairs of TTL5 neurons within inter-somatic distances of 50-100 μ m. The 10 microcircuits, constructed in this way, formed the basis for the *in silico* synaptic transmission experiments reported below.

Additionally, we also constructed five sets of TTL5 microcircuits, with each set containing 10 instances of circuits composed of a different number of unique morphologies. The additional unique morphologies were generated by jittering the section lengths of each neuron and branching angles by 25% of their original values. We verified that these new “cloned” neurons maintained their original Sholl and branching angle statistics. Thus, these neurons were statistically similar to the population of the 33 reconstructed TTL5 neurons.

The first set in the series of microcircuits with unique morphologies consisted of a single morphology of a reconstructed neuron (10 different reconstructed neurons were used to get 10 microcircuit instances). The second set again consisted of 10 circuits, but was composed of 3 unique variant morphologies derived from actual reconstructed neurons. The circuits in the third set were each composed of 10 unique variant morphologies. The fourth set was composed of 100 unique morphologies. In the fifth and final set of circuits, all model TTL5 neurons in each circuit were unique variant morphologies in terms of their precise branching angles and segment lengths, but maintained the statistics of the original reconstructed cell type (based on 33 reconstructed TTL5 morphological exemplars). In total, we constructed a total of 50 microcircuits (10 circuits each) for: a single unique morphology, 3 unique morphologies, 10 unique morphologies, 100 unique morphologies, and where all morphologies were unique.

Stochastic synapse model

At each putative synaptic location identified by the collision-detection algorithm, we implemented a *stochastic* model of synaptic transmission. This model guaranteed that post-synaptic responses would be different in every trial (Fuhrmann *et al.* 2002). The model was an extension of the phenomenological Tsodyks-Markram dynamic synapse model (Tsodyks & Markram, 1997), modified to incorporate NMDA receptor (NMDAR) kinetics as described by Jahr & Stevens (1990). The basic underlying assumptions were derived from the classical quantal model of synaptic transmission, in which a synaptic connection is

assumed to be composed of N independent release sites (Del Castillo & Katz, 1954; Korn & Faber, 1991), each of which has a probability of release, p , and contributes a quanta q to the post-synaptic response. Release from any particular site is independent of release from all other sites (Fuhrmann *et al.* 2002). Though we only used the model for unitary pre-synaptic APs, it also has the ability to represent both short-term facilitation and depression.

Parameters for model synapses were derived from experimental estimates (assuming normal distribution; mean \pm S.D.). For AMPA receptor (AMPA) kinetics: synaptic conductance g_{AMPA} (0.3 ± 0.2 nS; Yoshimura *et al.* 1999; Sarid *et al.* 2007; Rinaldi *et al.* 2008); rise time [$\tau_{riseAMPA}$] and decay time constants [$\tau_{decayAMPA}$] were 0.2 ms and 1.7 ± 0.18 ms, respectively; Häusser & Roth, 1997), utilization of synaptic efficacy U , analogous to the probability of neurotransmitter release (0.5 ± 0.02 ; Tsodyks & Markram 1997); time constant for recovery from depression D (671 ± 17 ms; Tsodyks & Markram, 1997) and time constant for recovery from facilitation F (17 ± 5 ms). For NMDAR kinetics: synaptic conductance g_{NMDAR} ($0.71 * g_{AMPA}$; Myme *et al.* 2003), $\tau_{riseNMDA}$ and $\tau_{decayNMDA}$, 0.29 ms and 43 ms respectively; Sarid *et al.* 2007). $[Mg^{2+}]_o$ was set to 1mM (Jahr & Stevens, 1990). The axonal conduction delay for each stochastic model synapse was computed using the axonal path distance to the soma. AP conduction velocity was set at 300 μ m/ms, based on experimental estimates by Stuart *et al.* (1997).

Biophysical model of the TTL5 neuron

Neuronal biophysics was simulated based on the approach developed by Druckmann *et al.* (2007) and Hay *et al.* (2011). Briefly, a model neuron was created with a 3D reconstructed morphology from *in vitro* experiments. The model neuron contained 653 compartments with an average length of about 19 μ m per compartment. We then used a multi-objective evolutionary search algorithm to obtain an optimized representation of experimentally measured somatic responses to prolonged injections of supra-threshold step current. The free parameters in the model were the maximal conductances of somatic and dendritic ion channels, as represented in the Hodgkin-Huxley formalism. The somatic response of the model and the back propagation of APs into the apical dendritic arbor matched the *in vitro* observations (Hay *et al.* 2011).

***In silico* stimulation and recording**

In silico experiments were performed in the NEURON (version 7.2) simulation environment (<http://www.neuron.yale.edu>; Hines & Carnevale, 1997) with a simulation time step (dt) of 0.025 ms. Simulations were run on a 128 processor rack of a BlueGene/P supercomputer accessed through the CADMOS consortium or on 32 processors of a SGI Prism parallel computer. All *in silico* experiments used the circuit, neuron and synapse models (see Stochastic Synapse Model), without fine-tuning.

To select neuron pairs for *in silico* experiments, we applied the same procedure as in previous *in vitro* studies (Markram *et al.* 1997). From each of 10 reconstructed microcircuits we randomly selected 200 pairs of TTL5 neurons within inter-somatic distances of 50-100 μm , thus creating a population of 2000 TTL5 neuron pairs. In the event an identical pair was sampled twice, the pair was discarded and a new pair was chosen to avoid a sampling bias in the statistical analysis of *in silico* synaptic properties. Furthermore, we performed additional analyses on a subset of modeled pairs of TTL5 neurons with synaptic contacts in the range of 4-8 to ensure strict comparability with the previously reported *in vitro* data.

To evoke unitary pre-synaptic APs in model neurons, we simulated square current pulses of 5 nA for a duration of 10 ms at the soma and measured the post-synaptic response in the target model neurons.

Data analysis

Data analysis was carried out in MATLAB (version 7.7). As a biological benchmark, we used *in vitro* measurements of latency of EPSP onset, rise time, amplitude, decay time constant, failures and the coefficient of variation (CV) of EPSP amplitude (n = 138; Markram *et al.* 1997). Data from model connections (n = 2000) were compared against this benchmark. Values for simulated connections were determined by averaging the data from 100 independent trials. Somatic EPSP amplitude was measured as the difference between baseline and peak voltage (see Fig. 3B, bottom trace, upward and downward arrows). Latency of EPSP onset was measured as time taken by an AP to fall from peak amplitude to 5% of peak EPSP amplitude (see Fig. 3B, bottom trace, dashed lines). Rise time was

measured as the time taken to rise from 20 to 80% peak EPSP amplitude (see Fig. 3B, right, bottom trace). The decay time constant was measured by fitting a single exponential (see Fig. 3C, bottom trace in black, marked τ_{EPSP} above downward vertical arrow) to the average EPSP in a region where the EPSP had decayed to about 80% of peak amplitude.

Reliability of synaptic transmission was evaluated using the same set of neuron pairs used to measure the average synaptic response properties by building a distribution of failures per connection. In each modeled connection, trials in which a pre-synaptic AP failed to evoke an EPSP were labeled as failures. The CV of EPSP amplitude, computed as S.D./mean amplitude, measured the variability of EPSPs. Differences between *in vitro* and *in silico* data were tested using Fisher's exact two sample test, with $\alpha = 0.01$.

Results

A recent study has shown that anatomical models of neocortical microcircuits derived from the incidental geometrical overlap of diverse 3D reconstructed morphologies yield cell-type specific patterns of synaptic innervation, which largely match the *in vitro* data and are invariant across different model microcircuits (Hill *et al.* 2011, submitted). It thus appears that the incidental overlap of axo-dendritic arbors is sufficient to pattern most synapses between neurons in a manner similar to that found in biological experiments and that morphological diversity renders such patterns invariant in the local microcircuit. In this study, we investigated whether the physiology of synaptic transmission also emerges naturally from the axo-dendritic overlap, and whether the morphological diversity also imparts invariance and robustness to the average physiological properties in the local microcircuit.

Anatomy of *in silico* connections

We examined the anatomy of synaptic innervation in single model connections, randomly sampled from many possible connections in a reconstructed microcircuit (see Methods; Fig. 1A). In this example, the pre-synaptic neuron (in red) established 8 contacts (black dots) on the post-synaptic neuron (in blue). Of these 8 synaptic contacts, 2 were located on terminal tufts and 6 on the basal dendrites. The post-synaptic dendrogram (Fig. 1B, right) revealed

that about 65% of the underlying synapses occurred on proximal branches of basal dendrites. This finding was consistent with *in vitro* observations (Markram *et al.* 1997). The patterns of synaptic innervation on the axon and dendrites also matched the *in vitro* data (data not shown; Hill *et al.* 2011, submitted). The average number of synaptic contacts per connection was $\sim 6 \pm 5$ (mean \pm S.D; $n = 2000$), as compared to 5.5 ± 1.1 in the *in vitro* data. Such a high variability for potential synaptic contacts arising through axo-dendritic touches in reconstructed neurons has been previously reported (Braitenberg & Schüz, 1998; Fares & Stepanyants, 2009). *In vitro* studies have shown that synaptic contacts between TTL5 neurons are rarely less than 4, and mostly lie within the range of 4 and 8 (Markram *et al.* 1997; Kalisman *et al.* 2005; Le Bé & Markram, 2006), suggesting that a form of microcircuit plasticity selectively maintains the number of synaptic contacts per connection within the observed range. Our *in silico* model currently lacks biophysical mechanisms of microcircuit plasticity, which explains the high variability of the mean number of synaptic contacts.

In our complete reconstructed *in silico* microcircuit (across the full dimensions), the probability of a connection between any two TTL5 neurons was of the order of 10-15%. Model TTL5 neurons received about 200 - 300 afferent synapses from about 40 - 60 neighboring TTL5 neurons, consistent with previous estimates (average of 250 afferent synapses from 50 TTL5 neurons; Markram *et al.* 1997; Song *et al.* 2005; see Fig. 2 where afferent synapses from other TTL5 neurons are shown as yellow dots). In the vicinity of a minicolumn (30-50 μm), this structural connectivity is closer to a *tabula rasa* like connectivity as previously reported (Kalisman *et al.* 2005).

In the *in silico* microcircuit, the proportion of synapses on distal apical dendrites was slightly lower than in *in vitro* observations (there was an overall match of about 90% compared against the *in vitro* data without taking the innervation of distal apical tufts into consideration; Hill *et al.* 2011, submitted). The discrepancy in the distal tuft dendrites might be due to poorer reconstructions of more distal arbors, while the discrepancy in the apical dendrites could be due to the possibility that some pyramidal neurons axons and dendrites grow upward together in tracts laid down by radial glial cells, where dendrites can be

brought into closer apposition with axons than normally possible with independently growing arbors (Yu *et al.* 2009).

Physiology of *in silico* connections

Model TTL5 neurons exhibited mean resting membrane potentials of -71 ± 2 mV, within the range of experimental observations (mean \pm S.D.; -69 ± 2 mV after correction for a liquid junction potential (LJP) offset of ~ 9 mV; Markram *et al.* 1997). The mean input resistance and membrane time constants were about 120 M Ω and 20 ms respectively, again within the range of experimental measurements. Quantal EPSC and EPSP amplitudes were ~ 20 pA and ~ 0.16 mV respectively, consistent with previous *in vitro* observations (Yoshimura *et al.* 1999; Simkus & Stricker, 2002; Myme *et al.* 2003; Silver *et al.* 2003).

For a valid comparison with *in vitro* results, we sampled 200 model neuron pairs from one of the microcircuits, generated by our model, choosing only pairs with intersomatic distances in the range ~ 50 -100 μm as sampled in experiments. We then applied *in silico* stimulation protocols that replicated those applied in the previous *in vitro* study (Markram *et al.* 1997). The mean EPSP onset latency in model connections was 1.8 ± 0.6 ms ($n = 200$; Fig. 1C), the mean 20-80 % rise time was 2 ± 0.95 ms (Fig. 1D). Simulated EPSPs had mean amplitudes of 1.3 ± 0.9 mV (Fig. 1E) and the mean decay time constant was 32 ± 6.05 ms (Fig. 1E). Overall, there were no significant differences between the *in silico* and the *in vitro* data ($P > 0.01$, $\alpha = 0.01$, two sample K-S test) without any fine-tuning of parameters of the model.

We then measured the synaptic transmission properties for 2000 pairs of neurons within inter-somatic distances of 100 μm extracted from all 10 microcircuits instances (200 pairs \times 10 microcircuits; see Methods), each of which contained TTL5 neurons in different locations with different morphologies and orientations (see Methods). Despite these differences, synaptic response properties were similar to the *in vitro* data for all circuits. In each case the means and standard deviation of the *in silico* data fell within the same ranges as the *in vitro* data. The mean latency of EPSP onset across all 2000 *in silico* pairs was 1.75 ± 0.6 ms, compared against an *in vitro* value of 1.7 ± 0.9 ms (Fig. 3D; Fisher's exact two sample test, $P > 0.01$, $\alpha = 0.01$). The mean rise time was 2.1 ± 0.8 ms, compared to an *in*

in vitro value of 2.9 ± 2.3 ms (Fig. 3E; Fisher's exact two sample test, $P > 0.01$, $\alpha = 0.01$). The mean EPSP amplitude was 1.3 ± 1 mV as against the *in vitro* value of 1.3 ± 1.1 mV (Fig. 3F; Fisher's exact two sample test, $P > 0.01$, $\alpha = 0.01$). The mean decay time constant was 31.6 ± 5.8 ms as against an *in vitro* value of 40 ± 18 ms (Fig. 3G; Fisher's exact two sample test, $P > 0.01$, $\alpha = 0.01$). Pairwise comparison between different microcircuits showed a high level of invariance (data not shown; $P > 0.01$, $\alpha = 0.01$, two sample K-S test for all pairs of circuits). This suggests that the overall structure of neuronal microcircuits and the behaviour of their synaptic connections are independent of the precise positioning, orientation and morphology of individual neurons.

In silico connections transmitted reliably with a mean failure rate of 13 ± 17.5 % ($n = 2000$). The distribution of transmission failures closely matched the *in vitro* data ($P > 0.01$, $\alpha = 0.01$, Fisher's exact two sample test; Fig. 4A and Table 1). The CV for simulated EPSPs (mean, 0.54 ± 0.25 ; $n = 2000$) was very similar to the *in vitro* data ($P > 0.01$, $\alpha = 0.01$, Fisher's exact two sample test; Fig. 4B and Table 1). The rate of transmission failures and the CV of simulated EPSPs decreased with an increase in EPSP amplitude and mirrored the *in vitro* data (Fig. 4C and D, respectively; data shown for an instance of 200 neuron pairs from a single microcircuit).

With an increase in the inter-somatic distance of sampled TTL5 pairs, our *in silico* model predicted that the mean number of synaptic contacts per connection is significantly lower than the *in vitro* mean of 5.5 contacts. The mean number of contacts decreased significantly at inter-somatic distances further from $100\mu\text{m}$ (see Fig. S2; two sampled K-S test, $\alpha = 0.05$, $** p < 0.05$). The mean post-synaptic responses *in silico* were smaller for TTL5 pairs at inter-somatic distances greater than $100\mu\text{m}$ (data not shown). Previous studies have shown that the connection probability between TTL5 neurons falls as a function of inter-somatic distance (Perin *et al.* 2011). With a decrease in the connection probability and the corresponding decrease in the mean number of synaptic contacts between pairs of TTL5 neurons, the *in silico* model predicts a decrease in the size of the mean post-synaptic response. However, the caveat is that we lack sufficient *in vitro* data for the post-synaptic responses of TTL5 neurons at different inter-somatic distances in order to validate the *in*

silico prediction.

As an additional analysis, to ensure strict comparability with the *in vitro* data, we chose the subset of modeled TTL5 pairs comprising between 4 and 8 synaptic contacts (data not shown; see methods), the latency of EPSP onset (1.8 ± 0.6 ms), 20-80% rise time (2 ± 0.8 ms), amplitude (1.2 ± 0.9 mV) and decay time (30 ± 8.5 ms) did not differ significantly from the *in vitro* data (data not shown; $P > 0.01$, $\alpha = 0.01$, two sample K-S test). However, the resulting latencies were marginally slower than reported *in vitro*. This discrepancy could be explained if the mean path distance between synapses and the soma were higher in neurons with at least 4 synaptic contacts than in those with less than 4 contacts or if the *in vitro* observations missed connections mediated by fewer than 4 contacts.

Morphological diversity TTL5 neurons renders invariant *in silico* synaptic transmission

In order to further assess how intrinsic morphological diversity renders the average physiological properties in a local microcircuit invariant, we studied the emergence of *in silico* synaptic response properties by constructing microcircuits in which the intrinsic morphological diversity was manipulated (see Methods). We observed a systematic reduction in the overall variability of average synaptic response property distributions in the local neocortical microcircuit by increasing in the intrinsic morphological diversity of the modelled TTL5 neurons (see Fig. 5). This result complements recent work, where the variability of the TTL5 structural synaptic innervation patterns has been shown to decrease with an increase in the diversity of the morphological composition of the local neocortical microcircuit (Hill *et al.* 2010, submitted). Strikingly, even a low number of 10 unique morphologies resulted in invariance of *in silico* synaptic transmission. Intrinsic morphological diversity therefore ensures that the average synaptic responses are invariant in the local neocortical microcircuit as a whole (the height of the error bar in every bin for the average synaptic response property distributions decreased with an increase in morphological diversity; see Fig. 5). This invariance of the average synaptic properties suggests that, at the level of the local neocortical microcircuit, the spatial positioning of synaptic appositions and consequently their physiological properties remain highly

invariant across animals belonging to the same species.

Robustness of *in silico* synaptic transmission

To investigate the influence of anatomical and physiological factors on average synaptic response properties in the local microcircuit, we conducted *in silico* experiments in which we systematically perturbed a range of different parameters, including axonal conduction delays, post-synaptic locations and conductances. In each experiment, we compared the behaviour of a set of 200 TTL5 pairs (from a single microcircuit instance) with and without the perturbation. The same set of pairs was used throughout for all perturbations.

As the first step, we assessed the impact of replacing the original axonal conduction delays and post-synaptic locations derived following the touch detection with values randomly selected from the *in vitro* data. For a given connection, we thus perturbed the axonal delay of each model synapse to its corresponding dendritic location. Surprisingly, this perturbation produced no significant change in distributions of synaptic properties ($P > 0.01$, $\alpha = 0.01$, two sample K-S test; Table 2). This suggests that the overall synaptic response properties of a microcircuit are independent of precise synaptic locations and axonal delays, even if axonal delays remain crucial for temporal summation and for other phenomena such as spike timing dependent plasticity.

To test the effects of the axonal conduction delay on its own, we set the delay for model synapses to a fixed value of 0.05 ms, and measured the effects on latency, 20-80% rise time, EPSP amplitude and decay time. As expected, this perturbation produced latency distributions that differed significantly from those observed in the control population ($P < 0.01$, $\alpha = 0.01$, two sample K-S test; Table 2). However, distributions of 20-80% rise time, EPSP amplitude and decay time constant were virtually unaffected ($P > 0.01$, $\alpha = 0.01$, two sample K-S test; Table 2). This suggests that at least at the level of the local neocortical microcircuit, precise axonal delays do not influence the rise time, EPSP amplitude and decay time constants.

Synaptic conductances in cortical neurons are believed to play a vital role in information processing learning and memory. To study the importance of this parameter, we set all

conductances in the model to a fixed value of 0.3 nS (the mean of the distribution of experimentally estimated synaptic conductance assigned to every synaptic contact in the *in silico* microcircuit; see Methods). Remarkably, the perturbation produced no significant change in the average synaptic response property distributions ($P > 0.01$, $\alpha = 0.01$, two sample K-S test; Table 2). This suggests that the overall distribution of synaptic properties across multiple TTL5 neurons is independent of the distribution of synaptic conductances at the level of the local neocortical microcircuit, even though synaptic conductances may be still be important for other phenomena such as local dendritic integration, synaptic plasticity, learning and memory.

To study the role of post-synaptic locations on their own, we replaced the locations in the original model (computed from neuron morphologies) with a uniform coverage of the entire dendritic arbor, measured first in terms of branch order and then in terms of path distance. Interestingly, these perturbations produced no significant change in the distributions of average EPSP amplitude and decay time constants ($P > 0.01$, $\alpha = 0.01$, two sample K-S test; Table 2). However, in the local microcircuit, these changes did lead to significant alterations in the distribution of average latency to EPSP onset and 20-80% rise time ($P < 0.01$, $\alpha = 0.01$; Table 2).

The post-synaptic locations in the original model were further manipulated by clustering them on dendritic segments with the same branch order. Interestingly, this perturbation also produced no significant change in the distributions of average latency of EPSP onset, amplitude and decay time constants ($P > 0.01$, $\alpha = 0.01$; Table 2). However, the rise times of synaptic responses were faster and the average rise time distribution was significantly different from the original *in silico* data in the local microcircuit ($P < 0.01$, $\alpha = 0.01$; Table 2).

An alternative clustering scheme, in which all synapses were clustered on 1° basal dendrites produced no significant change in the distribution of average EPSP decay time constants in the *in silico* microcircuit. However, the distributions of average latency of EPSP onset, rise time and amplitude were significantly altered ($P < 0.01$, $\alpha = 0.01$, two sample K-S test; Table 2). More specifically, the EPSP onset latency and rise times were both shorter, due to

the proximity of synapses to the soma. Amplitudes were higher due to lower dendritic filtering.

In two final *in silico* experiments, we replaced the diverse post-synaptic morphologies used to generate our neuron pairs with a single reconstructed morphology. Pre-synaptic morphologies and synaptic innervation patterns were left unchanged. In the first experiment, we used synaptic innervation patterns measured in terms of branch order. In the second we used patterns measured in terms of path distance. Strikingly, neither experiment showed any significant change in the distributions of average latency and EPSP amplitude, though we did observe significant alterations in rise and decay times (the latter only when with synaptic innervation patterns based on path distances) ($P < 0.01$, $\alpha = 0.01$; Table 2). These results suggest that the robustness of *in silico* synaptic response properties is partly due to morphological diversity in the local neocortical microcircuit.

Discussion

We have shown, in what we believe is the first study of its kind, that the incidental overlap of axo-dendritic arbors leads to biologically comparable properties of *in silico* synaptic transmission in the local neocortical microcircuit. A major prediction is that the average physiological properties are independent of the exact position, orientation and morphology of individual model neurons. A key finding that emerged from this result is that intrinsic morphological diversity renders the average physiological properties invariant across microcircuits and robust to perturbations.

Previous endeavors to create cortical microcircuits *in silico* have ranged from recurrent arrangement of “ball and stick” like neurons (Traub *et al.* 1992; Bush & Sejnowski, 1996) to models of feedforward synaptic connections in the rat barrel cortex, where the numbers and dendritic locations of synaptic contacts were drawn from the statistics measured *in vitro* (Sarid *et al.* 2007). In contrast, the connectivity data in our study is purely based on the geometrical overlap between axonal and dendritic arbors of reconstructed TTL5 morphologies. An additional advantage of constructing model circuits in the manner we described above is that realistic axonal delays can be matched to each synapse, thus

corresponding to the dendritic location of that synapse. Sarid *et al.* (2007) also used a lognormal distribution for the synaptic conductances in their *in silico* model and the distribution of EPSP amplitudes obtained in this way closely matched *in vitro* measurements. However, our work shows that the distribution of the amplitude of EPSPs can match the *in vitro* observations even when the distribution of conductances is collapsed to a constant value (0.3 nS per synaptic contact; Table 2) and that the morphological diversity of TTL5 neurons is a key factor in the robustness of the average synaptic response properties.

Previous studies have shown the emergence and disappearance of connections between TTL5 neuron *in vitro* over a period of several hours (Le Bé & Markram, 2006). It was observed that in the connections that emerged, the weaker ones (with 1-3 synaptic contacts) were eliminated, while the stronger connections (with 4-8 synaptic contacts) were retained in a Darwinian fashion. This mechanism of synaptic transmission through multiple synaptic contacts further reinforces the observation of a Gaussian-like distribution of synaptic contacts in the range of 4 and 8 between pairs of TTL5 neurons (Markram *et al.* 1997; Kalisman *et al.* 2005). Currently, our *in silico* model lacks a mechanism for microcircuit plasticity, which partly explains the fact that the distribution of synaptic contacts *in silico*, although having a comparable mean, has a higher variability compared to the *in vitro* data. The *in silico* model will be further refined to incorporate a mechanism of microcircuit plasticity in the future which would enable a more accurate match with the shape of the *in vitro* distribution of synaptic contacts per connection. Among other future refinements, the *in silico* model will contain reconstructed morphologies with autaptic contacts to mirror *in vitro* observations of autapses in TTL5 neurons and biophysical mechanisms of spike-timing dependent plasticity to study the effects of learning and memory in the local TTL5 microcircuit (Lübke *et al.* 1996; Perin *et al.* 2011).

Our results identify some of the key governing principles underlying the emergence of synaptic innervation pattern and post-synaptic response properties in the local TTL5 microcircuit. The *in silico* model provides new insights which would have been difficult or impossible to decipher through *in vitro* experiments alone. By actually building a detailed

unifying model of the TTL5 network based on 3D reconstructed neurons and comparing the results of *in silico* models to *in vitro* data, one can identify functional mechanisms that are not adequately represented in the *in silico* model and further refine the biological accuracy of the model.

References

Anwar H, Riachi I, Hill S, Schürmann F & Markram H (2009). An approach to Capturing Neuron Morphological Diversity. In *Computational Neuroscience: Realistic Modeling for Experimentalists*, ed. Schutter ED, pp. 211-232. The MIT Press, Cambridge.

Bush P & Sejnowski T (1996). Inhibition synchronizes sparsely connected cortical neurons within and between columns in realistic network models. *J Comput Neurosci* **3**, 91-110.

DeFelipe J & Fariñas I (1992). The pyramidal neuron of the cerebral cortex: morphological and chemical characteristics of the synaptic inputs. *Prog Neurobiol* **39**, 563-607.

Del Castillo J & Katz B (1954). Quantal components of the end-plate potential. *J Physiol* **124**, 560-573.

Feldmeyer D, Lübke J, Silver RA & Sakmann B (2002). Synaptic connections between layer 4 spiny neurone-layer 2/3 pyramidal cell pairs in juvenile rat barrel cortex: physiology and anatomy of interlaminar signalling within a cortical column. *J Physiol* **538**, 803-822.

Fuhrmann G, Segev I, Markram H & Tsodyks M (2002). Coding of temporal information by activity-dependent synapses. *J Neurophysiol* **87**, 140-148.

Gilbert CD & Wiesel TN (1979). Morphology and intracortical projections of functionally characterised neurones in the cat visual cortex. *Nature* **280**, 120-125.

Hausser M & Roth A (1997). Estimating the time course of the excitatory synaptic conductance in neocortical pyramidal cells using a novel voltage jump method. *J Neurosci* **17**, 7606-7625.

Hines ML & Carnevale NT (1997). The NEURON simulation environment. *Neural Comput* **9**, 1179-1209.

Jahr CE & Stevens CF (1990). A quantitative description of NMDA receptor-channel kinetic behavior. *J Neurosci* **10**, 1830-1837.

- Kalisman N, Silberberg G & Markram H (2005). The neocortical microcircuit as a tabula rasa. *Proc Natl Acad Sci U S A* **102**, 880-885.
- Kasper EM, Lübke J, Larkman AU & Blakemore C (1994). Pyramidal neurons in layer 5 of the rat visual cortex. III. Differential maturation of axon targeting, dendritic morphology, and electrophysiological properties. *J Comp Neurol* **339**, 495-518.
- Korn H & Faber DS (1991). Quantal analysis and synaptic efficacy in the CNS. *Trends Neurosci* **14**, 439-445.
- Larkman AU (1991). Dendritic morphology of pyramidal neurones of the visual cortex of the rat: I. Branching patterns. *J Comp Neurol* **306**, 307-319.
- Larkum ME, Zhu JJ & Sakmann B (1999). A new cellular mechanism for coupling inputs arriving at different cortical layers. *Nature* **398**, 338-341.
- Le Bé JV & Markram H (2006). Spontaneous and evoked synaptic rewiring in the neonatal neocortex. *Proc Natl Acad Sci U S A* **103**, 13214-13219.
- Lübke J, Roth A, Feldmeyer D & Sakmann B (2003). Morphometric analysis of the columnar innervation domain of neurons connecting layer 4 and layer 2/3 of juvenile rat barrel cortex. *Cereb Cortex* **13**, 1051-1063.
- Markram H (1997). A network of tufted layer 5 pyramidal neurons. *Cereb Cortex* **7**, 523-533.
- Markram H, Lübke J, Frotscher M, Roth A & Sakmann B (1997). Physiology and anatomy of synaptic connections between thick tufted pyramidal neurones in the developing rat neocortex. *J Physiol* **500 (Pt 2)**, 409-440.
- Mountcastle VB (1997). The columnar organization of the neocortex. *Brain* **120 (Pt 4)**, 701-722.
- Myme CI, Sugino K, Turrigiano GG & Nelson SB (2003). The NMDA-to-AMPA ratio at synapses onto layer 2/3 pyramidal neurons is conserved across prefrontal and visual cortices. *J Neurophysiol* **90**, 771-779.
- Peters A (1979). Thalamic Input to the Cerebral-Cortex. *Trends in Neurosciences* **2**, 183-185.
- Peters A (1987). Number of neurons and synapses in primary visual cortex. In *Cerebral Cortex*, ed. Jones EG & Peters A, pp. 267-294. Plenum, New York.

- Rinaldi T, Silberberg G & Markram H (2008). Hyperconnectivity of local neocortical microcircuitry induced by prenatal exposure to valproic acid. *Cereb Cortex* **18**, 763-770.
- Sarid L, Bruno R, Sakmann B, Segev I & Feldmeyer D (2007). Modeling a layer 4-to-layer 2/3 module of a single column in rat neocortex: interweaving in vitro and in vivo experimental observations. *Proc Natl Acad Sci U S A* **104**, 16353-16358.
- Shepherd GM, Stepanyants A, Bureau I, Chklovskii D & Svoboda K (2005). Geometric and functional organization of cortical circuits. *Nat Neurosci* **8**, 782-790.
- Silva LR, Amitai Y & Connors BW (1991). Intrinsic oscillations of neocortex generated by layer 5 pyramidal neurons. *Science* **251**, 432-435.
- Silver RA, Lübke J, Sakmann B & Feldmeyer D (2003). High-probability unquantal transmission at excitatory synapses in barrel cortex. *Science* **302**, 1981-1984.
- Simkus CR & Stricker C (2002). Properties of mEPSCs recorded in layer II neurones of rat barrel cortex. *J Physiol* **545**, 509-520.
- Song S, Sjöström PJ, Reigl M, Nelson S & Chklovskii DB (2005). Highly nonrandom features of synaptic connectivity in local cortical circuits. *PLoS Biol* **3**, e68.
- Spruston N (2008). Pyramidal neurons: dendritic structure and synaptic integration. *Nat Rev Neurosci* **9**, 206-221.
- Stepanyants A & Chklovskii DB (2005). Neurogeometry and potential synaptic connectivity. *Trends Neurosci* **28**, 387-394.
- Stepanyants A, Hof PR & Chklovskii DB (2002). Geometry and structural plasticity of synaptic connectivity. *Neuron* **34**, 275-288.
- Stuart G & Sakmann B (1995). Amplification of EPSPs by axosomatic sodium channels in neocortical pyramidal neurons. *Neuron* **15**, 1065-1076.
- Stuart G, Schiller J & Sakmann B (1997). Action potential initiation and propagation in rat neocortical pyramidal neurons. *J Physiol* **505 (Pt 3)**, 617-632.
- Thomson AM & Deuchars J (1994). Temporal and spatial properties of local circuits in neocortex. *Trends Neurosci* **17**, 119-126.
- Thomson AM, Deuchars J & West DC (1993). Large, deep layer pyramid-pyramid single axon EPSPs in slices of rat motor cortex display paired pulse and frequency-dependent depression, mediated presynaptically and self-facilitation, mediated postsynaptically. *J Neurophysiol* **70**, 2354-2369.

- Thomson AM, West DC, Wang Y & Bannister AP (2002). Synaptic connections and small circuits involving excitatory and inhibitory neurons in layers 2-5 of adult rat and cat neocortex: triple intracellular recordings and biocytin labelling in vitro. *Cereb Cortex* **12**, 936-953.
- Traub RD, Miles R & Buzsaki G (1992). Computer simulation of carbachol-driven rhythmic population oscillations in the CA3 region of the in vitro rat hippocampus. *J Physiol* **451**, 653-672.
- Tsodyks MV & Markram H (1997). The neural code between neocortical pyramidal neurons depends on neurotransmitter release probability. *Proc Natl Acad Sci U S A* **94**, 719-723.
- Wang Z & McCormick DA (1993). Control of firing mode of corticotectal and corticopontine layer V burst-generating neurons by norepinephrine, acetylcholine, and 1S,3R-ACPD. *J Neurosci* **13**, 2199-2216.
- Yoshimura Y, Kimura F & Tsumoto T (1999). Estimation of single channel conductance underlying synaptic transmission between pyramidal cells in the visual cortex. *Neuroscience* **88**, 347-352.
- Yu YC, Bultje RS, Wang X & Shi SH (2009). Specific synapses develop preferentially among sister excitatory neurons in the neocortex. *Nature* **458**, 501-504.
- Yuste R, Gutnick MJ, Saar D, Delaney KR & Tank DW (1994). Ca²⁺ accumulations in dendrites of neocortical pyramidal neurons: an apical band and evidence for two functional compartments. *Neuron* **13**, 23-43.

Author contributions

S.R, S.L.H and H.M conceived and designed the experiments, S.R performed the *in silico* experiments and analyzed the data, Y.W did all the *in vitro* morphological reconstructions and measured the innervation patterns, F.S and J.G.K designed and programmed the simulation framework. S.R and H.M drafted the manuscript. All authors discussed the results and critically commented on the manuscript.

Acknowledgements

This study was supported by Swiss Federal funding to the Blue Brain Project. Computations were in part performed on the CADMOS IBM BlueGene/P. The financial support for CADMOS and the Blue Gene/P system is provided by the Canton of Geneva, Canton of Vaud, Hans Wilsdorf Foundation, Louis-Jeantet Foundation, University of Geneva, University of Lausanne, and Ecole Polytechnique Fédérale de Lausanne.

We are indebted to Prof. Idan Segev for insightful discussions and comments on the manuscript and Etay Hay for the biophysical TTL5 model. We thank all members of the Blue Brain Project and the Laboratory of Neural Microcircuitry for their assistance throughout this study. We thank Mr. Richard Walker for editing the manuscript, Dr. Konstantinos Sfyraakis for the circuit building software, Drs. Eilif Müller, Daniel Keller, Imad Riachi, Martin Telefont & Ms. Shruti Muralidhar for helpful discussions. We gratefully acknowledge Drs. Rajnish Ranjan, Sébastien Lasserre, Juan Hernando, Georges Khazen and Michael Reimann, Albert Gidon & John Kenyon for discussions and technical assistance.

Table 1. Comparison of *in vitro* & *in silico* synaptic transmission

Synaptic transmission property	<i>in vitro</i> (mean ± S.D., n = 138)	<i>in silico</i> (mean ± S.D., n = 2000)
EPSP onset latency (ms)	1.7 ± 0.9	1.75 ± 0.6
20-80 % rise time (ms)	2.9 ± 2.3	2.1 ± 0.8
EPSP amplitude (mV)	1.3 ± 1.1	1.3 ± 1
Decay time constant (ms)	40 ± 18	31.6 ± 5.8
Failures (%)	14.3 ± 17.6	13 ± 17.5
CV of EPSP amplitude	0.52 ± 0.37	0.54 ± 0.25

Table 2. *In silico* synaptic response properties to perturbations in anatomical and physiological parameters in the local neocortical microcircuit (two sampled K-S test between control and perturbed data sets for comparison, $\alpha = 0.01$, ** $p < 0.01$)

Perturbation	<i>P</i>-value for Latency distribution	<i>P</i>-value for Rise distribution	<i>P</i>-value for time EPSP amplitude distribution	<i>P</i>-value for Decay constant distribution	<i>P</i>-value for time
Decouple axonal delays and post-synaptic locations	0.13	0.37	0.52	0.83	
Fixed axonal delay (0.05 ms)	1.21×10^{-46} **	0.77	0.98	0.99	
Fixed synaptic conductance per contact (0.3 nS)	0.98	0.91	0.85	0.99	
Uniform sampling of post-synaptic locations (dendritic branch orders)	5.43×10^{-4} **	5.5×10^{-4} **	0.02	0.3	
Uniform sampling of post-synaptic locations (dendritic path distances)	1.97×10^{-10} **	1.07×10^{-34} **	0.01	0.11	
Clustering synapses on dendritic sections with the same branch order	0.08	2.38×10^{-5} **	0.44	0.48	
Clustering synapses on 1° basal dendrites	2.85×10^{-9} **	2.99×10^{-74} **	8.91×10^{-6} **	0.23	
Single post-synaptic morphology: unchanged dendritic branch orders	0.03	0.16	0.37	6.93×10^{-12} **	
Single post-synaptic morphology: unchanged dendritic path distances	0.01	1.1×10^{-17} **	0.21	2.37×10^{-15} **	

Table and figure legends

Table 1. Comparison of *in vitro* and *in silico* synaptic transmission

Table shows a comparison of synaptic transmission properties *in vitro* (mean \pm S.D.; Markram *et al.* 1997) and *in silico*.

Table 2. *In silico* synaptic response properties to perturbations in anatomical and physiological parameters in the local neocortical microcircuit

Table shows the *P*-value of the average synaptic response property distributions of the latency of EPSP onset, 20-80% rise time, amplitude and decay time constant on comparison against the control data *in silico* (**, $P < 0.01$, $\alpha = 0.01$, two sample K-S test) following perturbations of anatomical and physiological model parameters in the local neocortical microcircuit.

Figure 1. Anatomy and Physiology of *in silico* synaptic connections

A, *In silico* TTL5 neuron pair. The pre-synaptic TTL5 neuron is shown in blue and the post-synaptic TTL5 neuron in red. The connection was mediated by 8 synaptic contacts (black dots, identified by the collision-detection algorithm). Of the 8 contacts, 2 were located on terminal tufts and 6 on basal dendrites. *B*, Left, branch order axogram (for the pre-synaptic blue TTL5 neuron). Right, branch order dendrogram (for the post-synaptic red TTL5 neuron) of synaptic contacts (black dots) mediating the modelled TTL5 connection shown in *A*. In the dendrogram, dashed lines in blue schematically represent the axon collaterals of the projecting TTL5 neuron. *C*, Histogram of latencies of somatic EPSP onset, measured from the peak of the presynaptic AP to the time whereby the EPSP reached 5% of its amplitude (for a set of 200 modeled connections from a single microcircuit). Inset, the mean latency for this set of *in silico* connections. *D*, Histogram of 20-80% EPSP rise times. *E*, Histogram of peak EPSP amplitudes. *F*, Histogram of decay time constants.

Figure 2. Prediction map of afferent TTL5 synapses onto a single TTL5 neuron *in silico*

The structural map of afferent synapses from neighbouring model TTL5 neurons onto a single model TTL5 neuron (the axon is the thinner arbor emerging from the bottom; all afferent TTL5 synapses are shown as yellow dots superimposed on the dendritic arbor). The single model neuron received 213 synapses from 58 neighbouring TTL5 neurons (on average, each modeled TTL5 neuron received 250 afferent synapses from 50 neighbouring TTL5 neurons; $n = 1000$).

Figure 3. Physiology of *in silico* synaptic transmission

A, Examples of five successive EPSPs (middle traces) in response to a pre-synaptic AP (top trace) in the modeled connection shown in Fig. 1A). Responses also show a failure. The bottom trace shows the average EPSP. **B**, Rise time measurement of the simulated EPSPs (lower traces), evoked by simulated APs (upper traces). A simulated EPSP represents an average over 100 trials. Dashed lines represent the mean latency (AP peak to 5% of the EPSP peak amplitude). Arrows point to 20% and 80 % rise time of the EPSP peak amplitude. **C**, Decay time course of a mean simulated EPSP. Single exponential fit is superimposed on the decay time course (τ_{EPSP}) of the mean EPSP (lower trace, vertical arrow above the black curve). **D**, Mean latency of EPSP onset in 2000 modeled connections. *In silico* data (blue bars) are compared against the *in vitro* data (red bars). The error bars represent the respective variability in S.D. units. **E**, Mean 20-80% rise time. **F**, Mean peak EPSP amplitude. **G**, Mean EPSP decay time constant.

Figure 4. Reliability of *in silico* synaptic transmission

A, Histogram of the percentage of transmission failures for modeled TTL5 connections ($n = 2000$). The error bars at the center of each bin represent variability in S.D. across different instances of modeled pairs. The mean percentage of failures *in silico* was $13 \pm 17.5\%$ compared against the *in vitro* data of $14.3 \pm 17.6\%$ ($n = 140$). **B**, histogram of CV of EPSP amplitude in modeled TTL5 connections. The mean CV of EPSP amplitude *in silico* was 0.54 ± 0.25 compared to 0.52 ± 0.37 ($n = 140$) *in vitro*. **C**, percentage of transmission

failures plotted as a function of simulated EPSP amplitude (shown only for a single instance of 200 modelled TTL5 pairs). The percentage of transmission failures decreased with increasing EPSP amplitude, almost mirroring observations in the biological benchmark data. **D**, CV of EPSP amplitude plotted as a function of simulated EPSP amplitude. The CV of EPSP amplitude decreased with increasing simulated EPSP amplitude, mirroring the *in vitro* data.

Figure 5. Intrinsic morphological diversity renders average synaptic response properties invariant in the local TTL5 microcircuit

A, Decrease in the mean latency of synaptic responses for 2000 TTL5 pairs sampled from microcircuits ($n = 10$), with a single cloned reconstructed morphology, 3 reconstructed morphologies, 10 reconstructed morphologies, 100 reconstructed morphologies, and when all clones were unique (blue bars, first five plots from top to bottom, see Methods). The error bars in black show the variability (in S.D.) at every bin (mean & S.D. across $n = 10$ microcircuits in each case; see Methods). The plot at the bottom shows a decrease in the variability of average synaptic response properties with an increase in the diversity of the different reconstructed TTL5 morphologies (S.D., black bars; $\alpha = 0.05$, Fishers's exact two sample test; **, $p < 0.05$). **B**, Decrease in the variability of mean rise time across microcircuits with increasing morphological diversity. **C**, Decrease in the variability of mean EPSP amplitude across microcircuits with increasing morphological diversity. **D**, Decrease in the variability of mean EPSP decay time constant across microcircuits with increasing morphological diversity.

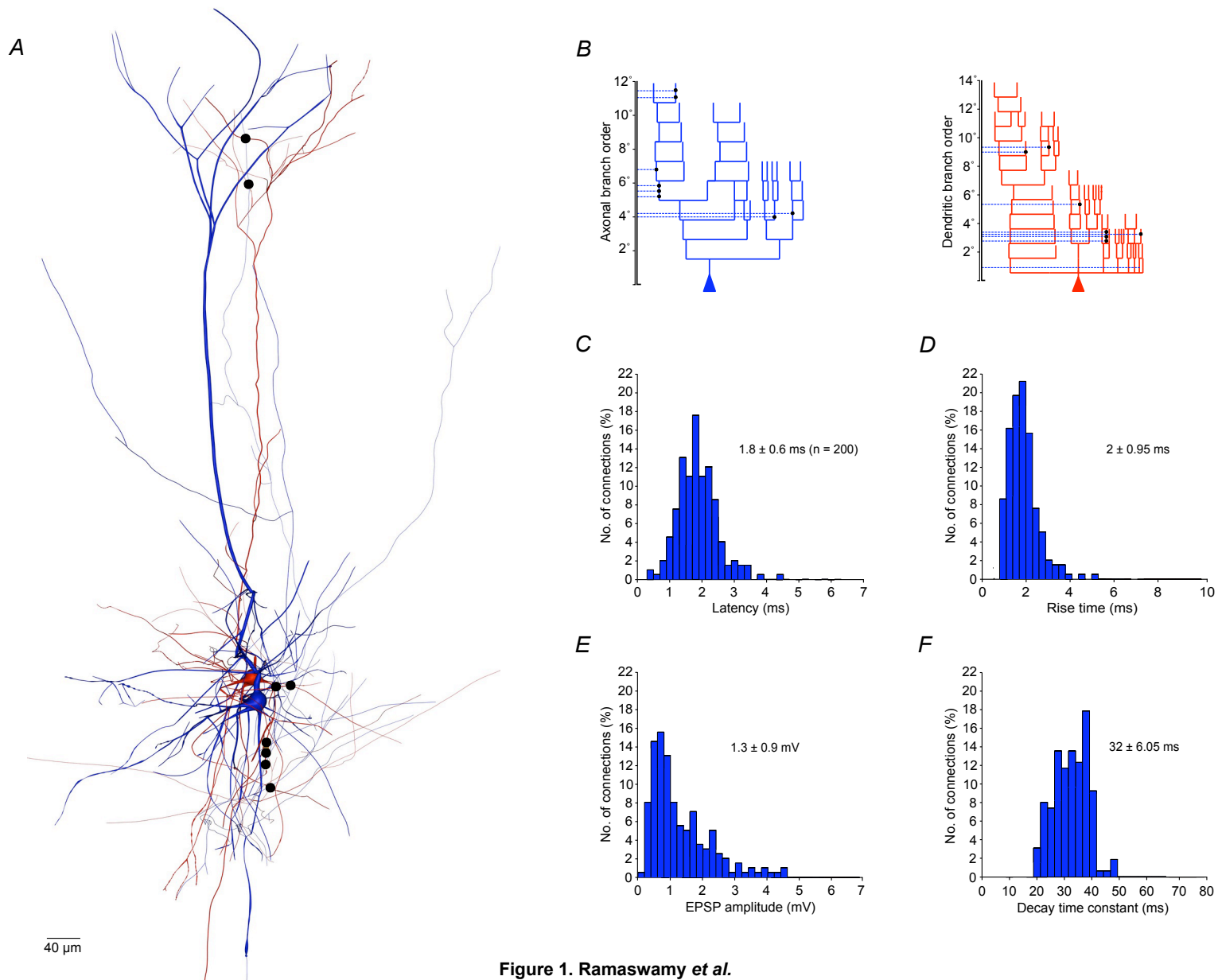




Figure 2. Ramaswamy *et al.*

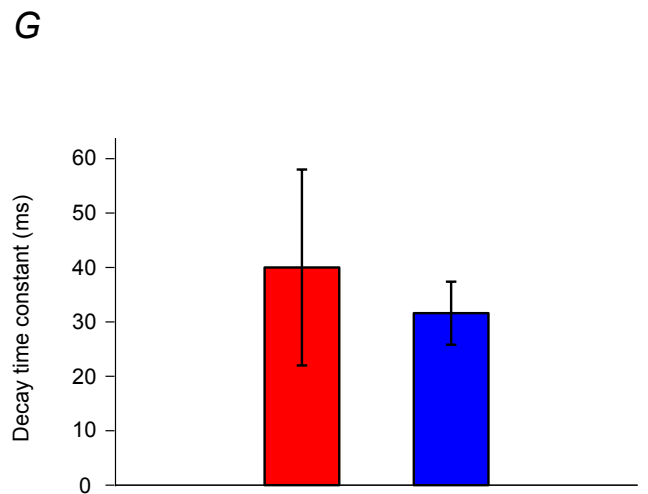
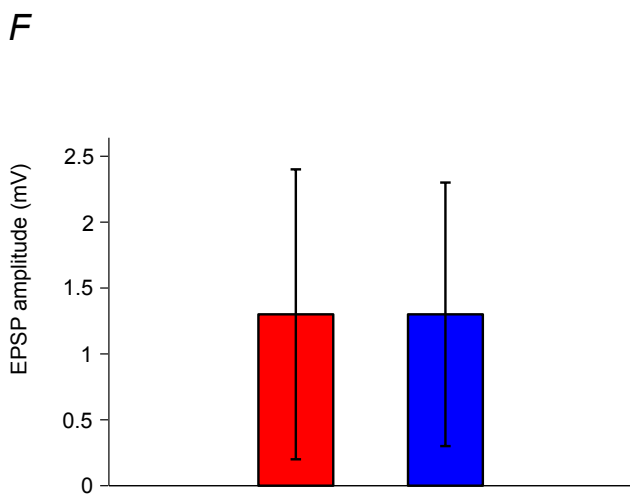
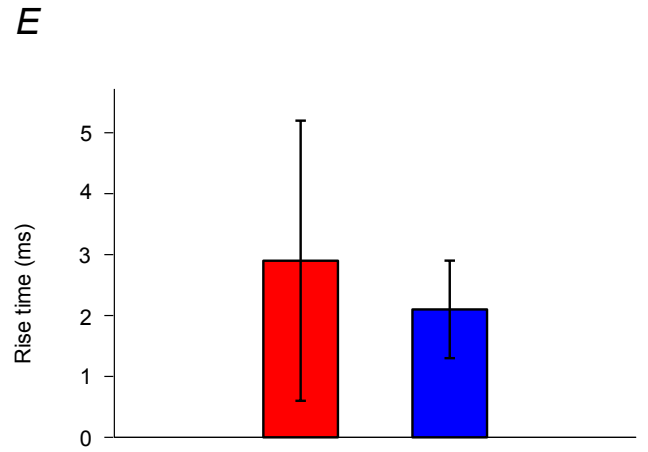
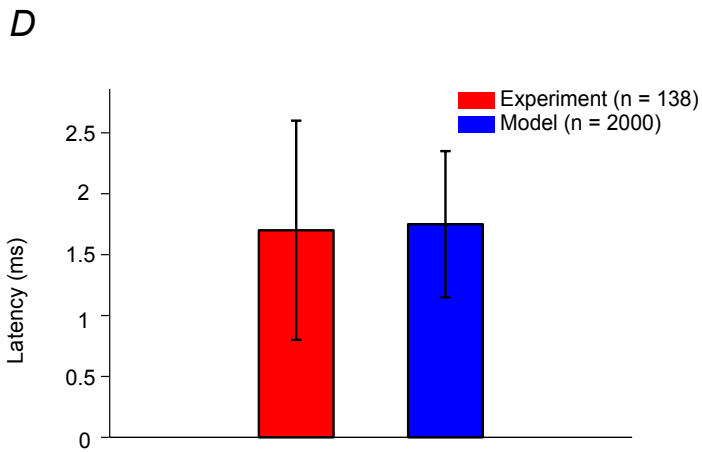
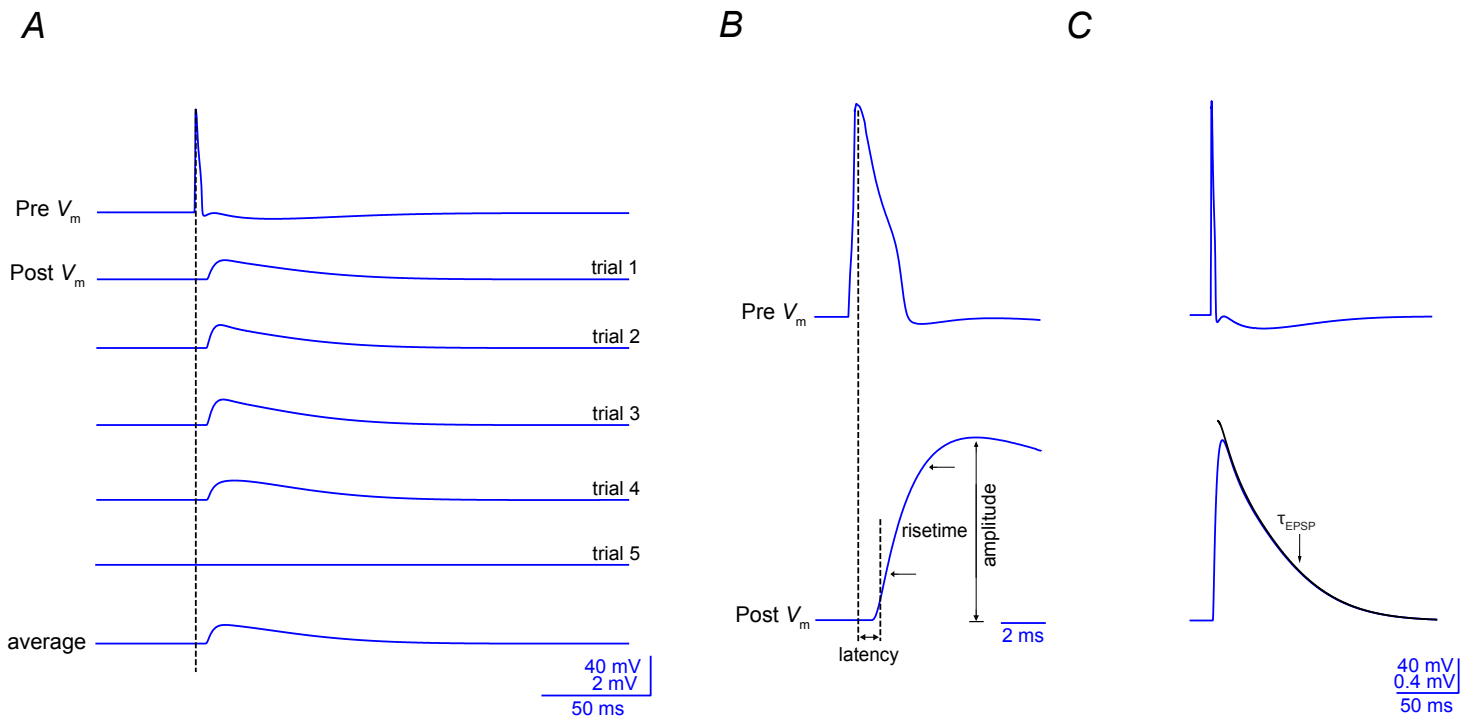


Figure 3. Ramaswamy *et al.*

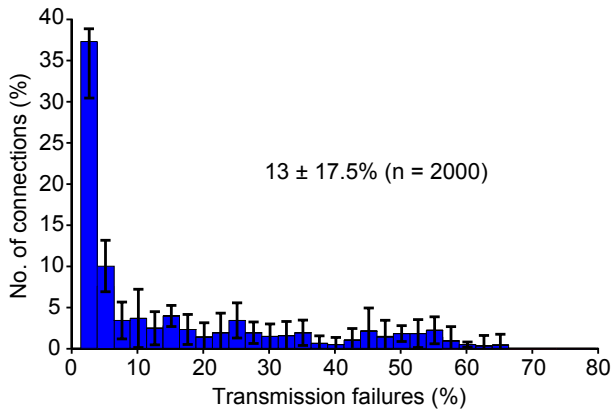
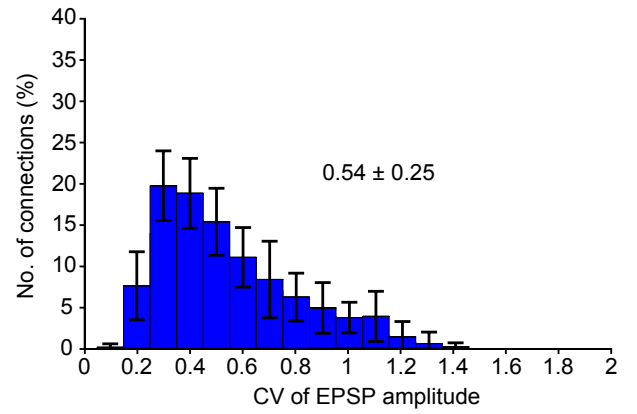
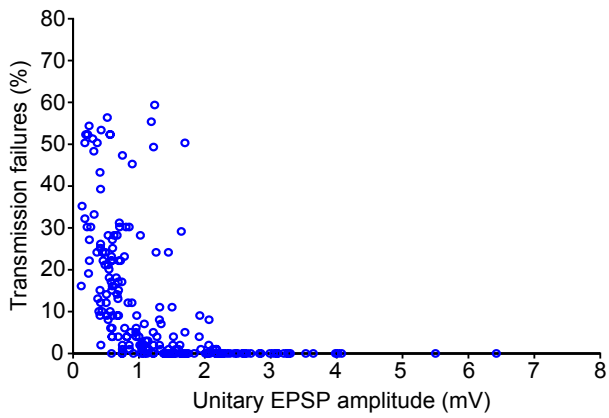
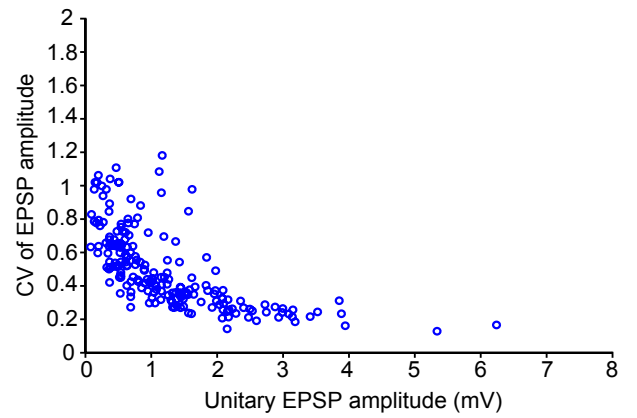
A**B****C****D**

Figure 4. Ramaswamy *et al.*

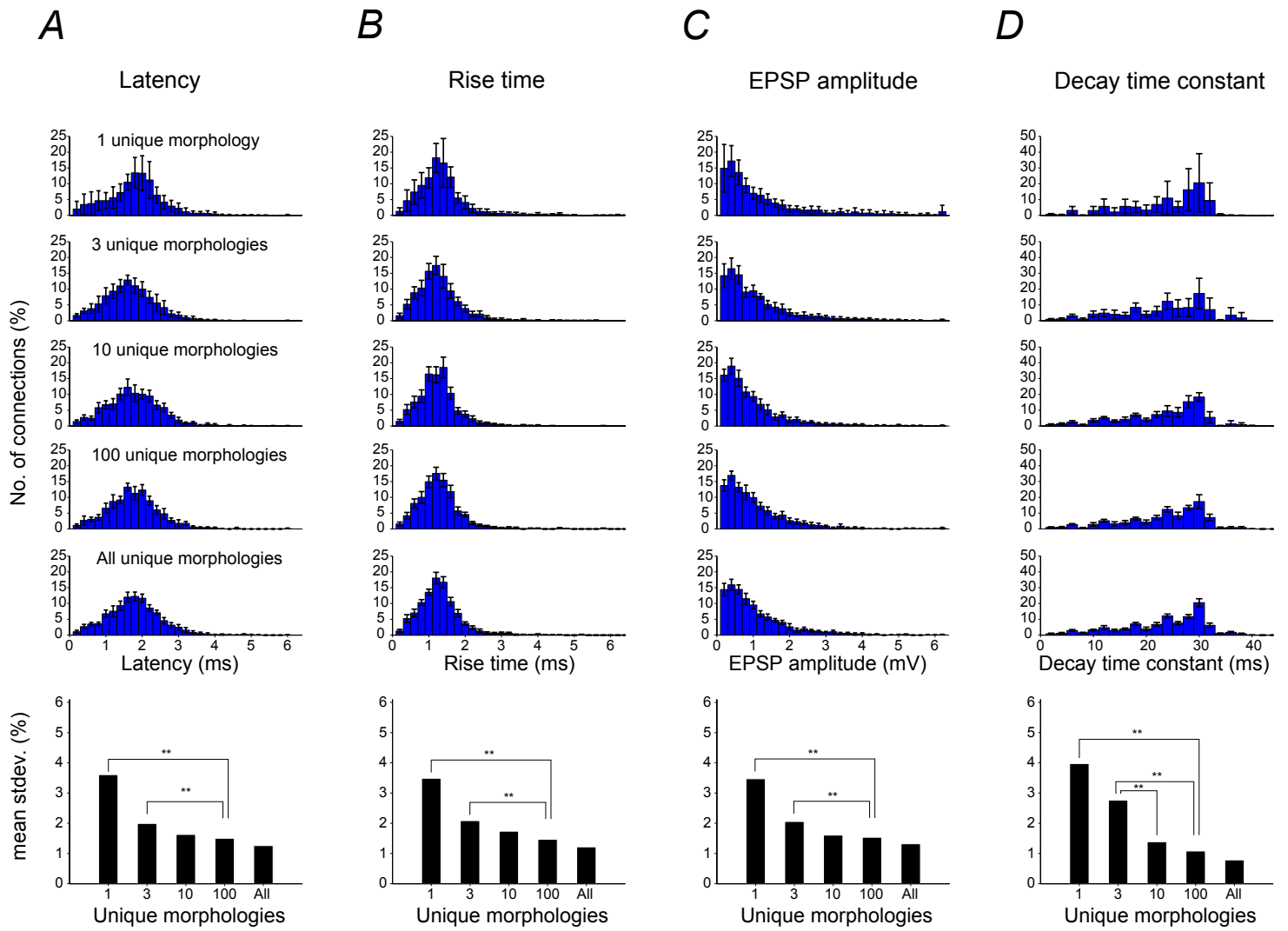


Figure 5. Ramaswamy *et al.*

Supporting online material, Ramaswamy *et al.*

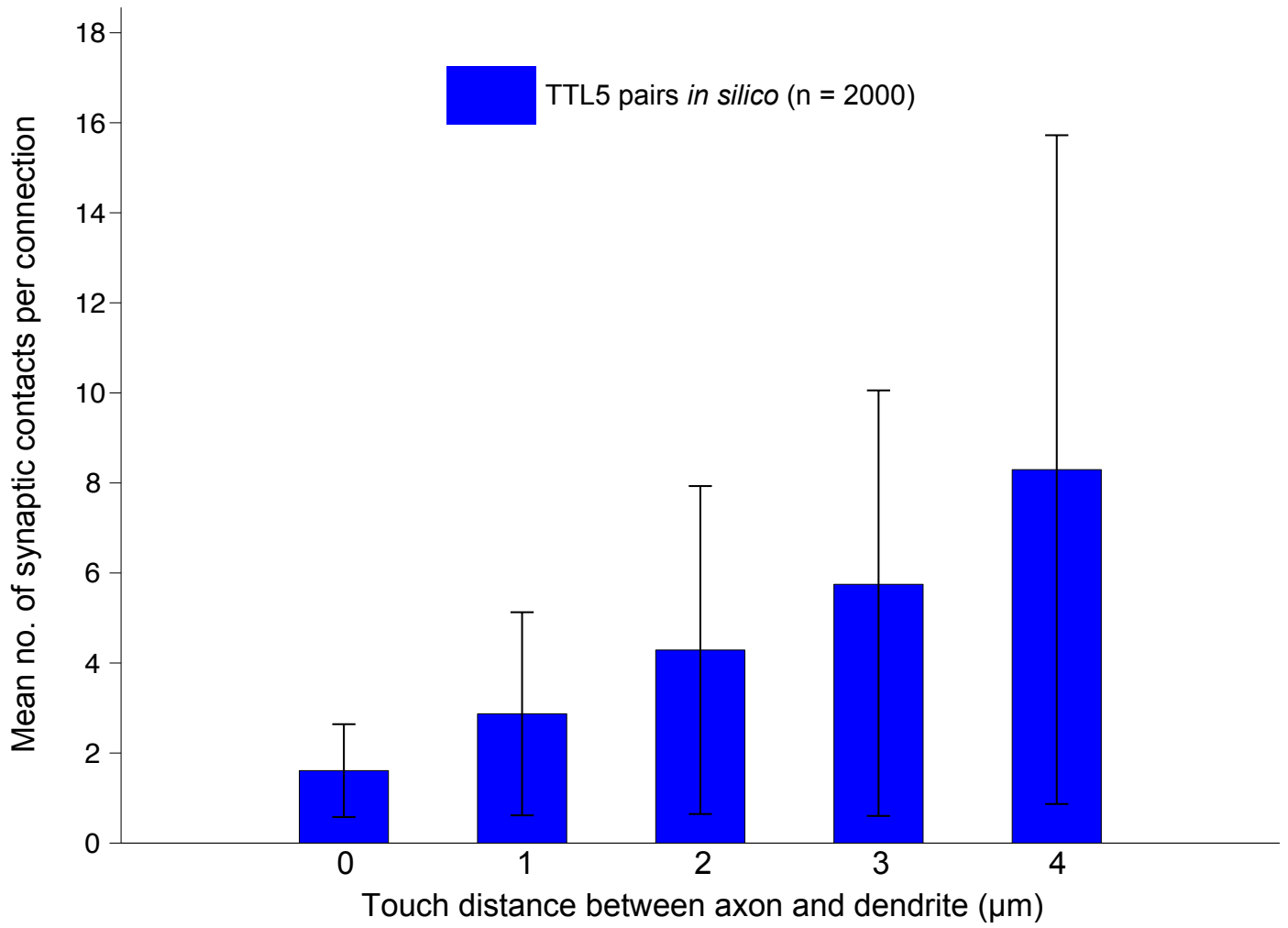
Supplementary figure legends

Figure S1. Axo-dendritic touch distance and mean number of synaptic contacts in pairs of TTL5 neurons

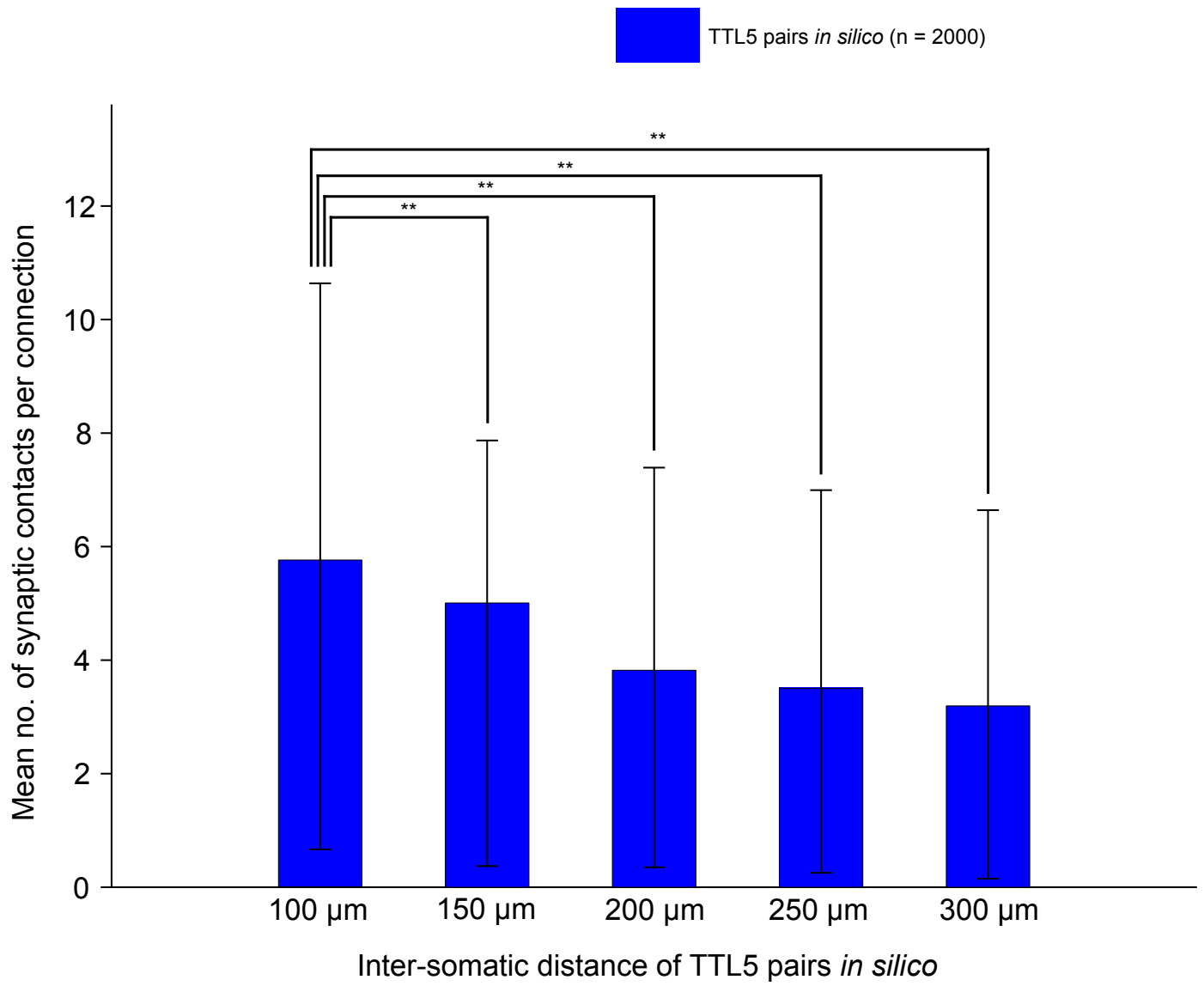
The axo-dendritic touch distance parameter for the identification of synaptic contacts was incrementally varied from 0 to 4 μm (0,1,2,3,4 μm) in different instances of *in silico* microcircuits (10 microcircuits for each axo-dendritic touch distance). The mean number of synaptic contacts (n = 2000 pairs; 200 pairs of TTL5 neurons each sampled across 10 microcircuit instances) varied from 2 at a touch distance of 0 μm to about 8 at a touch distance of 4 μm . The touch distance parameter of 3 μm gave rise to a mean of about 6 synaptic contacts, which is consistent with *in vitro* estimates.

Figure S2. Mean number of synaptic contacts decreases significantly between pairs of TTL5 neurons with an increase in the inter somatic distance

The *in silico* model predicts that the mean number of synaptic contacts decreases significantly between TTL5 neuron pairs with an increase in the inter-somatic distance for sampling pairs (n = 2000 pairs). The mean number of synaptic contacts decreased significantly at inter-somatic distances further from 100 μm (two sampled K-S test, $\alpha = 0.05$, ** $p < 0.05$).



Supplementary Figure S1. Ramaswamy *et al.*



Supplementary Figure S2. Ramaswamy *et al.*

INTRA- AND INTER-LAMINAR PYRAMIDAL PATHWAYS IN SILICO

"I have had my results for a long time: but I do not yet know how I am to arrive at them."

Carl Friedrich Gauss

In silico Synaptic Transmission of Intra- and Inter-laminar Excitatory Pathways in the Neocortex

Srikanth Ramaswamy¹, Sean L. Hill¹, James G. King¹, Yun Wang^{2,3}, Felix
Schürmann¹, Idan Segev⁴ and Henry Markram¹

¹ Brain Mind Institute, École Polytechnique Fédérale de Lausanne (EPFL), CH – 1015, Lausanne, Switzerland

² Caritas St. Elizabeth's Medical Center, Tufts University, Boston, MA 02135, USA

³ School of Optometry & Ophthalmology, Wenzhou Medical College, Wenzhou, Zhejiang, 325027, P.R.China

⁴ Institute of Life Sciences, Dept. of Neurobiology and Interdisciplinary Center for Neural Computation, Edmond Safra Campus, Givat Ram Hebrew University Jerusalem 91904, Israel

Corresponding Author: Henry Markram, PhD,
Brain Mind Institute, École Polytechnique Fédérale de Lausanne (EPFL),
CH – 1015, Lausanne, Switzerland
E-mail: henry.markram@epfl.ch
Ph. +41 21 693 9569
Fax. +41 21 693 5350

4.1 ABSTRACT

Recent work has shown that in an *in silico* network of 3D reconstructed thick tufted layer 5 pyramidal (TTL5) neurons, the overlap of axo-dendritic arbors gives rise to biologically comparable anatomical and physiological synaptic properties. We investigated the emergent physiology of *in silico* synaptic transmission between L2/3, L4, slender-tufted L5 (STL5) and L6 model pyramidal neurons (PCs). Intra- and inter-laminar *in silico* synaptic connections were constructed by arranging 3D reconstructed pyramidal neurons randomly in a volume equivalent to the respective layers of the neocortical column. The physical locations of the overlap of axo-dendritic arbours were identified and model synapses were formed at these locations. Experimentally derived parameters such as the axonal conduction delay, stochastic synaptic transmission, and quantal conductances were assigned to model synapses. An independently constructed biophysical neuron model, although built to capture the firing behaviour of TTL5 pyramidal neurons was generalized across all model pyramidal neurons. Some assumptions were made to ensure the biophysical relevance of this generalization. We found that the physiological properties of the resulting *in silico* synaptic connections largely matched *in vitro* observations. Our *in silico* model provides insight that the emergent synaptic properties are strikingly similar across different cortical regions, particularly the non-barrel and barrel somatosensory cortices. In addition, the *in silico* model also predicts the anatomy and physiology of inter-laminar synaptic connections between pyramidal neurons that have not been probed through *in vitro* experiments.

4.2 INTRODUCTION

The profound information processing ability of the mammalian brain can be attributed in part to computations between networks of pyramidal neurons (PCs) the local neocortical microcircuit. In the neocortex, PCs that are nearby tend to form the vast majority of synapses rather than the ones spread farther apart [Braitenberg et al. 1998]. Decades of research have generated vast amounts of information about the structure and function of PCs (for review see [Spruston 2008]). The manner in which a PC integrates synaptic input leading to an AP is central to its function. The dendrites of PCs are richly endowed with voltage gated ion channels that shape an EPSP as it traverses the dendritic arbor to reach the soma [Spruston 2008]. A characteristic feature of PCs is a clear distinction of the morphology comprising an apical trunk ascending from the apex of a pyramid-like soma, with oblique dendrites emanating at various angles from the trunk. The axon arborizes profusely within a distance of 300-500 μm to form local connections. The extent to which neocortical pyramidal cells function as a local network is determined by the strength and probability of their connections.

To understand how sensory signals from the periphery are transformed into electrical activity in the neocortex it is essential to elucidate the spatial-temporal dynamics of cortical signal processing and the underlying PC microcircuits [Lübke and Feldmeyer 2007b]. We have previously shown that in *in silico* models of TTL5 microcircuits, the anatomical loci of synapses

and the physiological properties of somatic EPSPs closely matched those recorded experimentally without the need for any fine-tuning (see Chapter 3). Furthermore, the average synaptic response properties were found to be robust and invariant due to intrinsic morphological diversity. In the present study, we extended our method of modeling TTL5 microcircuits to develop a complete *in silico* map of PC-PC synaptic transmission in a biologically accurate model of the neocortical column. We found that the average synaptic properties were robust and invariant due to morphological diversity across all PC-PC pathways modeled, which suggests that this diversity is a fundamental governing principle of neocortical function.

Excitatory synaptic connections between PCs in the supra- and infragranular layers were modeled by arranging 3D morphological reconstructions of PCs in their respective neocortical layers. The physical locations of the overlap of axo-dendritic arbours were identified and model synapses were formed at these locations. Experimentally derived parameters such as the axonal conduction delay, stochastic synaptic transmission, and quantal conductances were assigned to model synapses. An independently constructed biophysical neuron model, although built to capture the firing behaviour of TTL5 neurons was generalized across all model pyramidal neurons. Some assumptions were made to ensure the biophysical relevance of this generalization. We found that the physiological properties of the resulting *in silico* synaptic connections largely matched *in vitro* observations. Our *in silico* model provides insight that the emergent synaptic properties are strikingly similar across different cortical regions, particularly the non-barrel and barrel somatosensory cortices. In addition, the *in silico* model also predicts the anatomy and physiology of inter-laminar synaptic connections between pyramidal neurons that have not been probed through *in vitro* experiments.

4.3 METHODS

4.3.1 3D anatomical reconstruction of PC morphologies

Biocytin stained morphologies ($n = 19$ L2/3PCs, $n = 13$ L4PCs, $n = 6$ L4SSs, $n = 11$ L5STPCs & $n = 44$ L6CCPCs) were obtained from 300 μm thick sagittal brain slices from the somatosensory cortex of juvenile Wistar rats (aged 14-16 days). The methods used were compliant with Swiss national and institutional guidelines. Stained morphologies were reconstructed using the NeuroLucida system (MicroBrightField Inc., Colchester, VT, USA) and a brightfield light microscope (Olympus GmbH, Düsseldorf, Germany). The biocytin staining procedure led to $\sim 25\%$ shrinkage in terms of slice thickness and $\sim 10\%$ anisotropic shrinkage in terms of height and width. The reconstructed morphologies were corrected for shrinkage of thickness.

4.3.2 Morphology repair

The somata of PCs recorded *in vitro* tend to be chosen $\sim 50\text{-}100$ μm beneath the surface of the slice. As a result, the slicing procedure severs about 20-40% of their axonal and dendritic arbors. To partially recover their anatomy, we re-grew cut portions using an algorithm developed by

Anwar *et al.* (2009) [Anwar *et al.* 2010]. After compensating for measurement inaccuracies and tissue shrinkage, the algorithm repairs dendrites and axons separately, while maintaining the overall statistics of the neuron's morphology [Anwar *et al.* 2010]. The dendritic and axonal arbors were artificially cut and the algorithm attempted to regrow the cut arbor.

4.3.3 Constructing inter- and intra-laminar PC microcircuits

A 3D hexagonal volume was loaded ($377.7 \mu\text{m} \times 1520 \mu\text{m} \times 356.7 \mu\text{m}$) with randomly positioned model neurons derived from the diverse set of reconstructed PC morphologies mentioned above. A hexagon allows close packing of neurons and these dimensions were chosen such that the diameter of the hexagon accounted for the full extent of the dendritic arborization of TTL5 neurons, which are the neurons with the largest arbours in the local neocortical microcircuit. The density of neurons in the model circuit was appropriate for the juvenile rat somatosensory cortex (the density of neurons (per mm^3) in the modelled layers were - $\sim 41,000$ in L2/3, $\sim 42,000$ in L4, $\sim 35,000$ in L5 and $\sim 40,000$ in L6; [Peters and Jones 1999, Meyer *et al.* 2010]). We repeated this procedure 10 times, thus creating 10 potential PC microcircuits through methods described previously (see Chapter 3). In brief, synaptic contacts were identified using a collision-detection algorithm implemented on the BlueGene/P supercomputer. The algorithm detected all appositions between axonal arbors of pre-synaptic neurons and the dendrites of neighboring neurons. The potential synaptic contacts detected this way in each connection were then converted into functional synapses through an algorithm, constrained with the *in vitro* connection probability estimated for pairs within inter-somatic distances of 50-100 μm - 6% for L2/3PC connections, 25% for L4PC connections, 3% for L4SS-L2/3PC connections, 3% for L5STPC connections, 3% for L6CCPC connections and 1.3% for L6CTPC connections. The 10 microcircuits, constructed in this way, formed the basis for the *in silico* synaptic transmission experiments reported below.

4.3.4 Stochastic synapse model

At each putative synaptic location identified by the collision-detection algorithm, we implemented a stochastic model of synaptic transmission. This model guaranteed that post-synaptic responses would be different in every trial [Fuhrmann *et al.* 2002]. The model was an extension of the phenomenological Tsodyks-Markram dynamic synapse model [Tsodyks and Markram 1997], modified to incorporate NMDA receptor (NMDAR) kinetics as described by Jahr & Stevens (1990) [Jahr and Stevens 1990].

Parameters for model synapses were derived from experimental estimates (assuming normal distribution; mean \pm S.D.). For AMPA receptor (AMPA) kinetics: synaptic conductance g_{AMPA} ($0.3 \pm 0.2 \text{ nS}$; [Yoshimura *et al.* 1999, Sarid *et al.* 2007, Rinaldi *et al.* 2008]); rise time [τ_{riseAMPA}] and decay time constants [$\tau_{\text{decayAMPA}}$] were 0.2 ms and $1.7 \pm 0.18 \text{ ms}$,

respectively; [Häusser and Roth 1997]), utilization of synaptic efficacy U , analogous to the probability of neurotransmitter release (pathway specific release probability values were used):

- L2/3 PC – L2/3 PC, 0.46 ± 0.26 [Koester and Johnston 2005]
- L4PC – L4PC, 0.86 ± 0.09 [Brémaud et al. 2007]
- L4SS – L2/3PC, 0.79 ± 0.04 [Silver et al. 2003]
- L5STPC – L5STPC, 0.39 ± 0.04 [Le Bé et al. 2007]
- L6CCPC – L6CCPC, 0.61 ± 0.14 [Brémaud et al. 2007]

In some of the studies where the U parameter was obtained from, D and F parameters were not identified and therefore we used values estimated from TTL5 connections by for such of those pathways [Tsodyks and Markram 1997]. The time constant for recovery from depression D was (671 ± 17 ms; [Tsodyks and Markram 1997]) and the time constant for recovery from facilitation F (17 ± 5 ms) were used. For NMDAR kinetics: synaptic conductance g_{NMDAR} ($0.86 * g_{\text{AMPA}}$ for L4PC connections, $0.5 * g_{\text{AMPA}}$ for L4SS-L2/3PC connections, and $0.7 * g_{\text{AMPA}}$ for all other PC-PC connections modelled), τ_{riseNMDA} and $\tau_{\text{decayNMDA}}$ of 0.29 ms and 43 ms respectively [Sarid et al. 2007]. $[\text{Mg}^{2+}]_0$ was set to 1 mM [Jahr and Stevens 1990]. The axonal conduction delay for each stochastic model synapse was computed using the axonal path distance to the soma. AP conduction velocity was set at 300 $\mu\text{m}/\text{ms}$, based on experimental estimates by Stuart *et al.* (1997) [Stuart et al. 1997].

4.3.5 Biophysical pyramidal cell model

Neuronal biophysics was simulated based on the approach developed by Druckmann *et al.* (2007) and Hay *et al.* (2011) to model TTL5 neurons [Druckmann et al. 2007, Hay et al. 2011]. Briefly, a model pyramidal neuron was created with a 3D reconstructed morphology from *in vitro* experiments. The free parameters in the model were the maximal conductances of somatic and dendritic ion channels, as represented in the Hodgkin-Huxley formalism. The somatic response of the model and the back propagation of APs into the apical dendritic arbor matched the *in vitro* observations [Hay et al. 2011]. The model neuron was originally fit to a reconstructed TTL5 morphology and we generalized this model to PC morphologies across layers 2/3 to 6. Some assumptions were made to determine the intrinsic properties for the respective PC morphological classes by distributing the I_h conductance as an exponential function based on the absolute distance of the dendritic arbour [Kole et al. 2006b]. Spines were taken into account by scaling the specific membrane capacitance (C_m).

4.3.6 In silico stimulation and recording

In silico experiments were performed in the NEURON (version 7.2) simulation environment [Hines and Carnevale 1997] with a simulation time step (dt) of 0.025 ms. Simulations were

run on a 128 processor rack of a BlueGene/P supercomputer accessed through the CADMOS consortium or on 32 processors of a SGI Prism parallel computer. All *in silico* experiments used the circuit, neuron and synapse models on an as-is-where-is basis, without any fine-tuning. To select neuron pairs for *in silico* experiments, we applied the same procedure as in previous *in vitro* studies [Feldmeyer et al. 1999; 2002, Silver et al. 2003, Feldmeyer et al. 2006, Le Bé et al. 2007]. From each of the 10 reconstructed microcircuits we randomly selected 200 pairs of intra- and inter-laminar PC connections within inter-somatic distances in the range ~ 50 -100 μm , thus creating a population of 2000 excitatory pairs from each layer examined. To evoke unitary pre-synaptic APs in model PCs, we simulated square current pulses of 5 nA for a duration of 10 ms at the soma and measured the post-synaptic response in the target model neurons.

4.3.7 Data analysis

Data analysis was carried out in MATLAB (version 7.7). As biological benchmarks, we used *in vitro* measurements of the latency of EPSP onset, rise time, amplitude, decay time constant, failures and the coefficient of variation (CV) of EPSP amplitude for intra- and inter-laminar PC-PC pathways from [Feldmeyer et al. 1999; 2002, Silver et al. 2003, Mercer et al. 2005, Koester and Johnston 2005, Kole et al. 2006b, Feldmeyer et al. 2006, Le Bé et al. 2007]. Data from model connections for each inter- and intra-laminar PC-PC pathway studied here ($n = 2000$) were compared against their respective benchmark. Values for simulated connections were determined by averaging the data from 100 independent trials. Somatic EPSP amplitude was measured as the difference between baseline and peak voltage. Latency of EPSP onset was measured as time taken by an AP to fall from peak amplitude to 5% of peak EPSP amplitude. Rise time was measured as the time taken to rise from 20 to 80% peak EPSP amplitude. The decay time constant was measured by fitting a single exponential to the average EPSP in a region where the EPSP had decayed to about 80% of peak amplitude. Reliability of synaptic transmission was evaluated using the same set of neuron pairs used to measure synaptic transmission properties. Trials in which a pre-synaptic AP failed to evoke an EPSP were labeled as failures. The variability of EPSPs was measured by the CV of EPSP amplitude, computed as S.D./mean amplitude. Differences between *in vitro* and *in silico* data were tested using Fisher's exact two sample test, with $\alpha = 0.01$. The analysis protocols are consistent with *in vitro* experiments and were successfully replicated in a recent study characterizing the *in silico* synaptic transmission properties of modelled TTL5 connections (see Chapter 3).

4.4 RESULTS

Previous work has shown that the incidental overlap of axo-dendritic arbors between TTL5 neurons gives rise to biologically comparable properties *in silico* synaptic transmission of these connections (see Chapter 3). In this study, we investigated whether the physiological properties also emerge naturally from the axo-dendritic overlap of other PC-PC synaptic connections.

4.4.1 Intra-laminar connections

Anatomy of connections between L2/3PCs

We examined the anatomy of synaptic innervation in single model connections, randomly sampled from many possible connections in a reconstructed microcircuit of L2/3PCs. The mean number of synaptic contacts per connection was $\sim 2.6 \pm 2.4$ (mean \pm S.D; $n = 2000$), as compared against 2.8 ± 0.7 in the *in vitro* data.

Physiology of connections between L2/3PCs

The mean EPSP onset latency in model connections was 0.9 ± 0.3 ms ($n = 2000$; see Figure 4.1; Table 4.1), the mean 20-80 % rise time was 1.6 ± 0.3 ms (see Figure 4.1). Simulated EPSPs had mean amplitudes of 1.2 ± 0.7 mV (see Figure 4.1) and the mean decay time constant was 21.3 ± 6.32 ms (see Figure 4.1). The *in silico* latency of EPSP onset, amplitude ($P > 0.01$, $\alpha = 0.01$, Fisher's exact two sample test) These results were obtained without any fine-tuning of the model parameters.

We measured the synaptic transmission properties for 2000 pairs of neurons within inter-somatic distances of 100 μ m extracted from all 10 microcircuits instances (200 pairs \times 10 microcircuits; see Methods), each of which contained L2/3PCs in different locations with different morphologies and orientations. The average synaptic response properties were tested for similarity to the *in vitro* data in all modelled microcircuits. The mean latency of EPSP onset across all 2000 *in silico* L2/3PC pairs was 0.9 ± 0.3 ms, compared against an *in vitro* value of 1.1 ± 0.4 ms (see Figure 4.1; Fisher's exact two sample test, $P > 0.01$, $\alpha = 0.01$). The mean rise time was 1.6 ± 0.3 ms, compared to an *in vitro* value of 0.7 ± 0.2 ms [Feldmeyer et al. 2006] (see Figure 4.1; Fisher's exact two sample test, $P < 0.01$, $\alpha = 0.01$). However, another independent study by Kampa et al. (2006) estimate the 20-80% rise times between connected L2/3PC pairs to be 2.9 ± 1.29 ms [Kampa et al. 2006]. However, the inter-somatic distance of sampled L2/3PC pairs by Kampa et al. was in the range of 40-45 ms. It remains to be verified if the rise times can be sensitive to the inter-somatic sampling distance. The mean EPSP amplitude was 1.2 ± 0.7 mV as against the *in vitro* value of 1 ± 0.7 mV (see Figure 4.1; Fisher's exact two sample test, $P > 0.01$, $\alpha = 0.01$). The mean decay time constant was 21.3 ± 6.3 ms as against an *in vitro* value of 15.7 ± 4.5 ms (see Figure 4.1; Fisher's exact two sample test, $P > 0.01$, $\alpha = 0.01$). The mismatch of the rise time and the decay time constants in particular suggests that the model generalization from TTL5 to other PCs needs to be re-calibrated for a better fit of the passive properties (see Methods)

In silico connections transmitted reliably with a mean failure rate of $26.3 \pm 19.7\%$ ($n = 2000$). The distribution of transmission failures closely matched the *in vitro* data ($P > 0.01$, $\alpha = 0.01$, Fisher's exact two sample test; see Figure 4.1 and Table 4.2). The CV for simulated EPSPs (0.7 ± 0.3 ; $n = 2000$) was higher than the *in vitro* data ($P < 0.01$, $\alpha = 0.01$, Fisher's exact two

sample test; see Figure 4.1 and Table 4.2). The mismatch between the *in silico* and *in vitro* CV of EPSP amplitudes is perhaps due to the fact that the synapse model we describe is univesicular, while in reality these PC connections could be mediated by multivesicular release [Koester and Johnston 2005]. The rate of transmission failures and the CV of simulated EPSPs decreased with an increase in EPSP amplitude as expected from a binomial model of synaptic transmission (data not shown). This relationship is expected in a binomial model of synaptic transmission in which the main determinant of EPSP amplitude is the probability of neurotransmitter release.

Anatomy of connections between L4PCs

We examined the anatomy of synaptic innervation in single model connections, randomly sampled from many possible connections in a reconstructed microcircuit of L4PCs (see Methods). The mean number of synaptic contacts per connection was $\sim 3.35 \pm 3.22$ (mean \pm S.D; $n = 2000$), as compared to 3.4 ± 1 in the *in vitro* data.

Physiology of connections between L4PCs

We measured the synaptic transmission properties for 2000 pairs of neurons within inter-somatic distances of 100 μm extracted from all 10 microcircuits instances (200 pairs \times 10 microcircuits; see Methods), each of which contained L4PCs in different locations with different morphologies and orientations (see Methods). The *in silico* mean latency of EPSP onset across all 2000 L4PC pairs was 1.2 ± 0.4 ms, compared against an *in vitro* value of 1 ± 0.4 ms (see Figure 4.2; Fisher's exact two sample test, $P > 0.01$, $\alpha = 0.01$). The mean rise time was 1.6 ± 0.7 ms, compared to an *in vitro* value of 1.5 ± 0.5 ms (see Figure 4.2; Fisher's exact two sample test, $P > 0.01$, $\alpha = 0.01$). The mean EPSP amplitude was 1.6 ± 1.4 mV as against the *in vitro* value of 1.6 ± 1.5 mV (see Figure 4.2; Fisher's exact two sample test, $P > 0.01$, $\alpha = 0.01$). The mean decay time constant was 31 ± 5 ms as against an *in vitro* value of 17.8 ± 6.3 ms (see Figure 4.2; Fisher's exact two sample test, $P < 0.01$, $\alpha = 0.01$). The decay time could be different because due to the generalization step from TTL5 neuron models to other PCs, which would need a re-calibration of the passive property fits.

L4PC connections *in silico* transmitted reliably with a mean failure rate of $6.5 \pm 8.5\%$ ($n = 2000$). The distribution of transmission failures closely matched the *in vitro* data ($P > 0.01$, $\alpha = 0.01$, Fisher's exact two sample test; see Figure 4.2 and Table 4.2). The CV for simulated EPSPs (mean, 0.3 ± 0.14 ; $n = 2000$) was very similar to the *in vitro* data ($P > 0.01$, $\alpha = 0.01$, Fisher's exact two sample test; see Figure 4.2 and Table 4.2). The rate of transmission failures and the CV of simulated EPSPs decreased with an increase in EPSP amplitude, almost matching the *in vitro* data (data not shown).

Anatomy of connections between L5STPCs

We next examined the anatomy of synaptic innervation in single model connections, randomly sampled from many possible connections in a reconstructed microcircuit of L5STPCs (see Methods). The mean number of synaptic contacts per connection was $\sim 3.5 \pm 2$ (mean \pm S.D; $n = 2000$), as compared to 4 ± 1.3 in the *in vitro* data.

Physiology of connections between L5STPCs

Measurements of synaptic transmission properties for 2000 pairs of neurons within inter-somatic distances of 100 μm extracted from all 10 microcircuits instances were performed (200 pairs \times 10 microcircuits; see Methods), each of which contained L5STPCs in different locations with different morphologies and orientations (see Methods). The mean latency of EPSP onset across all 2000 *in silico* pairs was 1.2 ± 0.5 ms, compared against an *in vitro* value of 1.4 ± 0.2 ms (see Figure 4.3; Fisher's exact two sample test, $P > 0.01$, $\alpha = 0.01$). The mean rise time was 2 ± 1.05 ms, compared to an *in vitro* value of 2.7 ± 0.3 ms (see Figure 4.3; Fisher's exact two sample test, $P > 0.01$, $\alpha = 0.01$). The mean EPSP amplitude was 0.95 ± 0.9 mV as against the *in vitro* value of 0.8 ± 0.2 mV (see Figure 4.3; Fisher's exact two sample test, $P > 0.01$, $\alpha = 0.01$). The mean decay time constant was 26.5 ± 7.7 ms as against an *in vitro* value of 47 ± 7 ms (see Figure 4.3; Fisher's exact two sample test, $P > 0.01$, $\alpha = 0.01$).

L5STPC connections *in silico* transmitted reliably with a mean failure rate of 12.3 ± 2.1 % ($n = 2000$). The distribution of transmission failures closely matched the *in vitro* data ($P > 0.01$, $\alpha = 0.01$, Fisher's exact two sample test; see Figure 4.3 and Table 4.2). The CV for simulated EPSPs (mean, 0.7 ± 0.3 ; $n = 2000$) was very similar to the *in vitro* data ($P > 0.01$, $\alpha = 0.01$, Fisher's exact two sample test; see Figure 4.3 and Table 4.2). The rate of transmission failures and the CV of simulated EPSPs decreased with an increase in EPSP amplitude, almost mirroring the *in vitro* data (data not shown).

Anatomy of connections between L6PCs

We examined the anatomy of synaptic innervation in single model connections between L6CCPCs, randomly sampled from many possible connections in a reconstructed microcircuit of L6CCPCs (see Methods). The mean number of synaptic contacts per connection was $\sim 3.4 \pm 2.7$ (mean \pm S.D; $n = 2000$), as compared to 4 ± 0.25 in the *in vitro* data.

Physiology of connections between L6PCs

There have only been a couple of noteworthy studies to date on PC-PC microcircuits in the juvenile rat somatosensory cortex [Mercer et al. 2005] [Berger et al., in preparation]. Therefore, the available *in vitro* data set is rather sparse for the moment. In our measurement of synaptic transmission properties of *in silico* L6CCPC connections, we found that the mean latency of

EPSP onset *in silico* was 1.9 ± 0.7 ms as against the *in vitro* mean of 2.1 ± 0.7 ms ($P > 0.01$, $\alpha = 0.01$, Fisher's exact two sample test; see Table 1). The mean rise time *in silico* was 1.5 ± 0.4 ms as against the *in vitro* mean of 1.6 ± 0.7 ms ($P > 0.01$, $\alpha = 0.01$, Fisher's exact two sample test; see Table 4.2). The mean EPSP amplitude was 1 ± 0.6 ms as against the *in vitro* mean of 0.9 ± 0.7 ms ($P > 0.01$, $\alpha = 0.01$, Fisher's exact two sample test; see Table 4.2). Although the *in silico* model predicted a mean decay time constant of 30 ± 8.1 ms, both the *in vitro* studies cited above do not provide a relevant measurement for comparison.

The mean transmission failures predicted by the *in silico* model for L6CCPC connections was 2.5 ± 8 ms as against estimates of 2.7 from binomial analysis [Brémaud et al. 2007]. The mean CV of *in silico* EPSP amplitudes was 0.4 ± 0.2 compared against an estimated 0.47 from binomial analysis [Brémaud et al. 2007].

4.4.2 Inter-laminar connections

Connections between L4SS and L2/3PCs

The anatomy of connections between *in silico* L4SS and L2/3PC connections had a mean number of synaptic contacts 4.2 ± 4 as against a mean of 4.5 ± 0.5 . The axonal and dendritic branch order innervation patterns for *in silico* connections were close to *in vitro* measurements [Feldmeyer et al. 2002].

The emergent *in silico* synaptic physiology in terms of the latency of EPSP onset, rise time, amplitude and decay time constant for this connection still need sufficient validation. It appears that our assumption of using the AP conduction velocity of $300 \mu\text{m}/\text{ms}$ estimated by for TTL5 neurons [Stuart et al. 1997] might be inadequate to model the latency of inter-laminar synaptic pathways, since the axonal pathway of L4SS-L2/3PC connections has been reported to be longer [Feldmeyer et al. 2002]. This very likely implies a different AP conduction velocity value, despite the fact that the presynaptic axonal branch order innervation pattern is in agreement with observations in Feldmeyer et al. The mismatch in terms of the rise time and decay time constant of *in silico* EPSPs indicates that the passive properties of the biophysical L2/3PC neuron model needs to be recalibrated, despite the fact that the postsynaptic innervation patterns are in agreement with the biological benchmark [Feldmeyer et al. 2002].

However, in terms of the *in silico* transmission of failures and the CV of EPSP amplitude for L4SS-L2/3PC connections, the model predicted a mean of $5.9 \pm 8.9\%$ and 0.33 ± 0.14 closely matching the *in vitro* means of $5 \pm 8.8\%$ and 0.3 ± 0.13 , respectively.

Interestingly, the *in silico* mean EPSP amplitude and CV of EPSP amplitudes are consistent with a previous independent study that modelled synaptic interactions between L4SSs and L2/3PCs [Sarid et al. 2007]. However, in contrast to the *in silico* study by Sarid et al. [Sarid et al. 2007], where the numbers and dendritic locations of synaptic contacts were drawn from the statistics measured *in vitro* for the feedforward L4SS-L2/3PC connection, the connectivity data

in our study is purely based on the geometrical overlap between axonal and dendritic arbors of reconstructed L4SS and L2/3PC morphologies.

4.5 DISCUSSION

This study provides preliminary evidence on the emergence of the *in silico* excitatory synaptic network underlying signal flow in a model of the neocortical microcircuit. We show that the *in silico* synaptic transmission of intra- and inter-laminar pathways match *in vitro* data to a certain extent, and identify such of those areas of mismatch for further refinement. The emergence of local PC microcircuits and an important inter-laminar pathway, the feedforward excitatory pathway from L4 to L2/3 by sheer axo-dendritic apposition of reconstructed neurons assembled within the dimensions of a neocortical microcircuit is rather striking. Our detailed simulations provide strong indications that the AP conduction velocity for inter-laminar pathways could be very different from those of intra-laminar connections. Preliminary studies by Helmstaedter *et al.* (2008) [Helmstaedter *et al.* 2008] estimate the AP conduction velocity in thin unmyelinated axons from L4SSs to L2/3PCs to be around 200 $\mu\text{m}/\text{ms}$. Interestingly, the *in silico* NCC model already predicts that with an assigned AP conduction velocity of 300 $\mu\text{m}/\text{ms}$ estimated from thicker unmyelinated axons of TTL5 neurons from Stuart *et al.* (1997) [Stuart *et al.* 1997] to modelled inter-laminar L4SS-L2/3PC connections, the latency does not match *in vitro* observations and that a lower AP conduction velocity needs to be assigned for inter-laminar pathways. In the next stage of refinement, we aim to derive estimates of AP conduction velocities for pathways based on the diameter of the presynaptic axon in the neocortical column (NCC) model. This would enable the verification of the possibility that the axons providing intra-cortical connections represent ‘delay lines’ with highly tuned latencies, depending on their diameters and myelination and how they contribute to cortical information processing [Thomson and Bannister 2003].

Currently, the axonal arbours of reconstructed L2/3PCs do not extend to innervate TTL5 neurons. This pathway from L2/3PCs to TTL5 neurons is reported to be crucial for ‘binding’ different features of a sensory stimulus for cortical information processing [Thomson and Morris 2002, Kampa *et al.* 2006]. The next refinement of the NCC model will incorporate extensively reconstructed axonal arbours of L2/3PCs to model the L2/3PC to TTL5 neuron pathway.

Through building a biologically detailed microcircuit, strong indications from *in vitro* data on the likely existence of multi-vesicular release at synaptic boutons of PCs in supra-granular layers can also be verified. Our study demonstrates that building a detailed unifying model of the excitatory synaptic network based on 3D reconstructed neurons and comparing the results of *in silico* models to *in vitro* data, one can identify functional mechanisms that are not adequately represented in the *in silico* model and further refine the biological accuracy of the model.

4.6 AUTHOR CONTRIBUTIONS

SR, SLH, IS and HM conceived and designed the experiments. SR performed the literature survey, *in silico* experiments, and analyzed the data. YW did all the *in vitro* morphological reconstructions and measured the pre and postsynaptic innervation patterns. FS and JGK designed and programmed the simulation framework. SR and HM drafted the initial version of the manuscript.

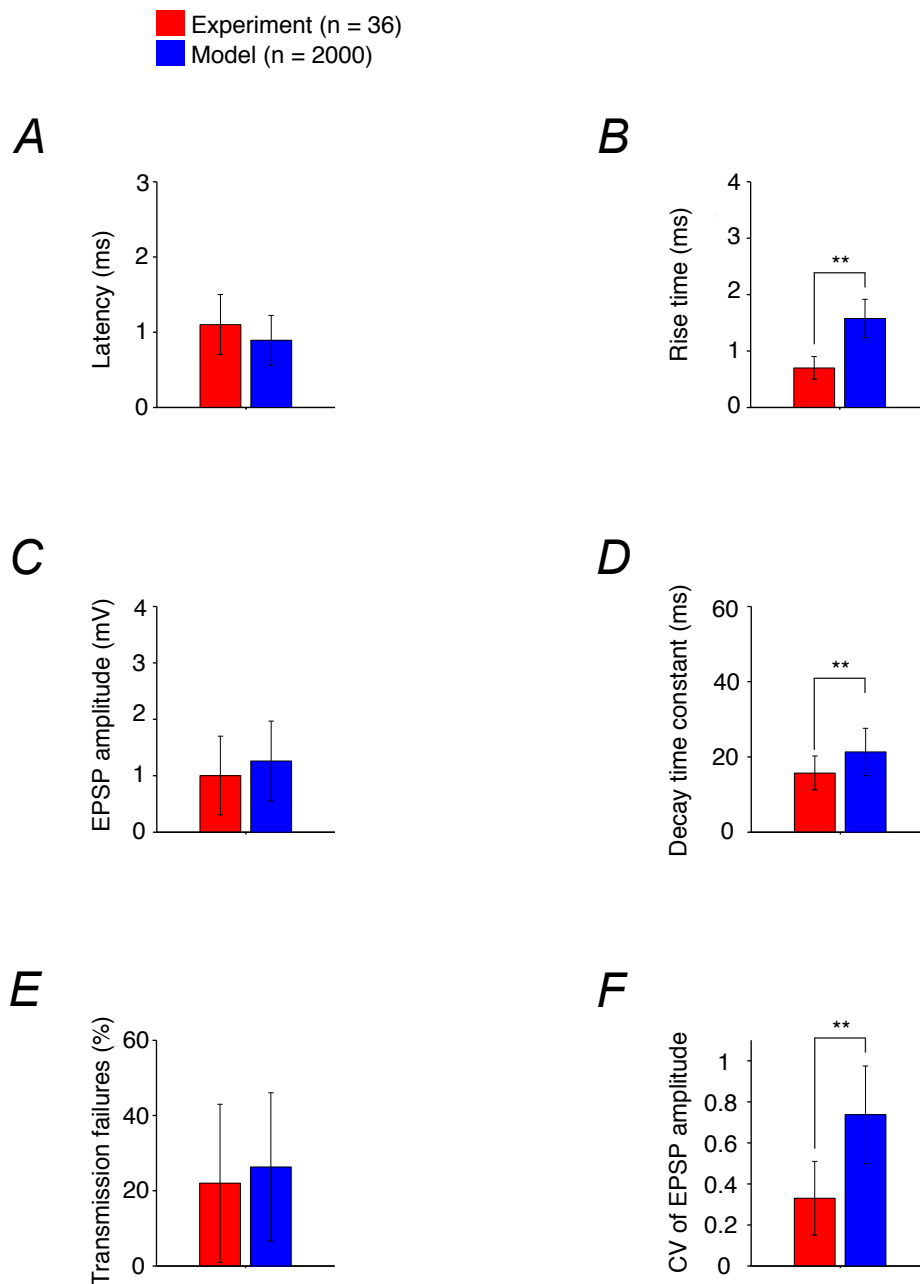


Figure 1. Ramaswamy *et al.*

Figure 4.1: The *in silico* mean latency to EPSP onset, 20 - 80% rise time, amplitude, decay time constant, transmission failures and CV of EPSP amplitude compared against *in vitro* data for L2/3PC connections. The bars in red are the mean *in vitro* measurements, corresponding mean *in silico* measurements are shown in blue. The error bar indicates the S.D. Statistical significance was tested using Fisher's exact two sample test, ** $P < 0.01$, $\alpha = 0.01$.

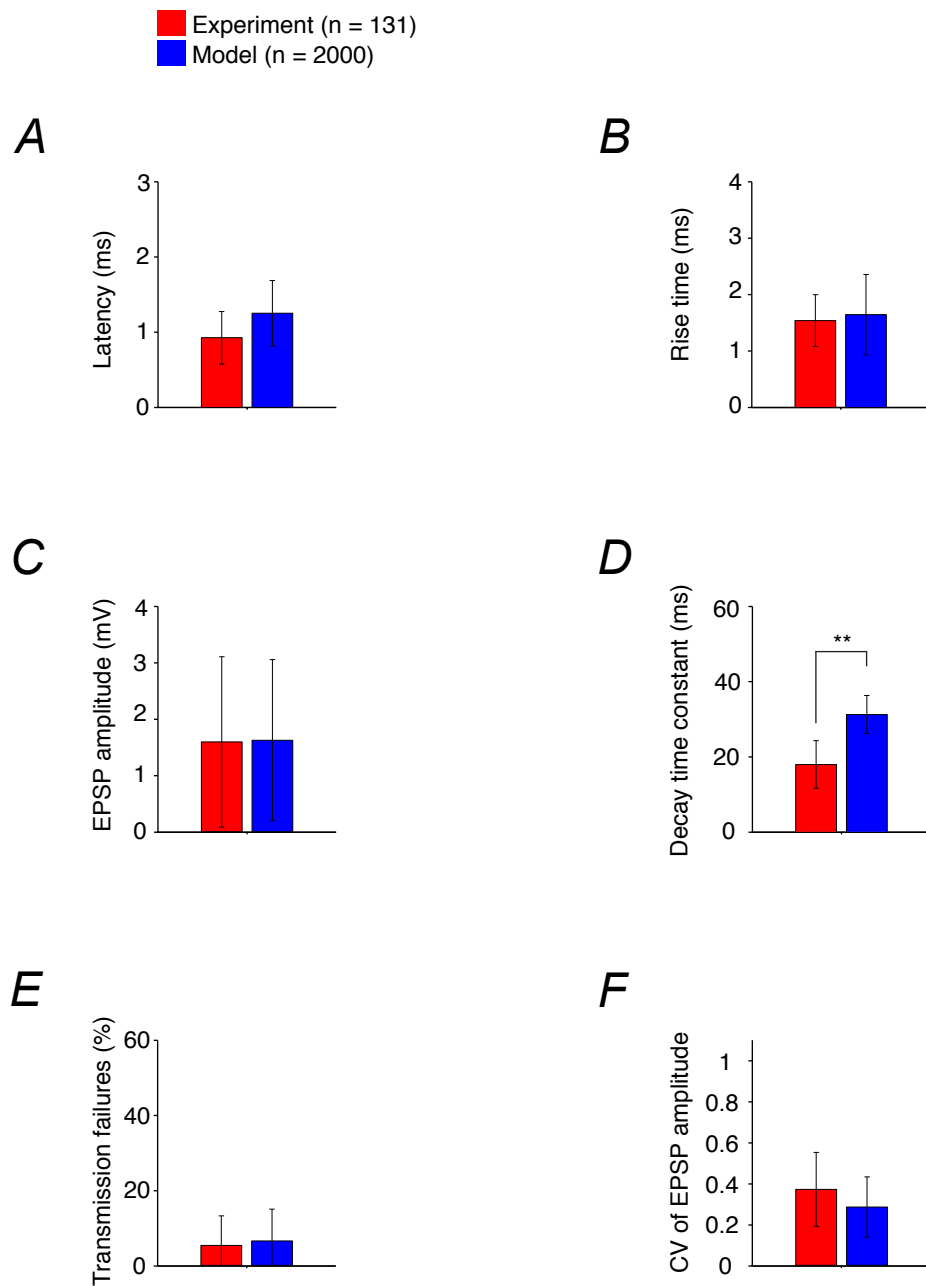


Figure 2. Ramaswamy *et al.*

Figure 4.2: The *in silico* mean latency to EPSP onset, 20 - 80% rise time, amplitude, decay time constant, transmission failures and CV of EPSP amplitude compared against *in vitro* data for L4PC connections. The bars in red are the mean *in vitro* measurements, corresponding mean *in silico* measurements are shown in blue. The error bar indicates the S.D. Statistical significance was tested using Fisher's exact two sample test, ** $P < 0.01$, $\alpha = 0.01$.

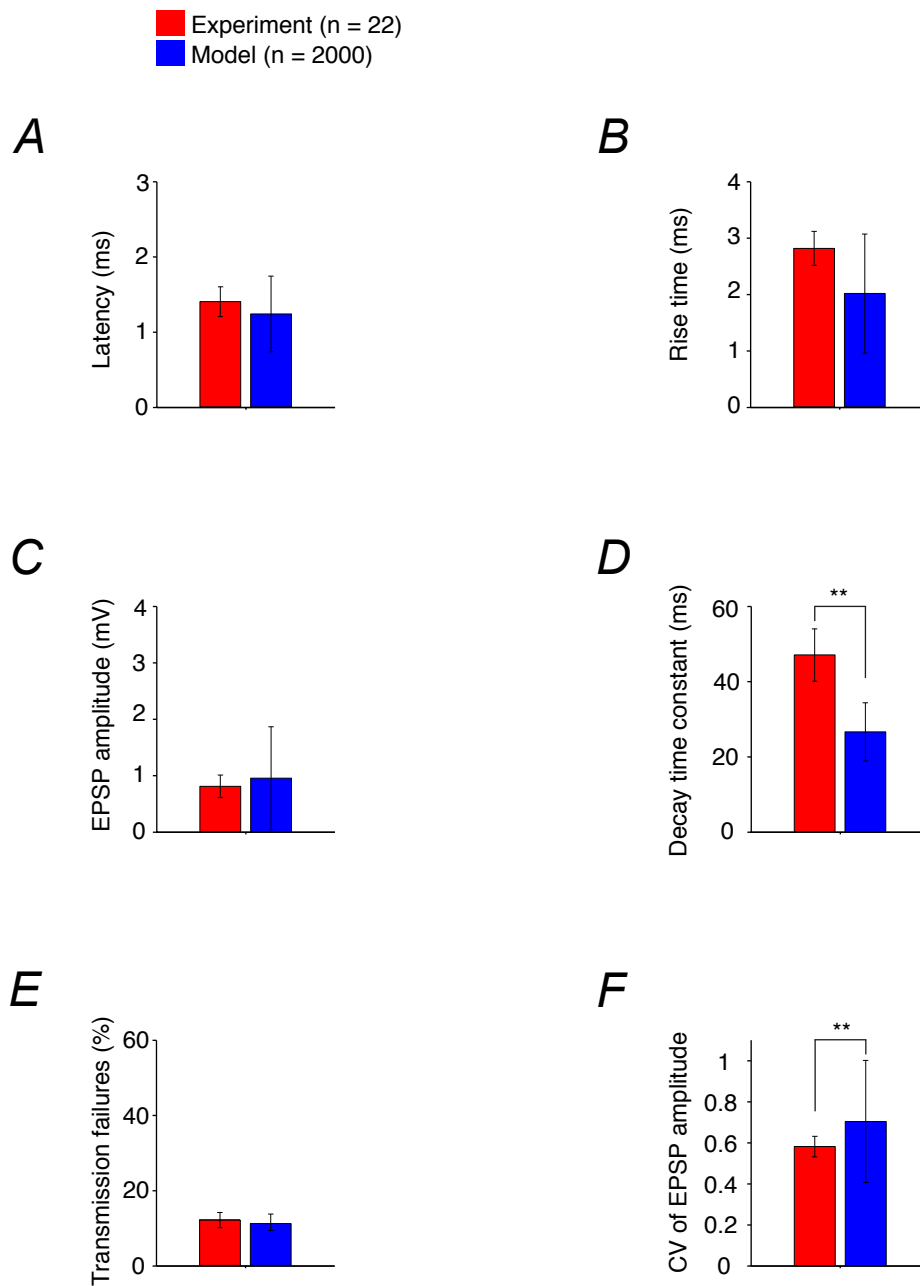


Figure 3. Ramaswamy *et al.*

Figure 4.3: The *in silico* mean latency to EPSP onset, 20 - 80% rise time, amplitude, decay time constant, transmission failures and CV of EPSP amplitude compared against *in vitro* data for L5STPC connections. The bars in red are the mean *in vitro* measurements, corresponding mean *in silico* measurements are shown in blue. The error bar indicates the S.D. Statistical significance was tested using Fisher's exact two sample test, ** $P < 0.01$, $\alpha = 0.01$.

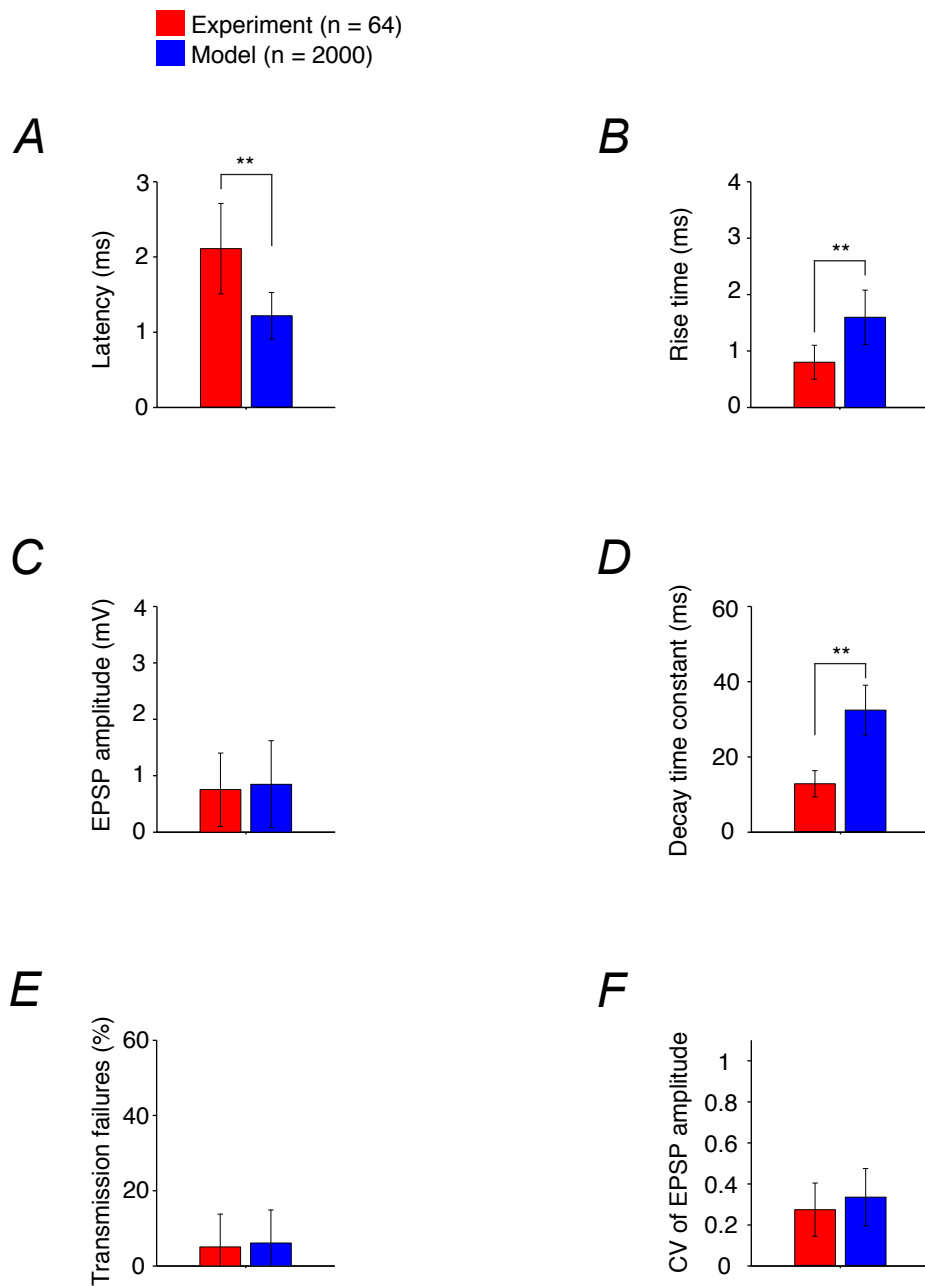


Figure 4. Ramaswamy *et al.*

Figure 4.4: The *in silico* mean latency to EPSP onset, 20 - 80% rise time, amplitude, decay time constant, transmission failures and CV of EPSP amplitude compared against *in vitro* data for L4SS - L2/3PC connections. The bars in red are the mean *in vitro* measurements, corresponding mean *in silico* measurements are shown in blue. The error bar indicates the S.D. Statistical significance was tested using Fisher's exact two sample test, ** $P < 0.01$, $\alpha = 0.01$.

Table 4.1: No. of synaptic contacts for *in silico* PC-PC connections (mean \pm S.D.). For every entry, the italicised values in parentheses indicate the *in vitro* mean \pm S.D.

<i>in silico</i> Pathway	No. of synaptic contacts/connection
L2/3PC-L2/3PC	2.6 \pm 2.4 (<i>2.8 \pm 0.7</i>)
L4PC - L4PC	3.35 \pm 3.22 (<i>3.4 \pm 1</i>)
L4SS - L2/3PC	4.2 \pm 4 (<i>4.5 \pm 0.5</i>)
L5STPC - L5STPC	3.5 \pm 2 (<i>4 \pm 1.3</i>)
L6CCPC - L6CCPC	3.4 \pm 2.7 (<i>4 \pm 0.25</i>)

Table 4.2: *In silico* synaptic transmission properties of PC-PC connections. For every entry, the italicised values in parentheses indicate the *in vitro* mean \pm S.D., where available. In case of a significant mismatch with *in vitro* data the corresponding *in silico* values are highlighted in red (Fisher's exact two sample test, $P < 0.01$, $\alpha = 0.01$).

<i>in silico</i> Pathway	EPSP Latency	Rise time	Amplitude	Decay	% Failures	CV of EPSP
L2/3PC-L2/3PC	0.9 \pm 0.3 (<i>1.1 \pm 0.4</i>)	1.6 \pm 0.3 (0.7 \pm 0.2)	1.2 \pm 0.7 (1 \pm 0.7)	21.3 \pm 6.32 (15.7 \pm 4.5)	26.3 \pm 19.7 (22 \pm 21)	0.7 \pm 0.2 (0.3 \pm 0.2)
L4PC - L4PC	1.2 \pm 0.4 (<i>1\pm0.4</i>)	1.6 \pm 0.7 (1.5 \pm 0.5)	1.6 \pm 1.4 (1.6 \pm 1.5)	31 \pm 5 (17.8 \pm 6.3)	6.5 \pm 8.5 (5.3 \pm 8)	0.3 \pm 0.14 (0.37 \pm 0.2)
L4SS - L2/3PC	1.2 \pm 0.3 (<i>2.1 \pm 0.6</i>)	1.5 \pm 0.5 (0.8 \pm 0.3)	0.8 \pm 0.7 (0.7 \pm 0.6)	32.3 \pm 6.6 (12.7 \pm 3.5)	5.9 \pm 8.9 (5 \pm 8.8)	0.33 \pm 0.14 (0.27 \pm 0.13)
L5STPC - L5STPC	1.2 \pm 0.5 (<i>1.4 \pm 0.2</i>)	2 \pm 1.05 (2.7 \pm 0.3)	0.95 \pm 0.9 (0.8 \pm 0.2)	26.5 \pm 7.7 (47 \pm 7)	12.3 \pm 2.1 (12 \pm 2)	0.7 \pm 0.3 (0.6 \pm 0.05)
L6CCPC - L6CCPC	1.9 \pm 0.7 (<i>2.1 \pm 0.8</i>)	1.5 \pm 0.4 (1.6 \pm 0.7)	1 \pm 0.6 (0.9 \pm 0.7)	30 \pm 8.1	2.5 \pm 8 (2.7)	0.4 \pm 0.2 (0.47)

INHIBITORY AND EXCITATORY PATHWAYS IN SILICO

“From reading too much, and sleeping too little, his brain dried up on him and he lost his judgement. ”

Miguel de Cervantes

In silico Synaptic Transmission of Inhibitory and Excitatory Pathways in the Neocortex

Srikanth Ramaswamy¹, Eilif Mueller¹, Werner van Geit,¹ Sean L. Hill¹, James G. King¹, Yun Wang^{2,3}, Felix Schürmann¹, Idan Segev⁴ and Henry Markram¹

¹ Brain Mind Institute, École Polytechnique Fédérale de Lausanne (EPFL), CH – 1015, Lausanne, Switzerland

² Caritas St. Elizabeth's Medical Center, Tufts University, Boston, MA 02135, USA

³ School of Optometry & Ophthalmology, Wenzhou Medical College, Wenzhou, Zhejiang, 325027, P.R.China

⁴ Institute of Life Sciences, Dept. of Neurobiology and Interdisciplinary Center for Neural Computation, Edmond Safra Campus, Givat Ram Hebrew University Jerusalem 91904, Israel

Corresponding Author: Henry Markram, PhD,
Brain Mind Institute, École Polytechnique Fédérale de Lausanne (EPFL),
CH – 1015, Lausanne, Switzerland
E-mail: henry.markram@epfl.ch
Ph. +41 21 693 9569
Fax. +41 21 693 5350

5.1 ABSTRACT

The functions performed by different neural microcircuits depend on the anatomical and physiological properties of the various synaptic pathways connecting neurons. Previous work has shown that the connectivity of reconstructed excitatory-inhibitory and inhibitory-excitatory axo-dendritic arbours significantly predicted the distributions of functional synapses in a model of the neocortical column (NCC). We investigated if the *in silico* physiology of synaptic connections also emerge from the statistical connectivity of axo-dendritic appositions in a biologically detailed model of the NCC.

5.2 INTRODUCTION

The gossamer of excitatory, inhibitory, feed-forward and feedback pathways endow the neocortical microcircuit with a high level of synaptic recurrence [Thomson et al. 2002, Markram et al. 2004, Szabadics et al. 2006]. Although excitatory pathways form an overwhelming majority, the *yin* of excitation is dynamically balanced by the *yang* of inhibition during cortical activity [Shu et al. 2003, Monier et al. 2003]. Normal cortical function is reliant on the activation of excitatory and inhibitory pathways, since an imbalance of excitation-inhibition leads to several pathologies including epilepsy [Cossart et al. 2001, Cobos et al. 2005], schizophrenia [Lewis et al. 2005], anxiety, hypersensitivity and depression [Homanics et al. 1997]. Pyramidal cells that principally mediate excitation have a rather stereotypical anatomy and electrophysiology, whereas the interneurons mediating inhibition are electrically highly diverse [Karube et al. 2004, Markram et al. 2004] and their anatomy is specialized to target specific regions of postsynaptic neurons [Somogyi et al. 1998]. In spite of tremendous advances in our knowledge of neocortical neurons and their synaptic interactions, not much is known about the properties of synaptic pathways that maintain the crucial excitation-inhibition balance.

Previous work has shown that when different reconstructed neuron types are independently and randomly positioned to build a model of the neocortical column (NCC), the statistical connectivity of axo-dendritic arbours significantly predicted the distributions of functional synapses (Hill *et al.*, submitted). Here, we discuss the emergent *in silico* synaptic response properties arising from the statistical connectivity of axo-dendritic appositions in the NCC model.

5.3 METHODS

5.3.1 3D Reconstruction

Three-dimensional neuron models were reconstructed from stained cells using the NeuroLucida system (MicroBrightField Inc., Colchester, VT, USA) and a brightfield light microscope (Olympus, Düsseldorf, Germany). After the staining procedure, there is ~25% shrinkage of the slice thickness and ~10% anisotropic shrinkage along the X- and Y-axes. Only shrinkage of thickness

is immediately accounted for and corrected. Shrinkage in the X- and Y-axes is accounted for in the morphology repair [Anwar et al. 2010].

5.3.2 Morphology Repair

The reconstructed neurons from slices usually have their somata about 50 μm beneath the slice surface. They thus lose part of their morphology. An algorithm by Anwar *et al.* [Anwar et al. 2010] attempts to recover the original anatomy of the missing part of the neuron. The algorithm preserves the morphological statistics of neuron in the repaired branches by using the intact part of the morphologies to build a statistical model that grows the cut portions. In a preparatory corrective and unraveling step, the algorithm corrects for measurement inaccuracies and tissue shrinkage while maintaining the neuron's morphological structure (branching frequency and angles). Dendrites and axons are then repaired separately. For the dendrites, we compute a dendritic 3D probability from the intact portion of the neuron, which describes the probabilistic behavior of a branch (continuing, terminating, bifurcating) of a particular order and type at a given distance from the soma. Using these Bayesian spatial distributions, the cut dendrites are regrown point by point. Axon repair is based on anatomical class statistical distributions, which are computed from a pool of the same class of neurons in the database. Sub-trees are pasted from the intact parts so that the regrown part matches the class statistics computed from the intact part. After the repair algorithm, neurons are statistically equivalent to *in vivo* neurons.

5.3.3 Circuit Building

Model microcircuits were built using the “BlueBuilder” application [Kozloski et al. 2008]. The locations of the somata were assigned randomly within their layer boundaries, the corresponding 3D morphologies were then loaded at these locations, and a touch-detection algorithm run to detect all structural appositions for all neurons in the circuit.

5.3.4 Touch detection

To account for bouton swelling and spine extension, any axo-dendritic apposition of less than 3 μm was considered a potential connection i.e. if the axon of neuron i came, at least once, within 3 μm of the dendrite of neuron j , i was said to be structurally connected to j .

5.3.5 Functionalizing structural appositions

The structural appositions in each connection were converted into functional synapses through an algorithm, constrained with *in vitro* connection probability values measured for pairs of neurons within inter-somatic distances of 50-100 μm . The microcircuits constructed in this way formed the basis for the *in silico* synaptic transmission experiments.

Table 5.1: Dynamics and parameters for *in silico* synaptic transmission in the NCC model. The parameters were mainly obtained from [Markram et al. 1997a; 1998, Gupta et al. 2000, Wang et al. 2006, Silberberg and Markram 2007]

Synapse type	Dynamics	g_{syn} (nS)	U	D(ms)	F(ms)	Decay time (ms)
I1	Inhibitory, facilitating	0.33 ± 0.27	0.016 ± 0.1	45 ± 21	376 ± 253	10.4 ± 6.2
I2	Inhibitory, depressing	0.49 ± 0.28	0.25 ± 0.13	706 ± 405	21 ± 9	8.3 ± 2.2
I3	Inhibitory, pseudo-linear	0.2 ± 0.05	0.32 ± 0.14	144 ± 80	62 ± 31	6.4 ± 1.7
E1	Excitatory, facilitating	0.3 ± 0.2	0.028 ± 0.02	194 ± 18	507 ± 37	1.7 ± 0.2
E2	Excitatory, depressing	0.3 ± 0.2	0.5 ± 0.02	671 ± 17	17 ± 5	1.7 ± 0.2
E3	Excitatory, pseudo-linear	0.3 ± 0.2	0.29 ± 0.02	329 ± 53	326 ± 66	1.7 ± 0.2

5.3.6 Dynamics and parameters of synaptic transmission

The dynamics of transmission for 6 classes of excitatory and inhibitory synapses in the NCC model are described below. Synaptic transmission was modelled with the Tsodyks-Markram phenomenological model with stochastic neurotransmitter release described in [Fuhrmann et al. 2002]. Experimentally derived values for the synaptic conductance g_{syn} (nS), utilization of synaptic efficacy (analogous to neurotransmitter release probability) U, time constant for recovery from depression D(ms), time constant for recovery from facilitation F(ms) and the conductance decay time (ms) are shown as mean \pm standard deviation (S.D.). The reversal potential for excitatory synapses E_{RevAMPA} was set to 0 mV, while the GABA_A reversal E_{RevGABA} was set to -80 mV [Silberberg and Markram 2007].

5.3.7 Mapping rules for synaptic transmission

The mapping rules to assign the dynamics of transmission for every putative synapse in the NCC model identified through the axo-dendritic overlap of 3D reconstructed neuronal arbours are described below.

5.3.8 Biophysical single neuron models

The biophysical single neuron models for both excitatory and inhibitory neurons were obtained from previously described techniques [Druckmann et al. 2007, Hay et al. 2011].

5.3.9 In silico stimulation and recording

In silico experiments were performed in the NEURON (version 7.2) simulation environment with a simulation time step (dt) of 0.025 ms [Hines and Carnevale 1997]. Simulations were run on a 128 processor rack of a BlueGene/P supercomputer accessed through the CADMOS consortium or on 32 processors of a SGI Prism parallel computer. All *in silico* experiments used the circuit,

neuron and synapse models "as-is-where-is", without any fine-tuning. To select neuron pairs for *in silico* experiments, we applied the same procedure as in previous *in vitro* studies [Gupta et al. 2000, Silberberg and Markram 2007]. From each of the 10 reconstructed microcircuits we randomly selected 200 pairs of intra- and inter-laminar PC connections within inter-somatic distances in the range $\sim 50\text{-}100\ \mu\text{m}$, thus creating a population of 2000 PC pairs from each layer examined. To evoke unitary pre-synaptic APs in model PCs, we simulated square current pulses of 5 nA for a duration of 10 ms at the soma and measured the post-synaptic response in the target model neurons.

5.3.10 Data analysis

Data analysis was carried out in MATLAB (version 7.7). We collected published data from various sources and consolidated them in a database of over 30 excitatory-excitatory, excitatory-inhibitory and inhibitory-excitatory synaptic pathways. This database served as the biological benchmark to compare the *in silico* synaptic response properties. In brief, this database contains the mean \pm S.D. of PSP amplitudes, 20 - 80% rise time, onset latency, half-width and decay time constants. Values for *in silico* connections were determined by averaging the data from 100 independent trials. Somatic EPSP amplitude was measured as the difference between baseline and peak voltage. Differences between *in vitro* and *in silico* data were tested using Fisher's exact two sample test, with $\alpha = 0.01$.

5.4 RESULTS

We characterized the anatomy and physiology in terms of the PSP amplitude of *in silico* synaptic response properties arising from the statistical connectivity of axo-dendritic appositions in the NCC model. The PSP amplitudes for several excitatory-inhibitory and inhibitory-excitatory pathways *in silico* were examined and compared against the respective biological benchmark where available. Furthermore, the *in silico* model generated predictions on the PSP amplitudes for several Excitatory-Inhibitory and Inhibitory-Excitatory pathways, which have not been characterized through *in vitro* experiments.

5.4.1 Anatomy of *in silico* Inhibitory-Excitatory and Excitatory-Inhibitory connections

The *in silico* anatomy of the mean number of synaptic contact per connection for Inhibitory-Excitatory and Excitatory-Inhibitory connections was compared against measurements from *in vitro* experiments. Pairs of synaptically connected neurons *in silico* within inter-somatic distances of 50-100 μm were sampled from the NCC model, in a manner consistent with *in vitro* experiments. The overall profile of the mean number of synaptic contacts per connection was not significantly different from *in vitro* observations ([Wang et al. 2002, Markram et al. 2004, Silberberg and Markram 2007]; see figure 5.1; test for statistical significance through Wilcoxon rank sum test, $\alpha = 0.05$). Some discrepancies were observed for specific Excitatory-Inhibitory

connections. This discrepancy could partly arise from the fact that currently, we do not have sufficient reconstructions for certain inhibitory interneuron types. Future versions of the *in silico* NCC model will be refined to include more reconstructions of layer-specific inhibitory interneuron types.

5.4.2 Physiology of *in silico* Inhibitory-Excitatory connections

IPSPs from Bipolar cells (BP) to Pyramidal cells (PC)

In silico IPSPs from BPs to L3PCs had amplitudes of 0.15 ± 0.1 mV ($n = 84$ pairs, within inter-somatic distances of $100 \mu\text{m}$) compared against 0.13 mV *in vitro* from Rozov *et al.* (2001) [Rozov *et al.* 2001], recorded at a holding potential of -57 mV. Out of several *in silico* BP to PC pathways across different layers in the NCC model, *in vitro* data for comparison currently exists only for connections from BP to L3PC (see figure 5.2).

The NCC model generated predictions on the IPSP amplitudes for other BP to PC pathways (see figure 5.2), which have not yet been characterized *in vitro*.

IPSPs from Bitufted cells (BTC) to PC

Simulated IPSPs from BTCs to L4SSs had amplitudes of about 0.2 ± 0.1 mV ($n = 6$ pairs, within inter-somatic distances of $100 \mu\text{m}$) compared against *in vitro* measurements with a mean of 0.48 ± 0.45 mV from Beierlein *et al.* (2003) [Beierlein *et al.* 2003] (see figure 5.3). The mismatch in the *in silico* and *in vitro* PSP amplitudes could be explained due to the fact that we currently do not match the mean number of synaptic contacts/connection recorded for this pathway (in the order of ~ 5 , [Beierlein *et al.* 2003]).

Out of several *in silico* BTC to PC pathways across different layers in the NCC model, *in vitro* data for comparison currently exists only for BTC to L3PC connections.

IPSPs from Chandelier cells (ChC) to PC

A complete *in vitro* characterization of the synaptic properties of ChC to PC connections is currently lacking. Therefore, simulated IPSPs from ChCs to PCs could not be compared against *in vitro* data and the values reported here are initial predictions from the *in silico* model (see figure 5.4).

In vitro experiments suggest that certain chemospecific attractor mechanisms align the axon closer towards the axon initial segment of Purkinje neurons [Ango *et al.* 2004]. In a similar manner, chemospecific mechanisms could act to guide the axons of ChCs closer towards the axon initial segment of PCs. Incorporating such mechanisms in the *in silico* model will provide stronger predictions on the functional role of the selective innervation of the axon initial segment by ChCs.

IPSPs from Double bouquet cells (DBC) to PC

Simulated IPSPs from DBCs to L₃PCs had amplitudes of 0.18 ± 0.35 mV ($n = 77$ pairs, within inter-somatic distances of 100 μ m) compared against *in vitro* measurements with a mean of 0.14 ± 0.3 mV from Ali *et al.* (2007) [Ali *et al.* 2007] (see figure 5.5). *In vitro* data to validate the *in silico* IPSP amplitudes of DBC to PC connections across other layers is currently lacking.

The *in silico* model provided predictions on the range of IPSP amplitudes from DBC to PC connections across different layers (see figure 5.5).

IPSPs from Large basket cells (LBC) to PC

Simulated IPSPs from LBCs to L₃PCs had amplitudes of 0.68 ± 0.5 mV ($n = 223$ pairs, within inter-somatic distances of 100 μ m) compared against *in vitro* measurements with a mean of 0.65 ± 0.44 mV from Thomson *et al.* (2002) [Thomson *et al.* 2002] (see figure 5.6). *In silico* IPSPs from LBCs to L₄SSs had amplitudes of 0.7 ± 0.25 mV ($n = 69$ pairs, within inter-somatic distances of 100 μ m) compared against *in vitro* values of 1.1 ± 0.8 mV from Beierlein *et al.* (2003) [Beierlein *et al.* 2003] (see figure 5.6). Mean amplitudes from LBCs to L₅TTPCs in the NCC model had amplitudes of 0.35 ± 0.2 mV ($n = 120$ pairs, within inter-somatic distances of 100 μ m; see figure 5.6). These values were significantly different from *in vitro* measurements from Thomson *et al.* (2002) [Thomson *et al.* 2002]. This discrepancy could arise due to a mismatch in the mean number of synaptic contacts for these connections in the NCC model (estimated at around 13 contacts per connection from *in vitro* experiments [Markram *et al.* 2004]).

The *in silico* model also gave predictions for IPSP amplitudes from LBC to PC connections (see figure 5.6).

IPSPs from Martinotti cells (MC) to PC

Simulated IPSPs from MCs to L₅TTPCs measured 0.3 ± 0.2 mV in amplitude ($n = 128$ pairs, within inter-somatic distances of 100 μ m) compared against *in vitro* measurements of 0.5 ± 0.4 mV, recorded at a holding potential of -57.3 mV from Silberberg & Markram (2007) [Silberberg and Markram 2007] (see figure 5.7).

The *in silico* predictions on the amplitudes of other MC to PC connections are also shown in figure 5.7.

IPSPs from Nest basket cells (NBC) to PC

Simulated IPSPs from NBCs to L₅TTPCs measured 0.9 ± 0.5 mV in amplitude ($n = 283$ pairs, within inter-somatic distances of 100 μ m) compared against *in vitro* measurements of 1.21 ± 1.18 mV from Blatow *et al.* (2003) [Blatow *et al.* 2003] (see figure 5.8).

The *in silico* predicted amplitudes of other NBC to PC connections are also indicated in figure 5.8.

IPSPs from Small basket cells (SBC) to PC

Simulated IPSPs from SBCs to L₃PCs measured 0.8 ± 0.2 mV in amplitude (n = 65 pairs, within inter-somatic distances of 100 μ m) compared against *in vitro* measurements of 1.22 ± 0.71 mV from Thomson *et al.* (1996) [Thomson *et al.* 1996] (see figure 5.9). From SBCs to L₅TTPCs, simulated IPSPs measured 0.7 ± 0.2 mV (n = 38 pairs, within inter-somatic distances of 100 μ m) compared against *in vitro* measurements of 1.1 ± 0.6 mV from Thomson *et al.* (1996) [Thomson *et al.* 1996] (see figure 5.9). These *in silico* experiments were performed by holding the postsynaptic PC at a membrane voltage of -55 mV to replicate the *in vitro* recording conditions [Thomson *et al.* 1996].

The *in silico* predictions on the amplitudes of other MC to PC connections are indicated in figure 5.9.

5.4.3 *Physiology of in silico Excitatory-Inhibitory connections*

EPSPs from Layer 2 PCs (L2PC) to Interneurons (IN)

Simulated EPSPs from L₂PCs to BTCs had amplitudes of 0.38 ± 0.3 mV (n = 100 pairs, within inter-somatic distances of 100 μ m) compared against *in vitro* measurements of 0.22 ± 0.19 mV from Koester & Johnston (2005) [Koester and Johnston 2005] (see figure 5.10). The NCC model predicted *in silico* EPSP amplitudes measuring 0.6 ± 0.1 mV for L₂PC to MC connections (n = 100 pairs, within inter-somatic distances of 100 μ m) compared against *in vitro* observations of 0.72 ± 0.08 mV from Lu *et al.* (2007) [Lu *et al.* 2007] (see figure 5.10).

The NCC model also generated predictions for EPSP amplitudes from L₂PC to other IN connections (see figure 5.10).

EPSPs from Layer 3 PCs (L3PC) to IN

The characterization of EPSP amplitudes from L₃PCs to other INs is by far the most extensive, in comparison to data sets for IPSP (see Physiology of *in silico* Inhibitory-Excitatory connections) or EPSP characterizations in other neocortical layers.

In silico EPSP amplitudes from L₃PC to NBCs measured 0.7 ± 0.3 mV (n = 150 pairs, within inter-somatic distances of 100 μ m) compared against *in vitro* measurements of 0.38 ± 0.25 mV from Blatow *et al.* (2003) [Blatow *et al.* 2003] (see figure 5.11). EPSP amplitudes *in silico* for connections from L₃PCs to LBCs were measured to be 1.3 ± 0.2 mV (n = 150 pairs, within inter-somatic distances of 100 μ m) compared against *in vitro* measurements of 1.9 ± 1.6 mV from Thomson *et al.* (2002) [Thomson *et al.* 2002] (see figure 5.11). For connections from L₃PCs to BTCs, the *in silico* EPSP amplitudes were 0.35 ± 0.2 mV (n = 150 pairs, within inter-somatic distances of 100 μ m) compared against *in vitro* measurements of 0.24 ± 0.2 mV from Ali *et al.* (2007) [Ali *et al.* 2007] (see figure 5.11). *In silico* EPSP amplitudes from L₃PCs to BPs measured 1 ± 0.2 mV (n = 63 pairs, within inter-somatic distances of 100 μ m) compared against *in vitro* measurements

of 1.35 mV from Rozov *et al.* (2001) [Rozov *et al.* 2001](see figure 5.11). *In silico* L3PC to DBC connections had amplitudes of 0.45 ± 0.4 mV ($n = 77$ pairs, within inter-somatic distances of 100 μm) as against *in vitro* amplitudes of 0.41 ± 0.2 mV from Thomson & Deuchars (1997) [Thomson and Deuchars 1997] (see figure 5.11). *In silico* EPSPs from L3PCs to MCs measured 0.7 ± 0.06 mV ($n = 82$ pairs, within inter-somatic distances of 100 μm) as against of 0.72 ± 0.08 mV from Lu *et al.* (2007) [Lu *et al.* 2007](see figure 5.11).

EPSPs from Layer 4 PCs (L4PC) to IN

Currently, there is a lack of *in vitro* data for interactions from L4PCs to IN types in layer 4. The NCC model provided predictions for the range of EPSP amplitudes from L4PCs to INs (see figure 5.12). Further *in vitro* experiments would be necessary to validate the predicted *in silico* amplitudes.

EPSPs from Layer 4 Spiny stellates (L4SS) to IN

In silico EPSP amplitudes from L4SSs to DBCs in layer 4 measured 0.42 ± 0.3 mV ($n = 59$ pairs, within inter-somatic distances of 100 μm) as against *in vitro* measurements of 0.3 ± 0.5 mV from Beierlein *et al.* (2003) [Beierlein *et al.* 2003](see figure 5.13).

The NCC model provided further predictions on EPSP amplitudes for connections from L4SSs to other IN types in layer 4 (see figure 5.13).

EPSPs from Layer 5 Slender-tufted PCs (L5STPC) to IN

Currently, there is a lack of *in vitro* data for interactions from L5STPCs to IN types in layer 5. The NCC model provided predictions for the range of *in silico* EPSP amplitudes from L5STPCs to IN types in layer 5 (see figure 5.14). Further *in vitro* experiments would be necessary to validate the predicted *in silico* amplitudes for connections from L5STPCs to INs in layer 5.

EPSPs from Layer 5 Thick-tufted PCs (L5TTPC) to IN

In silico EPSP amplitudes from L5TTPCs to SBCs in layer 5 were measured to be 1.9 ± 0.2 mV ($n = 46$ pairs, within inter-somatic distances of 100 μm) as against 1.95 ± 0.2 mV *in vitro* from Angulo *et al.* 1999 [Angulo *et al.* 1999] (see figure 5.15). EPSP amplitudes from L5TTPCs to DBCs in layer 5 were measured to be 0.6 ± 0.4 mV ($n = 34$ pairs, within inter-somatic distances of 100 μm) as against 0.65 ± 0.5 mV *in vitro* from Thomson & Deuchars (1997) [Thomson and Deuchars 1997] (see figure 5.15). From L5TTPCs to MCs in layer 5, *in silico* EPSP amplitudes measured 0.25 ± 0.3 mV ($n = 40$ pairs, within inter-somatic distances of 100 μm) as against 0.28 ± 0.3 mV *in vitro* from Silberberg & Markram (2007) [Silberberg and Markram 2007] (see figure 5.15).

The NCC model provided predictions for *in silico* EPSP amplitudes from L5TTPCs to IN types in layer 5 (see figure 5.15).

EPSPs from Layer 6 Cortico-cortical PCs (L6CCPC) to IN

Currently, there is a lack of *in vitro* data for interactions from L6CCPCs to IN types in layer 6. The NCC model provided predictions for the range of *in silico* EPSP amplitudes from L6CCPCs to IN types in layer 6 (see figure 5.16). Further *in vitro* experiments would be necessary to validate the predicted *in silico* amplitudes for connections from L6CCPCs to INs in layer 6 (see figure 5.16)

EPSPs from Layer 6 Cortico-thalamic PCs (L6CTPC) to IN

In silico EPSP amplitudes from L6CTPCs to SBCs in layer 6 were measured to be 0.25 ± 0.4 mV ($n = 53$ pairs, within inter-somatic distances of $100 \mu\text{m}$) as against 0.27 ± 0.4 mV *in vitro* (unpublished observations from Thomson *et al.*; see figure 5.17). EPSP amplitudes from L6CTPCs to MCs in layer 6 were measured to be 0.2 ± 0.15 mV ($n = 34$ pairs, within inter-somatic distances of $100 \mu\text{m}$) as against 0.17 ± 0.15 mV *in vitro* from West *et al.* (2006) [West *et al.* 2006] (see figure 5.17).

The NCC model provided predictions for the range of *in silico* EPSP amplitudes from L6CTPCs to other IN types in layer 6 (see figure 5.17).

5.5 DISCUSSION

These results demonstrate for the first time that when different reconstructed neuron types are independently and randomly positioned to build a model of the neocortical column (NCC), the statistical connectivity of axo-dendritic arbours gives rise to emergent *in silico* synaptic response properties. Some discrepancies were observed in the anatomical properties for the mean number of synaptic contacts per connection for certain Excitatory-Inhibitory connections. This discrepancy could partly arise from the fact that currently, we do not have sufficient reconstructions for certain inhibitory interneuron types. Future versions of the *in silico* NCC model will be refined to include more reconstructions of layer-specific inhibitory interneuron types. Among other crucial refinements, incorporating rules of chemospecific mechanisms that guide the axons of certain axo-axonic cells (for eg. ChCs) closer towards the axon initial segment of PCs, in the *in silico* model will provide stronger predictions on the functional role of the selective innervation of the axon initial segment by ChCs.

In an exhaustive *in silico* characterization of a myriad of excitatory-inhibitory and inhibitory-excitatory connections, we show that while quite a few *in silico* pathways match the *in vitro* values, there is a mismatch in some cases. This mismatch could arise due to several reasons, the foremost among them being the space-clamp error that could significantly underestimate the synaptic conductance values estimated from *in vitro* experiments. A correction must therefore be applied in order to compensate for this anomaly in the estimated synaptic conductance by

perhaps scaling them sufficiently such that the mismatching *in silico* IPSP amplitudes match *in vitro* observations.

Furthermore, the somatic GABA_a reversal potential is also a matter of debate. Previous studies have shown that the Cl⁻ pump is expressed as a somato-dendritic gradient in neurons in the juvenile rodent neocortex [Ben-Ari 2002]. It is known through studies of the Martinotti disynaptic loop that inhibitory depressing connections from MCs to PCs have a very hyperpolarized somatic GABA_a reversal of around -88 mV [Silberberg and Markram 2007]. It remains to be seen, however, if this is the case for only these connections due to the characteristic innervation of distal tufts of PCs from MCs or if connections from other interneurons to PCs also have a more hyperpolarized GABA_a reversal than usually predicted by the Nernst equation.

The single neuron models we currently use for inhibitory neurons are passive with somatically distributed ion channel mechanisms. Further studies call for investigating the effect of the integration of synaptic input through active dendrites, and for a characterization of ion channel types and their detailed distributions along dendrites of neocortical inhibitory interneurons.

Further refinements to the *in silico* model would also entail the incorporation of pathway specific slow inhibition by GABA_b, observed predominantly in the superficial layers of the neocortex by Olah *et al.* (2007) [Oláh *et al.* 2007] and Muralidhar *et al.* (in preparation).

The reconstructed *in silico* microcircuit can be used for purely exploratory studies to test the existence of specific connectivity motifs and the arising predictions could pave the way for the design of carefully targeted experiments to enable a better understanding of the principles of neocortical connectivity.

5.6 AUTHOR CONTRIBUTIONS

SR, EM, SLH, IS and HM conceived and designed the experiments. SR collected *in vitro* data through literature search, performed *in silico* experiments, and analyzed the data. WvG constructed the interneuron models. YW reconstructed the neuron morphologies. FS and JGK designed and programmed the simulation framework.

Table 5.2: Mapping rules for synaptic dynamics. For every given Morpho-Electrical (ME) type in the NCC model, the synapse type onto PCs and from PCs is indicated. Connections from INs to INs are of the type I₂ (inhibitory, depressing). The rules were mainly obtained from [Markram et al. 1997a; 1998, Gupta et al. 2000, Markram et al. 2004, Wang et al. 2006]. For an explanation of the ME types, see 4.

ME type	onto PCs	from PCs	ME type	onto PCs	from PCs
NGC cAD	I ₂	E ₂	LBC dFS	I ₂	E ₂
NGC cFS	I ₂	E ₂	LBC dST	I ₂	E ₂
NGC dNA	I ₂	E ₂	NBC bNA	I ₂	E ₂
MC bAD	I ₂	E ₁	NBC cAD	I ₂	E ₁
MC cAD	I ₂	E ₁	NBC bAD	I ₂	E ₁
MC cFS	I ₂	E ₁	NBC cFS	I ₃	E ₂
MC cNA	I ₂	E ₁	NBC cNA	I ₃	E ₂
MC dFS	I ₂	E ₁	NBC dFS	I ₂	E ₂
MC bST	I ₃	E ₁	NBC dST	I ₂	E ₂
BP bIS	I ₃	E ₂	NBC cST	I ₃	E ₂
BP bNA	I ₃	E ₂	NBC bST	I ₃	E ₂
BP cAD	I ₂	E ₂	SBC bNA	I ₂	E ₂
BP cNA	I ₁	E ₂	SBC cAD	I ₁	E ₂
BTC bAD	I ₂	E ₂	SBC cFS	I ₃	E ₂
BTC bIS	I ₂	E ₂	SBC cNA	I ₃	E ₂
BTC bNA	I ₁	E ₂	SBC dFS	I ₂	E ₂
BTC cAD	I ₂	E ₁	ChC cAD	I ₂	E ₂
BTC cFS	I ₁	E ₂	ChC dNA	I ₂	E ₂
BTC cNA	I ₃	E ₂	ChC cFS	I ₂	E ₂
DBC bAD	I ₂	E ₂	L2PC cAD	E ₂	E ₂
DBC bNA	I ₁	E ₂	L3PC cAD	E ₂	E ₂
DBC cAD	I ₂	E ₁	L4PC cAD	E ₂	E ₂
DBC cNA	I ₁	E ₂	L4SS cST	E ₂	E ₂
LBC bAD	I ₃	E ₂	L4SS cAD	E ₂	E ₂
LBC bNA	I ₂	E ₂	L5TTPC cAD	E ₂	E ₂
LBC cAD	I ₁	E ₁	L5UTPC cAD	E ₂	E ₂
LBC cFS	I ₂	E ₂	L6CTPC cAD	E ₂	E ₂
LBC cST	I ₂	E ₂	L6CCPC cAD	E ₂	E ₂
LBC cNA	I ₂	E ₂	L6CLPC cAD	E ₂	E ₂

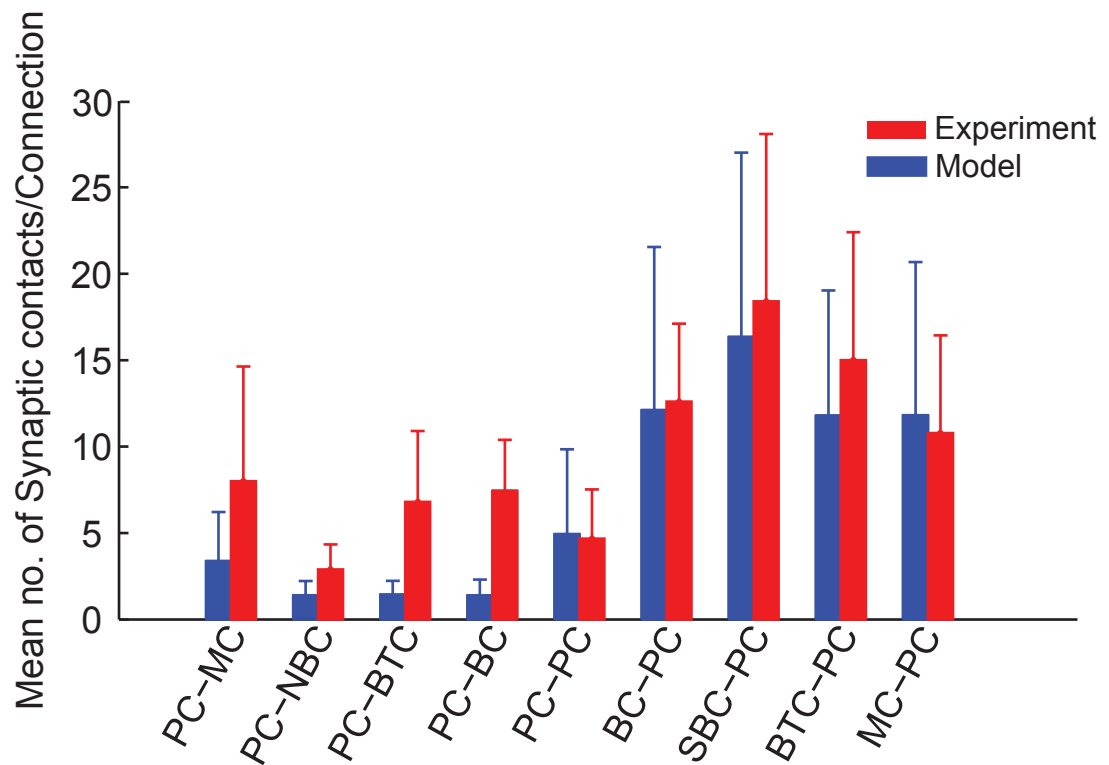


Figure 1. Mean number of synaptic contacts per connection

Figure 5.1: Mean number of synaptic contacts per connection for *in silico* Inhibitory-Excitatory and Excitatory-Inhibitory connections compared against *in vitro* data. Bars in red and blue respectively show the mean number of synaptic contacts per connection for *in vitro* and *in silico* pathways. The variability in terms of standard deviation is shown by vertical error bars.

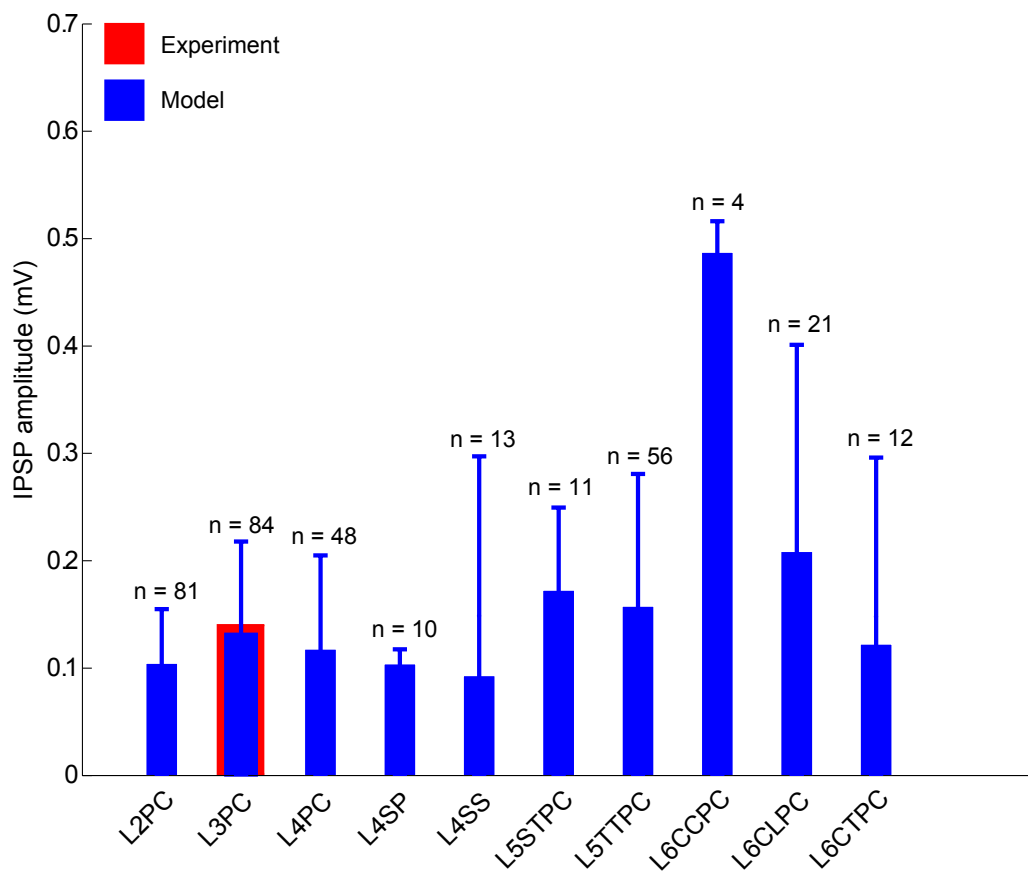


Figure 2. Mean IPSP amplitudes from BP to PC

Figure 5.2: Mean *in silico* IPSP amplitudes from BP to PCs

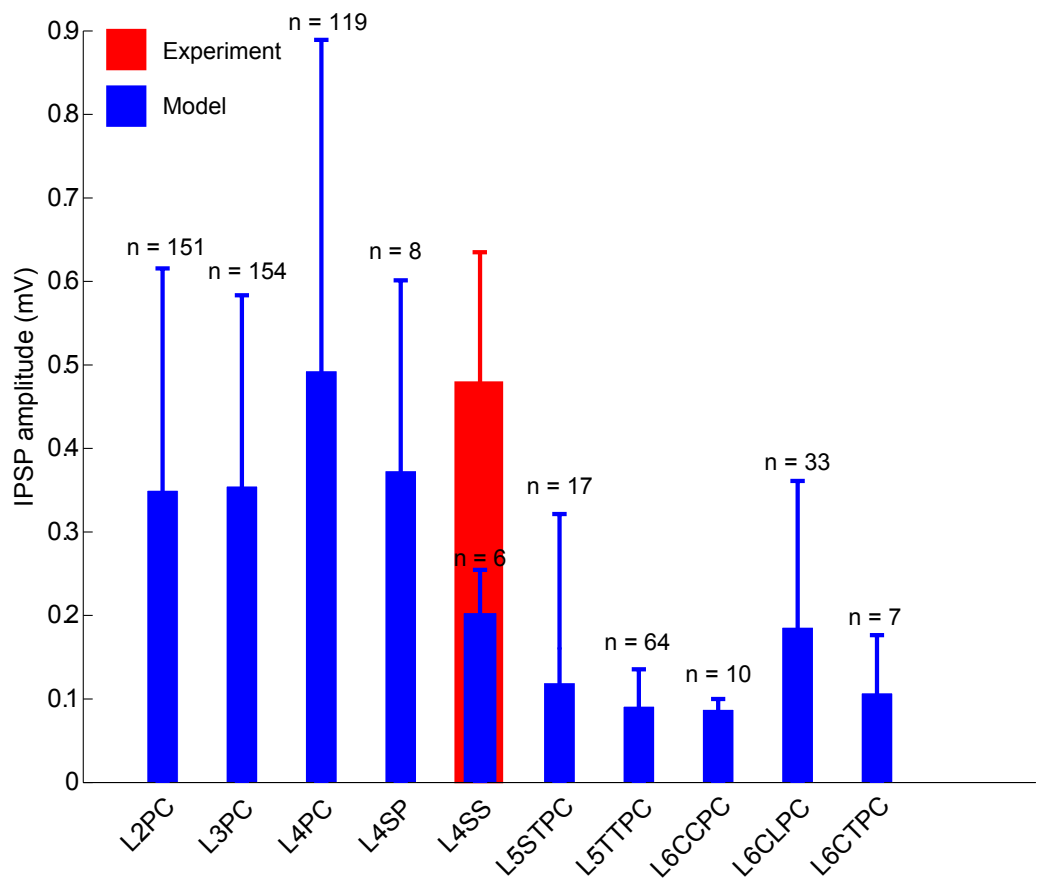


Figure 3. Mean IPSP amplitudes from BTC to PC

Figure 5.3: Mean IPSP amplitudes from BTC to PC

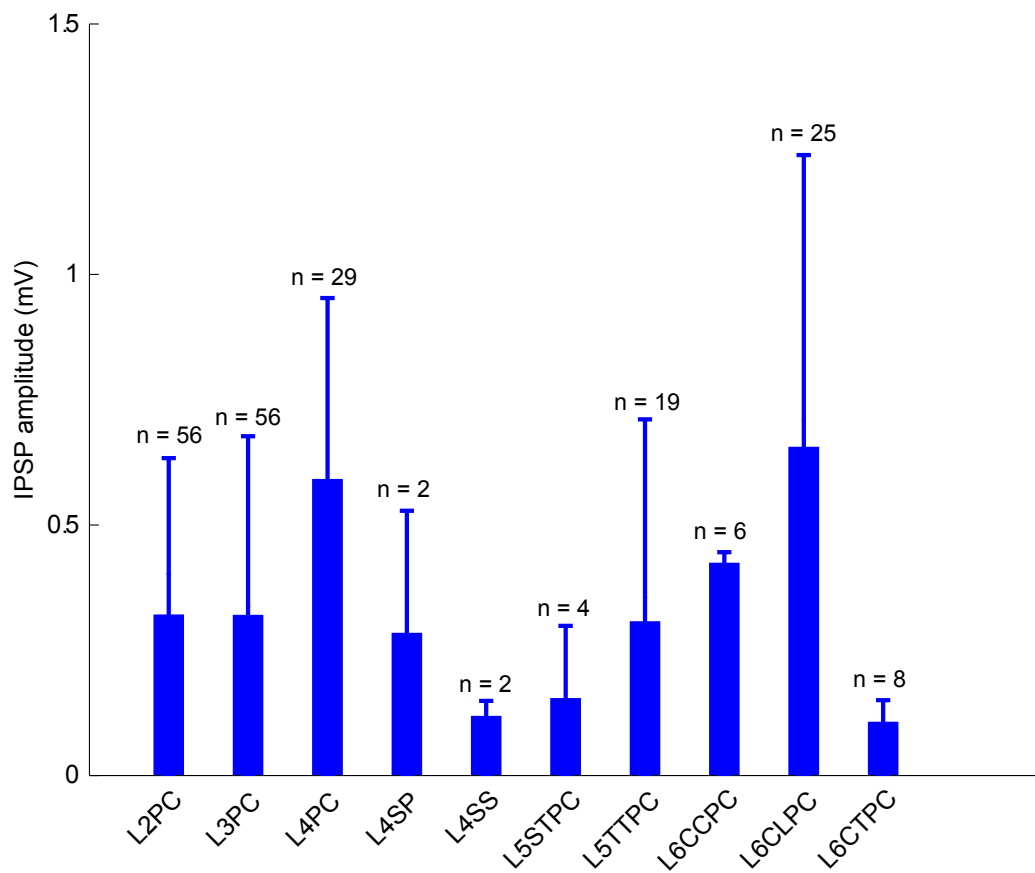


Figure 4. Mean IPSP amplitudes from ChC to PC

Figure 5.4: Mean IPSP amplitudes from ChC to PC

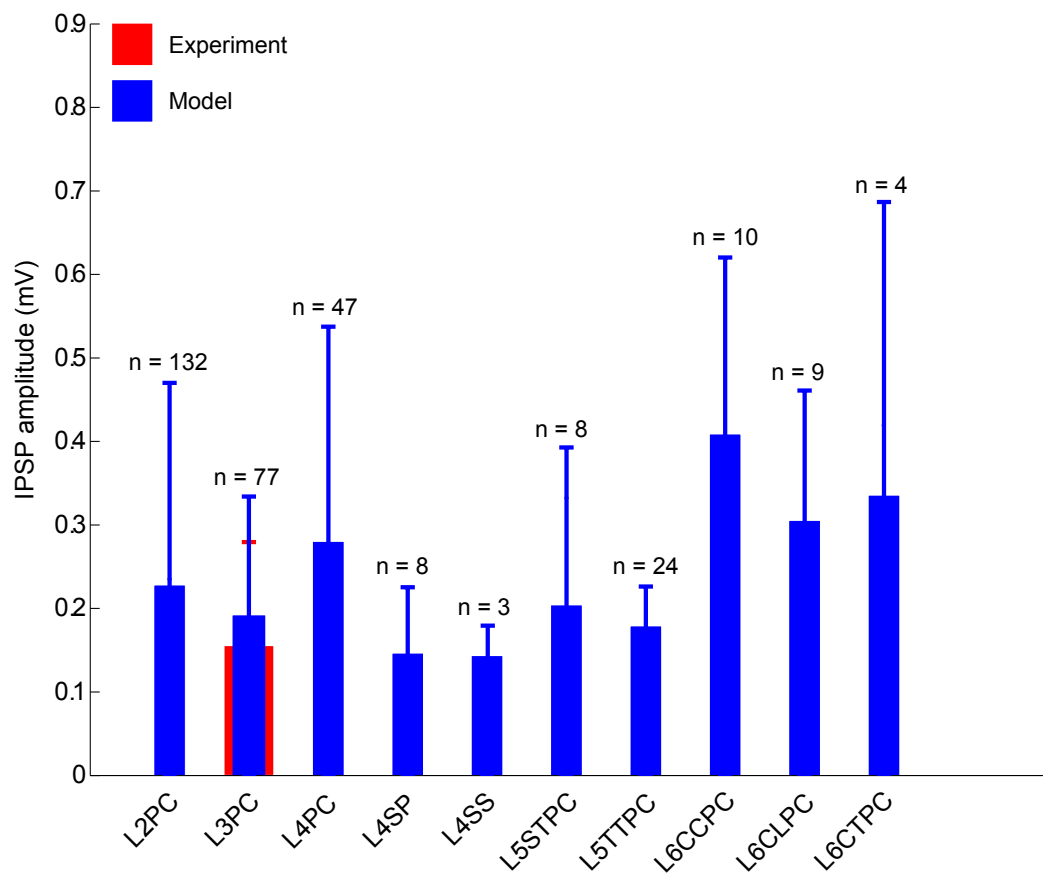


Figure 5. Mean IPSP amplitudes from DBC to PC

Figure 5.5: Mean IPSP amplitudes from DBC to PC

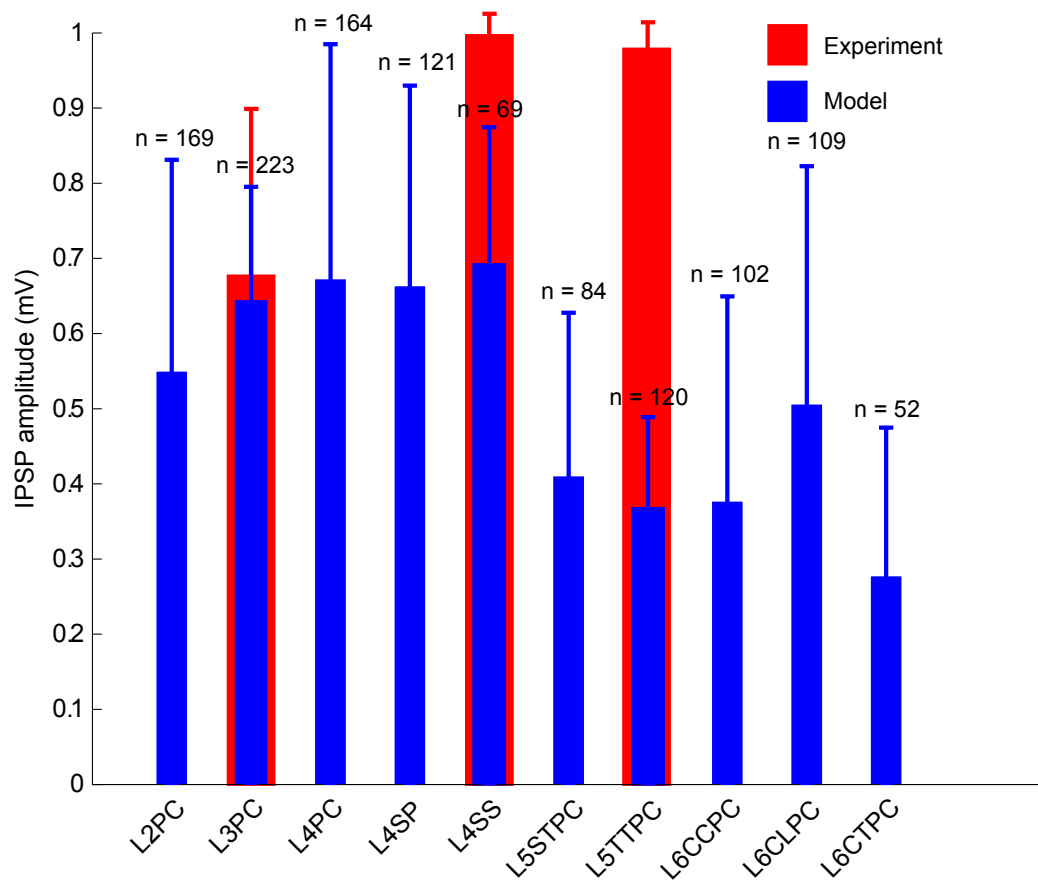


Figure 6. Mean IPSP amplitudes from LBC to PC

Figure 5.6: Mean IPSP amplitudes from LBC to PC

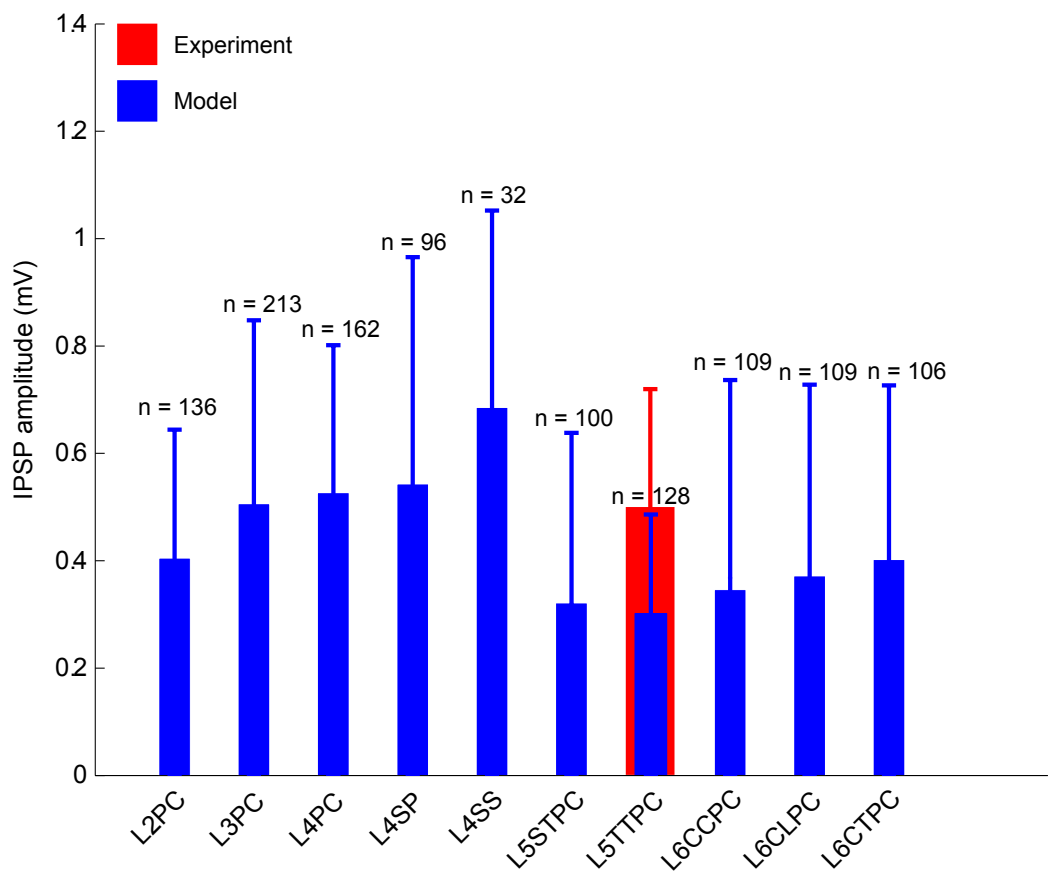


Figure 7. Mean IPSP amplitudes from MC to PC

Figure 5.7: Mean IPSP amplitudes from MC to PC

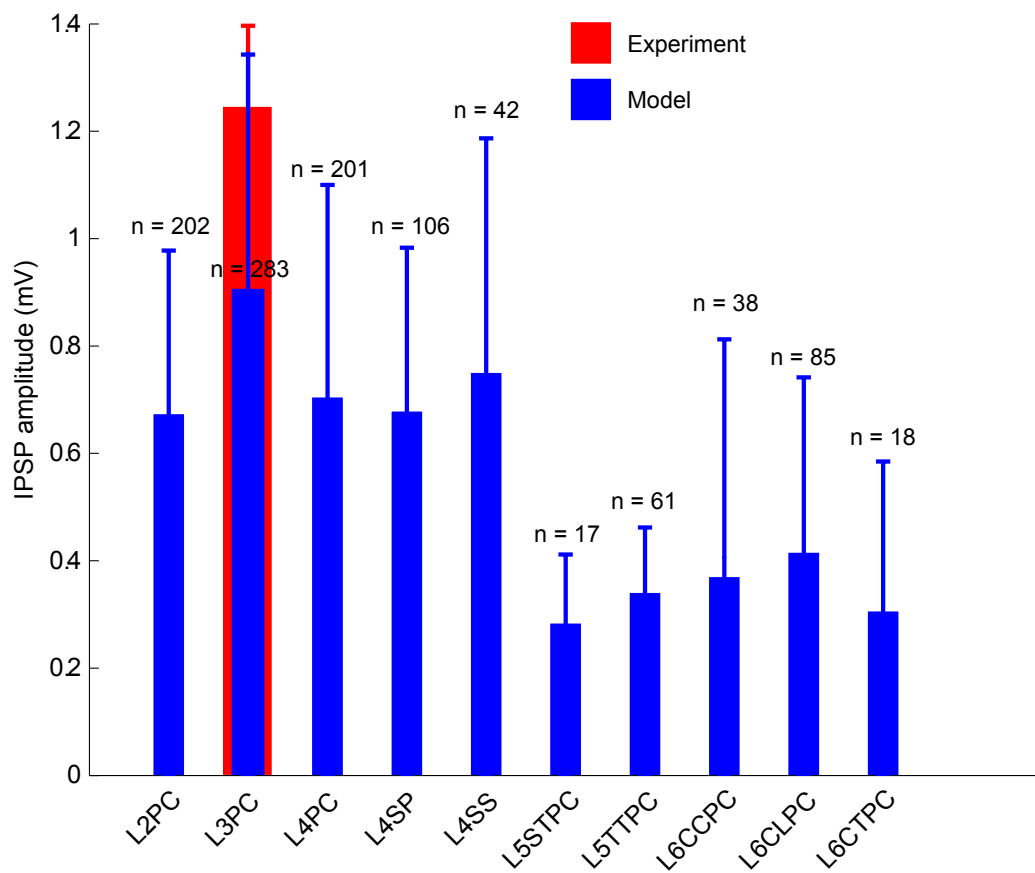


Figure 8. Mean IPSP amplitudes from NBC to PC

Figure 5.8: Mean IPSP amplitudes from NBC to PC

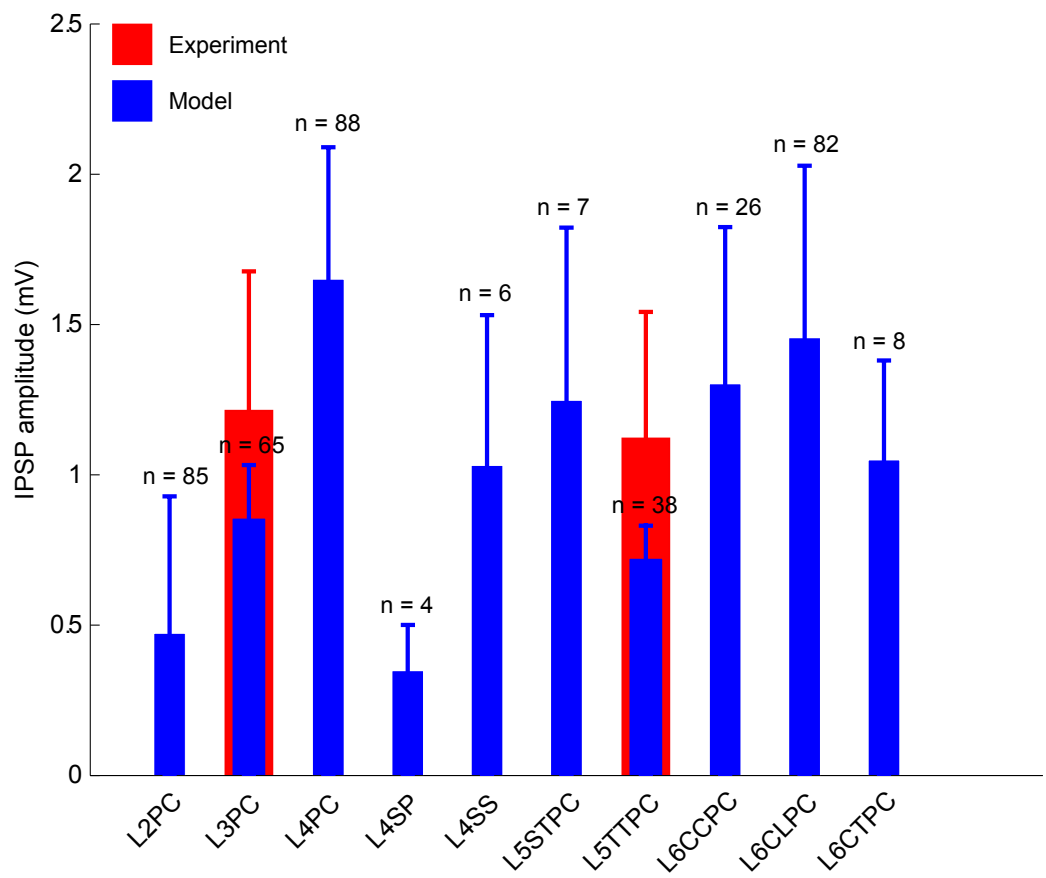


Figure 9. Mean IPSP amplitudes from SBC to PC

Figure 5.9: Mean IPSP amplitudes from SBC to PC

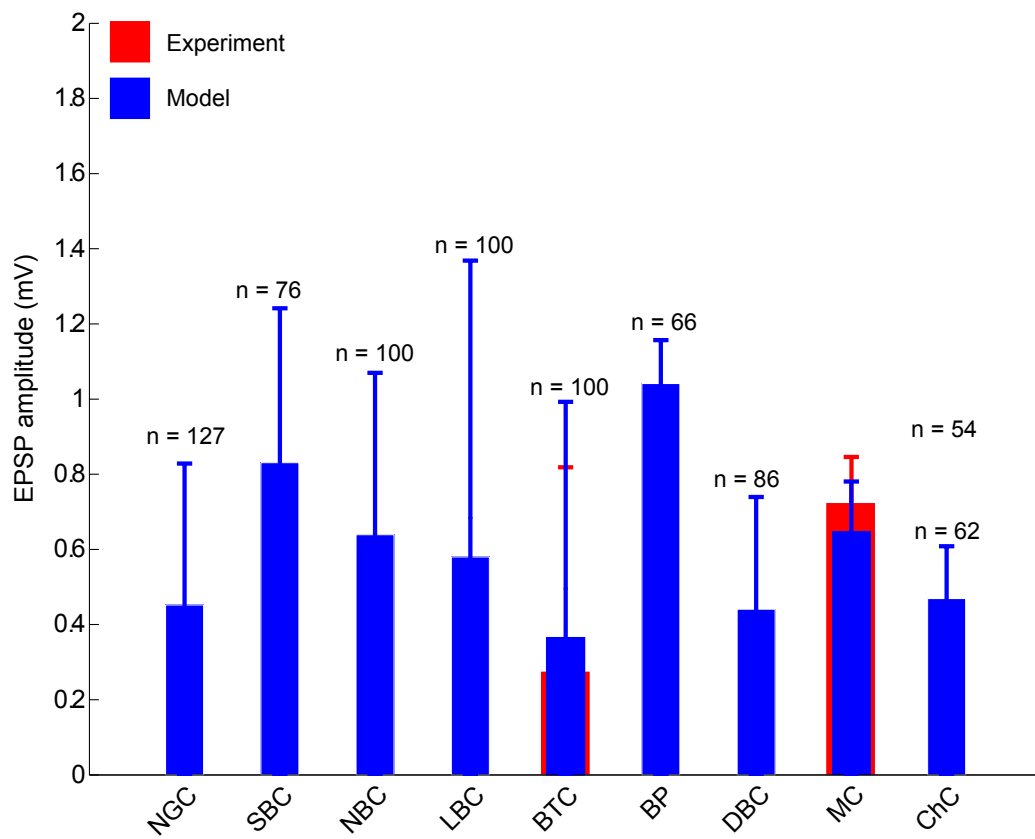


Figure 10. Mean EPSP amplitudes from L2PC to IN

Figure 5.10: Mean EPSP amplitudes from L2PC to IN

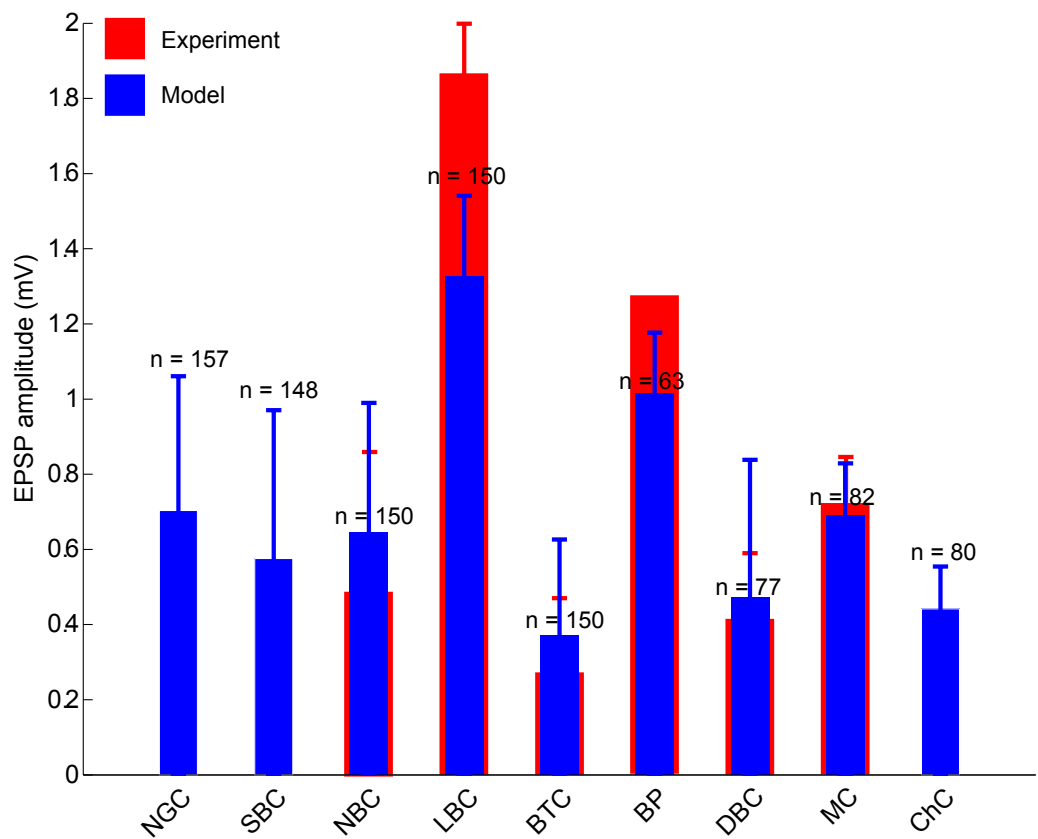


Figure 11. Mean EPSP amplitudes from L3PC to IN

Figure 5.11: Mean EPSP amplitudes from L₃PC to IN

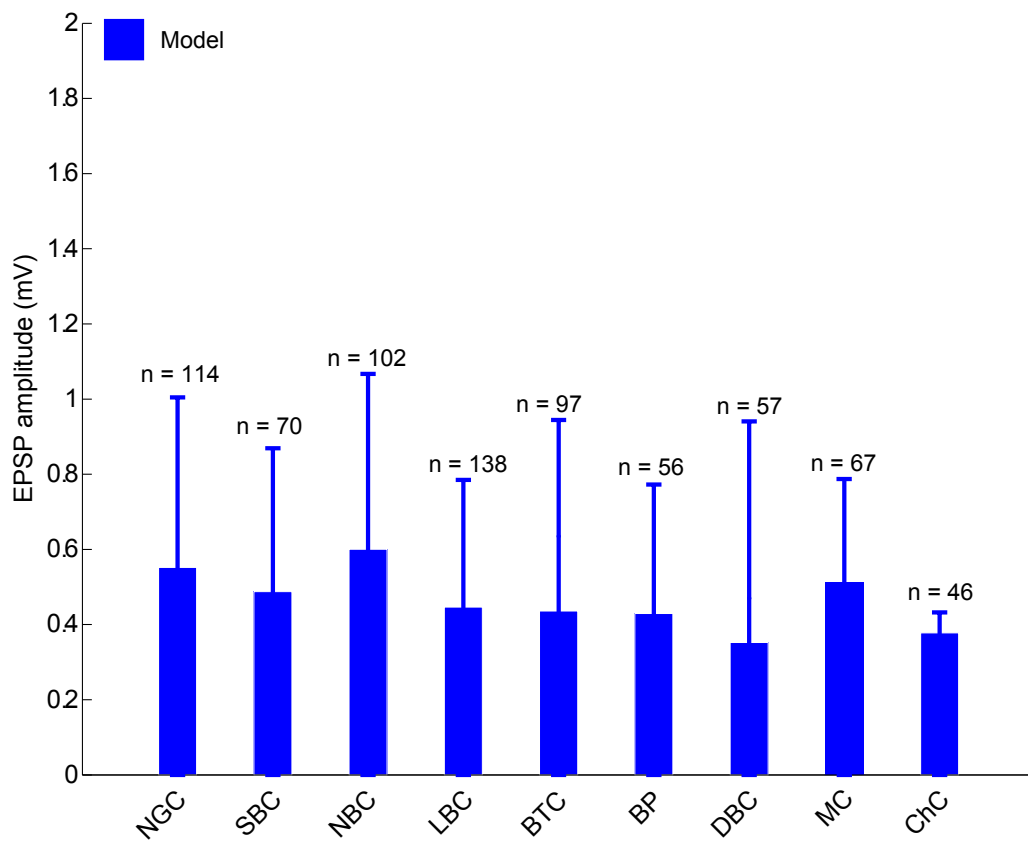


Figure 12. Mean EPSP amplitudes from L4PC to IN

Figure 5.12: Mean EPSP amplitudes from L4PC to IN

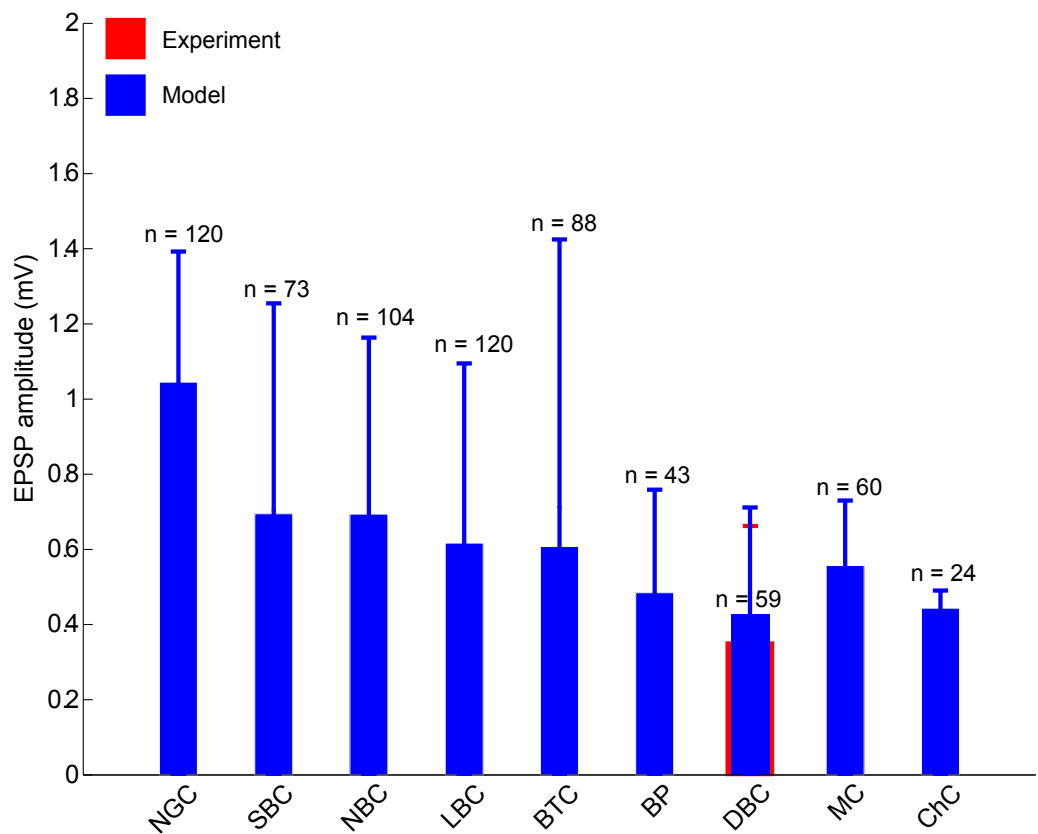


Figure 13. Mean EPSP amplitudes from L4SS to IN

Figure 5.13: Mean EPSP amplitudes from L4SS to IN

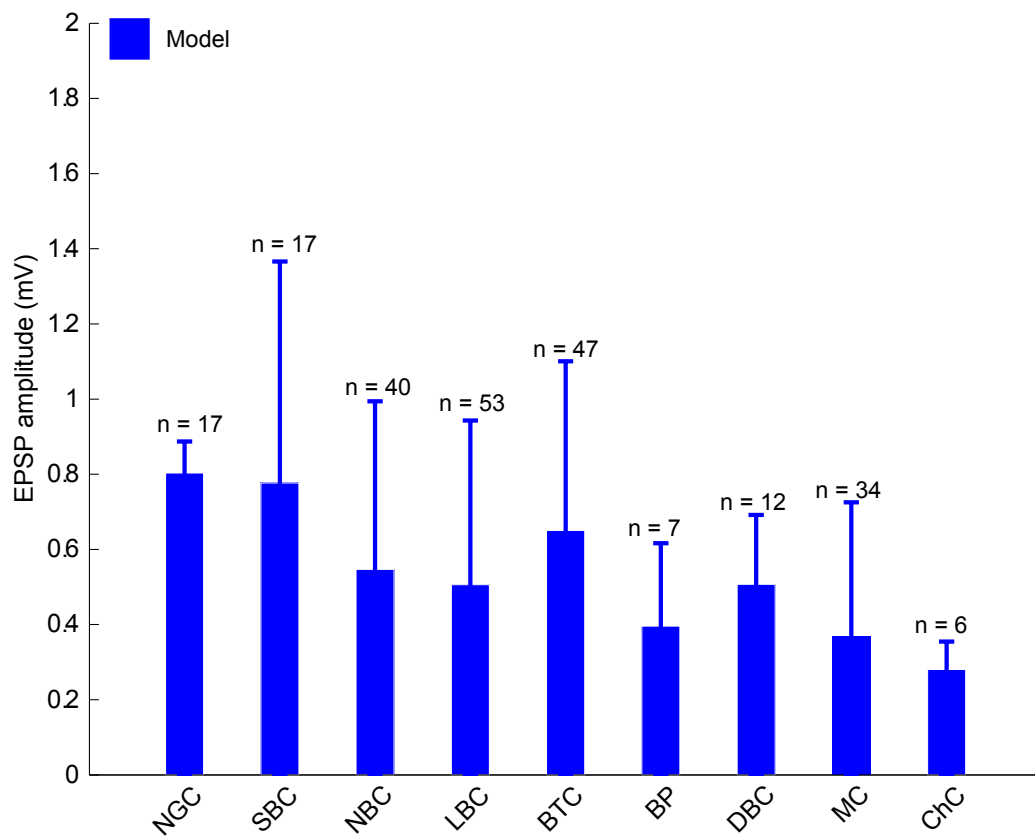


Figure 14. Mean EPSP amplitudes from L5STPC to IN

Figure 5.14: Mean EPSP amplitudes from L5STPC to IN

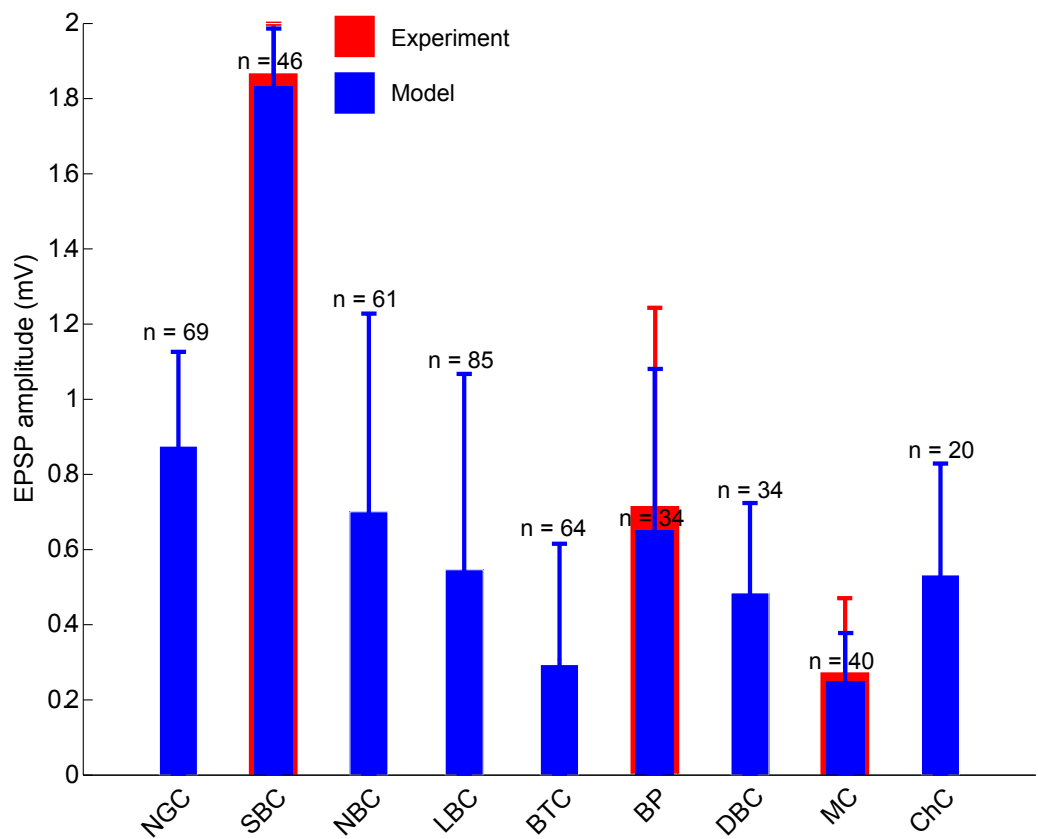


Figure 15. Mean EPSP amplitudes from L5TTPC to IN

Figure 5.15: Mean EPSP amplitudes from L5TTPC to IN

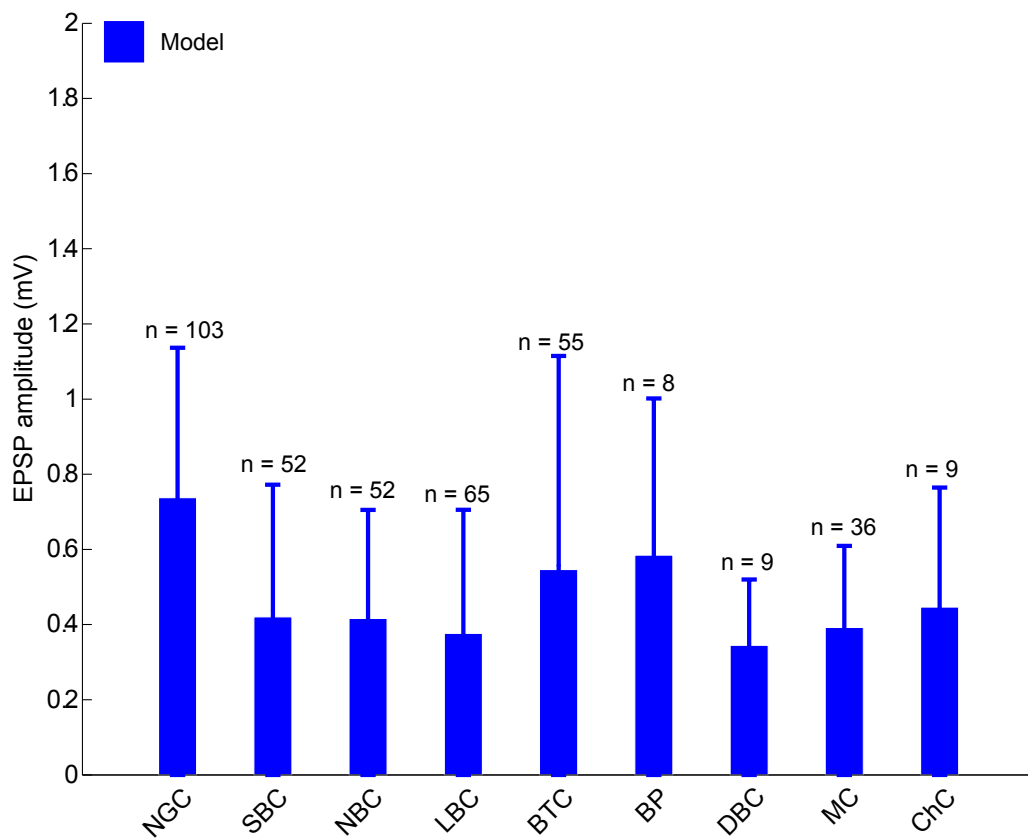


Figure 16. Mean EPSP amplitudes from L6CCPC to IN

Figure 5.16: Mean EPSP amplitudes from L6CCPC to IN

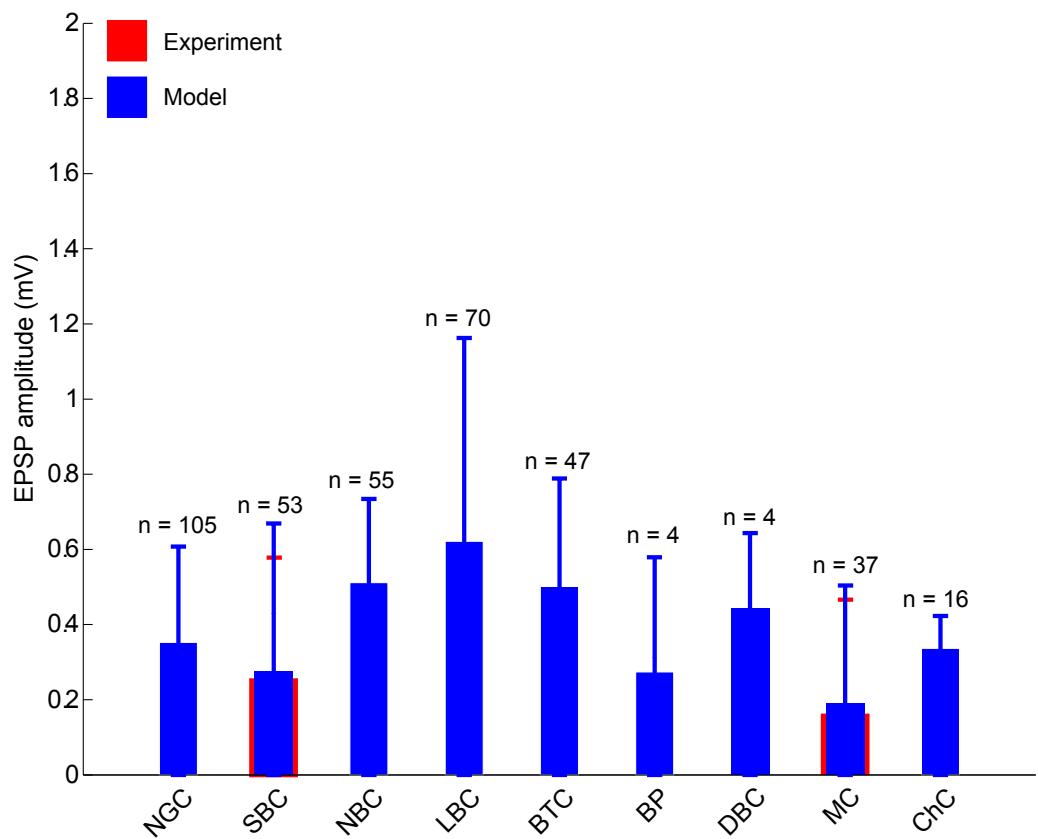


Figure 17. Mean EPSP amplitudes from L6CTPC to IN

Figure 5.17: Mean EPSP amplitudes from L6CTPC to IN

Part IV

CONCLUSIONS AND PERSPECTIVES ON FUTURE WORK

CONCLUSIONS AND PERSPECTIVES ON FUTURE WORK

"We do not see things as they are. We see them as we are."

The Talmud

In 1944, Alan Turing spoke about 'building the brain'. Several noteworthy endeavours since have tried to create machines that can think. Undoubtedly, many of these thinking machines have proven rather adept in performing noteworthy cognitive tasks, for instance like playing chess or even John Searle's 'Chinese room test'. But the question here is, how close are the working principles of these artificial thinking machines to a real brain? Reverse-engineering the brain through *in vitro* experiments to build a unifying facility to create detailed *in silico* not only holds promise to build 'real' thinking machines, but also the potential of uncovering the causes of several diseases plaguing the brain.

The Blue Brain Project (BBP) is the first comprehensive endeavour to build a unifying model of the neocortical column (NCC) by systematic data integration and biologically detailed simulations. Undertaken within the scope of the BBP, the research presented here lays the foundation to study the functional properties of *in silico* synaptic connectivity. In order to study the properties of *in silico* synaptic transmission in the NCC, it is critical to build faithful models of the various composite pieces that constitute the NCC - the morpho-electrical diversity of neocortical neurons and principles of synaptic communication derived from *in vitro* experiments.

I have shown that the functional properties of synaptic transmission (*i.e.* the latency of EPSP onset, rise time, amplitude, decay time constant, failures and CV of EPSP amplitude) emerge as a consequence of building the neocortical column guided by elementary first principles from biology. A fundamental result obtained from this thesis is the insight on how the fine anatomical structure of reconstructed thick-tufted layer 5 pyramidal (TTL5) neurons generates biologically comparable distributions of the functional properties of synaptic transmission. This study demonstrates that intrinsic morphological diversity renders the average synaptic response properties robust to perturbations of anatomical and physiological properties in the local microcircuit. Remarkably, morphological diversity also confers local microcircuit invariance of the average synaptic response properties by ensuring that the overall variability decreases as an increase in the diversity of morphologies. It might appear that nature has ensured to keep the morphological structure of pyramidal neurons is highly characteristic on the one hand while rendering each neuron morphologically unique by intrinsic diversity. This has led to the discovery of basic principles of "microcircuit level robustness and invariance", governing the function of the local microcircuit of TTL5 neurons.

Furthermore, I also demonstrate that the entire excitatory network of the neocortical microcircuit, consisting of intra- and inter-laminar pathways emerges as a consequence of reverse-engineering the neocortical microcircuit with reconstructed neurons through an *in silico* model. It appears that the principle of microcircuit level robustness and invariance described above is an idiosyncratic feature governing the function of local neocortical microcircuits.

The functions performed by different neural microcircuits depend on the anatomical and physiological properties of the various synaptic pathways connecting neurons. The balance of excitation and inhibition is critical to the normal function of the neocortical microcircuit. I also investigated the emergent *in silico* synaptic physiology of the myriad of excitatory-inhibitory and inhibitory-excitatory pathways in order to set the stage for the emergent dynamics of the NCC model.

The results emanating from this research lays the foundation for further exploratory studies of *in silico* synaptic transmission within the framework of the BBP. An immediate logical extension could be the characterization of synaptic transmission in *in silico* circuit motifs observed in biology, for example Martinotti disynaptic loops or polysynaptic connections between basket and pyramidal cells to investigate how the imbalance of excitation-inhibition leads to pathological states in networks of neurons. Furthermore, this sets the stage for the exploration of recurring motifs of connectivity that emerge as a result of the biologically constrained bottom-up construction of the NCC model. Such *in silico* predictions could go hand in hand to drive the design of specific *in vitro* experiments to test the operational advantages of certain recurring connectivity patterns.

The methods presented here to study *in silico* synaptic transmission is fundamental for further studies of neuromodulatory effects on the global dynamics of the neocortical microcircuit in a pathway specific manner. Furthermore, the methods I present also provide the foundation to study learning mechanisms at the level of synapses, which is something that can be extremely difficult if not impossible to study with current experimental techniques.

Pathophysiological disorders in the brain pose an exponentially increasing share of health-care budgets and a source of considerable suffering for mankind. *In silico* drug screening to modulate the dynamics of synaptic transmission is a targeted research direction based on the fundamental work in this thesis. Biologically detailed simulations of the pathophysiology of synaptic pathways will provide a better understanding of the the principle mechanism of drug action on the brain, and their possible side effects.

A thorough characterization of *in silico* synaptic transmission within the framework of the BBP will drive the development of novel therapeutics and treatments to alleviate brain disease.

"You must be the change you wish to see in the world."

Mahatma Gandhi

Part V

BIBLIOGRAPHY

BIBLIOGRAPHY

BIBLIOGRAPHY

- Ali AB, Bannister AP, Thomson AM (2007) Robust correlations between action potential duration and the properties of synaptic connections in layer 4 interneurons in neocortical slices from juvenile rats and adult rat and cat. *J Physiol* 580:149–69. (Cited on pages 108 and 109.)
- Allen F, Almasi G, Andreoni W, Beece D, Berne BJ, Bright A, Brunheroto J, Cascaval C, Castanos J, Coteus P, Crumley P, Curioni A, Denneau M, Donath W, Eleftheriou M, Fitch B, Fleischer B, Georgiou CJ, Germain R, Giampapa M, Gresh D, Gupta M, Haring R, Ho H, Hochschild P, Hummel S, Jonas T, Lieber D, Martyna G, Maturu K, Moreira J, Newns D, Newton M, Philhower R, Picunko T, Pitera J, Pitman M, Rand R, Royyuru A, Salapura V, Sanomiya A, Shah R, Sham Y, Singh S, Snir M, Suits F, Swetz R, Swope WC, Vishnumurthy N, Ward TJC, Warren H, Zhou R (2001) Blue gene: a vision for protein science using a petaflop supercomputer. *IBM Syst. J.* 40:310–327. (Cited on page 10.)
- Andjelic S, Gallopin T, Cauli B, Hill EL, Roux L, Badr S, Hu E, Tamás G, Lambolez B (2009) Glutamatergic nonpyramidal neurons from neocortical layer vi and their comparison with pyramidal and spiny stellate neurons. *J Neurophysiol* 101:641–54. (Cited on page 27.)
- Ango F, di Cristo G, Higashiyama H, Bennett V, Wu P, Huang ZJ (2004) Ankyrin-based subcellular gradient of neurofascin, an immunoglobulin family protein, directs gabaergic innervation at purkinje axon initial segment. *Cell* 119:257–72. (Cited on page 107.)
- Angulo MC, Rossier J, Audinat E (1999) Postsynaptic glutamate receptors and integrative properties of fast-spiking interneurons in the rat neocortex. *J Neurophysiol* 82:1295–302. (Cited on page 110.)
- Anwar H, Riachi I, Hill S, Schürmann F, Markram H (2010) *An approach to Capturing Neuron Morphological Diversity. In Computational Neuroscience: Realistic Modeling for Experimentalists* The MIT Press, Cambridge. (Cited on pages xix, 9, 24, 85, and 104.)
- Ascoli GA, Alonso-Nanclares L, Anderson SA, Barrionuevo G, Benavides-Piccione R, Burkhalter A, Buzsáki G, Cauli B, Defelipe J, Fairén A, Feldmeyer D, Fishell G, Fregnac Y, Freund TF, Gardner D, Gardner EP, Goldberg JH, Helmstaedter M, Hestrin S, Karube F, Kisvárdy ZF, Lambolez B, Lewis DA, Marin O, Markram H, Muñoz A, Packer A, Petersen CCH, Rockland KS, Rossier J, Rudy B, Somogyi P, Staiger JF, Tamas G, Thomson AM, Toledo-Rodriguez M, Wang Y, West DC, Yuste R (2008) Petilla terminology: nomenclature of features of gabaergic interneurons of the cerebral cortex. *Nat Rev Neurosci* 9:557–68. (Cited on pages xix and 25.)

- Beierlein M, Gibson JR, Connors BW (2003) Two dynamically distinct inhibitory networks in layer 4 of the neocortex. *J Neurophysiol* 90:2987–3000. (Cited on pages 107, 108, and 110.)
- Bekkers JM (2000a) Distribution and activation of voltage-gated potassium channels in cell-attached and outside-out patches from large layer 5 cortical pyramidal neurons of the rat. *J Physiol* 525 Pt 3:611–20. (Cited on page 20.)
- Bekkers JM (2000b) Properties of voltage-gated potassium currents in nucleated patches from large layer 5 cortical pyramidal neurons of the rat. *J Physiol* 525 Pt 3:593–609. (Cited on page 20.)
- Ben-Ari Y (2002) Excitatory actions of gaba during development: the nature of the nurture. *Nat Rev Neurosci* 3:728–39. (Cited on page 112.)
- Berger T, Larkum ME, Lüscher HR (2001) High i(h) channel density in the distal apical dendrite of layer v pyramidal cells increases bidirectional attenuation of epsps. *J Neurophysiol* 85:855–68. (Cited on page 26.)
- Bi GQ, Poo MM (1998) Synaptic modifications in cultured hippocampal neurons: dependence on spike timing, synaptic strength, and postsynaptic cell type. *J Neurosci* 18:10464–72. (Cited on page 32.)
- Blatow M, Rozov A, Katona I, Hormuzdi SG, Meyer AH, Whittington MA, Caputi A, Monyer H (2003) A novel network of multipolar bursting interneurons generates theta frequency oscillations in neocortex. *Neuron* 38:805–17. (Cited on pages 108 and 109.)
- Braitenberg V, Schüz A, Braitenberg V (1998) *Cortex: statistics and geometry of neuronal connectivity* Springer, Berlin, 2nd thoroughly rev. ed edition. (Cited on pages 26, 36, and 83.)
- Brémaud A, West DC, Thomson AM (2007) Binomial parameters differ across neocortical layers and with different classes of connections in adult rat and cat neocortex. *Proc Natl Acad Sci U S A* 104:14134–9. (Cited on pages 86 and 91.)
- Brown SP, Hestrin S (2009a) Cell-type identity: a key to unlocking the function of neocortical circuits. *Curr Opin Neurobiol* 19:415–21. (Cited on page 32.)
- Brown SP, Hestrin S (2009b) Intracortical circuits of pyramidal neurons reflect their long-range axonal targets. *Nature* 457:1133–6. (Cited on page 36.)
- Buhl EH, Tamás G, Szilágyi T, Stricker C, Paulsen O, Somogyi P (1997) Effect, number and location of synapses made by single pyramidal cells onto aspiny interneurons of cat visual cortex. *J Physiol* 500 (Pt 3):689–713. (Cited on page 32.)
- Bureau I, von Saint Paul F, Svoboda K (2006) Interdigitated paralemniscal and lemniscal pathways in the mouse barrel cortex. *PLoS Biol* 4:e382. (Cited on page 37.)

- Bush P, Sejnowski T (1996) Inhibition synchronizes sparsely connected cortical neurons within and between columns in realistic network models. *J Comput Neurosci* 3:91–110. (Cited on page 9.)
- Cauli B, Audinat E, Lambolez B, Angulo MC, Ropert N, Tsuzuki K, Hestrin S, Rossier J (1997) Molecular and physiological diversity of cortical nonpyramidal cells. *J Neurosci* 17:3894–906. (Cited on pages 24 and 27.)
- Cobos I, Calcagnotto ME, Vilaythong AJ, Thwin MT, Noebels JL, Baraban SC, Rubenstein JLR (2005) Mice lacking *dlx1* show subtype-specific loss of interneurons, reduced inhibition and epilepsy. *Nat Neurosci* 8:1059–68. (Cited on page 103.)
- Connors BW, Gutnick MJ (1990) Intrinsic firing patterns of diverse neocortical neurons. *Trends Neurosci* 13:99–104. (Cited on page 24.)
- Cossart R, Dinocourt C, Hirsch JC, Merchan-Perez A, De Felipe J, Ben-Ari Y, Esclapez M, Bernard C (2001) Dendritic but not somatic gabaergic inhibition is decreased in experimental epilepsy. *Nat Neurosci* 4:52–62. (Cited on page 103.)
- Craven KB, Zagotta WN (2006) Cng and hcn channels: two peas, one pod. *Annu Rev Physiol* 68:375–401. (Cited on page 21.)
- DeFelipe J (1999) Chandelier cells and epilepsy. *Brain* 122 (Pt 10):1807–22. (Cited on page 27.)
- DeFelipe J, Fariñas I (1992) The pyramidal neuron of the cerebral cortex: morphological and chemical characteristics of the synaptic inputs. *Prog Neurobiol* 39:563–607. (Cited on page 26.)
- DeFelipe J, Hendry SH, Hashikawa T, Molinari M, Jones EG (1990) A microcolumnar structure of monkey cerebral cortex revealed by immunocytochemical studies of double bouquet cell axons. *Neuroscience* 37:655–73. (Cited on page 28.)
- DeFelipe J, Hendry SH, Jones EG (1989) Visualization of chandelier cell axons by parvalbumin immunoreactivity in monkey cerebral cortex. *Proc Natl Acad Sci U S A* 86:2093–7. (Cited on page 28.)
- DeFelipe J, Alonso-Nanclares L, Arellano JI (2002) Microstructure of the neocortex: comparative aspects. *J Neurocytol* 31:299–316. (Cited on page 26.)
- DeFelipe J, Ballesteros-Yáñez I, Inda MC, Muñoz A (2006) Double-bouquet cells in the monkey and human cerebral cortex with special reference to areas 17 and 18. *Prog Brain Res* 154:15–32. (Cited on page 28.)
- Djurfeldt M, Lundqvist M, Johansson C, Rehn M, Ekeberg O, Lansner A (2008) Brain-scale simulation of the neocortex on the ibm blue gene/l supercomputer. *IBM Journal of Research and Development* 52:31–41. (Cited on page 9.)

- Druckmann S, Banitt Y, Gidon A, Schürmann F, Markram H, Segev I (2007) A novel multiple objective optimization framework for constraining conductance-based neuron models by experimental data. *Front Neurosci* 1:7–18. (Cited on pages 23, 28, 29, 86, and 105.)
- Druckmann S, Berger TK, Hill S, Schürmann F, Markram H, Segev I (2008) Evaluating automated parameter constraining procedures of neuron models by experimental and surrogate data. *Biol Cybern* 99:371–9. (Cited on pages 23, 28, and 29.)
- Eccles JC (1983) The horizontal (tangential) fibres system of lamina i of the cerebral neocortex. *Acta Morphol Hung* 31:261–84. (Cited on page 27.)
- Eccles JC (1964) *The physiology of synapses* Academic Press, New York. (Cited on page 32.)
- Feldmeyer D, Egger V, Lübke J, Sakmann B (1999) Reliable synaptic connections between pairs of excitatory layer 4 neurones within a single ‘barrel’ of developing rat somatosensory cortex. *J Physiol* 521 Pt 1:169–90. (Cited on page 87.)
- Feldmeyer D, Lübke J, Sakmann B (2006) Efficacy and connectivity of intracolumnar pairs of layer 2/3 pyramidal cells in the barrel cortex of juvenile rats. *J Physiol* 575:583–602. (Cited on pages 87 and 88.)
- Feldmeyer D, Lübke J, Silver RA, Sakmann B (2002) Synaptic connections between layer 4 spiny neurone-layer 2/3 pyramidal cell pairs in juvenile rat barrel cortex: physiology and anatomy of interlaminar signalling within a cortical column. *J Physiol* 538:803–22. (Cited on pages 87 and 91.)
- Froemke RC, Dan Y (2002) Spike-timing-dependent synaptic modification induced by natural spike trains. *Nature* 416:433–8. (Cited on page 32.)
- Fuhrmann G, Segev I, Markram H, Tsodyks M (2002) Coding of temporal information by activity-dependent synapses. *J Neurophysiol* 87:140–8. (Cited on pages 37, 85, and 105.)
- Goldberg JH, Lacefield CO, Yuste R (2004) Global dendritic calcium spikes in mouse layer 5 low threshold spiking interneurons: implications for control of pyramidal cell bursting. *J Physiol* 558:465–78. (Cited on page 27.)
- Grillner S, Markram H, De Schutter E, Silberberg G, LeBeau FEN (2005) Microcircuits in action—from cpgs to neocortex. *Trends Neurosci* 28:525–33. (Cited on pages xix and 33.)
- Gupta A, Wang Y, Markram H (2000) Organizing principles for a diversity of gabaergic interneurons and synapses in the neocortex. *Science* 287:273–8. (Cited on pages xxii, 3, 24, 27, 32, 105, 106, and 113.)
- Häusser M, Major G, Stuart GJ (2001) Differential shunting of epsps by action potentials. *Science* 291:138–41. (Cited on page 36.)

- Häusser M, Roth A (1997) Estimating the time course of the excitatory synaptic conductance in neocortical pyramidal cells using a novel voltage jump method. *J Neurosci* 17:7606–25. (Cited on page 86.)
- Häusser M, Spruston N, Stuart GJ (2000) Diversity and dynamics of dendritic signaling. *Science* 290:739–44. (Cited on page 36.)
- Häusser M (2004) Storing memories in dendritic channels. *Nat Neurosci* 7:98–100. (Cited on page 19.)
- Hay E, Hill S, Schürmann F, Markram H, Segev I (2011) Models of neocortical layer 5b pyramidal cells capturing a wide range of dendritic and perisomatic active properties. *PLoS Comput Biol* 7:e1002107. (Cited on pages 23, 28, 29, 86, and 105.)
- Hellwig B (2000) A quantitative analysis of the local connectivity between pyramidal neurons in layers 2/3 of the rat visual cortex. *Biol Cybern* 82:111–21. (Cited on page 36.)
- Helmstaedter M, Sakmann B, Feldmeyer D (2009) L2/3 interneuron groups defined by multiparameter analysis of axonal projection, dendritic geometry, and electrical excitability. *Cereb Cortex* 19:951–62. (Cited on page 24.)
- Helmstaedter M, Staiger JF, Sakmann B, Feldmeyer D (2008) Efficient recruitment of layer 2/3 interneurons by layer 4 input in single columns of rat somatosensory cortex. *J Neurosci* 28:8273–84. (Cited on page 92.)
- Hestrin S, Armstrong WE (1996) Morphology and physiology of cortical neurons in layer I. *J Neurosci* 16:5290–300. (Cited on page 28.)
- Hestrin S, Galarreta M (2005) Electrical synapses define networks of neocortical GABAergic neurons. *Trends Neurosci* 28:304–9. (Cited on page 25.)
- Hille B (1992) *Ionic channels of excitable membranes* Sinauer Associates, Sunderland, Mass., 2nd ed edition. (Cited on page 3.)
- Hines ML, Carnevale NT (1997) The neuron simulation environment. *Neural Comput* 9:1179–209. (Cited on pages 86 and 105.)
- Hines ML, Carnevale NT (2000) Expanding neuron's repertoire of mechanisms with nmodl. *Neural Comput* 12:995–1007. (Cited on page 11.)
- Hodgkin AL, Huxley AF (1952) A quantitative description of membrane current and its application to conduction and excitation in nerve. *J Physiol* 117:500–44. (Cited on page 21.)
- Holmgren C, Harkany T, Svennenfors B, Zilberter Y (2003) Pyramidal cell communication within local networks in layer 2/3 of rat neocortex. *J Physiol* 551:139–53. (Cited on page 36.)

- Homanics GE, DeLorey TM, Firestone LL, Quinlan JJ, Handforth A, Harrison NL, Krasowski MD, Rick CE, Korpi ER, Mäkelä R, Brilliant MH, Hagiwara N, Ferguson C, Snyder K, Olsen RW (1997) Mice devoid of gamma-aminobutyrate type a receptor beta3 subunit have epilepsy, cleft palate, and hypersensitive behavior. *Proc Natl Acad Sci U S A* 94:4143–8. (Cited on page 103.)
- Hubel DH, Wiesel TN (1959) Receptive fields of single neurones in the cat's striate cortex. *J Physiol* 148:574–91. (Cited on page 5.)
- Jahr CE, Stevens CF (1990) A quantitative description of nmda receptor-channel kinetic behavior. *J Neurosci* 10:1830–7. (Cited on pages 30, 85, and 86.)
- Jones EG (1975) Varieties and distribution of non-pyramidal cells in the somatic sensory cortex of the squirrel monkey. *J Comp Neurol* 160:205–67. (Cited on page 28.)
- Jones EG (2000) Microcolumns in the cerebral cortex. *Proc Natl Acad Sci U S A* 97:5019–21. (Cited on page 5.)
- Kalisman N, Silberberg G, Markram H (2003) Deriving physical connectivity from neuronal morphology. *Biol Cybern* 88:210–8. (Cited on page 36.)
- Kalisman N, Silberberg G, Markram H (2005) The neocortical microcircuit as a tabula rasa. *Proc Natl Acad Sci U S A* 102:880–5. (Cited on page 36.)
- Kampa BM, Letzkus JJ, Stuart GJ (2006) Cortical feed-forward networks for binding different streams of sensory information. *Nat Neurosci* 9:1472–3. (Cited on pages 88 and 92.)
- Kandel ER, Schwartz JH, Jessell TM (2000) *Principles of neural science* McGraw-Hill, Health Professions Division, New York, 4th ed edition. (Cited on page 5.)
- Karube F, Kubota Y, Kawaguchi Y (2004) Axon branching and synaptic bouton phenotypes in gabaergic nonpyramidal cell subtypes. *J Neurosci* 24:2853–65. (Cited on page 103.)
- Katz B, Miledi R (1968) The role of calcium in neuromuscular facilitation. *J Physiol* 195:481–92. (Cited on page 30.)
- Katz B (1969) *The release of neural transmitter substances*, Vol. 10 Thomas, Springfield, Ill. (Cited on page 30.)
- Kawaguchi Y (1995) Physiological subgroups of nonpyramidal cells with specific morphological characteristics in layer ii/iii of rat frontal cortex. *J Neurosci* 15:2638–55. (Cited on pages 24 and 27.)
- Kawaguchi Y, Kubota Y (1997) Gabaergic cell subtypes and their synaptic connections in rat frontal cortex. *Cereb Cortex* 7:476–86. (Cited on pages 24 and 27.)

- Kisvárday ZF, Gulyas A, Beroukas D, North JB, Chubb IW, Somogyi P (1990) Synapses, axonal and dendritic patterns of gaba-immunoreactive neurons in human cerebral cortex. *Brain* 113 (Pt 3):793–812. (Cited on page 28.)
- Klausberger T, Magill PJ, Márton LF, Roberts JDB, Cobden PM, Buzsáki G, Somogyi P (2003) Brain-state- and cell-type-specific firing of hippocampal interneurons in vivo. *Nature* 421:844–8. (Cited on pages 25 and 27.)
- Klausberger T, Somogyi P (2008) Neuronal diversity and temporal dynamics: the unity of hippocampal circuit operations. *Science* 321:53–7. (Cited on page 25.)
- Koester HJ, Johnston D (2005) Target cell-dependent normalization of transmitter release at neocortical synapses. *Science* 308:863–6. (Cited on pages 32, 86, 87, 89, and 109.)
- Kole MHP, Hallermann S, Stuart GJ (2006a) Single ih channels in pyramidal neuron dendrites: properties, distribution, and impact on action potential output. *J Neurosci* 26:1677–87. (Cited on page 21.)
- Kole MHP, Hallermann S, Stuart GJ (2006b) Single ih channels in pyramidal neuron dendrites: properties, distribution, and impact on action potential output. *J Neurosci* 26:1677–87. (Cited on pages 86 and 87.)
- Korn H, Faber DS (1991) Quantal analysis and synaptic efficacy in the cns. *Trends Neurosci* 14:439–45. (Cited on page 30.)
- Korngreen A, Sakmann B (2000) Voltage-gated k⁺ channels in layer 5 neocortical pyramidal neurones from young rats: subtypes and gradients. *J Physiol* 525 Pt 3:621–39. (Cited on page 20.)
- Kozloski J, Sfyarakis K, Hill S, Schürmann F, Peck CC, Markram H (2008) Identifying, tabulating, and analyzing contacts between branched neuron morphologies. *IBM Journal of Research and Development* 52:43–56. (Cited on page 104.)
- Lai HC, Jan LY (2006) The distribution and targeting of neuronal voltage-gated ion channels. *Nat Rev Neurosci* 7:548–62. (Cited on pages xviii, 3, and 8.)
- Larkum ME, Kaiser KM, Sakmann B (1999a) Calcium electrogenesis in distal apical dendrites of layer 5 pyramidal cells at a critical frequency of back-propagating action potentials. *Proc Natl Acad Sci U S A* 96:14600–4. (Cited on page 26.)
- Larkum ME, Zhu JJ, Sakmann B (1999b) A new cellular mechanism for coupling inputs arriving at different cortical layers. *Nature* 398:338–41. (Cited on page 26.)
- Le Bé JV, Silberberg G, Wang Y, Markram H (2007) Morphological, electrophysiological, and synaptic properties of corticocallosal pyramidal cells in the neonatal rat neocortex. *Cereb Cortex* 17:2204–13. (Cited on pages 86 and 87.)

- Lefort S, Tómm C, Floyd Sarria JC, Petersen CCH (2009) The excitatory neuronal network of the c2 barrel column in mouse primary somatosensory cortex. *Neuron* 61:301–16. (Cited on page 37.)
- Lewis DA, Lund JS (1990) Heterogeneity of chandelier neurons in monkey neocortex: corticotropin-releasing factor- and parvalbumin-immunoreactive populations. *J Comp Neurol* 293:599–615. (Cited on page 27.)
- Lewis DA, Hashimoto T, Volk DW (2005) Cortical inhibitory neurons and schizophrenia. *Nat Rev Neurosci* 6:312–24. (Cited on page 103.)
- Lien CC, Jonas P (2003) Kv3 potassium conductance is necessary and kinetically optimized for high-frequency action potential generation in hippocampal interneurons. *J Neurosci* 23:2058–68. (Cited on page 20.)
- Lorente de No R (1939) *Cerebral cortex: architecture, intracortical connections, motor projections* Oxford University Press, 3 edition. (Cited on page 24.)
- Lu Jt, Li Cy, Zhao JP, Poo Mm, Zhang Xh (2007) Spike-timing-dependent plasticity of neocortical excitatory synapses on inhibitory interneurons depends on target cell type. *J Neurosci* 27:9711–20. (Cited on pages 109 and 110.)
- Lübke J, Feldmeyer D (2007a) Excitatory signal flow and connectivity in a cortical column: focus on barrel cortex. *Brain Struct Funct* 212:3–17. (Cited on page 37.)
- Lübke J, Feldmeyer D (2007b) Excitatory signal flow and connectivity in a cortical column: focus on barrel cortex. *Brain Struct Funct* 212:3–17. (Cited on page 83.)
- Magee JC, Cook EP (2000) Somatic epsp amplitude is independent of synapse location in hippocampal pyramidal neurons. *Nat Neurosci* 3:895–903. (Cited on page 36.)
- Marin-Padilla M, Marin-Padilla TM (1982) Origin, prenatal development and structural organization of layer I of the human cerebral (motor) cortex. a golgi study. *Anat Embryol (Berl)* 164:161–206. (Cited on page 27.)
- Markram H (1997) A network of tufted layer 5 pyramidal neurons. (Cited on page 32.)
- Markram H, Helm PJ, Sakmann B (1995) Dendritic calcium transients evoked by single back-propagating action potentials in rat neocortical pyramidal neurons. *J Physiol* 485 (Pt 1):1–20. (Cited on page 26.)
- Markram H, Lübke J, Frotscher M, Roth A, Sakmann B (1997a) Physiology and anatomy of synaptic connections between thick tufted pyramidal neurones in the developing rat neocortex. *J Physiol* 500 (Pt 2):409–40. (Cited on pages xxii, 26, 32, 36, 105, and 113.)

- Markram H, Lübke J, Frotscher M, Sakmann B (1997b) Regulation of synaptic efficacy by coincidence of postsynaptic apss and epsps. *Science* 275:213–5. (Cited on pages 26 and 32.)
- Markram H, Pikus D, Gupta A, Tsodyks M (1998) Potential for multiple mechanisms, phenomena and algorithms for synaptic plasticity at single synapses. *Neuropharmacology* 37:489–500. (Cited on pages xx, 37, and 38.)
- Markram H, Sakmann B (1994) Calcium transients in dendrites of neocortical neurons evoked by single subthreshold excitatory postsynaptic potentials via low-voltage-activated calcium channels. *Proc Natl Acad Sci U S A* 91:5207–11. (Cited on page 26.)
- Markram H, Tsodyks M (1996) Redistribution of synaptic efficacy between neocortical pyramidal neurons. *Nature* 382:807–10. (Cited on page 26.)
- Markram H, Wang Y, Tsodyks M (1998) Differential signaling via the same axon of neocortical pyramidal neurons. *Proc Natl Acad Sci U S A* 95:5323–8. (Cited on pages xx, xxii, 27, 32, 34, 37, 105, and 113.)
- Markram H (2006) The blue brain project. *Nat Rev Neurosci* 7:153–60. (Cited on pages xviii, 3, 9, and 10.)
- Markram H (2008) Fixing the location and dimensions of functional neocortical columns. *HFSP J* 2:132–5. (Cited on page 5.)
- Markram H, Toledo-Rodriguez M, Wang Y, Gupta A, Silberberg G, Wu C (2004) Interneurons of the neocortical inhibitory system. *Nat Rev Neurosci* 5:793–807. (Cited on pages xxii, 24, 25, 26, 27, 28, 32, 103, 106, 108, and 113.)
- Martinotti C (1889) Contributo allo studio della corteccia cerebrale, ed all'origine centrale dei nervi. *Ann. Freniatr. Sci. Affini* 1:14–381. (Cited on page 27.)
- Mercer A, West DC, Morris OT, Kirchhecker S, Kerkhoff JE, Thomson AM (2005) Excitatory connections made by presynaptic cortico-cortical pyramidal cells in layer 6 of the neocortex. *Cereb Cortex* 15:1485–96. (Cited on pages 87 and 90.)
- Meyer HS, Wimmer VC, Oberlaender M, de Kock CPJ, Sakmann B, Helmstaedter M (2010) Number and laminar distribution of neurons in a thalamocortical projection column of rat vibrissal cortex. *Cereb Cortex* 20:2277–86. (Cited on page 85.)
- Migliore M, Shepherd GM (2002) Emerging rules for the distributions of active dendritic conductances. *Nat Rev Neurosci* 3:362–70. (Cited on page 6.)
- Monier C, Chavane F, Baudot P, Graham LJ, Frégnac Y (2003) Orientation and direction selectivity of synaptic inputs in visual cortical neurons: a diversity of combinations produces spike tuning. *Neuron* 37:663–80. (Cited on page 103.)

- Moor RJ (2010) Neuron model life-cycle Master's thesis, Kirchoff Institute for Physics, University of Heidelberg. (Cited on pages 13 and 224.)
- Mountcastle VB (1957) Modality and topographic properties of single neurons of cat's somatic sensory cortex. *J Neurophysiol* 20:408–34. (Cited on page 5.)
- Mountcastle VB (1997) The columnar organization of the neocortex. *Brain* 120 (Pt 4):701–22. (Cited on pages 3 and 5.)
- Nicoll A, Larkman A, Blakemore C (1993) Modulation of epsp shape and efficacy by intrinsic membrane conductances in rat neocortical pyramidal neurons in vitro. *J Physiol* 468:693–710. (Cited on page 21.)
- Nowak L, Bregestovski P, Ascher P, Herbet A, Prochiantz A (1984) Magnesium gates glutamate-activated channels in mouse central neurones. *Nature* 307:462–5. (Cited on page 30.)
- Oláh S, Komlósi G, Szabadics J, Varga C, Tóth E, Barzó P, Tamás G (2007) Output of neurogliaform cells to various neuron types in the human and rat cerebral cortex. *Front Neural Circuits* 1:4. (Cited on page 112.)
- Perin R, Berger TK, Markram H (2011) A synaptic organizing principle for cortical neuronal groups. *Proc Natl Acad Sci U S A* 108:5419–24. (Cited on page 36.)
- Perrier JF, Alaburda A, Hounsgaard J (2002) Spinal plasticity mediated by postsynaptic l-type ca2+ channels. *Brain Res Brain Res Rev* 40:223–9. (Cited on page 19.)
- Peters A, Feldman ML (1976) The projection of the lateral geniculate nucleus to area 17 of the rat cerebral cortex. i. general description. *J Neurocytol* 5:63–84. (Cited on page 36.)
- Peters A, Jones EG (1999) *Cerebral cortex* Plenum Press, New York. (Cited on pages 26 and 85.)
- Petersen CCH (2007) The functional organization of the barrel cortex. *Neuron* 56:339–55. (Cited on page 5.)
- Powell TP, Mountcastle VB (1959) Some aspects of the functional organization of the cortex of the postcentral gyrus of the monkey: a correlation of findings obtained in a single unit analysis with cytoarchitecture. *Bull Johns Hopkins Hosp* 105:133–62. (Cited on page 5.)
- Purves D, Riddle DR, LaMantia AS (1992) Iterated patterns of brain circuitry (or how the cortex gets its spots). *Trends Neurosci* 15:362–8. (Cited on page 5.)
- Rakic P (1975) Local circuit neurons. *Neurosci Res Program Bull* 13:295–416. (Cited on page 25.)
- Ranjan R (2011) Engineering Neuron Models : from Ion Channels to Electrical Behavior Ph.D. diss., Ecole Polytechnique Fédérale de Lausanne. (Cited on pages 13 and 21.)

- Reyes A, Lujan R, Rozov A, Burnashev N, Somogyi P, Sakmann B (1998) Target-cell-specific facilitation and depression in neocortical circuits. *Nat Neurosci* 1:279–85. (Cited on pages xx, 32, and 35.)
- Rinaldi T, Silberberg G, Markram H (2008) Hyperconnectivity of local neocortical microcircuitry induced by prenatal exposure to valproic acid. *Cereb Cortex* 18:763–70. (Cited on page 85.)
- Robinson RB, Siegelbaum SA (2003) Hyperpolarization-activated cation currents: from molecules to physiological function. *Annu Rev Physiol* 65:453–80. (Cited on page 21.)
- Romand S, Wang Y, Toledo-Rodriguez M, Markram H (2011) Morphological development of thick-tufted layer v pyramidal cells in the rat somatosensory cortex. *Front Neuroanat* 5:5. (Cited on pages xviii and 7.)
- Rozov A, Jerecic J, Sakmann B, Burnashev N (2001) Ampa receptor channels with long-lasting desensitization in bipolar interneurons contribute to synaptic depression in a novel feedback circuit in layer 2/3 of rat neocortex. *J Neurosci* 21:8062–71. (Cited on pages 107 and 110.)
- Sarid L, Bruno R, Sakmann B, Segev I, Feldmeyer D (2007) Modeling a layer 4-to-layer 2/3 module of a single column in rat neocortex: interweaving in vitro and in vivo experimental observations. *Proc Natl Acad Sci U S A* 104:16353–8. (Cited on pages 85, 86, and 91.)
- Schiller J, Schiller Y, Stuart G, Sakmann B (1997) Calcium action potentials restricted to distal apical dendrites of rat neocortical pyramidal neurons. *J Physiol* 505 (Pt 3):605–16. (Cited on page 26.)
- Schoppa NE, Westbrook GL (1999) Regulation of synaptic timing in the olfactory bulb by an a-type potassium current. *Nat Neurosci* 2:1106–13. (Cited on page 19.)
- Shu Y, Hasenstaub A, McCormick DA (2003) Turning on and off recurrent balanced cortical activity. *Nature* 423:288–93. (Cited on page 103.)
- Silberberg G, Gupta A, Markram H (2002) Stereotypy in neocortical microcircuits. *Trends Neurosci* 25:227–30. (Cited on page 5.)
- Silberberg G, Markram H (2007) Disynaptic inhibition between neocortical pyramidal cells mediated by martinotti cells. *Neuron* 53:735–46. (Cited on pages xxii, 27, 36, 105, 106, 108, 110, and 112.)
- Silver RA, Lubke J, Sakmann B, Feldmeyer D (2003) High-probability uniquantal transmission at excitatory synapses in barrel cortex. *Science* 302:1981–4. (Cited on pages 86 and 87.)
- Sjöström PJ, Turrigiano GG, Nelson SB (2001) Rate, timing, and cooperativity jointly determine cortical synaptic plasticity. *Neuron* 32:1149–64. (Cited on pages 19 and 32.)

- Sjöström PJ, Turrigiano GG, Nelson SB (2007) Multiple forms of long-term plasticity at unitary neocortical layer 5 synapses. *Neuropharmacology* 52:176–84. (Cited on page 32.)
- Somogyi P (1977) A specific 'axo-axonal' interneuron in the visual cortex of the rat. *Brain Res* 136:345–50. (Cited on page 27.)
- Somogyi P (1979) An interneurone making synapses specifically on the axon initial segment of pyramidal cells in the cerebral cortex of the cat [proceedings]. *J Physiol* 296:18P–19P. (Cited on page 27.)
- Somogyi P, Cowey A (1981) Combined golgi and electron microscopic study on the synapses formed by double bouquet cells in the visual cortex of the cat and monkey. *J Comp Neurol* 195:547–66. (Cited on page 28.)
- Somogyi P, Freund TF, Cowey A (1982) The axo-axonic interneuron in the cerebral cortex of the rat, cat and monkey. *Neuroscience* 7:2577–607. (Cited on page 27.)
- Somogyi P, Tamás G, Lujan R, Buhl EH (1998) Salient features of synaptic organisation in the cerebral cortex. *Brain Res Brain Res Rev* 26:113–35. (Cited on pages 24, 32, 36, and 103.)
- Song S, Sjöström PJ, Reigl M, Nelson S, Chklovskii DB (2005) Highly nonrandom features of synaptic connectivity in local cortical circuits. *PLoS Biol* 3:e68. (Cited on page 36.)
- Spruston N (2008) Pyramidal neurons: dendritic structure and synaptic integration. *Nat Rev Neurosci* 9:206–21. (Cited on page 83.)
- Stuart G, Schiller J, Sakmann B (1997) Action potential initiation and propagation in rat neocortical pyramidal neurons. *J Physiol* 505 (Pt 3):617–32. (Cited on pages 86, 91, and 92.)
- Stuart GJ, Sakmann B (1994) Active propagation of somatic action potentials into neocortical pyramidal cell dendrites. *Nature* 367:69–72. (Cited on pages 21 and 26.)
- Stuart G, Spruston N, Häusser M (2007) *Dendrites* Oxford University Press, Oxford, 2nd edition. (Cited on page 21.)
- Swindale NV (1998) Cortical organization: modules, polymaps and mosaics. *Curr Biol* 8:R270–3. (Cited on page 5.)
- Szabadics J, Varga C, Molnár G, Oláh S, Barzó P, Tamás G (2006) Excitatory effect of gabaergic axo-axonic cells in cortical microcircuits. *Science* 311:233–5. (Cited on pages 27 and 103.)
- Tamás G, Lorincz A, Simon A, Szabadics J (2003) Identified sources and targets of slow inhibition in the neocortex. *Science* 299:1902–5. (Cited on page 28.)
- Thomson AM, Deuchars J (1997) Synaptic interactions in neocortical local circuits: dual intracellular recordings in vitro. *Cereb Cortex* 7:510–22. (Cited on page 110.)

- Thomson AM, Deuchars J, West DC (1993) Large, deep layer pyramid-pyramid single axon epsps in slices of rat motor cortex display paired pulse and frequency-dependent depression, mediated presynaptically and self-facilitation, mediated postsynaptically. *J Neurophysiol* 70:2354–69. (Cited on page 32.)
- Thomson AM, West DC, Hahn J, Deuchars J (1996) Single axon ipsp elicited in pyramidal cells by three classes of interneurons in slices of rat neocortex. *J Physiol* 496 (Pt 1):81–102. (Cited on page 109.)
- Thomson AM, Bannister AP (2003) Interlaminar connections in the neocortex. *Cereb Cortex* 13:5–14. (Cited on page 92.)
- Thomson AM, Lamy C (2007) Functional maps of neocortical local circuitry. *Front Neurosci* 1:19–42. (Cited on pages 3, 36, and 37.)
- Thomson AM, Morris OT (2002) Selectivity in the inter-laminar connections made by neocortical neurones. *J Neurocytol* 31:239–46. (Cited on page 92.)
- Thomson AM, West DC, Wang Y, Bannister AP (2002) Synaptic connections and small circuits involving excitatory and inhibitory neurons in layers 2-5 of adult rat and cat neocortex: triple intracellular recordings and biocytin labelling in vitro. *Cereb Cortex* 12:936–53. (Cited on pages 36, 103, 108, and 109.)
- Toledo-Rodriguez M, Blumenfeld B, Wu C, Luo J, Attali B, Goodman P, Markram H (2004) Correlation maps allow neuronal electrical properties to be predicted from single-cell gene expression profiles in rat neocortex. *Cereb Cortex* 14:1310–27. (Cited on page 20.)
- Toledo-Rodriguez M, El Manira A, Wallén P, Svirskis G, Hounsgaard J (2005a) Cellular signalling properties in microcircuits. *Trends Neurosci* 28:534–40. (Cited on pages xviii, 3, 6, 19, 20, and 24.)
- Toledo-Rodriguez M, Goodman P, Illic M, Wu C, Markram H (2005b) Neuropeptide and calcium-binding protein gene expression profiles predict neuronal anatomical type in the juvenile rat. *J Physiol* 567:401–13. (Cited on page 27.)
- Tomioka R, Okamoto K, Furuta T, Fujiyama F, Iwasato T, Yanagawa Y, Obata K, Kaneko T, Tamamaki N (2005) Demonstration of long-range gabaergic connections distributed throughout the mouse neocortex. *Eur J Neurosci* 21:1587–600. (Cited on page 26.)
- Traub RD, Miles R, Buzsáki G (1992) Computer simulation of carbachol-driven rhythmic population oscillations in the ca3 region of the in vitro rat hippocampus. *J Physiol* 451:653–72. (Cited on page 9.)
- Tsodyks MV, Markram H (1997) The neural code between neocortical pyramidal neurons depends on neurotransmitter release probability. *Proc Natl Acad Sci U S A* 94:719–23. (Cited on pages 37, 85, and 86.)

- Valverde F (1978) The organization of area 18 in the monkey. a golgi study. *Anat Embryol (Berl)* 154:305–34. (Cited on page 28.)
- Vercelli AE, Garbossa D, Curtetti R, Innocenti GM (2004) Somatodendritic minicolumns of output neurons in the rat visual cortex. *Eur J Neurosci* 20:495–502. (Cited on page 28.)
- Wahle P (1993) Differential regulation of substance p and somatostatin in martinotti cells of the developing cat visual cortex. *J Comp Neurol* 329:519–38. (Cited on page 27.)
- Wang Y, Gupta A, Toledo-Rodriguez M, Wu CZ, Markram H (2002) Anatomical, physiological, molecular and circuit properties of nest basket cells in the developing somatosensory cortex. *Cereb Cortex* 12:395–410. (Cited on pages 27 and 106.)
- Wang Y, Markram H, Goodman PH, Berger TK, Ma J, Goldman-Rakic PS (2006) Heterogeneity in the pyramidal network of the medial prefrontal cortex. *Nat Neurosci* 9:534–42. (Cited on pages xxii, 105, and 113.)
- Wang Y, Toledo-Rodriguez M, Gupta A, Wu C, Silberberg G, Luo J, Markram H (2004) Anatomical, physiological and molecular properties of martinotti cells in the somatosensory cortex of the juvenile rat. *J Physiol* 561:65–90. (Cited on page 27.)
- Watts J, Thomson AM (2005) Excitatory and inhibitory connections show selectivity in the neocortex. *J Physiol* 562:89–97. (Cited on page 36.)
- West DC, Mercer A, Kirchhecker S, Morris OT, Thomson AM (2006) Layer 6 cortico-thalamic pyramidal cells preferentially innervate interneurons and generate facilitating epsps. *Cereb Cortex* 16:200–11. (Cited on page 111.)
- White EL, Keller A (1989) *Cortical circuits: synaptic organization of the cerebral cortex—structure, function, and theory* Birkhäuser, Boston. (Cited on page 26.)
- Williams SR, Stuart GJ (2002) Dependence of epsp efficacy on synapse location in neocortical pyramidal neurons. *Science* 295:1907–10. (Cited on page 21.)
- Woodruff A, Xu Q, Anderson SA, Yuste R (2009) Depolarizing effect of neocortical chandelier neurons. *Front Neural Circuits* 3:15. (Cited on page 27.)
- Woodruff AR, Anderson SA, Yuste R (2010) The enigmatic function of chandelier cells. *Front Neurosci* 4:201. (Cited on page 27.)
- Yoshimura Y, Kimura F, Tsumoto T (1999) Estimation of single channel conductance underlying synaptic transmission between pyramidal cells in the visual cortex. *Neuroscience* 88:347–52. (Cited on page 85.)
- Zucker RS, Regehr WG (2002) Short-term synaptic plasticity. *Annu Rev Physiol* 64:355–405. (Cited on page 32.)

Part VI

APPENDIX

THE THICK-TUFTED LAYER 5 PYRAMIDAL NEURON

**MANUSCRIPT FOR SUBMISSION TO THE JOURNAL OF
PHYSIOLOGY**

TITLE: The Thick Tufted Layer 5 Pyramidal Neuron

AUTHORS: Srikanth Ramaswamy, Yun Wang, Idan Segev and Henry Markram

**AUTHOR AFFILIATIONS: Brain Mind Institute, Ecole Polytechnique Fédérale de
Lausanne (EPFL), CH – 1015, Lausanne, Switzerland**

CORRESPONDING AUTHOR: Henry Markram, PhD,

Brain Mind Institute,

Ecole Polytechnique Fédérale de Lausanne (EPFL),

CH – 1015, Lausanne, Switzerland

e-mail: henry.markram@epfl.ch

Ph. +41 21 693 9569

Fax. +41 21 693 5350

**KEYWORDS: Layer 5 pyramidal neuron, apical and basal dendrites, dendritic
properties, axonal properties, action potential initiation and propagation, synaptic
properties, synaptic plasticity, pathophysiology**

Abstract

The thick tufted layer 5 (TTL5) pyramidal neuron is the most extensively studied neuron in the mammalian neocortex and has become a benchmark excitatory neuron. The TTL5 neuron integrates information across all neocortical layers and is the final common pathway for information flow from the neocortex to subcortical structures. This neuron has the widest local axonal and dendritic arborization and therefore sets the maximal dimensions of the local neocortical microcircuitry. Several studies over the past two decades have probed the anatomy, physiology, biophysics, pharmacology, synaptic transmission and plasticity, role of dendritic integration in neocortical information processing, learning, memory, and disease. This review summarizes key breakthroughs in our understanding of the diverse roles of TTL5 neurons in cortical function.

Abbreviations ACh, acetylcholine; AIS, axon initial segment; AMPAR, AMPA receptor; AP, action potential; bAP, back-propagating action potential; bAC, back-propagation activated Ca^{2+} spike; BDNF, brain-derived neurotrophic factor; BK, large-conductance Ca^{2+} dependent K^+ channel; CV, coefficient of variation; DA, dopamine; HCN, hyperpolarization-activated cation; IR-DIC, infrared differential interference contrast; KAR, kainate receptor; KCC2, K^+/Cl^- co-transporter; L2/3PC, layer 2/3 pyramidal neuron; TTL5, thick tufted layer 5; NMDAR, NMDA receptor; P, postnatal day; PSD, postsynaptic density; RSE, redistribution of synaptic efficacy; SK, large-conductance Ca^{2+} dependent K^+ channel; STDP, spike-timing dependent synaptic plasticity; VPA, valproic acid.

Introduction

The mammalian neocortex is endowed with a daunting diversity of neurons. These neurons are classified into excitatory pyramidal neurons or inhibitory interneurons. Pyramidal neurons exist in all layers of the neocortex except layer 1, forming the most abundant neuron type. In particular, TTL5 neurons are one of the most extensively studied neocortical cell types (Markram, 1997; Markram *et al.* 1997a; Spruston, 2008).

TTL5 neurons mainly project to subcortical regions and are characterized by an exquisite stereotypical morphology consisting of a pyramid like soma, and two distinct dendritic domains: the apical and basal dendrites. A single primary axon emerges from the TTL5 soma, before branching exuberantly and projecting to subcortical structures, establishing numerous excitatory glutamatergic synaptic connections spanning its length. The past couple of decades have witnessed several enlightening revelations on the functional roles of TTL5 neurons; through a combination of IR-DIC microscopy and *in vitro* patch-clamp recordings from neocortical brain slices (Stuart *et al.* 1993; Stuart & Sakmann, 1994; Markram & Sakmann, 1994; Stuart & Spruston, 1995; Markram *et al.* 1997a; Larkum *et al.* 2001; Davie *et al.* 2006; Nevian *et al.* 2007; Larkum *et al.* 2009), and through *in vivo* whole cell recordings (Helmchen *et al.* 1999; Svoboda *et al.* 1997) and more recently with microendoscopy for targeted recordings in freely moving animals (Murayama *et al.* 2007; Murayama & Larkum, 2009a; Murayama & Larkum, 2009b).

A recent comprehensive review has focussed on the dendritic structure and synaptic integration in hippocampal and neocortical pyramidal neurons (see Spruston, 2008). However, the intent of this review is two fold; to integrate the knowlegde from a vast body of existing literature specific to TTL5 neurons, providing insights on the dendritic properties and synaptic integration, axonal structure, AP initiation and propagation, synaptic dynamics, structural and functional synaptic plasticity and pathophysiology down to a succinct summary, and to articulate key questions, the answers to which would further our understanding of how the properties of TTL5 neurons influence neocortical function.

Dendritic properties

Characteristics of dendritic structure

The elaborate dendritic arbour of TTL5 neurons is characterized by an apical trunk ascending from the apex of the soma with oblique dendrites emanating at various angles from the apical trunk, terminating with a crown like tuft in layer 1, and basal dendrites emerging radially from the base of the soma. TTL5 neurons receive a bulk of glutamatergic synaptic inputs on basal and proximal oblique dendrites (Thomson *et al.* 1993; Markram, 1997; Markram *et al.* 1997a), while GABA-ergic inputs are primarily

received by the soma, proximal dendrites and axon, but could also be received by distal terminal tufts (for review see Markram *et al.* 2004; see also Silberberg & Markram, 2007). The mechanisms underlying synaptic integration in specific dendritic input domains of TTL5 neurons are not completely understood yet, raising several tantalizing questions.

Detailed morphological analyses by Romand *et al.* (2011) have revealed that the TTL5 dendritic arbour is characterized by distinct growing rates and properties of alterations over different stages of development. During the postnatal day (P) 7 to P14 period almost all dendritic compartments grow fast with a disappearance of filopodia-like segments along the apical dendrites; During the P14 to P21 period, the growth is mostly localized on specified segments of each compartment with a marked increase in the densities of spines; Finally, during the P21 to P60 period, the number of basal dendritic segments significantly increase at certain branch orders, while some oblique dendritic segments are lengthened or thickened. Therefore, the developmental changes of the TTL5 dendritic arbour can be categorized into two modes: the fast overall growth during the initial period and the slow localized growth (thickening of the intermediate segments or lengthening of the terminal segments) over subsequent periods. The differential regulation in the arborization of dendritic compartments during various developmental stages supports the notion that multiple functional compartments may serve to integrate distinct signal transduction systems, enhancing the information processing potential of TTL5 neurons.

TTL5 dendrites are richly endowed with spines, which directly receive most of the excitatory synaptic input (Peters & Kaiserman-Abramof, 1970; Peters, 1987; Larkman, 1991). The functional relevance of spines is not fully understood yet, however, some general speculations have been made through theoretical studies and *in vitro* slice experiments, a) Spines serve to optimize the filling of a large number of afferent synapses onto a dendrite by increasing the dendritic surface area (Stepanyants *et al.* 2002) b) Spines could check the diffusion of critical molecules away from the synapse, serving as individual biochemical compartments (Koch & Zador, 1993; for review see Nimchinsky *et al.* 2002) c) Spines could play a regulatory role on the electrical properties of neurons (Koch & Zador, 1993; Yuste & Denk, 1995; Yuste *et al.* 2000; Tsay & Yuste, 2002; Araya *et al.* 2006; Araya *et al.* 2007; Palmer & Stuart, 2009). The spine head is the site of a tiny,

amorphous structure called the postsynaptic density (PSD). Prominent in excitatory synapses, the PSD houses AMPA and NMDA receptors (AMPA & NMDAR, respectively) attached to large protein “signaling machines” that regulate the strength of synaptic transmission (Kennedy, 1997; Kennedy, 2000). *In vivo* imaging approaches have revealed the existence of spines with varying sizes in neocortical pyramidal cells, thin transient spines and thick persistent spines, suggesting functional roles in regulating time-scales for synaptic plasticity (Trachtenberg *et al.* 2002; Holtmaat *et al.* 2005; Holtmaat *et al.* 2006).

Dendritic excitability and local regenerative potentials

Stuart & Sakmann (1994) performed direct patch-clamp recordings of TTL5 apical dendrites *in vitro* and demonstrated *prima facie* that an axo-somatic action potential (AP) back-propagates into the dendritic arbour. A back-propagating action potential (bAP) serves as a retrograde signal, conveying the level of neuronal output activity to the dendrites. Indeed, bAPs attenuate in amplitude as they propagate from proximal to distal locations along the somato-dendritic axis (Stuart & Sakmann, 1994; for reviews see Stuart *et al.* 1997; Waters *et al.* 2004). Preliminary computational modelling studies have indicated that the morphology of the TTL5 dendritic arbour impacts the back-propagation of APs (Vetter *et al.* 2001).

Through simultaneous recordings of membrane voltage and $[Ca^{2+}]_i$ in TTL5 apical dendrites, Markram & Sakmann (1994) demonstrated that EPSPs caused a transient increase in $[Ca^{2+}]_i$ mediated by the opening of low voltage activated Ca^{2+} channels. The study by Markram & Sakmann (1994) provided additional insights that dendrites do not function as mere passive cables at low frequency synaptic activity. Furthermore, bAPs in proximal apical dendrites were also found to evoke transient $[Ca^{2+}]_i$ (Markram *et al.* 1995; Schiller *et al.* 1995; Helmchen *et al.* 1996). TTL5 distal apical dendrites were found to amplify glutamatergic inputs through local Ca^{2+} spikes, thus controlling the synaptic efficacy of cortico-cortical inputs to TTL5 neurons (Schiller *et al.* 1997).

TTL5 dendrites operate as coincidence detectors by summing local spikes from individual branches with other inputs to evoke AP firing. Conventionally, this implies the coincident activation of a sufficient number of inputs to reach AP firing threshold (for reviews see

Yuste *et al.* 2000; Segev & London, 2000; London & Häusser, 2005). A “critical frequency” of AP firing (~100 Hz) can elicit a regenerative Ca^{2+} spike in apical and basal dendrites (Larkum *et al.* 1999; Kampa *et al.* 2006). While local Ca^{2+} spikes are generated upon dendritic synaptic input coincident with bAPs, their initiation can be restrained by dendritic GABA_B mediated inhibition (Perez-Garci *et al.* 2006). Coincident summation of distal synaptic input with the BAP gives rise to a so-called back-propagation activated Ca^{2+} spike (BAC) consequently causing a burst of APs at the soma, which was first demonstrated by Larkum *et al.* (2000).

Previous endeavours at inferring the integrative properties of thin TTL5 dendrites have either employed computational modelling or optical imaging techniques (Schiller *et al.* 2000; Antic, 2003; Milojkovic *et al.* 2004; Milojkovic *et al.* 2005; Kampa *et al.* 2006). Although informative, a primary bottleneck of optical imaging is that the technique is only semi-quantitative, and has led to controversial inferences on the integrative properties of TTL5 dendrites. Pioneering work by Nevian *et al.* (2007) revealed the fundamental principles of synaptic integration in TTL5 basal dendrites through direct dendritic patch-clamp recordings. Simultaneous dendritic and somatic recordings of spontaneous events in TTL5 basal dendrites revealed a dendrite to soma EPSP attenuation of up to 40 fold at dendritic locations ~140 μm away from the soma. Contrastingly, the backward spread of EPSPs from the soma to basal dendrites was efficient with very little attenuation. Kampa *et al.* (2006) provided first hand evidence of bAPs encroaching the TTL5 basal dendritic arbour, and discovered that APs depolarized the distal basal dendrites during high-frequency burst firing following the generation of indispensable local dendritic Ca^{2+} spikes. Nevian *et al.* (2007) further provided critical insights on the attenuation of bAPs in TTL5 basal dendrites, and reported that when scaled to the relative size of apical and basal dendrites, the attenuation of bAPs in TTL5 apical and basal dendrites were almost identical. In addition to local Ca^{2+} spikes, Na^+ and NMDA spikes can also be initiated in the TTL5 dendritic arbour (Nevian *et al.* 2007; Schiller *et al.* 2000; Kampa *et al.* 2006; Rhodes, 2006; Major *et al.* 2008; Polsky *et al.* 2009; Larkum *et al.* 2009). By means of glutamate uncaging, Schiller *et al.* (2000) demonstrated that synaptically evoked potentials in basal dendrites were in fact NMDA spikes, usually followed by a large local Ca^{2+} influx. This study also identified that localized NMDA spikes potentially confer a degree of

parallel processing and independent decision-making in TTL5 basal dendritic branches.

A long-standing view has held that TTL5 dendrites sum synaptic input either linearly or supra-linearly (Nettleton & Spain, 2000; Ulrich, 2003; for review see Silver, 2010). Biophysical modelling approaches have suggested that the “arithmetic” of local summation in thin dendrites endows them with an ability to serve as independent computational “subunits”, which sigmoidally modulate their inputs prior to global summation. A study by Polsky *et al.* (2004) combined confocal imaging and dual-site focal synaptic stimulation of TTL5 basal dendrites to reveal that nearby inputs on the same dendritic branch summed sigmoidally, whereas widely separated inputs or inputs to different branches summed linearly. These findings by Polsky *et al.* (2004) provided experimental support for a previous theoretical postulate of a two-layer “neural network” model of thin-branch synaptic integration in pyramidal neurons (Poirazi *et al.* 2003).

Although previous computational modelling studies have hypothesized plausible explanations for synaptic integration in terminal tufts, these fine structures have proven rather difficult for direct experimental access (Rhodes & Llinás, 2001). Only recently did Larkum *et al.* (2009) demonstrate that NMDA spikes form the dominant mechanism through which distal synaptic input influences TTL5 neurons to reach AP firing threshold, additionally also providing the basis for parallel processing of top-down input received by terminal tufts. These experiments by Larkum *et al.* (2009) lead to a whole new unifying principle of synaptic integration, where TTL5 basal and terminal tuft dendrites integrate inputs through the recruitment of local NMDA spikes, relative to the fixed apical Ca^{2+} and axo-somatic Na^+ zones of integration.

How influential are TTL5 distal synaptic inputs in AP initiation as against their more proximal counterparts? Distal synapses are expected to exert lesser influence on axo-somatic AP initiation, mainly due to the charge loss following the flow of current from the dendrites to the soma and the axon (for reviews see: Spruston *et al.* 1994; Stuart *et al.* 1997b; Magee, 2000; also see Stuart & Spruston, 1998). Do ‘disadvantaged’ distal synapses scale their conductance accordingly, rendering themselves eligible to ‘veto’ their say on AP initiation (Häusser, 2001; Rumsey & Abbott, 2006; for reviews see: Segev & London, 2000; Magee, 2000; Williams & Stuart, 2003a)? Contrary to such synaptic

scaling observed in CA1 pyramidal neurons (Magee & Cook, 2000), Williams & Stuart (2002; 2003b) provided direct evidence that the amplitude and time course of both excitatory and inhibitory dendritic synaptic input in TTL5 neurons are influenced by voltage-gated conductances, thus revealing a site dependent mechanism for synaptic efficacy.

Dendrites with small diameters have high input impedance, therefore thin distal dendrites give rise to large local synaptic responses reducing the driving force for synaptic current. Distal synapses could also considerably influence AP initiation by activating voltage-gated conductances, which increase charge entry and consequently initiate local dendritic spikes (for reviews see: Magee, 2000; Spruston, 2008).

TTL5 neurons are bombarded with synaptic input during active network states *in vivo* (Pare *et al.* 1998; Borg-Graham *et al.* 1998; Destexhe *et al.* 2001; for review see Destexhe *et al.* 2003). Modelling studies have predicted that such ongoing activity attenuates synaptic potentials as they propagate across the dendritic arbour (Bernander *et al.* 1991; Ho & Destexhe, 2000; for review see London & Segev, 2001; Chance *et al.* 2002; Rudolph & Destexhe, 2003). Ongoing synaptic activity thus dictates the efficacy of dendritic synaptic input that activates dendritic spikes through local synaptic integration to forward-propagate to the axonal AP initiation site. This regime of distributed processing is believed to have implications on the computational power of cortical pyramidal neurons (Mel, 1993; Häusser & Mel, 2001; Williams & Stuart, 2003a). What do we know about such processing regimes under high-conductance states during active network states *in vivo*? The first experiments to test the existence of such a regime by mimicking *in vivo* like synaptic conductance levels *in vitro* were performed by Williams (2004), demonstrating that conductance is highly compartmentalized in TTL5 neurons, and that the dendritic arbour is optimized to independently carry out axo-somatic and apical dendritic integration under high synaptic conductance states. Additional evidence also suggests that distal excitatory synaptic inputs decisively control the synaptic output of TTL5 neurons, powerfully influencing neocortical network activity as a consequence (Williams, 2005).

Dendritic voltage-gated conductances

The dendrites of TTL5 neurons express A-type and persistent K^+ channels, transient and persistent Na^+ channels, hyperpolarization-activated cation (HCN) channels, a plethora of Ca^{2+} channels, and large and small conductance (BK & SK, respectively) Ca^{2+} dependent K^+ channels, all of which profoundly influence the integration of synaptic input (Huguenard *et al.* 1989; Reuveni *et al.* 1993; Markram & Sakmann, 1994; Stuart & Sakmann, 1994; Crill, 1996; Korngreen & Sakmann 2000; Bekkers, 2000*a*; Bekkers 2000*b*; Reyes, 2001; Benhassine & Berger, 2005; Kole *et al.* 2006; Almog & Korngreen, 2008; Benhassine & Berger, 2009). A-type K^+ channels decrease in density along the somato-dendritic axis and thus serve in defining a distal, low threshold region for the initiation of dendritic regenerative potentials (Korngreen & Sakmann, 2000; Bekkers 2000*b*; Schaefer *et al.* 2007).

Transient Na^+ channels are distributed uniformly along the somato-dendritic axis and are crucial in sustaining bAPs and local dendritic spikes (Huguenard *et al.* 1989; Stuart & Sakmann, 1994). Persistent Na^+ channels are uniformly distributed along the somato-dendritic axis and are believed to amplify the synaptic current in apical dendrites (Schwindt & Crill, 1995; Mittmann *et al.* 1997; Astman *et al.* 2006).

HCN channels carry the depolarizing I_h current activated by hyperpolarization, and are important for dendritic excitability. These channels, which are exponentially distributed along the somato-dendritic axis, profoundly influence the time course of synaptic input and cause spatially independent integration of synaptic input onto apical and basal dendrites in TTL5 neurons (Williams & Stuart, 2000; Berger *et al.* 2001; Lörincz *et al.* 2002; Berger *et al.* 2003; Kole *et al.* 2006). An interplay between the I_h current and the membrane capacitance endows band-pass filtering abilities to TTL5 neurons, thus favouring frequency tuning (Ulrich, 2002). Recent evidence indicates that an age-dependent increase in dendritic HCN channel density ensures the development of TTL5 neurons from compact temporal integrators to compartmentalized integrators of basal and apical dendritic synaptic input (Atkinson & Williams, 2009). A myriad of low (T-type) and high (L, N, P/Q and R types) voltage activated Ca^{2+} channels exist in TTL5 neurons (Reuveni *et al.* 1993; Markram & Sakmann, 1994; Almog & Korngreen, 2009).

Ca²⁺ channels are critical in regulating neurotransmitter release, generating and sustaining regenerative dendritic events and burst firing of APs (Markram & Sakmann, 1994; Schiller *et al.* 1997; Stuart *et al.* 1997; Ohana & Sakmann, 1998; Koester & Sakmann, 1998; Williams & Stuart, 1999; Larkum *et al.* 2000). BK channels are homogeneously distributed along the somato-dendritic axis of TTL5 neurons, and their activation reduces the occurrence of local dendritic Ca²⁺ spikes thus rendering dendrites less excitable. BK channels do not influence the temporal window to initiate bACs, thus actively decoupling the axo-somatic and the dendritic AP initiation zones during high-frequency inputs (Benhassine & Berger, 2005; Benhassine & Berger, 2009).

Axonal Properties

Characteristics of axonal structure

The lone TTL5 axon emerges from the soma, projecting towards the white matter while giving off several collateral stems that further bifurcate and ramify within the neocortex. The TTL5 axon initial segment (AIS) marks the origin of the axonal arbour and is uniquely innervated by GABAergic axo-axonic synapses established by Chandelier cells (Somogyi 1997; Szabadics *et al.* 2006; for reviews see Somogyi *et al.* 1998; Markram *et al.* 2004). This arrangement is believed to further refine the functional compartmentalization of TTL5 neurons (see Characteristics of dendritic structure).

Initiation and Propagation of APs

Preliminary insights on AP initiation in the unmyelinated AIS were gained almost half a century ago (Coombs *et al.* 1957, Fatt, 1957; Fuortes *et al.* 1957; Eccles, 1964; Palay *et al.* 1968; Peters *et al.* 1968). Through the years, numerous studies have also suggested the initiation of APs within dendrites of cortical pyramidal neurons (Spencer & Kandel, 1961; Wong *et al.* 1979; Deschênes, 1981; Herreras, 1990; Pockberger, 1991; Turner *et al.* 1991; Amitai *et al.* 1993; Yuste *et al.* 1994; Markram & Sakmann, 1994; Regehr & Armstrong, 1994; Markram *et al.* 1995; Hirsch *et al.* 1995; Mainen *et al.* 1995; Johnston *et al.* 1996; Schiller *et al.* 1997; Schwindt & Crill, 1997; Stuart *et al.* 1997a; Stuart *et al.* 1997b; Paré & Lang, 1998; Larkum *et al.* 1999; Larkum *et al.* 2000; Zhu *et al.* 2000; Schiller *et al.* 2000; Oakley *et al.* 2001a; Oakley *et al.* 2001b; Antic *et al.* 2003; Polsky *et al.* 2004;

Kampa *et al.* 2006; Gordon *et al.* 2006; Nevian *et al.* 2007; Major *et al.* 2008; Polsky *et al.* 2009; Larkum *et al.* 2009). However, a growing body of evidence conclusively indicates that APs in TTL5 neurons are often initiated in the low threshold axon rather than at the site of dendritic synaptic input (Stuart *et al.* 1997a; Colbert & Pan, 2002; Palmer & Stuart, 2006; Shu *et al.* 2006; Kole *et al.* 2007; Kole *et al.* 2008; Fleidervish *et al.* 2010). Palmer & Stuart (2006) demonstrated that AP initiation in TTL5 neurons occurs at the distal site of the AIS, about 35 μm away from the axon hillock.

How do APs propagate following their initiation? APs in TTL5 neurons orthogradely propagate into the axonal arbour, and retrogradely propagate to invade the dendritic arbour (Stuart *et al.* 1997). The retrograde propagation of APs signals the level of neuronal output to the dendritic tree (see Dendritic excitability and local regenerative potentials; Amitai *et al.* 1994; Stuart & Sakmann, 1994; Markram & Sakmann, 1994; Markram *et al.* 1995; Schiller *et al.* 1995; Schiller *et al.* 1997; Stuart *et al.* 1997a; Larkum *et al.* 1999; Larkum *et al.* 2000; Kampa *et al.* 2006; Nevian *et al.* 2007; Larkum *et al.* 2009).

Axonal APs have also been reported to occur before somatic APs, with the latency difference between the onset of axonal and somatic APs increasing at distal axonal locations (Stuart *et al.* 1997a). The latency difference between the peak of somatic and axonal APs increase with axonal recordings more distal from the soma, leading to an AP conduction velocity estimate of about 300 $\mu\text{m}/\text{ms}$ (Stuart *et al.* 1997a). Axonal APs back-propagating into the TTL5 dendritic tree undergo distance and frequency dependent attenuation (Stuart & Sakmann 1994; Stuart *et al.* 1997a). The latency difference between the onset and peak of somatic and dendritic bAPs have also been found to increase as a function of distance from the soma (Stuart *et al.* 1997a).

Several unique features distinguish AP initiation in TTL5 neurons. One such prominent feature is the characteristic rapid rise at the foot of the somatic AP, which leads to a so-called “kink” (Naundorf *et al.* 2007; McCormick *et al.* 2007). Detailed recordings from TTL5 neurons and computational modelling have revealed that this kink in the AP, exclusive to TTL5 neurons (Shu *et al.* 2007) could be attributed to axonal AP initiation, owing in part to the high density of Na^+ channels housed in the AIS (McCormick *et al.* 2006; Inda *et al.* 2006). The structural evidence for a high Na^+ channel density in the AIS

of cortical pyramidal neurons is both plentiful and conclusive (Inda *et al.* 2006; Kole *et al.* 2008; Lörincz & Nusser, 2010), but what functional relevance does this confer? Although it is tempting to subscribe to the interpretation that AP initiation is succored by a high Na⁺ channel density that renders a low threshold in the AIS of TTL5 neurons, the dilemma is far from resolved. Colbert & Pan (2002) suggested that the biophysics of axonal channels and not a high Na⁺ channel density underlies AP initiation in TTL5 neurons, whereas several studies have tried to affirm that AP initiation is aided by a high Na⁺ channel density in the AIS of TTL5 neurons (Kole *et al.* 2008; Hu *et al.* 2009). Yet another recent study reports that the density of Na⁺ channels in the AIS of TTL5 neurons is only 3 fold greater than in the soma (Fleidervish *et al.* 2010), contradicting previous estimates of Na⁺ channel density almost 50 fold greater than in proximal dendrites (Kole *et al.* 2008). Although Kole *et al.* (2008) demonstrated that the disruption of the tight anchoring of Na⁺ channels to the actin cytoskeleton increases the measurement of the inward Na⁺ current in the AIS of TTL5 neurons and pointed the potential pitfalls about previous interpretations on similar Na⁺ channel densities (Colbert & Pan, 2002), the mystery surrounding the functional advantages of a high Na⁺ channel density in the AIS is yet to be unraveled.

The AIS of TTL5 neurons also supports a high density of local voltage-gated D-type K⁺ channels, which play a pivotal role in integrating slow sub-threshold input and sculpting the AP waveform and duration (Kole *et al.* 2007b). Furthermore, D-type K⁺ channels also regulate neurotransmitter release and critically modulate the efficacy of synaptic connections between TTL5 neurons (Bekkers & Delaney, 2001; Kole *et al.* 2007b).

Intrinsic firing properties

Voltage-gated conductances contribute to AP initiation and influence the intrinsic properties of TTL5 neurons, such as the threshold for AP initiation, AP after-hyperpolarization and after-depolarization, and the firing mode. TTL5 neurons mostly respond to depolarizing somatic current injections through a distinctive firing pattern with spike-frequency adaptation, but can also discharge a burst of APs (Connors *et al.* 1982; McCormick *et al.* 1985; Connors & Gutnick, 1990; Mason & Larkman, 1990; Chagnac-Amitai *et al.* 1990; Silva *et al.* 1991; Amitai, 1994; Kasper *et al.* 1994a; Kasper

et al. 1994*b*; Kasper *et al.* 1994*c*; Schwindt *et al.* 1997; Williams & Stuart, 1999; Schubert *et al.* 2001; Steriade, 2004; Schubert *et al.* 2006; Groh *et al.* 2010).

Modelling and experimental studies have demonstrated that bursts of APs are generated through the activation of Ca²⁺ channels, prior to the back-propagation of APs into the TTL5 dendritic arbour (Rhodes & Gray, 1994; Mainen & Sejnowski, 1996; Williams & Stuart, 1999). The importance of burst firing is critically dependent upon the fidelity of information transfer (Lisman, 1997; Williams & Stuart, 1999). For instance, a pertinent question here is if all APs during a burst discharge propagate reliably into the TTL5 axonal arbour resulting in neurotransmitter release, and what are the postsynaptic consequences following such release? It is rather unambiguous that postsynaptic responses between TTL5 neurons exhibit frequency-dependent depression during a low frequency train of APs, typically < 100 Hz (Thomson *et al.* 1993; Markram & Tsodyks, 1996*a*; Markram & Tsodyks, 1996*b*; Markram, 1997; Markram *et al.* 1997*a*; Thomson, 1997; Tsodyks & Markram, 1997). Therefore, high frequency bursts of APs likely lead to unreliable postsynaptic responses, casting doubts on the relevance of burst firing in TTL5 neurons. Williams & Stuart (1999) discovered significance of burst firing, indicating that these bursts served to enhance synaptic coupling between TTL5 neurons through distinct and synergistic pre- and postsynaptic amplification mechanisms during bursts of APs. The activation of dendritic Ca²⁺ channels by bAPs was discovered to be indispensable in the generation of burst firing in TTL5 neurons (Williams & Stuart, 1999).

Synaptic properties

In vitro paired recordings by Markram *et al.* (1997*a*) have furthered fundamental know-how on the anatomical and physiological properties of TTL5 synaptic connections.

Anatomical properties of synaptic connections

Light and electron microscopic examinations of biocytin filled pre- and postsynaptic TTL5 neurons have both revealed fine-grain details on the morphology of axonal and dendritic arbours, the mean number and the spatial innervation pattern of potential synaptic contacts (Markram, 1997; Markram *et al.* 1997*a*). TTL5 neurons are connected with a probability of ~ 10% through about 4 to 8 potential synaptic contacts (mean ± S.D.

of 5.5 ± 1.1 contacts; Markram *et al.* 1997a). However, this numerical information is based on *in vitro* recordings from 300 μm thick neocortical slices where axons and dendrites are potentially severed due to the slicing procedure, and thus could very well represent lower estimates (Markram, 1997; Markram *et al.* 1997a). Potential synapses have been found to be distributed across the entire dendritic arbour, however, despite this heterogeneous spatial innervation TTL5 synapses are predisposed to occur at specific dendritic locations. A majority of potential synaptic contacts underlying connections between TTL5 neurons are located on secondary and tertiary branches of basal dendrites, about 80-120 μm from the soma. The densities of synapses on primary, secondary and tertiary branches of basal dendrites have been found to be strikingly similar (Markram, 1997; Markram *et al.* 1997a). A given TTL5 neuron can also potentially innervate its own dendritic arbour, establishing a so-called autapse (Van der Loos & Glaser, 1972; Lübke *et al.* 1996). Remarkably, the spatial locations of autapses in TTL5 neurons have been found to mirror that of synapses, implying highly common principles of synapse formation in local TTL5 microcircuits (Lübke *et al.* 1996).

Inhibitory interneurons innervate TTL5 neurons by establishing GABA-ergic synaptic contacts preferentially onto proximal dendrites and soma, axon, and distal dendritic tufts (for reviews see: Somogyi *et al.* 1998; Markram *et al.* 2004; Thomson & Lamy, 2007). While basket cells mostly target proximal dendrites and somata of TTL5 neurons (Gupta *et al.* 2000; Wang *et al.* 2002), Chandelier cells exclusively target the AIS (Somogyi, 1977; Szabadics *et al.* 2006) and Martinotti cells innervate distal TTL5 tufts (Silberberg & Markram, 2007).

“I innervate, therefore I am”. From an estimated 300-500 TTL5 neurons in a local cortical module (diameter of 300 μm ; Szentágothai, 1975), a connection probability of $\sim 10\%$, and about 5 potential synapses per connection, a single TTL5 neuron could be potentially innervated from as many as 40 neighbouring TTL5 neurons, receiving about 200 afferent TTL5 synapses on one hand, and innervating a similar number of TTL5 neurons on the other (Peters, 1987; Markram, 1997; Markram *et al.* 1997a; Song *et al.* 2005).

Physiological properties of synaptic connections

The response of monosynaptic glutamatergic connections between TTL5 neurons in the juvenile mammalian somatosensory cortex displays characteristic short-term frequency dependent depression, with a high initial probability of neurotransmitter release (Thomson *et al.* 1993; Thomson & West, 1993; Markram & Tsodyks, 1996; Markram *et al.* 1997a; Tsodyks & Markram, 1997; Thomson, 1997; Reyes *et al.* 1998; Reyes & Sakmann, 1999). Although this phenomenon is mostly ubiquitous across several neocortical areas in juvenile animals, an exception is the prefrontal cortex where the response of monosynaptic connections between TTL5 neurons is marked by facilitating synapses with pronounced augmentation (Wang *et al.* 2006; Berger *et al.* 2009). Monosynaptic connections between TTL5 neurons in the mature mammalian neocortex have been found to be predominantly facilitating (Williams & Atkinson, 2007).

A conspicuous trait of TTL5 synaptic depression is that once a certain “limiting” activation frequency is surpassed, postsynaptic responses show a decrease in amplitude inversely proportional to the activation frequency, termed the 1/f rule of synaptic depression (Tsodyks & Markram, 1997; Abbott *et al.* 1997). For instance, according to this rule the average amplitude of the postsynaptic response at an activation frequency of 40 Hz is half the amplitude at that of 20 Hz. The various mechanisms underlying frequency dependent synaptic depression in TTL5 neurons are not fully understood yet (O’Donovan & Rinzel, 1997). However, the phenomenon of synaptic depression has been found to be independent of the activation of postsynaptic voltage-gated channels or polysynaptic dendritic inhibition or shunting (Markram & Tsodyks, 1996). It is believed that both pre and postsynaptic factors influence depression (Markram *et al.* 1997a). Some preliminary experiments with the bath application of 100 μ M cyclothiazide to block AMPAR desensitization did not abolish depression altogether, however, the rate of depression was slowed and the rate of recovery from depression and the EPSP amplitudes were found to increase in response to a presynaptic stimulus with a train of APs (Markram, 1997). AMPAR desensitization could therefore play a prominent role in sculpting TTL5 synaptic responses mediated by frequency-dependent depressing synapses (Trussell & Fischbach, 1989; Jones & Westbrook, 1996; Markram, 1997).

GABA-ergic inputs onto TTL5 neurons display both frequency dependent depression and

facilitation (Thomson *et al.* 1996; Gupta *et al.* 2000, Silberberg & Markram, 2007; Ali & Thomson, 2007). Markram *et al.* (1998) showed that the very same axon of a TTL5 neuron innervating a neighbouring TTL5 neuron through depressing synapses on one hand can also innervate an interneuron through facilitating synapses on the other, implying that the different characteristics of the target neurons underlie qualitative differences in synaptic properties. This discovery uncovered a differential signaling mechanism in neocortical information processing regulated by selective synaptic modifications.

Monosynaptic unitary EPSPs evoked by a single presynaptic AP in juvenile synaptic connections between TTL5 neurons ($n = 138$) typically have amplitudes in the range of 0.15 to 5.5 mV with a mean of 1.3 ± 1.1 mV, a mean EPSP onset latency of 1.7 ± 0.9 ms, a mean 20-80% rise time of 2.6 ± 2.3 ms, and a mean decay time constant of 40 ± 18 ms at mean membrane potentials of -60 ± 2 mV (Markram *et al.* 1997a). The rather wide range of EPSP amplitudes could potentially arise from the number of release sites, the probability of neurotransmitter release or the quantal size, which form the basis of the classical quantal model of synaptic transmission (Del Castillo & Katz, 1954, Korn & Faber, 1991). By means of statistical analysis, Loebel *et al.* (2009) predicted that multiple release sites mediate synaptic transmission between TTL5 neurons, however, further experimental corroborations are mandatory to ascertain this prediction. Synaptic transmission between TTL5 neurons is highly reliable with a low mean percentage of transmission failures of 14.3 ± 17.6 , and a mean coefficient of variation (CV) of EPSP amplitude of 0.52 ± 0.37 (Markram *et al.* 1997a).

Unitary EPSPs in monosynaptic TTL5 connections are voltage dependent, with an increase in magnitude of the amplitude, decay time constant and the voltage time integral at membrane potentials higher than -60 mV (Markram *et al.* 1997a). The amplification of EPSPs at more depolarized membrane potentials could be attributed to several sources, including increased current flow through NMDA receptors, block of I_h currents, and activation of low-threshold Ca^{2+} or persistent somatic Na^+ channels (Markram & Sakmann, 1994; Stuart & Sakmann, 1995; Schwindt & Crill, 1995). At hyperpolarized membrane potentials, the postsynaptic response between TTL5 neurons is mainly mediated by AMPA receptors (AMPA receptors) with fast kinetics, and at more depolarized

membrane potentials NMDA receptors (NMDARs) mediate the postsynaptic response with comparatively slow kinetics (Markram *et al.* 1997a). The typical rise and decay time course of AMPA conductances are about 0.2 ms and 1.7 ms, respectively (Häusser & Roth, 1997).

The time course of Mg^{2+} block and unblock of NMDARs determines the extent of their activation by depolarization and has critical implications for spike-timing dependent synaptic plasticity (STDP) by delivering precision to the temporal window (Kampa *et al.* 2004). A spatial concentration of AMPAR and NMDAR “hot-spots” along the TTL5 apical dendrite reveals a somato-dendritic gradient of glutamate sensitivity (Dodt *et al.* 1998). Interestingly, stimulation of these glutamate receptor hot spots facilitates the triggering of both Na^+ and Ca^{2+} spikes, implying that these hot spots serve as initiation zones for dendritic regenerative potentials (Dodt *et al.* 1998; Frick *et al.* 2001). The repertoire of ionotropic glutamate receptors in TTL5 neurons also includes kainate receptors (KAR), although studies confirming their functional relevance are rather scarce. KARs display kinetics on time-scales similar to AMPARs and are differentially distributed as an increasing somato-dendritic gradient (Eder *et al.* 2003).

Several prevalent polysynaptic pathways have been identified in the neocortex, where an assortment of GABA-ergic interneurons mediates connections between neighbouring pyramidal cells. It has also been discovered that pyramidal cells in supra-granular layers exert strong inhibitory effects on neighbouring pyramidal cells through the direct activation of nerve terminals of GABA-ergic interneuron, bypassing their somato-dendritic domain (Ren *et al.* 2007). The emergent dynamics of polysynaptic pathways through the mediation of GABA-ergic interneurons display a rich variety of temporal and spatial patterns, ensuring a balance of Yin-like inhibition and Yang-like excitation, critical for cortical function (McBain & Fisahn, 2001). Intriguingly, in these polysynaptic pathways inhibition is induced by discharge of local pyramidal cells, and excitation is caused by specific GABA-ergic interneurons (Kapfer *et al.* 2007; Silberberg, 2008).

Pioneering studies to characterize the properties of such polysynaptic pathways between TTL5 neurons were carried out by Silberberg & Markram (2007). Inhibitory responses

were evoked in TTL5 neurons following presynaptic stimulation of individual neighbouring TTL5 neurons with trains of APs. Strikingly, the probability for inhibition between TTL5 neurons was more than twice that of direct excitation, and inhibitory responses increased as a function of rate and duration of presynaptic discharge. Simultaneous somatic and dendritic recordings indicated the TTL5 distal tuft dendrites as the origin of inhibition. Whole cell recordings from local TTL5 neurons and neighbouring interneurons combined with morphological reconstructions corroborated that the mediating GABA-ergic interneurons were Martinotti cells (Silberberg & Markram, 2007).

Remarkably, during high-frequency discharges the Martinotti pathway is activated, and renders inhibitory interactions between TTL5 neurons, which are otherwise predominantly excitatory during low-frequency discharges through monosynaptic connections. The Martinotti pathway prevents over-activation of TTL5 neurons, and is therefore crucial in preventing epilepsy (Silberberg & Markram, 2007). By exclusively innervating distal tufts of TTL5 neurons in supra-granular neocortical layers, the Martinotti pathway serves akin to a “fire-extinguisher” by preventing the prolonged regeneration of dendritic Ca^{2+} spikes in TTL5 neurons and consequent high-frequency bursting, thereby maintaining cortical function by ensuring a balance of inhibition and excitation. An elegant study by Berger *et al.* (2009) revealed that the Martinotti pathway is not exclusive to the somatosensory cortex alone and is strikingly ubiquitous in its occurrence as a motif across a multitude of neocortical areas, however its precise role, for instance, in synaptic plasticity entails further investigation.

Synaptic plasticity

Synapses are plastic, governed by temporal patterns of pre and postsynaptic activity. The process of synaptic plasticity is widely believed to underlie learning and memory. Postsynaptic activity is shaped by the active and passive properties of the dendritic arbour. Dendritic excitability associated with a synapse regulates the plastic properties of the synapse over several time scales and stages of development (Turrigiano, 1999; Desai *et al.* 2000; Sjöström *et al.* 2001; Sjöström *et al.* 2008).

Plasticity in Local Microcircuits: The Ability to Rewire

Structurally, the local neocortical microcircuit is a *tabula rasa*, with each TTL5 axon forming several appositions with all neighbouring TTL5 dendrites (Kalisman *et al.* 2003; Kalisman *et al.* 2005). However, functionally, the constituent neurons of the microcircuit are very fickle in choosing their postsynaptic partners, with synapses established only onto a small fraction of these targets (Kalisman *et al.* 2005). This blueprint equips the neocortical microcircuit with a high potential for plasticity, enabling the formation of a multitude of functional microcircuits, which are incessantly transformed owing to the activity of their inherent neurons.

Kalisman *et al.* (2005) demonstrated through an elegant study that in the local TTL5 microcircuit the *tabula rasa* geometrical connectivity confers all possible connections, potentially allowing the reconfiguring of the microcircuit without any remodelling of arbours but simply by the genesis or termination of synapses (boutins and spines) at existing physical appositions. This puts forth the pertinent question if the microcircuit is in a state of spontaneous preparedness to rapidly turn connections between TTL5 neurons on or off without any further re-growing of axons or dendrites?

Le Bé & Markram (2006) provided evidence for a novel form of microcircuit plasticity where complete connections between TTL5 neurons consisting of several synaptic contacts were turned on and off over a time scale of hours. Through simultaneous multiple direct patch-clamp recordings of synaptically connected TTL5 neurons in sagittal slices, Le Bé & Markram (2006) discovered that connections spontaneously emerged and disappeared on the time scale of several hours. New connections were found to appear by bath and periodic puff application of glutamate, while the disappearance of connections were unaffected, indicating that excitation mediated by glutamate catalysed the formation of new connections (Le Bé & Markram, 2006). The same study also provided insights on the strength of emerging and disappearing connections in that emergent connections were found to be weaker than existing ones. Interestingly, the synaptic connections that disappeared over a span of time were preferentially the weaker ones with fewer synapses. This may underlie the co-operative mechanism that drives the formation of multi-synapse connections in the neocortex (Stepanyants *et al.* 2009).

Such a phenomenon of microcircuit plasticity is likely triggered by new experiences, which removes the weakest connections and provides a grace period to test the merit of new emergent connections for their retention or elimination, endowing microcircuits with the ability to choose stronger and thus ‘fitter’ connections in a “Darwinian” fashion (Le Bé & Markram, 2006).

Hebbian Synaptic Modifications through Redistribution of Synaptic Efficacy (RSE)

BAPs trigger synaptic modifications as they collide in time or miss time incoming EPSPs, revealing a delicate line between Hebbian and anti-Hebbian synaptic modifications (Markram *et al.* 1997b; Sjöström *et al.* 2001; Bi & Poo, 2001; Sjöström & Häusser, 2006; Sjöström *et al.* 2007; Kampa *et al.* 2006; Letzkus *et al.* 2006; Kampa *et al.* 2007; Sjöström *et al.* 2008; cite the new History of STDP in Frontiers). The consequent change in synaptic strength from Hebbian pairing is not a uniform amplification of responses at all frequencies, but arises due to a redistribution of available synaptic efficacy (Markram & Tsodyks, 1996a; Markram & Tsodyks, 1996b).

Traditionally, synaptic plasticity has been evaluated by measuring the change in the amplitude of synaptic responses evoked by single-shock extracellular electrical stimulation of presynaptic fibres (Bliss & Lomo, 1973). Markram & Tsodyks (1996b) demonstrated that it is not possible to extrapolate the general behaviour of a synapse by unitary responses, but using a train of presynaptic APs was essential to monitor the changes in gain at a synapse. This was the first demonstration of the redistribution of synaptic efficacy (RSE), where the absolute synaptic efficacy of connections between TTL5 neurons remained unaffected following high-frequency presynaptic stimulation (Markram & Tsodyks, 1996a; Markram & Tsodyks, 1996b). It was also discovered that the entire synaptic response to the high-frequency presynaptic AP train was not uniformly increased, but instead the existing synaptic efficacy was redistributed (Markram & Tsodyks, 1996b). The same study also suggested likely mechanisms contributing to the increased use of the existing efficacy in TTL5 synapses, through either an increase in the probability of neurotransmitter release after pairing or by an increase in the affinity of postsynaptic glutamatergic receptors, provided the receptors are not fully saturated (Markram & Tsodyks, 1996b).

Dendritic Excitability and Synaptic Plasticity: Two Sides of the Same Coin

Recent advances have revealed that not only are synapses plastic, but also the dendritic arbour itself. Although the morphology of the dendritic arbour remains mostly untransformed, its electrical properties can change in an activity-dependent manner over seconds to hours and perhaps even days, implying that dendritic learning rules exist in conjunction with synaptic rules (Sjöström *et al.* 2007; Sjöström *et al.* 2008). Synapses convey information through the dendrites to the soma, triggering axonal APs as the final output. This process is symbiotic, where synaptic activity regulates dendritic excitability, and the dendritic arbour in turn exerts influence in inducing synaptic plasticity.

A back-propagating AP invading the TTL5 dendritic arbour sparks synaptic modification (Markram *et al.* 1997b; Sjöström *et al.* 2001; Dan & Poo, 2004; Sjöström & Häusser, 2006; Sjöström *et al.* 2007; Kampa *et al.* 2006; Letzkus *et al.* 2006; Dan & Poo, 2006; Kampa *et al.* 2007; Sjöström *et al.* 2008). Through paired whole-cell recordings from TTL5 neurons, Markram *et al.* (1997b) made a watershed discovery where the coincidence of postsynaptic APs and unitary EPSPs was found to induce changes in EPSP amplitude. Markram *et al.* measured the effect of controlling the relative timing of pre- and postsynaptic APs on the synaptic strength of a pair of TTL5 neurons. If the presynaptic AP preceded the postsynaptic AP by as little as 10 ms, the connection was “strengthened”, leading to long-term potentiation (LTP). On the contrary, if the postsynaptic AP preceded the presynaptic AP, the connection was “weakened”, causing long-term depression (LTD). This discovery ushered in a refreshing perspective on Hebbian synaptic plasticity (Hebb, 1949; Markram *et al.* 1997b). The phenomenon of the regulation of synaptic efficacy by coincidental APs and EPSPs, christened spike-timing dependent synaptic plasticity (STDP) has established itself as an attractive model for learning at the level of single cells across several brain regions (Markram *et al.* 1997b; Magee & Johnston, 1997; Bi & Poo, 1998; Abbott & Nelson, 2000; Koch & Segev, 2000; Sjöström *et al.* 2001; Sjöström *et al.* 2007; Kampa *et al.* 2007; Sjöström *et al.* 2008; Sjöström & Gerstner, 2010). The change of the synapse plotted as a function of the relative timing of pre- and postsynaptic APs is referred to as the STDP function or learning window and varies between synapse types (Abbott & Nelson, 2000).

In classical STDP, the felicitous timing of postsynaptic APs induces LTP by depolarizing

and unblocking glutamate-bound NMDA receptors (Magee & Johnston, 1997; Markram *et al.* 1997b; Kampa *et al.* 2007). Under situations wherein BAPs completely fail to invade the dendritic arbour, STDP can still be induced if the BAPs are salvaged by sufficient postsynaptic depolarization. This can either be achieved by current injection during whole-cell recordings or by evoking bursts of APs (Sjöström *et al.* 2001; Sjöström & Häusser, 2006; Kampa *et al.* 2006; Letzkus *et al.* 2006). High-frequency bursts of APs occur naturally in TTL5 neurons and influence the initiation of dendritic spikes, consequently depolarizing the dendritic arbour (Lisman, 1997; Williams & Stuart, 1999; Larkum *et al.* 1999; Kampa & Stuart, 2006). It has been demonstrated that only AP bursts above a critical frequency (~100 Hz) of firing initiate dendritic spikes (Larkum *et al.* 1999; Kampa & Stuart, 2006). Compelling evidence also shows that AP bursts are required to exceed a critical frequency to bring about STDP, implying an essential requirement of dendritic spikes (Kampa *et al.* 2006). Similarly, the induction of STDP at synapses on basal and apical dendrites of TTL5 neurons can be blocked by the inhibition of dendritic spikes by voltage-gated Ca^{2+} channel antagonists (Kampa *et al.* 2006; Letzkus *et al.* 2006). In summary, all these key findings strongly indicate that global dendritic spikes during AP burst firing are indispensable for the induction of LTP during low frequency pairing.

The subsequent question then is how dependent is STDP induction on the dendritic location of synapses? Synapses onto different regions of the TTL5 dendritic arbour transmit different kinds of information, which could be integrated in several different ways. In concurrence with this notion, proximal synapses function by directly depolarizing the axo-somatic compartment, whereas information conveyed by distal synapses is mostly integrated through the initiation of regenerative dendritic spikes. Recent studies have focused on deciphering the relevance of dendritic synapse location for STDP induction in neocortical pyramidal neurons. The first study to address the location dependence of STDP indicated that the time window for LTD induction in layer 2/3 pyramidal neurons (L2/3PCs) is broader for inputs from distal synapses (Froemke *et al.* 2006). It was discovered that Ca^{2+} dependent suppression of NMDARs in the distal dendrites led to a broadening of the time window for LTD induction. Two other studies have investigated distance dependent STDP induction in TTL5 neurons. Sjöström &

Häusser (2006) demonstrated that pairing trains of APs and EPSPs at positive times led to LTP at proximal inputs. Contrastingly, the same paradigm induced LTD at distally located inputs. Distal LTD was induced even while postsynaptic firing was absent, but could be transformed to LTP fostered by BAPs following sufficient dendritic current injection. Letzkus *et al.* (2006) complementarily demonstrated that pairing unitary layer 2/3 inputs with bursts of APs at positive times led to LTP at proximal synapses and LTD at distal synapses in TTL5 neurons. On the contrary, negative pairings had the opposite effect, inducing LTD at proximal inputs and LTP of distal inputs in TTL5 neurons (Letzkus *et al.* 2006). Recent work by Gordon *et al.* (2006) demonstrated that TTL5 basal dendrites manifest “compartments” of plasticity. While synapses onto proximal basal dendrites are modified when paired with the global activity of the neuron, in distal basal dendrites NMDA spikes serve as a local postsynaptic signal for induction of LTP (Gordon *et al.* 2006).

Modulation of intrinsic excitability and plasticity

Several studies have investigated the influence of neuromodulators like dopamine (DA), and acetylcholine (ACh) on neuronal activity in rat neocortex, which have been found to be generally inhibitory (Gulledge & Jaffe, 1998; Gulledge & Jaffe, 2001; Gulledge & Stuart, 2005). Gulledge & Jaffe (1998) measured the effect of DA on the membrane properties of TTL5 neurons in the rat prefrontal cortex, and discovered that over a range of concentrations, DA decreased the excitability of TTL5 neurons. In another study, Gulledge & Jaffe (2001) demonstrated that the dopaminergic modulation of TTL5 neurons in the rat prefrontal cortex occurs through at least three different mechanisms; a) DA was found to inhibit AP generation by enhancing spontaneous inhibitory synaptic input b) DA decreased the input resistance of TTL5 neurons c) DA triggered a delayed and prolonged enhancement of excitability. Although DA inhibits AP generation in TTL5 neurons in the prefrontal cortex, it does not influence the back-propagation of APs, and the initiation of local dendritic spikes in these neurons (Gulledge & Stuart, 2003). These results indicate that DA probably does not play a modulatory role on the dendritic properties of TTL5 neurons in the prefrontal cortex, however this entails further investigation. ACh brings about RSE and reduces the rate of synaptic depression between TTL5 neurons without affecting the so-called stationary EPSPs following presynaptic

stimulation with a train of APs, suggesting that ACh attenuates temporal coding in TTL5 neurons (Markram & Tsodyks, 1997).

Synaptic plasticity can be modulated through the influence of exclusive dendritic domains in TTL5 neurons. Gordon *et al.* (2006) found that pairing of APs and EPSPs led to LTP induction in proximal basal dendrites, however, in distal basal dendrites LTP could be induced only when synaptic activation strong enough to initiate local NMDA spikes was paired with the local application of brain-derived neurotrophic factor (BDNF) that served as a “gating molecule”. Although BDNF is known to have a modulatory effect on cortical synaptic plasticity (Desai *et al.* 1999), experiments by Gordon *et al.* (2006) could, for instance, provide a basis to differentiate between synapses occurring on proximal and distal parts of the TTL5 basal dendritic arbour, aided by BDNF application. Cholinergic modulation can directly influence synaptic plasticity by shifting the polarity of plasticity, suggesting different modes for Hebbian modifications in TTL5 neurons (Stiefel *et al.* 2005).

Pathophysiology of the TTL5 neuron

Over the years, a wealth of information has accumulated on TTL5 function, however, what is our current understanding about TTL5 dysfunction? TTL5 dysfunction can lead to a number of maladies such as schizophrenia, epilepsy, autism, anxiety and depression to name a few, thus critically affecting cortical information processing (Black *et al.* 2004; Traub *et al.* 2005; Lytton, 2007).

Schizophrenia is a devastating neuropathology, marked by deterioration in the process of thinking and emotional responsiveness. The basal dendritic arbour in prefrontal cortical TTL5 neurons atrophies in size due to schizophrenia, and the consequent abnormal dendritic outgrowth leads to a reduction in cortical neuropil, therefore causing a decrease in connectivity between TTL5 neurons (Black *et al.* 2004). The reduced prefrontal neuropil could also be associated with less dopaminergic innervation of the deep layers of the prefrontal cortex, owing to schizophrenia (Garey *et al.* 1998; Black *et al.* 2004).

Epilepsy is one of several episodic disorders of the brain, characterized by recurrent synchronous neuronal activity. Epilepsy is not necessarily a single disorder, but manifests

itself in several forms, including multiple sclerosis, transient ischaemic attacks and migraine, all dynamical disorders that become apparent over time (Khosravani & Zamponi, 2006; Lytton, 2007). Recent evidence indicates that distinct forms of epilepsy are linked to changes in the efficacy of the I_h current carried by HCN channels (Di Pasquale *et al.* 1997; Santoro & Baram, 2003).

The deficit in I_h mediated functions may contribute to the development and onset of spontaneously occurring hyper-excitability in neocortical pyramidal neurons in a rat model of absence seizures (Strauss *et al.* 2003). Furthermore, through a genetic rat model of absence epilepsy, Kole *et al.* (2007a) showed that an experimentally observed loss of dendritic I_h recruits dendritic Ca^{2+} channels to amplify back-propagating AP triggered dendritic Ca^{2+} spikes, causing an increase in burst firing. Thus, the deficit of dendritic HCN channels in TTL5 neurons provides a somato-dendritic mechanism for increasing the synchronization of cortical output, and is therefore likely to play an important role in the generation of absence seizures (Kole *et al.* 2007a). Additionally, recent experiments have shown that sensory deprivation in the neocortex increases the intrinsic excitability of TTL5 neurons through epileptic seizures from increased dendritic Ca^{2+} , arising through a deficit of HCN expression (Breton & Stuart, 2009). These preliminary findings have contributed to a better understanding of the cortical basis of idiopathic generalized epilepsies and bolsters the idea that the mechanisms involved in HCN expression hold promise as therapeutic targets for the treatment of absence seizures.

The K^+/Cl^- co-transporter (KCC2) is important in maintaining low $[Cl^-]_i$, resulting in hyperpolarizing GABA responses. A decrease in KCC2 after neuronal injuries result in increases in $[Cl^-]_i$ and enhanced neuronal excitability in TTL5 neurons due to depolarizing GABA responses (Jin *et al.* 2006). Through the gramicidin perforated-patch technique to measure the GABA-ergic reversal potential in rat neocortical slices, Jin *et al.* (2006) explored the potential functional consequence of KCC2 downregulation in chronically injured neocortex. The study found that a positive shift in the GABA-ergic reversal potential due to Cl^- extrusion, directly attributed to KCC2 downregulation caused epileptogenesis in pathophysiological TTL5 neurons.

Autism is a developmental disorder of neurological origin, primarily affecting social

cognition. The etiology of autism has not been conclusively established yet, but genetic and environmental alterations are believed to cause vulnerability to this neuropathology (Rubenstein & Merzenich, 2003; Rinaldi *et al.* 2007a; Rinaldi *et al.* 2007b; Markram *et al.* 2007). Recent studies have focussed on animal models of autism, to explore changes in molecular, synaptic and cellular properties in pathological TTL5 neurons.

Rinaldi *et al.* (2007) investigated the postnatal effects of embryonic exposure to valproic acid (VPA) on TTL5 neurons of juvenile rat somatosensory cortex through whole cell patch-clamp recordings, and discovered that a single prenatal injection of VPA caused a significant enhancement of the local recurrent connectivity formed by TTL5 neurons. The connections between these pathological TTL5 neurons led to weaker synaptic responses, and their intrinsic excitability was also weakened. Furthermore, the mean number of potential synaptic contacts diminished from about 5.5 in control TTL5 neurons to about 3.3 in pathological TTL5 neurons, following exposure to VPA (Rinaldi *et al.* 2007a). Through another study, Rinaldi *et al.* (2007b) demonstrated that a single prenatal injection of VPA caused a surprisingly selective enhancement of NMDAR subunits NR2A and NR2B. This selective enhancement translated into enhanced NMDAR mediated synaptic currents and a marked amplification of synaptic plasticity through LTP in TTL5 neurons. These results provide preliminary revelations of some of the core symptoms observed in humans prenatally exposed to VPA, and hold promise for the therapeutic treatment of autism.

Two Decades of Research into TTL5 function: What Lies Ahead?

We have endeavoured to review the dendritic, axonal, synaptic properties and plasticity of TTL5 neurons, and to a lesser extent that of pathophysiological TTL5 neurons through a treasure-trove of discoveries in the past two decades. Although we certainly know much more from where we started, this is still just the tip of the iceberg. What lies beneath? With the advent of newer approaches for targeted recording of TTL5 neurons *in vivo* and *in vitro*, and detailed computational models of TTL5 neurons and their synaptic interactions, the future holds immense promise to explore and understand the crucial roles of these exquisite hallmark neurons in neocortical information processing (Markram, 2006; Luo *et al.* 2008; Kitamura *et al.* 2008; Petreanu *et al.* 2009; Murayama & Larkum,

2009).

A degree of inevitable recurrence exists in the description of some key properties in this review. An interdependence is evident between dendritic excitability and synaptic plasticity and vice-versa, where on one hand activity-dependent regulation of dendritic excitability induces synaptic plasticity, and synaptic plasticity controls dendritic computations on the other. Some illuminating questions to be answered could be if the phenomenon of coincidence detection by BACs is omnipresent in the entire neocortical pyramidal network, and not just restricted to TTL5 neurons alone.

The computational advantages bestowed by separate basal and apical dendritic compartments in TTL5 neurons has been extensively investigated, however, further quantitative investigations are imperative to peel out the distinct benefits of having oblique dendrites arising from the main apical trunk, for instance. Furthermore, gaining a grasp of how a single TTL5 neuron is actively modulated by a myriad of excitatory and inhibitory synapses impinging onto its various dendritic domains is a “bare necessity” to better understand the essence of TTL5 function and dysfunction. The continuous pursuit to answer several of these questions will lead us closer to uncovering the holy grail of neocortical function.

References

Acker CD & Antic SD (2009). Quantitative assessment of the distributions of membrane conductances involved in action potential backpropagation along basal dendrites. *J Neurophysiol* **101**, 1524-1541.

Ali AB, Bannister AP & Thomson AM (2007). Robust correlations between action potential duration and the properties of synaptic connections in layer 4 interneurons in neocortical slices from juvenile rats and adult rat and cat. *J Physiol* **580**, 149-169.

Almog M & Korngreen A (2009). Characterization of voltage-gated Ca²⁺ conductances in layer 5 neocortical pyramidal neurons from rats. *PLoS One* **4**, e4841.

Amitai Y, Friedman A, Connors BW & Gutnick MJ (1993). Regenerative activity in apical dendrites of pyramidal cells in neocortex. *Cereb Cortex* **3**, 26-38.

Antic SD (2003). Action potentials in basal and oblique dendrites of rat neocortical pyramidal neurons. *J Physiol* **550**, 35-50.

Araya R, Jiang J, Eiselthel KB & Yuste R (2006). The spine neck filters membrane potentials. *Proc Natl Acad Sci U S A* **103**, 17961-17966.

Araya R, Nikolenko V, Eiselthel KB & Yuste R (2007). Sodium channels amplify spine potentials. *Proc Natl Acad Sci U S A* **104**, 12347-12352.

Astman N, Gutnick MJ & Fleidervish IA (2006). Persistent sodium current in layer 5 neocortical neurons is primarily generated in the proximal axon. *J Neurosci* **26**, 3465-3473.

Atkinson SE & Williams SR (2009). Postnatal development of dendritic synaptic integration in rat neocortical pyramidal neurons. *J Neurophysiol* **102**, 735-751.

Bandrowski AE, Huguenard JR & Prince DA (2003). Baseline glutamate levels affect group I and II mGluRs in layer V pyramidal neurons of rat sensorimotor cortex. *J Neurophysiol* **89**, 1308-1316.

Bar-Yehuda D & Korngreen A (2007). Cellular and network contributions to excitability of layer 5 neocortical pyramidal neurons in the rat. *PLoS One* **2**, e1209.

Bekkers JM (2000a). Distribution and activation of voltage-gated potassium channels in cell-attached and outside-out patches from large layer 5 cortical pyramidal neurons of the rat. *J Physiol* **525**, 611-620.

Bekkers JM (2000b). Properties of voltage-gated potassium currents in nucleated patches from large layer 5 cortical pyramidal neurons of the rat. *J Physiol* **525**, 593-609.

Bekkers JM & Delaney AJ (2001). Modulation of excitability by alpha-dendrotoxin-sensitive potassium channels in neocortical pyramidal neurons. *J Neurosci* **21**, 6553-6560.

Benhassine N & Berger T (2005). Homogeneous distribution of large-conductance calcium-dependent potassium channels on soma and apical dendrite of rat neocortical layer 5 pyramidal neurons. *Eur J Neurosci* **21**, 914-926.

Benhassine N & Berger T (2009). Large-conductance calcium-dependent potassium channels prevent dendritic excitability in neocortical pyramidal neurons. *Pflugers Arch* **457**, 1133-1145.

Berger T, Larkum ME & Luscher HR (2001). High I(h) channel density in the distal apical dendrite of layer V pyramidal cells increases bidirectional attenuation of EPSPs. *J Neurophysiol* **85**, 855-868.

Berger T & Luscher HR (2003). Timing and precision of spike initiation in layer V pyramidal cells of the rat somatosensory cortex. *Cereb Cortex* **13**, 274-281.

Berger T, Senn W & Luscher HR (2003). Hyperpolarization-activated current Ih disconnects somatic and dendritic spike initiation zones in layer V pyramidal neurons. *J Neurophysiol* **90**, 2428-2437.

Berger TK, Perin R, Silberberg G & Markram H (2009). Frequency-dependent disynaptic inhibition in the pyramidal network: a ubiquitous pathway in the developing rat neocortex. *J Physiol* **587**, 5411-5425.

Bernander O, Douglas RJ, Martin KA & Koch C (1991). Synaptic background activity influences spatiotemporal integration in single pyramidal cells. *Proc Natl Acad Sci U S A* **88**, 11569-11573.

Bi GQ & Poo MM (1998). Synaptic modifications in cultured hippocampal neurons: dependence on spike timing, synaptic strength, and postsynaptic cell type. *J Neurosci* **18**, 10464-10472.

Black JE, Kodish IM, Grossman AW, Klintsova AY, Orlovskaya D, Vostrikov V, Uranova N & Greenough WT (2004). Pathology of layer V pyramidal neurons in the prefrontal cortex of patients with schizophrenia. *Am J Psychiatry* **161**, 742-744.

Borg-Graham LJ, Monier C & Fregnac Y (1998). Visual input evokes transient and strong shunting inhibition in visual cortical neurons. *Nature* **393**, 369-373.

Breton JD & Stuart GJ (2009). Loss of sensory input increases the intrinsic excitability of layer 5 pyramidal neurons in rat barrel cortex. *J Physiol* **587**, 5107-5119.

Brown SP & Hestrin S (2009). Intracortical circuits of pyramidal neurons reflect their long-range axonal targets. *Nature* **457**, 1133-1136.

Chance FS, Abbott LF & Reyes AD (2002). Gain modulation from background synaptic input. *Neuron* **35**, 773-782.

Colbert CM & Pan E (2002). Ion channel properties underlying axonal action potential initiation in pyramidal neurons. *Nat Neurosci* **5**, 533-538.

Connors BW & Gutnick MJ (1990). Intrinsic firing patterns of diverse neocortical neurons. *Trends Neurosci* **13**, 99-104.

- Connors BW, Gutnick MJ & Prince DA (1982). Electrophysiological properties of neocortical neurons in vitro. *J Neurophysiol* **48**, 1302-1320.
- Coombs JS, Curtis DR & Eccles JC (1957). The interpretation of spike potentials of motoneurons. *J Physiol* **139**, 198-231.
- Crill WE (1996). Persistent sodium current in mammalian central neurons. *Annu Rev Physiol* **58**, 349-362.
- Davie JT, Kole MH, Letzkus JJ, Rancz EA, Spruston N, Stuart GJ & Hausser M (2006). Dendritic patch-clamp recording. *Nat Protoc* **1**, 1235-1247.
- DeFelipe J & Farinas I (1992). The pyramidal neuron of the cerebral cortex: morphological and chemical characteristics of the synaptic inputs. *Prog Neurobiol* **39**, 563-607.
- Desai NS, Rutherford LC & Turrigiano GG (1999a). BDNF regulates the intrinsic excitability of cortical neurons. *Learn Mem* **6**, 284-291.
- Desai NS, Rutherford LC & Turrigiano GG (1999b). Plasticity in the intrinsic excitability of cortical pyramidal neurons. *Nat Neurosci* **2**, 515-520.
- Deschenes M (1981). Dendritic spikes induced in fast pyramidal tract neurons by thalamic stimulation. *Exp Brain Res* **43**, 304-308.
- Destexhe A, Rudolph M, Fellous JM & Sejnowski TJ (2001). Fluctuating synaptic conductances recreate in vivo-like activity in neocortical neurons. *Neuroscience* **107**, 13-24.
- Destexhe A, Rudolph M & Pare D (2003). The high-conductance state of neocortical neurons in vivo. *Nat Rev Neurosci* **4**, 739-751.
- Di Pasquale E, Keegan KD & Noebels JL (1997). Increased excitability and inward rectification in layer V cortical pyramidal neurons in the epileptic mutant mouse Stargazer. *J Neurophysiol* **77**, 621-631.
- Dotdt HU, Frick A, Kampe K & Zieglgansberger W (1998). NMDA and AMPA receptors on neocortical neurons are differentially distributed. *Eur J Neurosci* **10**, 3351-3357.
- Eder M, Becker K, Rammes G, Schierloh A, Azad SC, Zieglgansberger W & Dotdt HU (2003). Distribution and properties of functional postsynaptic kainate receptors on neocortical layer V pyramidal neurons. *J Neurosci* **23**, 6660-6670.
- Eder M, Zieglgansberger W & Dotdt HU (2002). Neocortical long-term potentiation and long-term depression: site of expression investigated by infrared-guided laser stimulation. *J Neurosci* **22**, 7558-7568.

Fatt P (1957). Sequence of events in synaptic activation of a motoneurone. *J Neurophysiol* **20**, 61-80.

Frick A, Zieglgansberger W & Dodt HU (2001). Glutamate receptors form hot spots on apical dendrites of neocortical pyramidal neurons. *J Neurophysiol* **86**, 1412-1421.

Froemke RC, Poo MM & Dan Y (2005). Spike-timing-dependent synaptic plasticity depends on dendritic location. *Nature* **434**, 221-225.

Fuortes MG, Frank K & Becker MC (1957). Steps in the production of motoneuron spikes. *J Gen Physiol* **40**, 735-752.

Garey LJ, Ong WY, Patel TS, Kanani M, Davis A, Mortimer AM, Barnes TR & Hirsch SR (1998). Reduced dendritic spine density on cerebral cortical pyramidal neurons in schizophrenia. *J Neurol Neurosurg Psychiatry* **65**, 446-453.

Gordon U, Polsky A & Schiller J (2006). Plasticity compartments in basal dendrites of neocortical pyramidal neurons. *J Neurosci* **26**, 12717-12726.

Groh A, Meyer HS, Schmidt EF, Heintz N, Sakmann B & Krieger P (2010). Cell-type specific properties of pyramidal neurons in neocortex underlying a layout that is modifiable depending on the cortical area. *Cereb Cortex* **20**, 826-836.

Gulledge AT & Jaffe DB (1998). Dopamine decreases the excitability of layer V pyramidal cells in the rat prefrontal cortex. *J Neurosci* **18**, 9139-9151.

Gulledge AT & Jaffe DB (2001). Multiple effects of dopamine on layer V pyramidal cell excitability in rat prefrontal cortex. *J Neurophysiol* **86**, 586-595.

Gulledge AT & Stuart GJ (2003). Action potential initiation and propagation in layer 5 pyramidal neurons of the rat prefrontal cortex: absence of dopamine modulation. *J Neurosci* **23**, 11363-11372.

Gupta A, Wang Y & Markram H (2000). Organizing principles for a diversity of GABAergic interneurons and synapses in the neocortex. *Science* **287**, 273-278.

Hausser M (2001). Synaptic function: dendritic democracy. *Curr Biol* **11**, R10-12.

Hausser M & Mel B (2003). Dendrites: bug or feature? *Curr Opin Neurobiol* **13**, 372-383.

Hausser M & Roth A (1997). Estimating the time course of the excitatory synaptic conductance in neocortical pyramidal cells using a novel voltage jump method. *J Neurosci* **17**, 7606-7625.

Helmchen F, Imoto K & Sakmann B (1996). Ca^{2+} buffering and action potential-evoked Ca^{2+} signaling in dendrites of pyramidal neurons. *Biophys J* **70**, 1069-1081.

Helmchen F, Svoboda K, Denk W & Tank DW (1999). In vivo dendritic calcium dynamics in deep-layer cortical pyramidal neurons. *Nat Neurosci* **2**, 989-996.

Herreras O (1990). Propagating dendritic action potential mediates synaptic transmission in CA1 pyramidal cells in situ. *J Neurophysiol* **64**, 1429-1441.

Hirsch JA, Alonso JM & Reid RC (1995). Visually evoked calcium action potentials in cat striate cortex. *Nature* **378**, 612-616.

Ho N & Destexhe A (2000). Synaptic background activity enhances the responsiveness of neocortical pyramidal neurons. *J Neurophysiol* **84**, 1488-1496.

Holtmaat A, Wilbrecht L, Knott GW, Welker E & Svoboda K (2006). Experience-dependent and cell-type-specific spine growth in the neocortex. *Nature* **441**, 979-983.

Holtmaat AJ, Trachtenberg JT, Wilbrecht L, Shepherd GM, Zhang X, Knott GW & Svoboda K (2005). Transient and persistent dendritic spines in the neocortex in vivo. *Neuron* **45**, 279-291.

Huguenard JR, Hamill OP & Prince DA (1989). Sodium channels in dendrites of rat cortical pyramidal neurons. *Proc Natl Acad Sci U S A* **86**, 2473-2477.

Inda MC, DeFelipe J & Munoz A (2006). Voltage-gated ion channels in the axon initial segment of human cortical pyramidal cells and their relationship with chandelier cells. *Proc Natl Acad Sci U S A* **103**, 2920-2925.

Jin X, Prince DA & Huguenard JR (2006). Enhanced excitatory synaptic connectivity in layer v pyramidal neurons of chronically injured epileptogenic neocortex in rats. *J Neurosci* **26**, 4891-4900.

Johnston D, Magee JC, Colbert CM & Cristie BR (1996). Active properties of neuronal dendrites. *Annu Rev Neurosci* **19**, 165-186.

Jones MV & Westbrook GL (1996). The impact of receptor desensitization on fast synaptic transmission. *Trends Neurosci* **19**, 96-101.

Kalisman N, Silberberg G & Markram H (2003). Deriving physical connectivity from neuronal morphology. *Biol Cybern* **88**, 210-218.

Kalisman N, Silberberg G & Markram H (2005). The neocortical microcircuit as a tabula rasa. *Proc Natl Acad Sci U S A* **102**, 880-885.

Kampa BM, Clements J, Jonas P & Stuart GJ (2004). Kinetics of Mg²⁺ unblock of NMDA receptors: implications for spike-timing dependent synaptic plasticity. *J Physiol* **556**, 337-345.

Kampa BM, Letzkus JJ & Stuart GJ (2006). Requirement of dendritic calcium spikes for induction of spike-timing-dependent synaptic plasticity. *J Physiol* **574**, 283-290.

Kampa BM, Letzkus JJ & Stuart GJ (2007). Dendritic mechanisms controlling spike-timing-dependent synaptic plasticity. *Trends Neurosci* **30**, 456-463.

Kampa BM & Stuart GJ (2006). Calcium spikes in basal dendrites of layer 5 pyramidal neurons during action potential bursts. *J Neurosci* **26**, 7424-7432.

Kang J, Huguenard JR & Prince DA (2000). Voltage-gated potassium channels activated during action potentials in layer V neocortical pyramidal neurons. *J Neurophysiol* **83**, 70-80.

Kapfer C, Glickfeld LL, Atallah BV & Scanziani M (2007). Supralinear increase of recurrent inhibition during sparse activity in the somatosensory cortex. *Nat Neurosci* **10**, 743-753.

Kasper EM, Larkman AU, Lubke J & Blakemore C (1994a). Pyramidal neurons in layer 5 of the rat visual cortex. I. Correlation among cell morphology, intrinsic electrophysiological properties, and axon targets. *J Comp Neurol* **339**, 459-474.

Kasper EM, Larkman AU, Lubke J & Blakemore C (1994b). Pyramidal neurons in layer 5 of the rat visual cortex. II. Development of electrophysiological properties. *J Comp Neurol* **339**, 475-494.

Kasper EM, Lubke J, Larkman AU & Blakemore C (1994c). Pyramidal neurons in layer 5 of the rat visual cortex. III. Differential maturation of axon targeting, dendritic morphology, and electrophysiological properties. *J Comp Neurol* **339**, 495-518.

Kawaguchi Y & Kubota Y (1997). GABAergic cell subtypes and their synaptic connections in rat frontal cortex. *Cereb Cortex* **7**, 476-486.

Kennedy MB (1997). The postsynaptic density at glutamatergic synapses. *Trends Neurosci* **20**, 264-268.

Kennedy MB (2000). Signal-processing machines at the postsynaptic density. *Science* **290**, 750-754.

Khosravani H & Zamponi GW (2006). Voltage-gated calcium channels and idiopathic generalized epilepsies. *Physiol Rev* **86**, 941-966.

Koch C & Zador A (1993). The function of dendritic spines: devices subserving biochemical rather than electrical compartmentalization. *J Neurosci* **13**, 413-422.

Koester HJ & Sakmann B (1998). Calcium dynamics in single spines during coincident pre- and postsynaptic activity depend on relative timing of back-propagating action potentials and subthreshold excitatory postsynaptic potentials. *Proc Natl Acad Sci U S A* **95**, 9596-9601.

Kole MH, Brauer AU & Stuart GJ (2007a). Inherited cortical HCN1 channel loss amplifies dendritic calcium electrogenesis and burst firing in a rat absence epilepsy model. *J Physiol* **578**, 507-525.

Kole MH, Hallermann S & Stuart GJ (2006). Single I_h channels in pyramidal neuron dendrites: properties, distribution, and impact on action potential output. *J Neurosci* **26**, 1677-1687.

Kole MH, Ilschner SU, Kampa BM, Williams SR, Ruben PC & Stuart GJ (2008). Action potential generation requires a high sodium channel density in the axon initial segment. *Nat Neurosci* **11**, 178-186.

Kole MH, Letzkus JJ & Stuart GJ (2007b). Axon initial segment Kv1 channels control axonal action potential waveform and synaptic efficacy. *Neuron* **55**, 633-647.

Korngreen A & Sakmann B (2000). Voltage-gated K⁺ channels in layer 5 neocortical pyramidal neurones from young rats: subtypes and gradients. *J Physiol* **525 Pt 3**, 621-639.

Kumar SS, Bacci A, Kharazia V & Huguenard JR (2002). A developmental switch of AMPA receptor subunits in neocortical pyramidal neurons. *J Neurosci* **22**, 3005-3015.

Kumar SS & Huguenard JR (2003). Pathway-specific differences in subunit composition of synaptic NMDA receptors on pyramidal neurons in neocortex. *J Neurosci* **23**, 10074-10083.

Larkman A & Mason A (1990). Correlations between morphology and electrophysiology of pyramidal neurons in slices of rat visual cortex. I. Establishment of cell classes. *J Neurosci* **10**, 1407-1414.

Larkum ME, Kaiser KM & Sakmann B (1999a). Calcium electrogenesis in distal apical dendrites of layer 5 pyramidal cells at a critical frequency of back-propagating action potentials. *Proc Natl Acad Sci U S A* **96**, 14600-14604.

Larkum ME, Nevian T, Sandler M, Polsky A & Schiller J (2009). Synaptic integration in tuft dendrites of layer 5 pyramidal neurons: a new unifying principle. *Science* **325**, 756-760.

Larkum ME, Senn W & Luscher HR (2004). Top-down dendritic input increases the gain of layer 5 pyramidal neurons. *Cereb Cortex* **14**, 1059-1070.

Larkum ME, Zhu JJ & Sakmann B (1999b). A new cellular mechanism for coupling inputs arriving at different cortical layers. *Nature* **398**, 338-341.

Larkum ME, Zhu JJ & Sakmann B (2001). Dendritic mechanisms underlying the coupling of the dendritic with the axonal action potential initiation zone of adult rat layer 5 pyramidal neurons. *J Physiol* **533**, 447-466.

Le Bé JV & Markram H (2006). Spontaneous and evoked synaptic rewiring in the neonatal neocortex. *Proc Natl Acad Sci U S A* **103**, 13214-13219.

Letzkus JJ, Kampa BM & Stuart GJ (2006). Learning rules for spike timing-dependent plasticity depend on dendritic synapse location. *J Neurosci* **26**, 10420-10429.

Lisman JE (1997). Bursts as a unit of neural information: making unreliable synapses reliable. *Trends Neurosci* **20**, 38-43.

Loebel A, Silberberg G, Helbig D, Markram H, Tsodyks M & Richardson MJ (2009). Multiquantal release underlies the distribution of synaptic efficacies in the neocortex. *Front Comput Neurosci* **3**, 27.

London M & Häusser M (2005). Dendritic computation. *Annu Rev Neurosci* **28**, 503-532.

London M & Segev I (2001). Synaptic scaling in vitro and in vivo. *Nat Neurosci* **4**, 853-855.

Lorincz A, Notomi T, Tamas G, Shigemoto R & Nusser Z (2002). Polarized and compartment-dependent distribution of HCN1 in pyramidal cell dendrites. *Nat Neurosci* **5**, 1185-1193.

Luo L, Callaway EM & Svoboda K (2008). Genetic dissection of neural circuits. *Neuron* **57**, 634-660.

Lytton WW (2008). Computer modelling of epilepsy. *Nat Rev Neurosci* **9**, 626-637.

Magee JC (2000). Dendritic integration of excitatory synaptic input. *Nat Rev Neurosci* **1**, 181-190.

Magee JC & Cook EP (2000). Somatic EPSP amplitude is independent of synapse location in hippocampal pyramidal neurons. *Nat Neurosci* **3**, 895-903.

Magee JC & Johnston D (1997). A synaptically controlled, associative signal for Hebbian plasticity in hippocampal neurons. *Science* **275**, 209-213.

Mainen ZF, Joerges J, Huguenard JR & Sejnowski TJ (1995). A model of spike initiation in neocortical pyramidal neurons. *Neuron* **15**, 1427-1439.

Mainen ZF & Sejnowski TJ (1995). Reliability of spike timing in neocortical neurons. *Science* **268**, 1503-1506.

Mainen ZF & Sejnowski TJ (1996). Influence of dendritic structure on firing pattern in model neocortical neurons. *Nature* **382**, 363-366.

Major G, Polsky A, Denk W, Schiller J & Tank DW (2008). Spatiotemporally graded NMDA spike/plateau potentials in basal dendrites of neocortical pyramidal neurons. *J Neurophysiol* **99**, 2584-2601.

Margrie TW, Meyer AH, Caputi A, Monyer H, Hasan MT, Schaefer AT, Denk W & Brecht M (2003). Targeted whole-cell recordings in the mammalian brain in vivo. *Neuron* **39**, 911-918.

Markram H (2006). The blue brain project. *Nat Rev Neurosci* **7**, 153-160.

Markram H, Helm PJ & Sakmann B (1995). Dendritic calcium transients evoked by single back-propagating action potentials in rat neocortical pyramidal neurons. *J Physiol* **485 (Pt 1)**, 1-20.

Markram H, Lubke J, Frotscher M, Roth A & Sakmann B (1997a). Physiology and anatomy of synaptic connections between thick tufted pyramidal neurones in the developing rat neocortex. *J Physiol* **500 (Pt 2)**, 409-440.

Markram H, Lubke J, Frotscher M & Sakmann B (1997b). Regulation of synaptic efficacy by coincidence of postsynaptic APs and EPSPs. *Science* **275**, 213-215.

Markram H, Pikus D, Gupta A & Tsodyks M (1998a). Potential for multiple mechanisms, phenomena and algorithms for synaptic plasticity at single synapses. *Neuropharmacology* **37**, 489-500.

Markram H, Roth A & Helmchen F (1998b). Competitive calcium binding: implications for dendritic calcium signaling. *J Comput Neurosci* **5**, 331-348.

Markram H & Sakmann B (1994). Calcium transients in dendrites of neocortical neurons evoked by single subthreshold excitatory postsynaptic potentials via low-voltage-activated calcium channels. *Proc Natl Acad Sci U S A* **91**, 5207-5211.

Markram H, Toledo-Rodriguez M, Wang Y, Gupta A, Silberberg G & Wu C (2004). Interneurons of the neocortical inhibitory system. *Nat Rev Neurosci* **5**, 793-807.

Markram H & Tsodyks M (1996a). Redistribution of synaptic efficacy between neocortical pyramidal neurons. *Nature* **382**, 807-810.

Markram H & Tsodyks M (1996b). Redistribution of synaptic efficacy: a mechanism to generate infinite synaptic input diversity from a homogeneous population of neurons without changing absolute synaptic efficacies. *J Physiol Paris* **90**, 229-232.

Markram H, Wang Y & Tsodyks M (1998c). Differential signaling via the same axon of neocortical pyramidal neurons. *Proc Natl Acad Sci U S A* **95**, 5323-5328.

Mason A & Larkman A (1990). Correlations between morphology and electrophysiology of pyramidal neurons in slices of rat visual cortex. II. Electrophysiology. *J Neurosci* **10**, 1415-1428.

McCormick DA, Shu Y & Yu Y (2007). Neurophysiology: Hodgkin and Huxley model--still standing? *Nature* **445**, E1-2; discussion E2-3.

Mel BW (1993). Synaptic integration in an excitable dendritic tree. *J Neurophysiol* **70**, 1086-1101.

Milojkovic BA, Radojicic MS, Goldman-Rakic PS & Antic SD (2004). Burst generation in rat pyramidal neurones by regenerative potentials elicited in a restricted part of the basilar dendritic tree. *J Physiol* **558**, 193-211.

Milojkovic BA, Wuskell JP, Loew LM & Antic SD (2005). Initiation of sodium spikelets in basal dendrites of neocortical pyramidal neurons. *J Membr Biol* **208**, 155-169.

Milojkovic BA, Zhou WL & Antic SD (2007). Voltage and calcium transients in basal dendrites of the rat prefrontal cortex. *J Physiol* **585**, 447-468.

Mittmann T, Linton SM, Schwandt P & Crill W (1997). Evidence for persistent Na⁺ current in apical dendrites of rat neocortical neurons from imaging of Na⁺-sensitive dye. *J Neurophysiol* **78**, 1188-1192.

Murayama M & Larkum ME (2009a). Enhanced dendritic activity in awake rats. *Proc Natl Acad Sci U S A* **106**, 20482-20486.

Murayama M & Larkum ME (2009b). In vivo dendritic calcium imaging with a fiberoptic periscope system. *Nat Protoc* **4**, 1551-1559.

Naundorf B, Wolf F & Volgushev M (2006). Unique features of action potential initiation in cortical neurons. *Nature* **440**, 1060-1063.

Nettleton JS & Spain WJ (2000). Linear to supralinear summation of AMPA-mediated EPSPs in neocortical pyramidal neurons. *J Neurophysiol* **83**, 3310-3322.

- Nevian T, Larkum ME, Polsky A & Schiller J (2007). Properties of basal dendrites of layer 5 pyramidal neurons: a direct patch-clamp recording study. *Nat Neurosci* **10**, 206-214.
- Nimchinsky EA, Sabatini BL & Svoboda K (2002). Structure and function of dendritic spines. *Annu Rev Physiol* **64**, 313-353.
- Oakley JC, Schwindt PC & Crill WE (2001a). Dendritic calcium spikes in layer 5 pyramidal neurons amplify and limit transmission of ligand-gated dendritic current to soma. *J Neurophysiol* **86**, 514-527.
- Oakley JC, Schwindt PC & Crill WE (2001b). Initiation and propagation of regenerative Ca(2+)-dependent potentials in dendrites of layer 5 pyramidal neurons. *J Neurophysiol* **86**, 503-513.
- Ohana O & Sakmann B (1998). Transmitter release modulation in nerve terminals of rat neocortical pyramidal cells by intracellular calcium buffers. *J Physiol* **513** (Pt 1), 135-148.
- Palay SL, Sotelo C, Peters A & Orkand PM (1968). The axon hillock and the initial segment. *J Cell Biol* **38**, 193-201.
- Palmer LM & Stuart GJ (2006). Site of action potential initiation in layer 5 pyramidal neurons. *J Neurosci* **26**, 1854-1863.
- Palmer LM & Stuart GJ (2009). Membrane potential changes in dendritic spines during action potentials and synaptic input. *J Neurosci* **29**, 6897-6903.
- Pare D & Lang EJ (1998). Calcium electrogenesis in neocortical pyramidal neurons in vivo. *Eur J Neurosci* **10**, 3164-3170.
- Pare D, Shink E, Gaudreau H, Destexhe A & Lang EJ (1998). Impact of spontaneous synaptic activity on the resting properties of cat neocortical pyramidal neurons In vivo. *J Neurophysiol* **79**, 1450-1460.
- Peters A & Kaiserman-Abramof IR (1970). The small pyramidal neuron of the rat cerebral cortex. The perikaryon, dendrites and spines. *Am J Anat* **127**, 321-355.
- Peters A, Proskauer CC & Kaiserman-Abramof IR (1968). The small pyramidal neuron of the rat cerebral cortex. The axon hillock and initial segment. *J Cell Biol* **39**, 604-619.
- Pockberger H (1991). Electrophysiological and morphological properties of rat motor cortex neurons in vivo. *Brain Res* **539**, 181-190.
- Polsky A, Mel B & Schiller J (2009). Encoding and decoding bursts by NMDA spikes in basal dendrites of layer 5 pyramidal neurons. *J Neurosci* **29**, 11891-11903.

- Polsky A, Mel BW & Schiller J (2004). Computational subunits in thin dendrites of pyramidal cells. *Nat Neurosci* **7**, 621-627.
- Potez S & Larkum ME (2008). Effect of common anesthetics on dendritic properties in layer 5 neocortical pyramidal neurons. *J Neurophysiol* **99**, 1394-1407.
- Regehr WG & Armstrong CM (1994). Dendritic function. Where does it all begin? *Curr Biol* **4**, 436-439.
- Ren M, Yoshimura Y, Takada N, Horibe S & Komatsu Y (2007). Specialized inhibitory synaptic actions between nearby neocortical pyramidal neurons. *Science* **316**, 758-761.
- Reuveni I, Friedman A, Amitai Y & Gutnick MJ (1993). Stepwise repolarization from Ca²⁺ plateaus in neocortical pyramidal cells: evidence for nonhomogeneous distribution of HVA Ca²⁺ channels in dendrites. *J Neurosci* **13**, 4609-4621.
- Reyes A (2001). Influence of dendritic conductances on the input-output properties of neurons. *Annu Rev Neurosci* **24**, 653-675.
- Reyes A, Lujan R, Rozov A, Burnashev N, Somogyi P & Sakmann B (1998). Target-cell-specific facilitation and depression in neocortical circuits. *Nat Neurosci* **1**, 279-285.
- Reyes A & Sakmann B (1999). Developmental switch in the short-term modification of unitary EPSPs evoked in layer 2/3 and layer 5 pyramidal neurons of rat neocortex. *J Neurosci* **19**, 3827-3835.
- Rhodes P (2006). The properties and implications of NMDA spikes in neocortical pyramidal cells. *J Neurosci* **26**, 6704-6715.
- Rhodes PA & Gray CM (1994). Simulations of Intrinsically Bursting Neocortical Pyramidal Neurons. *Neural Computation* **6**, 1086-1110.
- Rinaldi T, Kulangara K, Antonello K & Markram H (2007). Elevated NMDA receptor levels and enhanced postsynaptic long-term potentiation induced by prenatal exposure to valproic acid. *Proc Natl Acad Sci U S A* **104**, 13501-13506.
- Rinaldi T, Perrodin C & Markram H (2008a). Hyper-connectivity and hyper-plasticity in the medial prefrontal cortex in the valproic Acid animal model of autism. *Front Neural Circuits* **2**, 4.
- Rinaldi T, Silberberg G & Markram H (2008b). Hyperconnectivity of local neocortical microcircuitry induced by prenatal exposure to valproic acid. *Cereb Cortex* **18**, 763-770.

- Rubenstein JL & Merzenich MM (2003). Model of autism: increased ratio of excitation/inhibition in key neural systems. *Genes Brain Behav* **2**, 255-267.
- Rudolph M & Destexhe A (2003). A fast-conducting, stochastic integrative mode for neocortical neurons in vivo. *J Neurosci* **23**, 2466-2476.
- Rumsey CC & Abbott LF (2006). Synaptic democracy in active dendrites. *J Neurophysiol* **96**, 2307-2318.
- Santoro B & Baram TZ (2003). The multiple personalities of h-channels. *Trends Neurosci* **26**, 550-554.
- Schaefer AT, Helmstaedter M, Schmitt AC, Bar-Yehuda D, Almog M, Ben-Porat H, Sakmann B & Korngreen A (2007). Dendritic voltage-gated K⁺ conductance gradient in pyramidal neurones of neocortical layer 5B from rats. *J Physiol* **579**, 737-752.
- Schiller J, Helmchen F & Sakmann B (1995). Spatial profile of dendritic calcium transients evoked by action potentials in rat neocortical pyramidal neurones. *J Physiol* **487 (Pt 3)**, 583-600.
- Schiller J, Major G, Koester HJ & Schiller Y (2000). NMDA spikes in basal dendrites of cortical pyramidal neurons. *Nature* **404**, 285-289.
- Schiller J, Schiller Y & Clapham DE (1998). NMDA receptors amplify calcium influx into dendritic spines during associative pre- and postsynaptic activation. *Nat Neurosci* **1**, 114-118.
- Schiller J, Schiller Y, Stuart G & Sakmann B (1997). Calcium action potentials restricted to distal apical dendrites of rat neocortical pyramidal neurons. *J Physiol* **505 (Pt 3)**, 605-616.
- Schubert D, Kotter R, Luhmann HJ & Staiger JF (2006). Morphology, electrophysiology and functional input connectivity of pyramidal neurons characterizes a genuine layer va in the primary somatosensory cortex. *Cereb Cortex* **16**, 223-236.
- Schubert D, Staiger JF, Cho N, Kotter R, Zilles K & Luhmann HJ (2001). Layer-specific intracolumnar and transcolumar functional connectivity of layer V pyramidal cells in rat barrel cortex. *J Neurosci* **21**, 3580-3592.
- Schwindt P, O'Brien JA & Crill W (1997). Quantitative analysis of firing properties of pyramidal neurons from layer 5 of rat sensorimotor cortex. *J Neurophysiol* **77**, 2484-2498.
- Schwindt PC & Crill WE (1995). Amplification of synaptic current by persistent sodium conductance in apical dendrite of neocortical neurons. *J Neurophysiol* **74**, 2220-2224.

Schwindt PC & Crill WE (1997). Local and propagated dendritic action potentials evoked by glutamate iontophoresis on rat neocortical pyramidal neurons. *J Neurophysiol* **77**, 2466-2483.

Segev I & London M (2000). Untangling dendrites with quantitative models. *Science* **290**, 744-750.

Shu Y, Duque A, Yu Y, Haider B & McCormick DA (2007). Properties of action-potential initiation in neocortical pyramidal cells: evidence from whole cell axon recordings. *J Neurophysiol* **97**, 746-760.

Silberberg G (2008). Polysynaptic subcircuits in the neocortex: spatial and temporal diversity. *Curr Opin Neurobiol* **18**, 332-337.

Silberberg G & Markram H (2007). Disynaptic inhibition between neocortical pyramidal cells mediated by Martinotti cells. *Neuron* **53**, 735-746.

Silberberg G, Wu C & Markram H (2004). Synaptic dynamics control the timing of neuronal excitation in the activated neocortical microcircuit. *J Physiol* **556**, 19-27.

Silva LR, Amitai Y & Connors BW (1991). Intrinsic oscillations of neocortex generated by layer 5 pyramidal neurons. *Science* **251**, 432-435.

Silver RA (2010). Neuronal arithmetic. *Nat Rev Neurosci* **11**, 474-489.

Sjostrom PJ & Hausser M (2006). A cooperative switch determines the sign of synaptic plasticity in distal dendrites of neocortical pyramidal neurons. *Neuron* **51**, 227-238.

Sjostrom PJ, Rancz EA, Roth A & Hausser M (2008). Dendritic excitability and synaptic plasticity. *Physiol Rev* **88**, 769-840.

Sjostrom PJ, Turrigiano GG & Nelson SB (2001). Rate, timing, and cooperativity jointly determine cortical synaptic plasticity. *Neuron* **32**, 1149-1164.

Sjostrom PJ, Turrigiano GG & Nelson SB (2003). Neocortical LTD via coincident activation of presynaptic NMDA and cannabinoid receptors. *Neuron* **39**, 641-654.

Sjostrom PJ, Turrigiano GG & Nelson SB (2007). Multiple forms of long-term plasticity at unitary neocortical layer 5 synapses. *Neuropharmacology* **52**, 176-184.

Somogyi P, Tamas G, Lujan R & Buhl EH (1998). Salient features of synaptic organisation in the cerebral cortex. *Brain Res Brain Res Rev* **26**, 113-135.

Song S, Sjostrom PJ, Reigl M, Nelson S & Chklovskii DB (2005). Highly nonrandom features of synaptic connectivity in local cortical circuits. *PLoS Biol* **3**, e68.

Spruston N (2008). Pyramidal neurons: dendritic structure and synaptic integration. *Nat Rev Neurosci* **9**, 206-221.

Spruston N, Jaffe DB & Johnston D (1994). Dendritic attenuation of synaptic potentials and currents: the role of passive membrane properties. *Trends Neurosci* **17**, 161-166.

Stepanyants A, Hof PR & Chklovskii DB (2002). Geometry and structural plasticity of synaptic connectivity. *Neuron* **34**, 275-288.

Steriade M (2004). Neocortical cell classes are flexible entities. *Nat Rev Neurosci* **5**, 121-134.

Stiefel KM, Tennigkeit F & Singer W (2005). Synaptic plasticity in the absence of backpropagating spikes of layer II inputs to layer V pyramidal cells in rat visual cortex. *Eur J Neurosci* **21**, 2605-2610.

Strauss U, Kole MH, Brauer AU, Pahnke J, Bajorat R, Rolfs A, Nitsch R & Deisz RA (2004). An impaired neocortical I_h is associated with enhanced excitability and absence epilepsy. *Eur J Neurosci* **19**, 3048-3058.

Stuart G (1999). Voltage-activated sodium channels amplify inhibition in neocortical pyramidal neurons. *Nat Neurosci* **2**, 144-150.

Stuart G, Schiller J & Sakmann B (1997a). Action potential initiation and propagation in rat neocortical pyramidal neurons. *J Physiol* **505 (Pt 3)**, 617-632.

Stuart G & Spruston N (1995). Probing dendritic function with patch pipettes. *Curr Opin Neurobiol* **5**, 389-394.

Stuart G & Spruston N (1998). Determinants of voltage attenuation in neocortical pyramidal neuron dendrites. *J Neurosci* **18**, 3501-3510.

Stuart G, Spruston N, Sakmann B & Hausser M (1997b). Action potential initiation and backpropagation in neurons of the mammalian CNS. *Trends Neurosci* **20**, 125-131.

Stuart GJ, Dodt HU & Sakmann B (1993). Patch-clamp recordings from the soma and dendrites of neurons in brain slices using infrared video microscopy. *Pflugers Arch* **423**, 511-518.

Stuart GJ & Hausser M (2001). Dendritic coincidence detection of EPSPs and action potentials. *Nat Neurosci* **4**, 63-71.

Stuart GJ & Sakmann B (1994). Active propagation of somatic action potentials into neocortical pyramidal cell dendrites. *Nature* **367**, 69-72.

Szabadics J, Varga C, Molnar G, Olah S, Barzo P & Tamas G (2006). Excitatory effect of GABAergic axo-axonic cells in cortical microcircuits. *Science* **311**, 233-235.

Thomson AM (1997). Activity-dependent properties of synaptic transmission at two classes of connections made by rat neocortical pyramidal axons in vitro. *J Physiol* **502** (Pt 1), 131-147.

Toledo-Rodriguez M, Blumenfeld B, Wu C, Luo J, Attali B, Goodman P & Markram H (2004). Correlation maps allow neuronal electrical properties to be predicted from single-cell gene expression profiles in rat neocortex. *Cereb Cortex* **14**, 1310-1327.

Trachtenberg JT, Chen BE, Knott GW, Feng G, Sanes JR, Welker E & Svoboda K (2002). Long-term in vivo imaging of experience-dependent synaptic plasticity in adult cortex. *Nature* **420**, 788-794.

Traub RD, Contreras D, Cunningham MO, Murray H, LeBeau FE, Roopun A, Bibbig A, Wilent WB, Higley MJ & Whittington MA (2005). Single-column thalamocortical network model exhibiting gamma oscillations, sleep spindles, and epileptogenic bursts. *J Neurophysiol* **93**, 2194-2232.

Trussell LO & Fischbach GD (1989). Glutamate receptor desensitization and its role in synaptic transmission. *Neuron* **3**, 209-218.

Tsay D & Yuste R (2004). On the electrical function of dendritic spines. *Trends Neurosci* **27**, 77-83.

Tsodyks MV & Markram H (1997). The neural code between neocortical pyramidal neurons depends on neurotransmitter release probability. *Proc Natl Acad Sci U S A* **94**, 719-723.

Turner RW, Meyers DE, Richardson TL & Barker JL (1991). The site for initiation of action potential discharge over the somatodendritic axis of rat hippocampal CA1 pyramidal neurons. *J Neurosci* **11**, 2270-2280.

Turrigiano GG (1999). Homeostatic plasticity in neuronal networks: the more things change, the more they stay the same. *Trends Neurosci* **22**, 221-227.

Ulrich D (2002). Dendritic resonance in rat neocortical pyramidal cells. *J Neurophysiol* **87**, 2753-2759.

Wang Y, Gupta A & Markram H (1999). Anatomical and functional differentiation of glutamatergic synaptic innervation in the neocortex. *J Physiol Paris* **93**, 305-317.

Wang Y, Markram H, Goodman PH, Berger TK, Ma J & Goldman-Rakic PS (2006). Heterogeneity in the pyramidal network of the medial prefrontal cortex. *Nat Neurosci* **9**, 534-542.

- Waters J, Schaefer A & Sakmann B (2005). Backpropagating action potentials in neurones: measurement, mechanisms and potential functions. *Prog Biophys Mol Bio* **87**, 145-170.
- Williams SR (2004). Spatial compartmentalization and functional impact of conductance in pyramidal neurons. *Nat Neurosci* **7**, 961-967.
- Williams SR (2005). Encoding and decoding of dendritic excitation during active states in pyramidal neurons. *J Neurosci* **25**, 5894-5902.
- Williams SR & Stuart GJ (1999). Mechanisms and consequences of action potential burst firing in rat neocortical pyramidal neurons. *J Physiol* **521 Pt 2**, 467-482.
- Williams SR & Stuart GJ (2000a). Backpropagation of physiological spike trains in neocortical pyramidal neurons: implications for temporal coding in dendrites. *J Neurosci* **20**, 8238-8246.
- Williams SR & Stuart GJ (2000b). Site independence of EPSP time course is mediated by dendritic I(h) in neocortical pyramidal neurons. *J Neurophysiol* **83**, 3177-3182.
- Williams SR & Stuart GJ (2002). Dependence of EPSP efficacy on synapse location in neocortical pyramidal neurons. *Science* **295**, 1907-1910.
- Williams SR & Stuart GJ (2003). Role of dendritic synapse location in the control of action potential output. *Trends Neurosci* **26**, 147-154.
- Wong RK, Prince DA & Basbaum AI (1979). Intradendritic recordings from hippocampal neurons. *Proc Natl Acad Sci U S A* **76**, 986-990.
- Yuste R & Denk W (1995). Dendritic spines as basic functional units of neuronal integration. *Nature* **375**, 682-684.
- Yuste R, Gutnick MJ, Saar D, Delaney KR & Tank DW (1994). Ca²⁺ accumulations in dendrites of neocortical pyramidal neurons: an apical band and evidence for two functional compartments. *Neuron* **13**, 23-43.
- Yuste R, Majewska A & Holthoff K (2000). From form to function: calcium compartmentalization in dendritic spines. *Nat Neurosci* **3**, 653-659.
- Zhou WL, Yan P, Wuskell JP, Loew LM & Antic SD (2008). Dynamics of action potential backpropagation in basal dendrites of prefrontal cortical pyramidal neurons. *Eur J Neurosci* **27**, 923-936.

Zhu JJ (2000). Maturation of layer 5 neocortical pyramidal neurons: amplifying salient layer 1 and layer 4 inputs by Ca²⁺ action potentials in adult rat tuft dendrites. *J Physiol* **526 Pt 3**, 571-587.

Manuscript submitted to Frontiers in Neuroinformatics

**Channelpedia: an integrative and interactive database for ion
channels**

Rajnish Ranjan, Georges Khazen, Luca Gambazzi, Srikanth Ramaswamy,

Sean Hill, Felix Schuermann & Henry Markram

Brain Mind Institute
Ecole Polytechnique Fédérale de Lausanne (EPFL),
Station 15, CH-1015 Lausanne, Switzerland

Correspondence:

Henry Markram

AAB 110, Brain Mind Institute

Ecole Polytechnique Fédérale de Lausanne (EPFL),

Station 15, CH-1015 Lausanne, Switzerland

henry.markram@epfl.ch

ABSTRACT

Ion channels are membrane proteins that selectively conduct ions across the cell membrane. The flux of ions through ion channels drives electrical and biochemical processes in cells and plays a critical role in shaping the electrical properties of neurons. The past three decades have witnessed extensive research to characterize the molecular, structural and biophysical properties of ion channels. This began to elucidate the role ion channels play in neuronal function and led to the development of computational models of ion channel function. Although there have been substantial efforts to consolidate these findings into easily accessible and coherent online resources, a single comprehensive resource is still lacking. The success of these initiatives has been hindered by the sheer diversity of approaches and variety in data formats. Here, we present an information management framework which is combination of a database and a discussion platform, where researchers can collaborate and synthesize information from literature. “*Channelpedia*” is an example of this framework which is designed to store information related to ion channels and models. It is a knowledge base system centered on models of genetically expressed ion channels and cross-referenced to other online databases. It encourages researchers to contribute, build and refine the knowledge base through interactive wiki-like interfaces. Equipped to automatically update references, *Channelpedia* integrates and highlights recent publications with relevant information in the database. It is web based, freely accessible and currently contains 187 annotated ion channels with 45 Hodgkin-Huxley models.

Keywords: Ion channel, Kinetics, Hodgkin-Huxley model, Database, Information management, Structured wiki

INTRODUCTION

The mammalian brain expresses about 350-500 ion channel genes and their variants (Ashburner et al., 2000). Ion channels are trans-membrane proteins that control the active and passive electrical behavior of a cell by selectively conducting ions across the cell membrane. Researchers have been working extensively to address the genetic, proteomic, structural, biophysical and functional properties of these ion channels and to build computational models that capture their biophysical and kinetic behavior. In 1952, Hodgkin and Huxley developed a mathematical model of ionic conductances to demonstrate their role in the electrical behavior of excitable nerve cells (Hodgkin and Huxley, 1952). Since then, these models have been widely used to build ion channel models and to construct biologically realistic neuron models. Ion channel models and their integration in neuronal models have allowed a better understanding of a) the role of any particular ion channel in generating different electrical behaviors of neurons, b) the differential role of ion channels in different neurons, c) the effect of neuromodulators on neuronal activity at the microcircuit and network levels. The influence of ion channels on such a broad spectrum of issues has resulted in a significant amount of scientific information.

In general, the management of information generated through scientific research becomes exceedingly complex due to sheer volume, continuously evolving data formats and the inherent diversity of research methodology. For example, there are 60,000 different articles relating to biology alone added on PubMed every month. In ion channel research alone, there are currently about 800 papers published every month (Fig 1a). Ion channel models are an example of continuously evolving data format, since they go through a number of iterations to capture the complex kinetics of an ion channel by successively adding biophysical details. These complexities arise due to the channel's inherent properties, interaction with other molecules and

experimental environments (intracellular and extracellular conditions, temperature and pH). Management of such information is a challenging task that involves maintenance, dedication and follow-up. Therefore, efficient information management is vital and applicable to every field of research and connecting small but highly specialized databases is becoming increasingly important to manage this huge and diverse information.

There have been several efforts made to document ion channel information. IUPHAR (Harmar et al., 2009) is currently the most comprehensive resource available for ion channels but lacks the computational models necessary for neuronal modeling. ModelDB (Hines et al., 2004) on the other hand contains some ion channel models but is not designed to manage ion channel models hence does not contain ion channel related information and not cross-referenced to other ion channel resources like Rat Genome and Nucleotide databases. Additionally, such resources have a rigid database structure, which makes them easily accessible and searchable but unsuitable for unstructured data as curators can add information only to predefined fields. Generally file upload and attachments are the only way to support unstructured data in such a system. The rigidity of these resources makes them ideal core sources for data mining, but additional on-line tools are needed to create meta-platforms that integrate multiple resources with unstructured information. Wikipedia (contributors, 2004) currently provides an ideal platform for unstructured data, and systematic addition of new information. Moreover, multiple contributors on Wikipedia can speed up the process of consolidating the data. Thus, so far, efforts to summarize the ion channel knowledgebase have been inadequate due to a lack of a framework supporting both unstructured and structured data. Review articles and very selected books are currently the only means by which published literature is being summarized and integrated (Brammar, 1998;Hille, 2001;Biel et al., 2009).

To manage scientific information efficiently, we propose a framework concept which integrates five main aspects of information management; a) Navigation, b) Structured data, c) Unstructured data, d) Data synthesis and, e) Reference management.

Easy navigation of data is an essential part of information management and requires logical grouping and hierarchical ordering. Data from published scientific research can be organized into two main categories: 1) Unstructured; data that are not quantifiable and have storage formats that are prone to change over time, 2) Structured; data that are quantifiable and have storage formats that rarely change. For example, the distribution profiles of ion channels on neurons are not fully constrained, generally being described in qualitative terms such as “Nav1.6 is known to be expressed in the axon initial segment of L2/3 pyramidal neurons” and is thus categorized under unstructured data. In contrast, data about gene ID and sequence of most of the ion channels would fall under structured data since their data format is fully constrained. Structured data are easily sorted into appropriate fields within the database and can be queried directly. Data synthesis is a conceptual process where unstructured data is synthesized into structured data. Information source for all data is managed with reference management.

We demonstrate the proposed framework by implementing an ion channel knowledgebase, “*Channelpedia*”. *Channelpedia* is a freely accessible web application that combines the functionality of unstructured wiki-like data and yet has the advantages of a structured database. It provides a framework, which enables the collective contribution of researchers to build a comprehensive resource for ion channel information. Additionally, it has a built-in referencing system that automatically filters new publications from PubMed and adds them to their respective categories, thus automating the acquisition and sorting of newly acquired information. It also notifies curators and researchers of newly published and relevant data.

METHODS AND RESULTS

Overview

The framework consists of five main modules: (Fig 1b). 1) Navigation, 2) Unstructured data, 3) Structured data, 4) Discussion and synthesis, 5) Reference management. Navigation enables easy browsing of data items grouped under category and subcategories. Unstructured data is stored as editable text and images. Structured data contains predefined fields for data with known formats and links with available online resources. Data synthesis is a proposed conceptual process where unstructured data could be converted into structured data. It provides a conducive environment for discussion among contributors. This may eventually lead to the conversion of unstructured data into structured, formatted data. For example, a discussion on HCN distribution could conclude as an exponential distribution over apical dendrites and parameters can be stored in a structured data instead of just descriptive language like “HCN is known to be distributed exponentially on pyramidal cells”. The reference management module is used to automatically find relevant literature from PubMed. It integrates an automated web crawler to download relevant article abstracts and adds them to respective categories. It allows contributors to be notified whenever there are new publications to be curated.

The framework supports users associated with the following roles: 1) Visitor; can access all the data but are not allowed to make any changes, 2) Contributor; needs a framework account to update or add new information from literature or to upload experimental data, 3) Administrator; needs a framework account to add/delete/change user credentials and database structure.

Data source

Contributors and existing online resources are the two main sources of data. The unstructured data (Fig 1c) is populated by contributors, who can freely edit formatted text and upload images without violating copyright agreements. Structured data contains data from existing online resources managed by administrator using automated scripts. Experimental data from literature is uploaded by contributors and stored as structured data.

Implementation

Database, formatted text support, reference crawler, web interface and a web server are the basic components required for the proposed framework. There are many tools available to support these functionalities (Fig 1d).

Channelpedia

Channelpedia (<http://www.Channelpedia.net>) is implemented as an example of the proposed framework (Fig 2). The main page supports easy navigation to 187 ion channels in different categories and sub categories. The current version of *Channelpedia* contains the following sections to store unstructured and structured information: Introduction, Genes, Ontologies, Interactions, Structure, Expression, Distribution, Function, Kinetics and Models. It supports three different user (Administrator, Contributor and Visitor) credentials to populate data (Fig 3). Structured data contains genetic information such as gene ID, symbol, name, synonyms and descriptions from the Rat Genome Database (<http://rgd.mcw.edu/>) (Twigger et al., 2007) which is then cross-referenced to other online resources using Ruby scripts (Matsumoto, 2011). Information related to genes and transcript sequences are obtained from Ensembl (Flicek et al., 2011) protein accession, peptide sequences are obtained from Uniprot (Jain et al., 2009); published interactions are obtained from the IntAct database (Aranda et al., 2010); complete GO

annotations (process, Function, and Component) are obtained from the Gene Ontology database (Ashburner et al., 2000); 3D structures of the channels were queried from the protein data bank (PDB) (Berman et al., 2000). Additionally, gene expression data obtained from single cell multiplex RT-PCR experiments performed in our lab (Toledo-Rodriguez et al., 2004) are also included in the database (Fig 3).

Models

Hodgkin-Huxley models of ion channels are built from published literature using a custom Matlab tool. Apart from description of kinetics and experimental details like temperature, cell-type and age of the animal, Channelpedia also contains a plot of the model response to a step voltage protocol (Fig 4). Authorized users can upload models to *Channelpedia* using a predefined customized XML schema. Uploaded models are available in XML or Neuron NMODL descriptions for all users (Hines and Carnevale, 2000;, 2001).

Reference management

References are handled in Channelpedia as a two step process. First step includes weekly automated download and keyword based classification of ion channel related abstracts from PubMed (Fig 5). Channelpedia contains ~180,000 abstracts and they are available under reference section of Channelpedia and categorized under different sections for each channel subtype. Second step involves contributors to identify the paper of interest and select them for respective ion channel page. These references are initially highlighted in red on the ion channel page. They will be marked up to blue when they are used (referenced) by contributors in the ion channel page (Fig 5). This feature enables verified integration of new information to ion channel page and allows contributors to identify unread publication for curation.

Implementation

MySQL is used as a database backend and Ruby on Rails framework implements the structure of the application. *Channelpedia* also uses several plugins or gems for other functionalities. The list of Ruby gems used are: Nokogiri for XML parsing, OpenURI as a wrapper for net/http, Hpricot for HTML parsing, Mechanize for web automation, bluecloth for wiki formatting and Attachment_fu plugin for file uploads (Fig 6).

DISCUSSION AND FUTURE DIRECTIONS

Scientific information is multidimensional and all of its aspects need to be documented and stored systematically. The volume of peer-reviewed papers published is already very large and continues to grow. Ideally, a provision should be made to store raw data, analysis code, analysis results and hypothesis in a machine-readable format instead of a descriptive language. Significant technological and administrative advancement is required to tackle this problem.

In this study we have proposed a framework concept as an alternate solution. We demonstrate this by implementing “*Channelpedia*” which facilitates building of an ion channel knowledge base to accommodate both structured and unstructured data. The structured data reside in ‘queryable’ database structures whereas unstructured data remain in wiki-like formatted text and image format. Although there is no automatic way to convert unstructured data into structured data, the framework is designed in such a way that by adding relevant database tables and tags to these tables, it will be possible to move the desired data into a structured format. For example, *Channelpedia* currently only supports Hodgkin-Huxley models but by adding database table “MarkovModels” with appropriate entities *Channelpedia* will be able to support Markov models in the structured database.

Temperature coefficient factor (Q_{10}) is used to capture the effect of temperature on gating kinetics. In most of the ion channel models Q_{10} factor is approximated to 2.3, whereas in reality it could vary between 2 and 30 (Dhaka et al., 2006). To keep such modifications and assumptions tractable we propose to add a separate model for each assumption. Therefore current models in *Channelpedia* do not contain Q_{10} factor.

Ion channel kinetics are often modified to achieve desired results in neuronal modeling. It becomes difficult to find the kinetics of the original model after several such modifications. For example, the Kv2.1 ion channel model used in (Johnson and McIntyre, 2008) contains activation parameter $v_{1/2} = -22\text{mV}$, citing (Chan et al., 2007) with $v_{1/2} 17.5\text{mV}$, whereas, experimental data reports this value to be -18mV (Baranauskas et al., 1999). *Channelpedia* with its Wiki-like functionality can provide an ideal platform to track such changes.

Data on ion channel interactions, 3D structure, expression in brain regions, cellular distribution and function in neuronal activity are currently limited in *Channelpedia*. Although references are automatically curated, it would require significant amount of manual effort to summarize published literature. We are actively adding more information from literature expect more user contributions to make it a more reliable and comprehensive database for ion channels.

Currently it supports very limited APIs (Application programming interface) but future versions of *Channelpedia* will include support for ontology and generic query to access any aspect of the data. Using ontologies along with APIs would be an ideal way to connect multiple *Channelpedia*-like, small, but specialized databases.

Channelpedia is an example where we have combined the functionality of structured and unstructured data management along with intelligent automated reference handling. A generic

implementation of this tool, which users can customize to their specific needs, could make this approach generally useful to other domains of research.

Contributions

Channelpedia was conceived and constructed as part of the Blue Brain Project's general aim to build brain models with biological accuracy and its specific aim to model each type of neuron according to the specific ion channels expressed. A number of researchers have contributed to the construction of *Channelpedia*: for literature search (Rajnish Ranjan, Srikanth Ramaswamy, Geetanjali Saha, Mehgana Katiki, Albert Gidon, Etay Hay, Shaul Druckmann & Michael Schartner); for prototype design & implementation (Rajnish Ranjan, Albert Gidon, James G. King, Etay Hay, Srikanth Ramaswamy, Felix Schuermann, Sean Hill, Shaul Druckmann, Adnan Abid & Thomas McColgan); for ion channel models (Rajnish Ranjan, Albert Gideon, Etay Hay, Shaul Druckmann & Mehgana Katiki); for cross referencing (Rajnish Ranjan & Georges Khazen); for data entry (Rajnish Ranjan, Georges Khazen & Martin Telefont); for maintenance (Rajnish Ranjan & Luca Gambazzi); for the final implementation (Rajnish Ranjan, Luca Gambazzi, James G. King, & John Kenyon). Rajnish Ranjan, Srikanth Ramaswamy, Henry Markram and Georges Khazen wrote the manuscript.

Acknowledgements

This work was performed within the framework of the Blue Brain Project and was supported by the respective EPFL project fund. We thank all the mentioned contributors for their help in the development of *Channelpedia*. We thank Shruti Muralidhar and Dr. Abdel Elhamdani for their comments on the manuscript, and Melissa Cochrane for help in editing the article.

References

- Aranda, B., Achuthan, P., Alam-Faruque, Y., Armean, I., Bridge, A., Derow, C., Feuermann, M., Ghanbarian, A.T., Kerrien, S., Khadake, J., Kerssemakers, J., Leroy, C., Menden, M., Michaut, M., Montecchi-Palazzi, L., Neuhauser, S.N., Orchard, S., Perreau, V., Roechert, B., Van Eijk, K., and Hermjakob, H. (2010). The IntAct molecular interaction database in 2010. *Nucleic Acids Res* 38, D525-531.
- Ashburner, M., Ball, C.A., Blake, J.A., Botstein, D., Butler, H., Cherry, J.M., Davis, A.P., Dolinski, K., Dwight, S.S., Eppig, J.T., Harris, M.A., Hill, D.P., Issel-Tarver, L., Kasarskis, A., Lewis, S., Matese, J.C., Richardson, J.E., Ringwald, M., Rubin, G.M., and Sherlock, G. (2000). Gene ontology: tool for the unification of biology. The Gene Ontology Consortium. *Nat Genet* 25, 25-29.
- Baranauskas, G., Tkatch, T., and Surmeier, D.J. (1999). Delayed rectifier currents in rat globus pallidus neurons are attributable to Kv2.1 and Kv3.1/3.2 K(+) channels. *J Neurosci* 19, 6394-6404.
- Berman, H.M., Westbrook, J., Feng, Z., Gilliland, G., Bhat, T.N., Weissig, H., Shindyalov, I.N., and Bourne, P.E. (2000). The Protein Data Bank. *Nucleic Acids Res* 28, 235-242.
- Biel, M., Wahl-Schott, C., Michalakakis, S., and Zong, X. (2009). Hyperpolarization-activated cation channels: from genes to function. *Physiol Rev* 89, 847-885.
- Brammar, E.C.C.A.W.J. (1998). *Ion Channel Factsbook Voltage-Gated Channels*. Academic Press.
- Chan, C.S., Guzman, J.N., Ilijic, E., Mercer, J.N., Rick, C., Tkatch, T., Meredith, G.E., and Surmeier, D.J. (2007). 'Rejuvenation' protects neurons in mouse models of Parkinson's disease. *Nature* 447, 1081-1086.
- Contributors, W. (2004). "Ion channel" *Wikipedia, The Free Encyclopedia* [Online]. Available: http://en.wikipedia.org/wiki/Ion_channel (accessed February 10, 2011) [Accessed].
- Dhaka, A., Viswanath, V., and Patapoutian, A. (2006). Trp ion channels and temperature sensation. *Annu Rev Neurosci* 29, 135-161.
- Flicek, P., Amode, M.R., Barrell, D., Beal, K., Brent, S., Chen, Y., Clapham, P., Coates, G., Fairley, S., Fitzgerald, S., Gordon, L., Hendrix, M., Hourlier, T., Johnson, N., Kahari, A., Keefe, D., Keenan, S., Kinsella, R., Kokocinski, F., Kulesha, E., Larsson, P., Longden, I., McLaren, W., Overduin, B., Pritchard, B., Riat, H.S., Rios, D., Ritchie, G.R., Ruffier, M., Schuster, M., Sobral, D., Spudich, G., Tang, Y.A., Trevanion, S., Vandrovcova, J., Vilella, A.J., White, S., Wilder, S.P., Zadissa, A., Zamora, J., Aken, B.L., Birney, E., Cunningham, F., Dunham, I., Durbin, R., Fernandez-Suarez, X.M., Herrero, J., Hubbard, T.J., Parker, A., Proctor, G., Vogel, J., and Searle, S.M. (2011). Ensembl 2011. *Nucleic Acids Res* 39, D800-806.
- Harmar, A.J., Hills, R.A., Rosser, E.M., Jones, M., Buneman, O.P., Dunbar, D.R., Greenhill, S.D., Hale, V.A., Sharman, J.L., Bonner, T.I., Catterall, W.A., Davenport, A.P., Delagrangé, P., Dollery, C.T., Foord, S.M., Gutman, G.A., Laudet, V., Neubig, R.R., Ohlstein, E.H., Olsen, R.W., Peters, J., Pin, J.P., Ruffolo, R.R., Searls, D.B., Wright, M.W., and Spedding, M. (2009). IUPHAR-DB: the IUPHAR database of G protein-coupled receptors and ion channels. *Nucleic Acids Res* 37, D680-685.
- Hille, B. (2001). *Ion channels of excitable membranes*. Sunderland, Mass.: Sinauer.
- Hines, M.L., and Carnevale, N.T. (2000). Expanding NEURON's repertoire of mechanisms with NMODL. *Neural Comput* 12, 995-1007.
- Hines, M.L., and Carnevale, N.T. (2001). NEURON: a tool for neuroscientists. *Neuroscientist* 7, 123-135.
- Hines, M.L., Morse, T., Migliore, M., Carnevale, N.T., and Shepherd, G.M. (2004). ModelDB: A Database to Support Computational Neuroscience. *J Comput Neurosci* 17, 7-11.
- Hodgkin, A.L., and Huxley, A.F. (1952). A quantitative description of membrane current and its application to conduction and excitation in nerve. *J Physiol* 117, 500-544.

- Jain, E., Bairoch, A., Duvaud, S., Phan, I., Redaschi, N., Suzek, B.E., Martin, M.J., Mcgarvey, P., and Gasteiger, E. (2009). Infrastructure for the life sciences: design and implementation of the UniProt website. *BMC Bioinformatics* 10, 136.
- Johnson, M.D., and McIntyre, C.C. (2008). Quantifying the neural elements activated and inhibited by globus pallidus deep brain stimulation. *J Neurophysiol* 100, 2549-2563.
- Matsumoto, Y.M. (2011). *Ruby A programmer's best friend* [Online]. Available: <http://www.ruby-lang.org/en/> [Accessed].
- Toledo-Rodriguez, M., Blumenfeld, B., Wu, C., Luo, J., Attali, B., Goodman, P., and Markram, H. (2004). Correlation maps allow neuronal electrical properties to be predicted from single-cell gene expression profiles in rat neocortex. *Cereb Cortex* 14, 1310-1327.
- Twigger, S.N., Shimoyama, M., Bromberg, S., Kwitek, A.E., and Jacob, H.J. (2007). The Rat Genome Database, update 2007--easing the path from disease to data and back again. *Nucleic Acids Res* 35, D658-662.

Figure legends

Figure 1.

a) Histogram of yearly ion channel publications, generated from 180,000 ion channel references present in the Channelpedia reference database. b) The proposed framework for scientific information management. c) The data source and possible user credentials. d) The possible choices for current implementation.

Figure 2.

An overview of the Channelpedia functionality with the Kv1.2 ion channel as an example.

Figure 3.

The data sources for Channelpedia, with a breakup of areas accessible to administrators, contributors and visitors.

Figure 4.

Example of the Nav1.3 ion channel kinetics model in *Channelpedia*, with the activation and inactivation kinetics and time constants, representation as a .mod file in the NEURON simulation environment, and in a custom XML format.

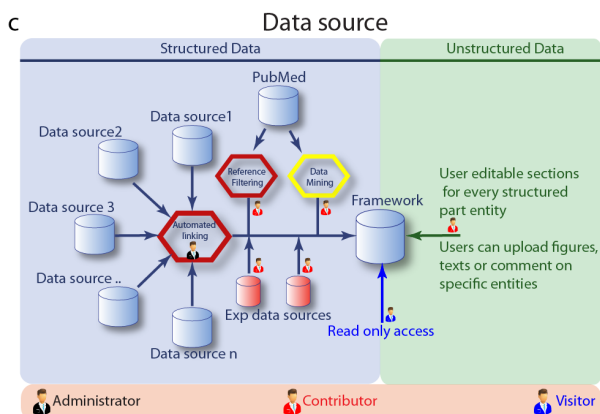
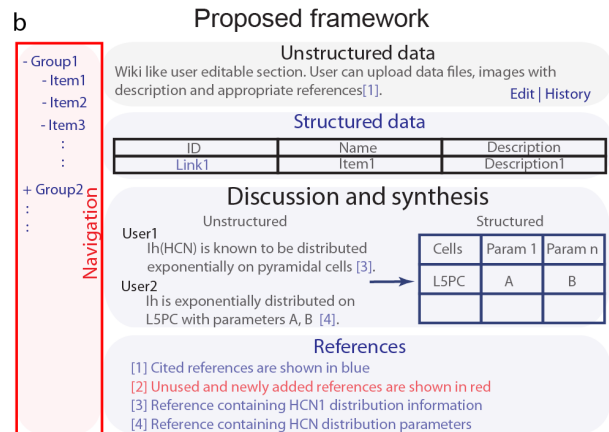
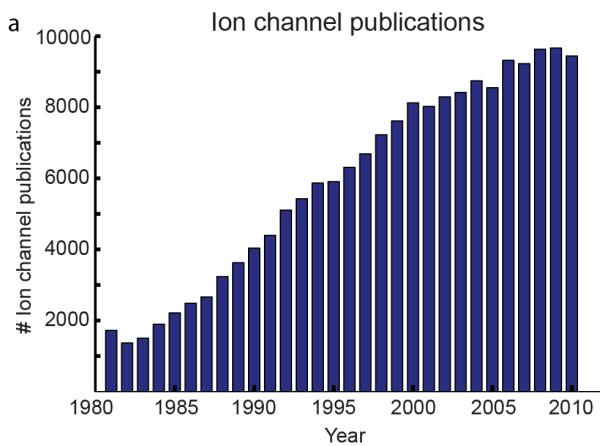
Figure 5.

The reference management structure, showing the step-by-step process to download a reference from pubmed and its usage in *Channelpedia*.

Figure 6.

The overall architecture of *Channelpedia*, and tools used to manage the database, file upload, wiki formatting, web automation, HTML and XML parsing.

Figure 1. a) Histogram of yearly ion channel publications, generated from 180,000 ion channel references present in the Channelpedia reference database. b) The proposed framework for scientific information management. c) The data source and possible user credentials. d) The possible choices for current implementation.



d Possible implementations

Database	Main plug-in	Language
MySQL	Bluecloth	Ruby on Rails, XML
Text file, RDBMS	Twiki	Perl
MySQL, PostgreSQL	MediaWiki	PHP
Text file based	Docuwiki	PHP
MySQL, PostgreSQL	Instiki	Ruby on Rails
RDBMS	JAMWiki	Java, servlets, JSP
MySQL, PostgreSQL	Pimki	Ruby
MySQL	WikkaWiki	PHP
MySQL, HSQLDB	XWiki	Java
ZODB	Zwiki	Python
MySQL, PostgreSQL	Wagn	Ruby on Rails

Figure 2. An overview of the Channelpedia functionality with the Kv1.2 ion channel as an example.

CHANNELPEDIA

IC Families

- Expand all
- Collapse all
- K**
 - Kv1**
 - Kv2**
 - Kv2.1**
 - Kv2.2**
 - Kv3**
 - Kv4**
 - Kv5**
 - Kv6**
 - Kv7**
 - Kv8**
 - Kv9**
 - Kv10**
 - Kv11**
 - Kv12**
 - Kir**
 - KCNQ**
 - KCa**
 - KvG**
- Na**
- Ca**
- Cl**
- Ih**
- A**
- M**
- TRP**

Kv1.2
Unstructured data

Introduction

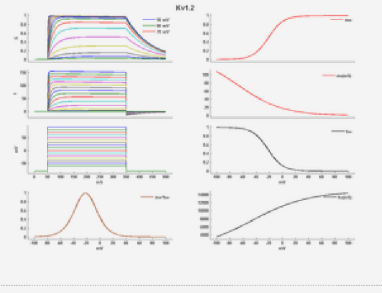
Potassium voltage-gated channel subfamily A member 2 also known as Kv1.2 is a protein that in humans is encoded by the KCNA2 gene.

Genes
Structured data [Edit](#) [History](#)

RGD ID	Chromosome	Position	Species
2950	2	202560152-202564305	Rat
10830	3	106904485-106909797	Mouse
735518	1	111145776-111148345	Human

Models
Hodgkin-Huxley model

Animal	rat
CellType	Oocyte
Age	0 Days
Temperature	20.0°C
Reversal	-65.0 mV
Ion	K +
Ligand ion	
Ref	Sprunger L K et.al; Eur. J. Pharmacol. 1996 Oct 31
mpower	1.0
mInf	$1.0000/(1+ \exp((v - -21.0000)/-11.3943))$
mTau	$150.0000/(1+ \exp((v - -67.5600)/34.1479))$
hpower	1.0
hInf	$1.0000/(1+ \exp((v - -22.0000)/11.3943))$
hTau	$15000.0000/(1+ \exp((v - -46.5600)/-44.1479))$



[MOD xml](#)

REFERENCES

REPORTS

SEARCH IN WIKI

References
Reference management

[1] An activation gating switch in Kv1.2 is localized to a threonine residue in the S2-S3 linker. [2] *Biophys. J.*, 2007 Dec 15 ,93(4173-86). [Download](#)

[2] The glycosylation state of Kv1.2 potassium channels affects trafficking, gating, and simulated action potentials. [3] *Brain Res.*, 2007 May 4 ,1144(1-10). [Download](#)

[3] Inhibition by bis(7)-tacrine of native delayed rectifier and KV1.2 encoded potassium channels. [4] *Neurosci. Lett.*, 2007 Jan 29 ,412(108-13). [Download](#)

Figure 3. The data sources for Channelpedia, with a breakup of areas accessible to administrators, contributors and visitors.

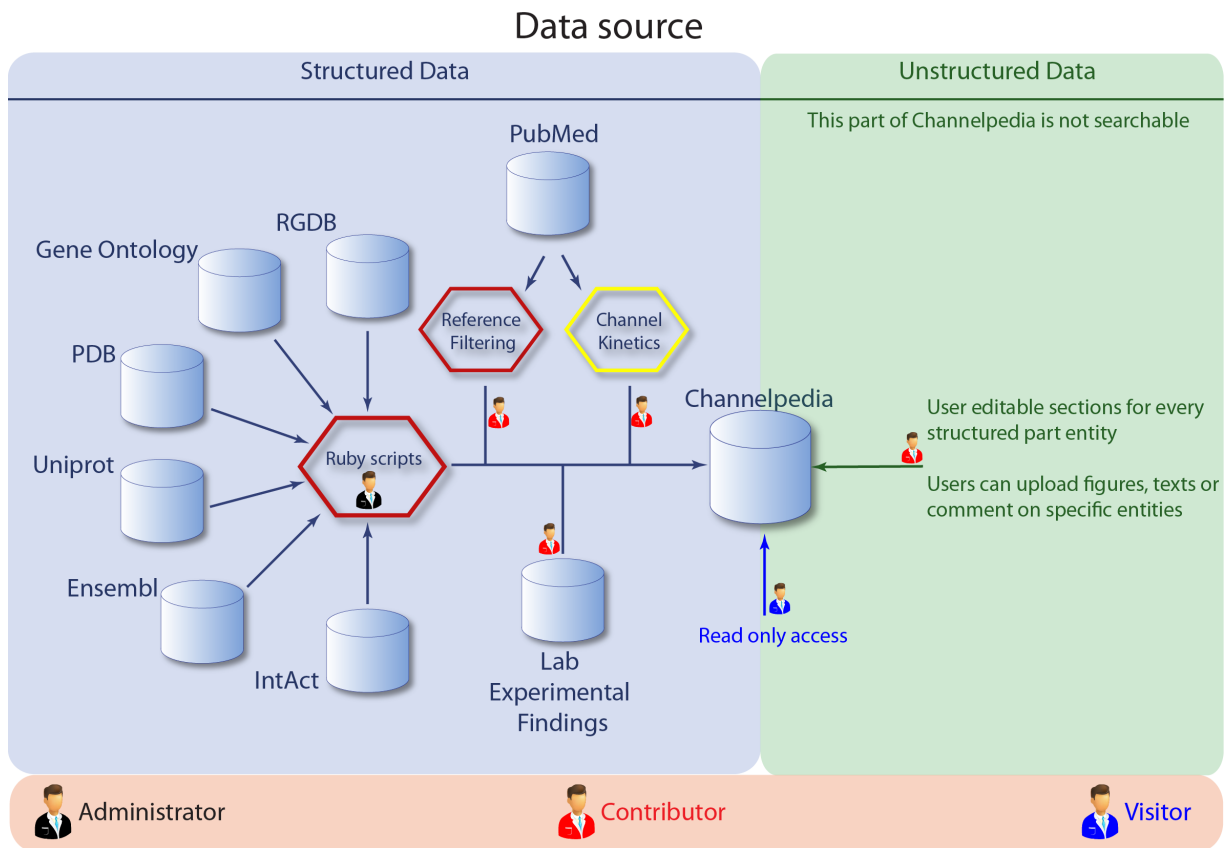


Figure 4. Example of the Nav1.3 ion channel kinetics model in *Channelpedia*, with the activation and inactivation kinetics and time constants, representation as a MOD file in the NEURON simulation environment, and in a custom XML format.

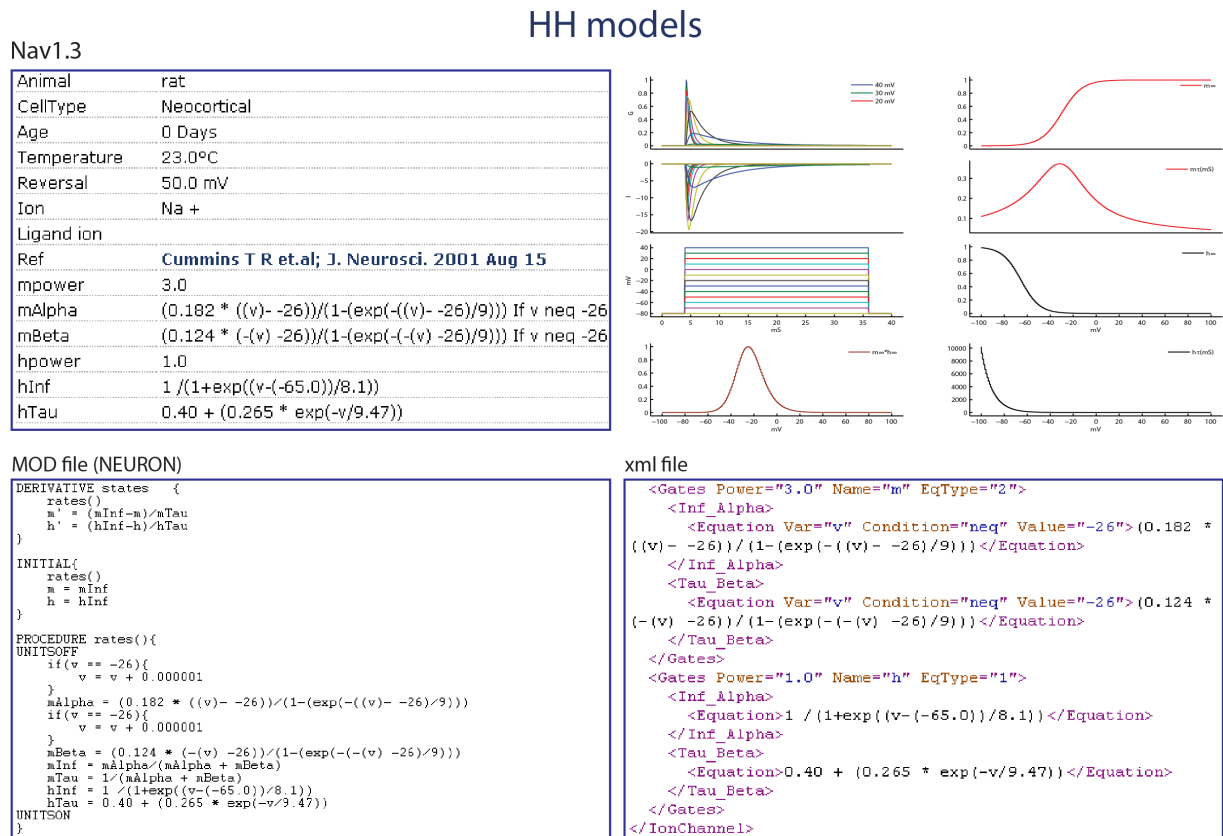


Figure 5. The reference management structure, showing the step-by-step process to download a reference from Pubmed and its usage in *Channelpedia*.

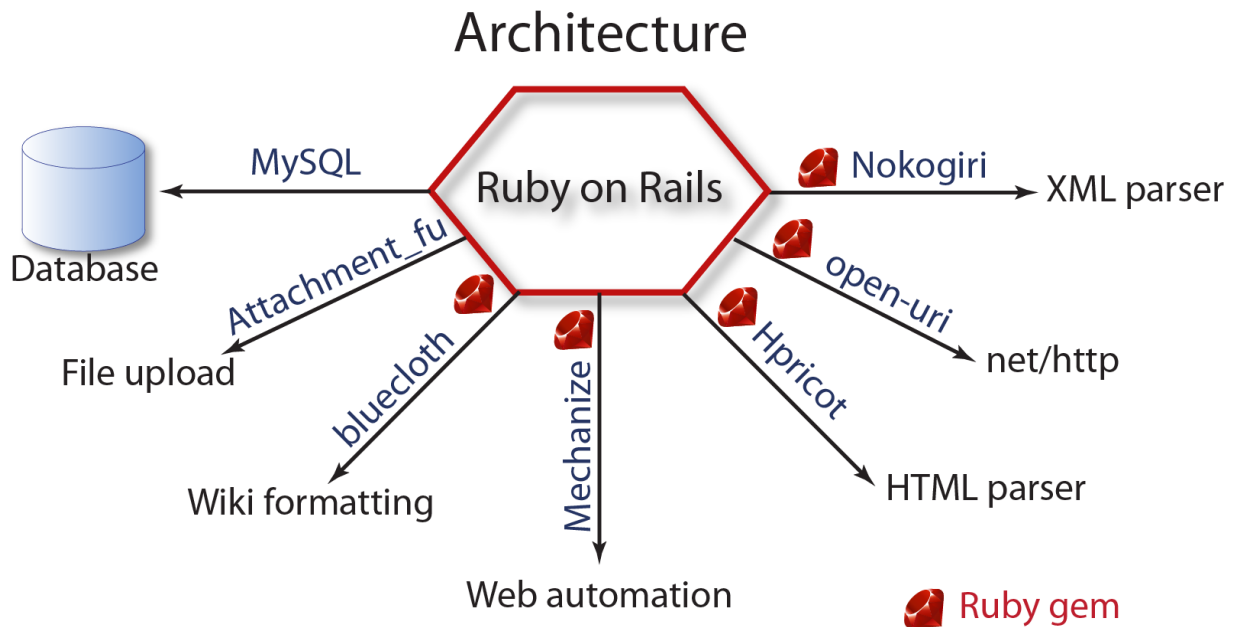


CHANNELPEDIA	REFERENCES	ADMIN
Channelpedia status		
Functions	Total no of references in channelpedia = 178625	
Show log	Total no of references in pubmed = 178813	
Users	References to be downloaded = 188	
Reports	Intermediate states of the Kv1.2 voltage sensor from atomistic molecular dynamics simulations. , 2011 Mar 28 ,() Kv1.2	
Download Abstracts	Rings of charge within the extracellular vestibule influence ion permeation of the 5-HT3A receptor. , 2011 Mar 15 ,()	
Status	A simplified bacterial "Pore" provides insight into the assembly, stability and structure of sodium channels. , 2011 Mar 15 ,()	
Configuration	Alternative mitochondrial electron transfer as a novel strategy for neuroprotection. , 2011 Mar 18 ,()	
List used ref	Conservation of Na+ versus K+ by the rat cortical collecting duct. , 2011 Mar 30 ,() Kir1.1	
List no pdf	The effect of altitude-induced hypoxia on heart disease: do acute, intermittent, and chronic exposures provide cardioprotection? <i>High Alt. Med. Biol.</i> , 2011 Spring ,12(45-55).	

References

- [1] Effects of Bmk AS on Nav1.2 expressed in *Xenopus laevis* oocytes. [210] *Cell Biol. Toxicol.*, 2008 Apr ,24(143-9). Download
- [2] Impaired Nav1.2 function and reduced cell surface expression in benign familial neonatal-infantile seizures. [211] *Epilepsia*, 2008 Sep ,49(1535-45). Download
- [3] Molecular changes in neurons in multiple sclerosis: altered axonal expression of Nav1.2 and Nav1.6 sodium channels and Na+ /Ca2+ exchanger. [404] *Proc. Natl. Acad. Sci. U.S.A.*, 2004 May 25 ,101(8168-73). Download

Figure 6. The overall architecture of *Channelpedia*, and tools used to manage the database, file upload, wiki formatting, web automation, HTML and XML parsing.



SINGLE NEURON STATUS REPORT

The prototype status reports provide a preview into the basic active and passive properties of single neuron models that go into building the NCC model. The purpose of these reports is to verify the generalization of electrical firing types which were optimized using a single morphological instance across different morphologies that could receive this e-type (see Chapter 2).

The prototype report was initially designed and implemented in Matlab and was later ported into the Python programming language by Ruben J. Moor as part of his Master's thesis [Moor 2010] and James G. King of the BBP.

In brief, the report contains the following information -

1. A summary of the electrical properties of a given single neuron - including the passive membrane properties like the input resistance R_{in} , membrane time constant τ_m , resting membrane potential V_m , specific membrane resistance R_m , specific membrane capacitance C_m , and the axial resistance R_a
2. The somatic response to injection of current steps at intensities of 1.5, 2.0 and 2.5 times relative to the model threshold current
3. A drawing of the morphological type showing the different sections of the morphology
4. A pictorial representation of ion channels used by this single neuron model across various sections of the morphology
5. A bar plot showing the conductance densities of ion channels across various sections of the morphology
6. The results of the multi-objective optimization algorithm with the computed parameters for the distribution of conductances and their distribution profiles across different sections of the morphology
7. A comparison of model features per MorphoElectrical (ME) type class to the biological distributions (obtained through experimental traces) for several features used as objectives for the multi-objective optimization algorithm - AP height, AHP depth, time to first spike, AP width, inter-spike interval, adaptation index and mean firing frequency (see Chapter 2)
8. For these feature distributions, the Gaussian curve shown in blue represents the mean \pm S.D. of the biological feature from experimental traces. The green bars show the generalization of features for representatives of a given ME type class (for an explanation of the ME-types, see Glossary of terms 4). The dashed line in green represents the feature value of the so called exemplar morphology, which is used to obtain the electrical firing model through the multi-objective optimization algorithm. A single neuron model was considered to have been validated if the feature value fell within 3 S.D.s of the biological mean feature value

Single MEtype report - runid 89

etype: cADpyr

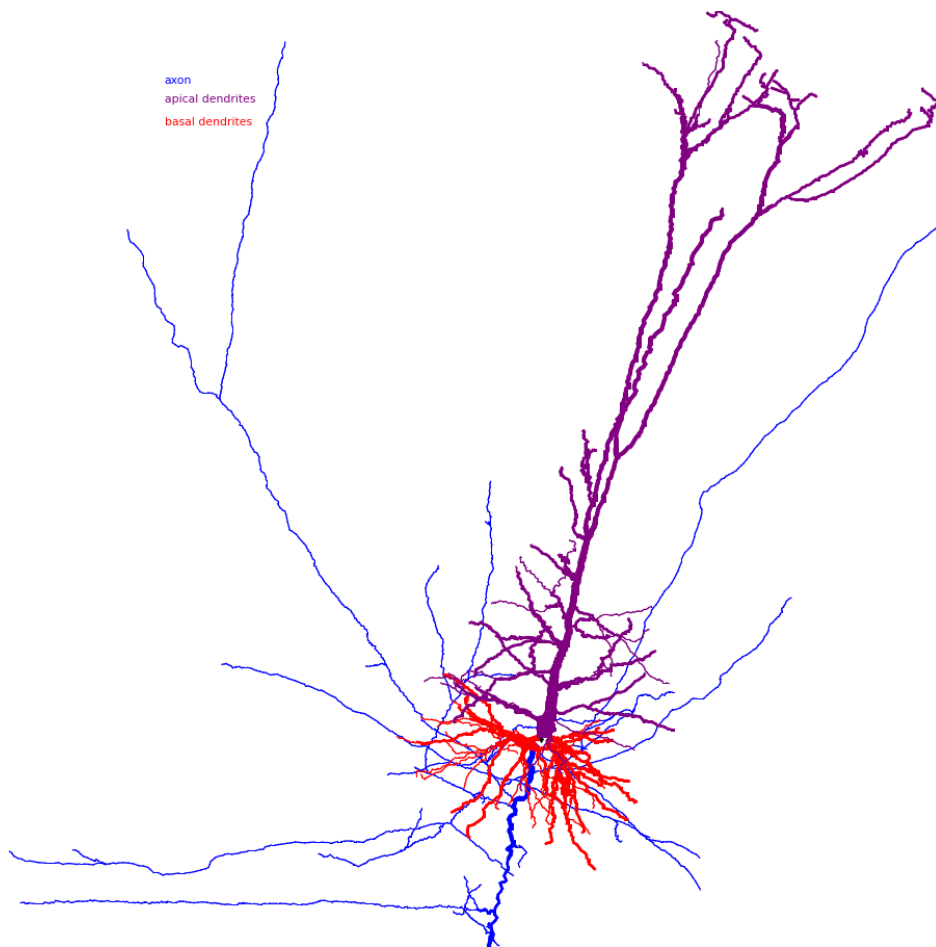
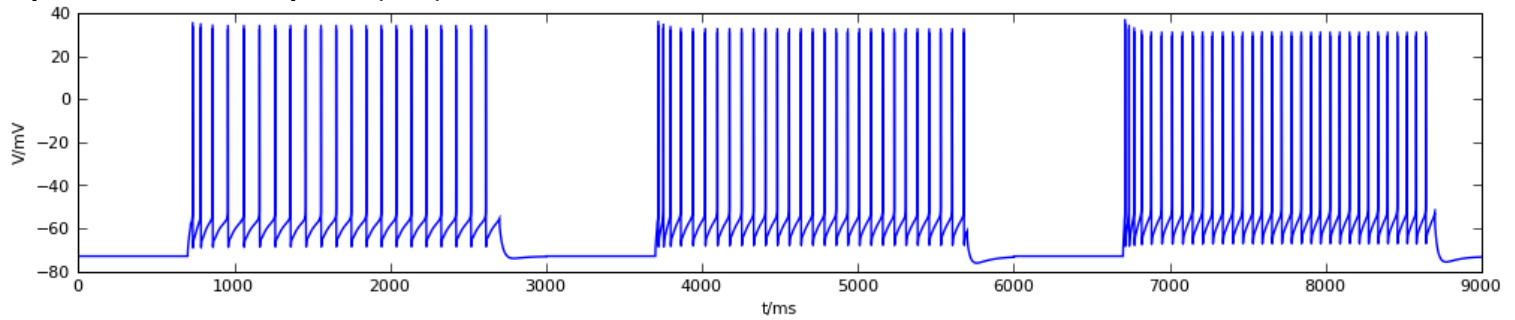
mtype: L5PC

Summary of electrical properties

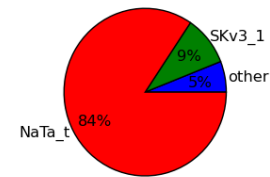
Eproto ID	228	MEtype ID	1295
mtype	L5PC	etype	cADpyr
morphology name	C060112A7_axon(x1.25)_corrected	metype name	cADpyr228_L5PC_5_C060112A7_axon(x1.25)_corrected
Rm (Ω cm ²)	10000	Ra (Ω cm)	80
Cm (μ F)	1	Rin (M Ω)	46.8018
τ (ms)	21.2876	resting potential (mV)	-72.6073

mtypes assigned to this e-type: L2PC, L3PC, L4PC, L4SP, L5PC, L5STPC, L5TTPC, L5UTPC, L6CCPC, L6CLPC, L6CTPC

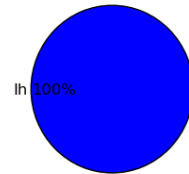
Response to current steps: 1.5, 2.0, 2.5 relative to the threshold current



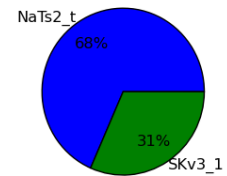
Conductances: apic



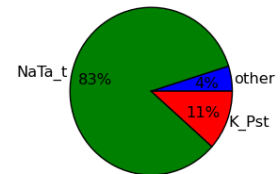
Conductances: dend

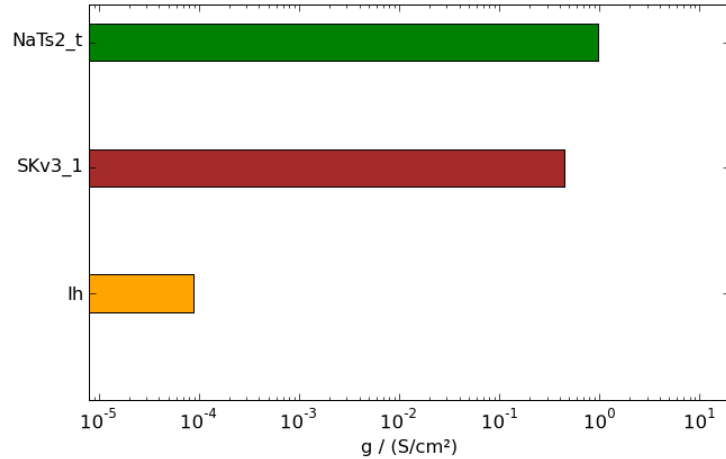
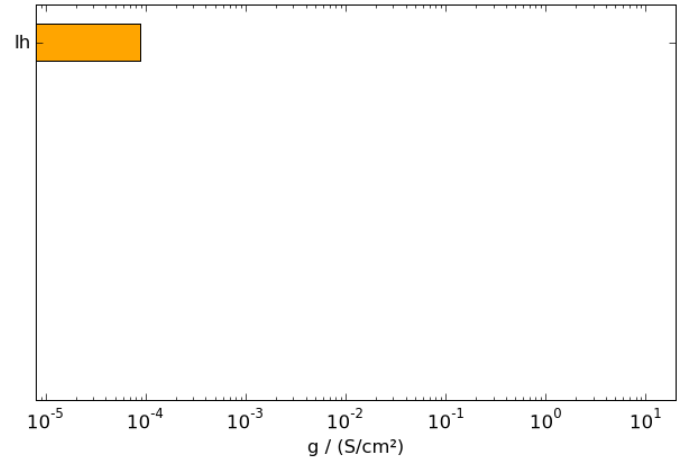
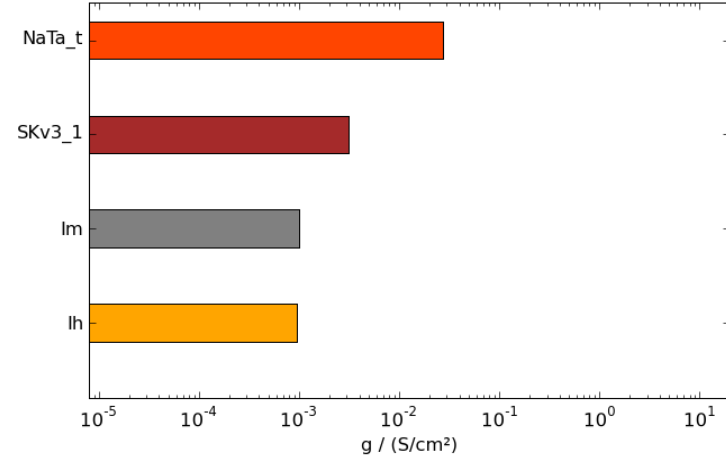
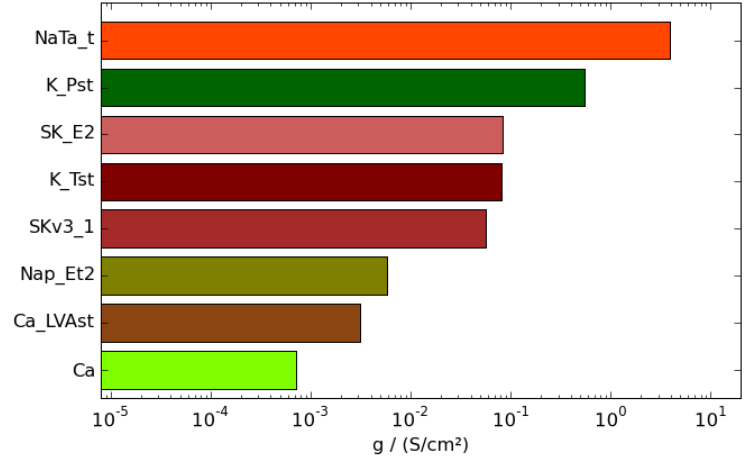


Conductances: soma



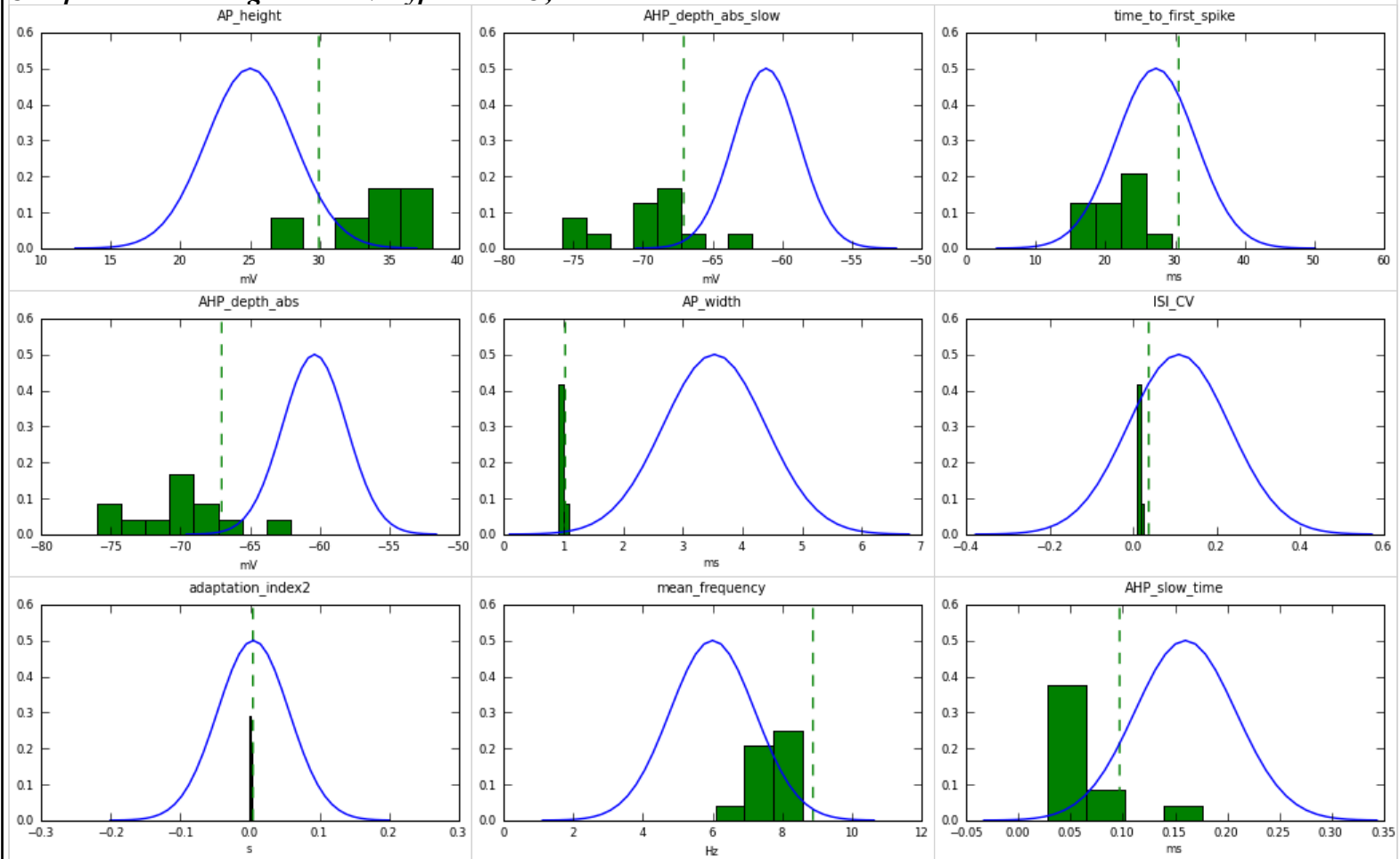
Conductances: axon



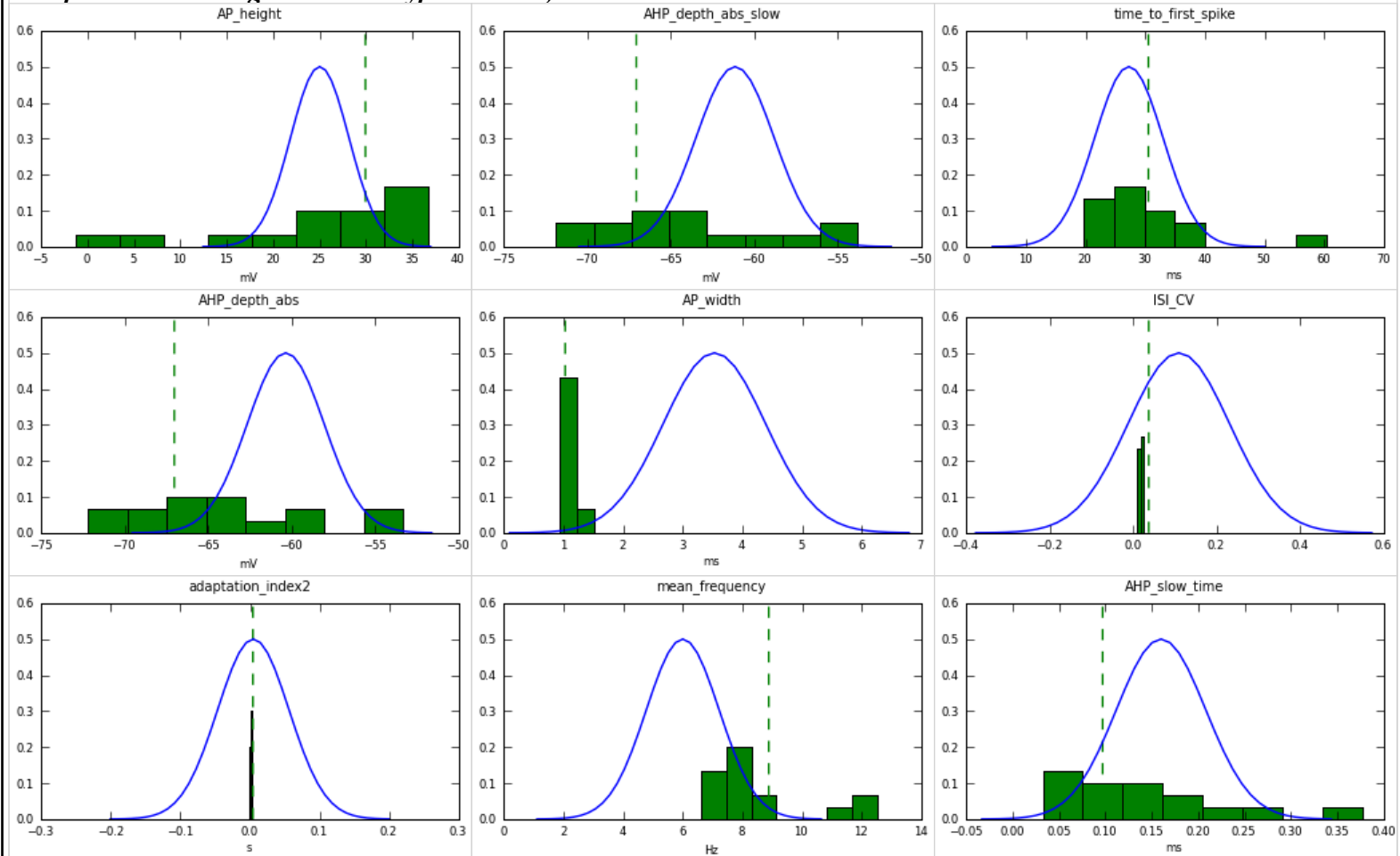
Conductance: soma, norm. distance 0.0**Conductance: dend, norm. distance 0.5****Conductance: apic, norm. distance 0.5****Conductance: axon, norm. distance 0.5****GA results**

current	section	f(x)	f(0)	f(1)
Ca	axon		0.000701	0.000701
Ca_LVAst	axon		0.00311	0.00311
lh	soma		8e-05	8e-05
	dend		8e-05	8e-05
	apic		9.7392e-05	0.0061400475374
Im	apic		0.001	0.001
K_Pst	axon		0.545	0.545
K_Tst	axon		0.0815	0.0815
NaTa_t	axon		3.96	3.96
	apic		0.0276	0.0276
NaTs2_t	soma		0.971	0.971
Nap_Et2	axon		0.00576	0.00576
SK_E2	axon		0.0824	0.0824
SKv3_1	axon		0.0559	0.0559
	soma		0.448	0.448
	apic		0.00314	0.00314

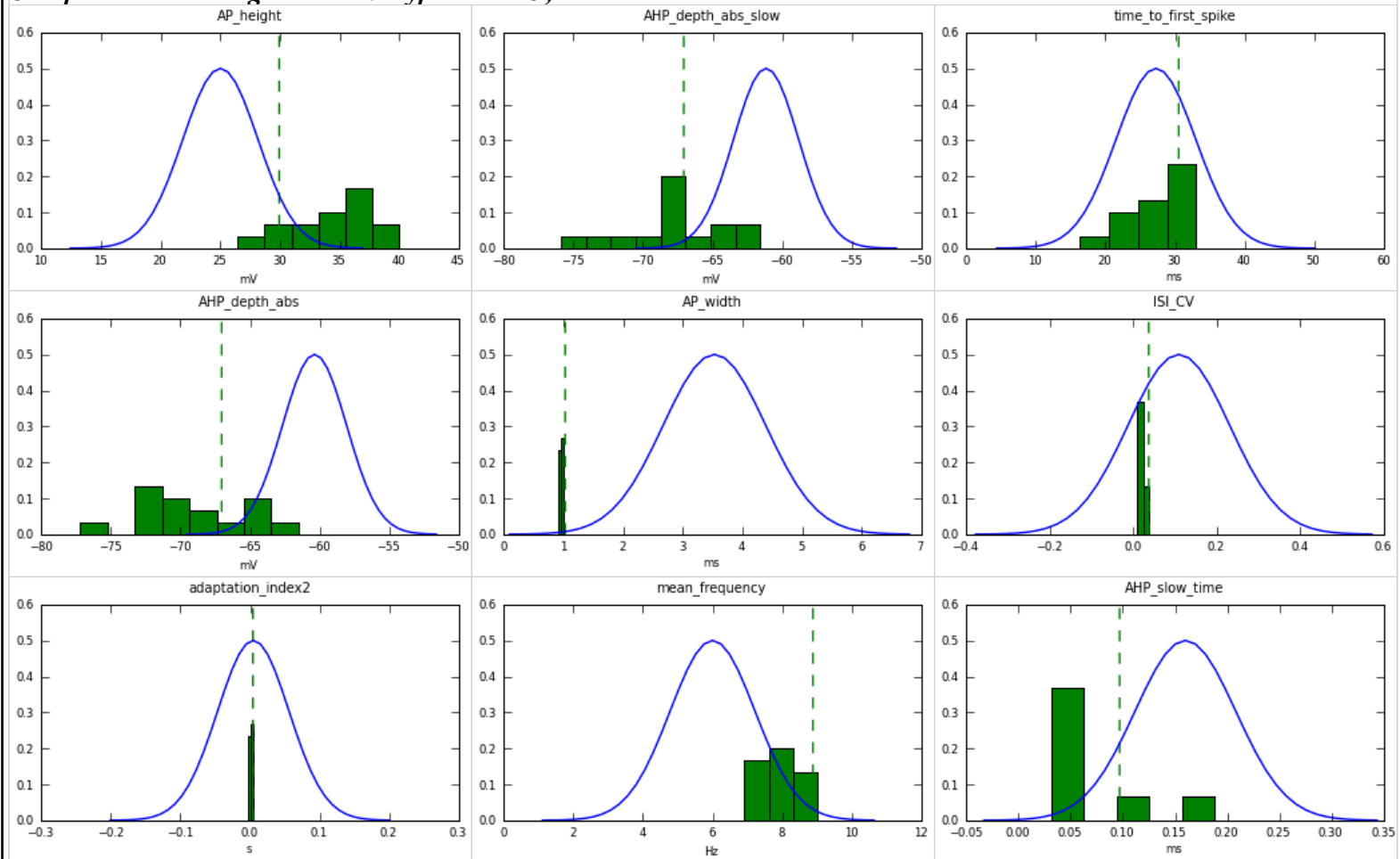
Comparison to biological data $MType = L2PC, n = 12$



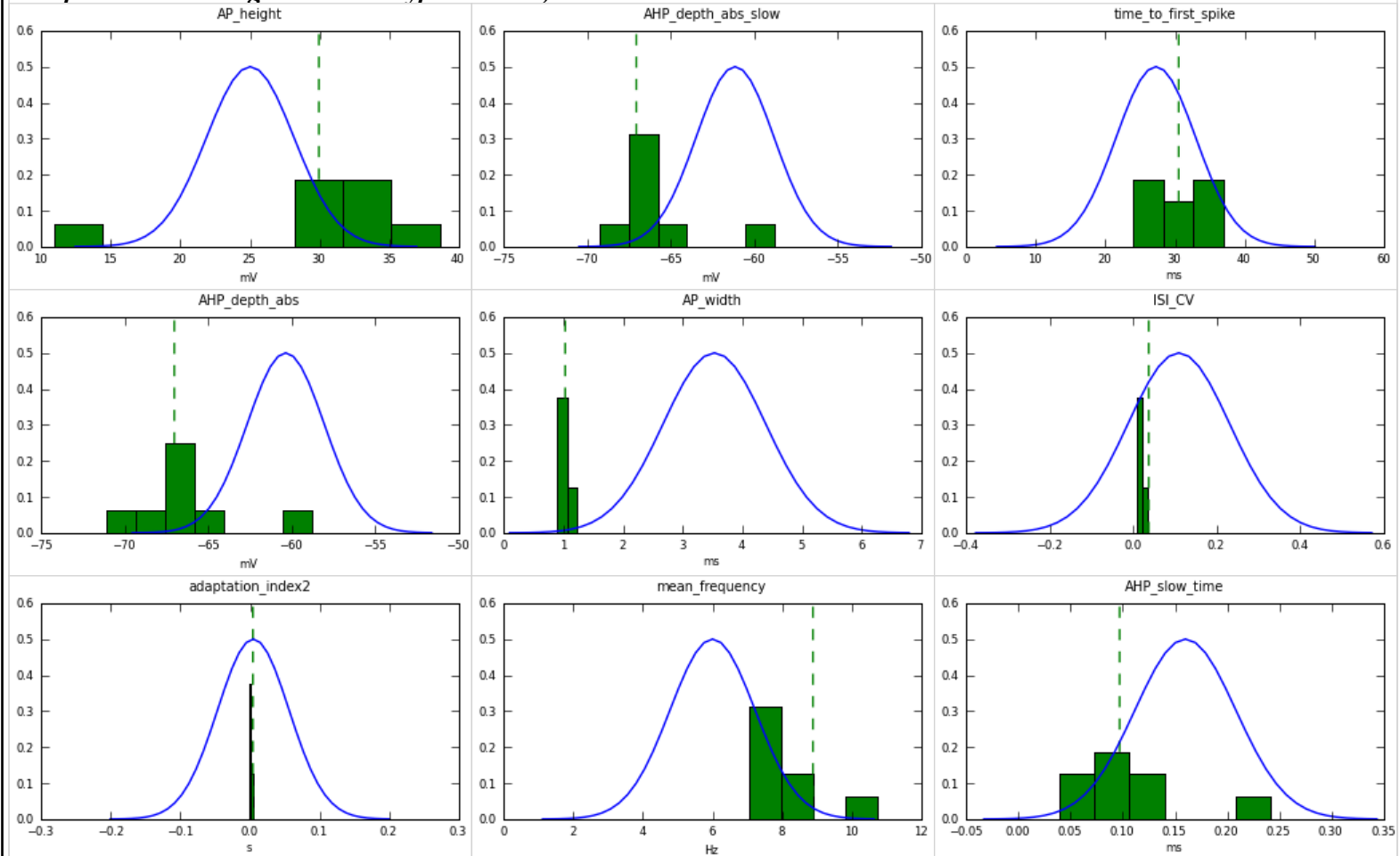
Comparison to biological data $MType = L3PC, n = 15$



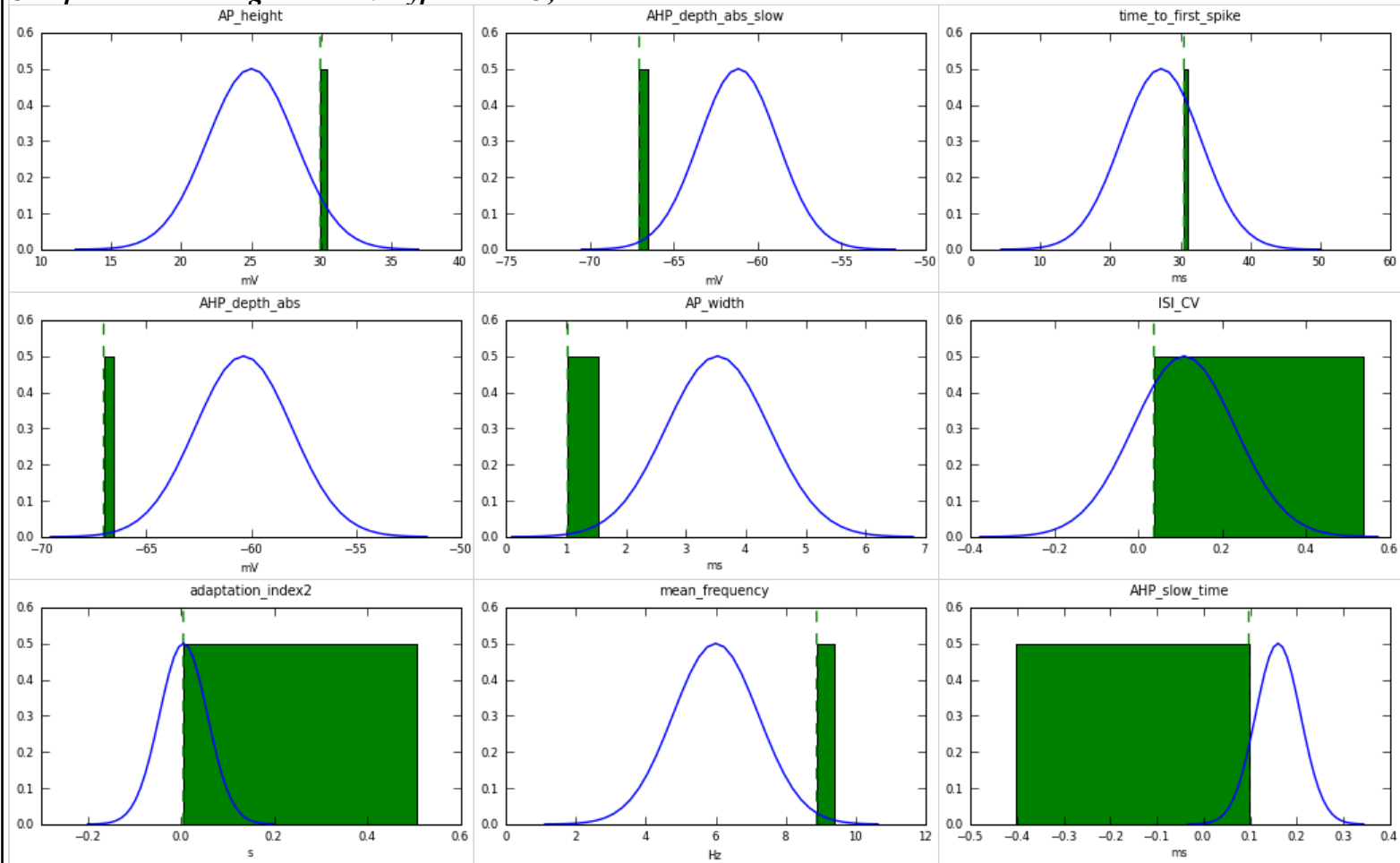
Comparison to biological data $MType = LAPC, n = 15$



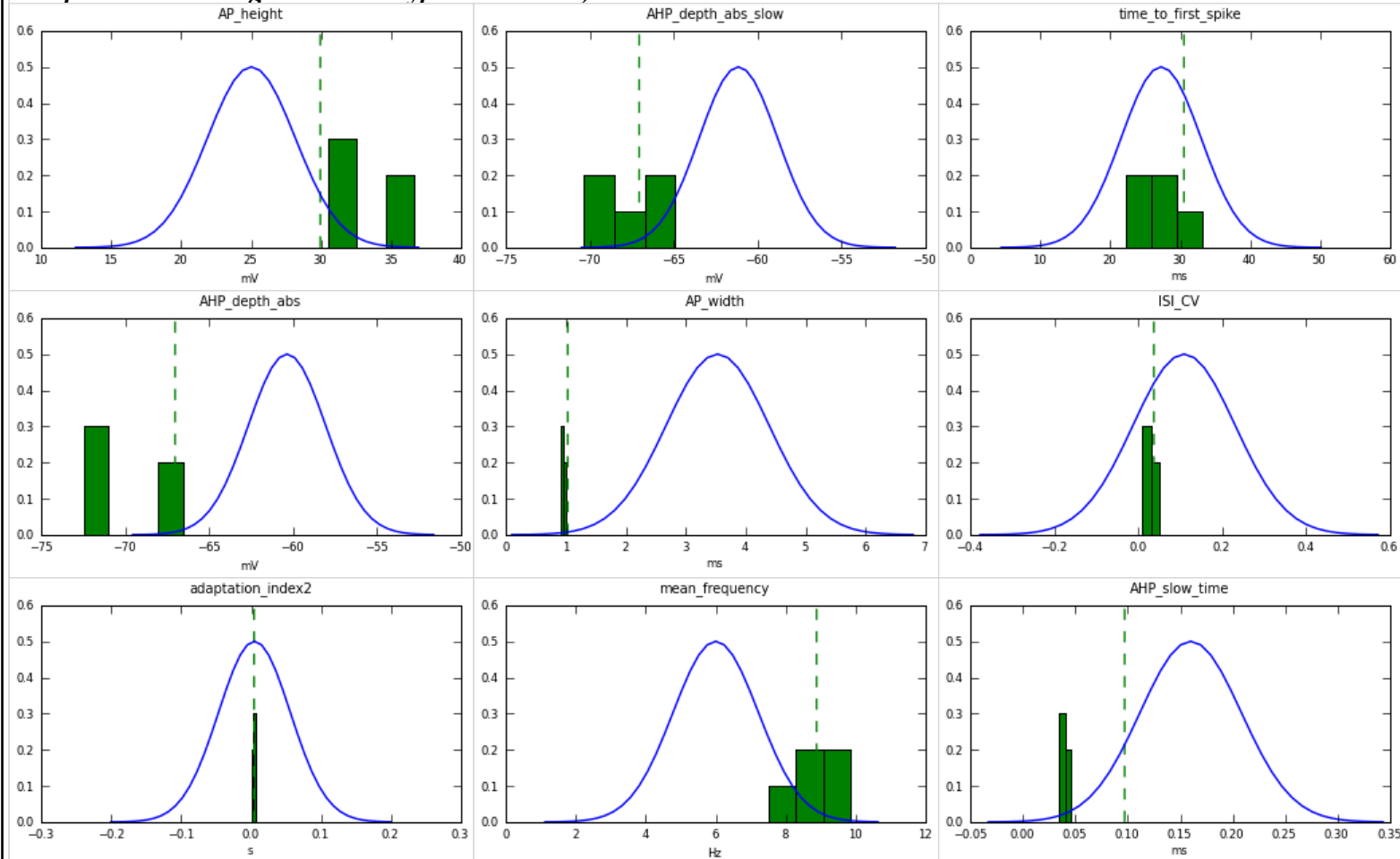
Comparison to biological data $MType = LASP, n = 8$



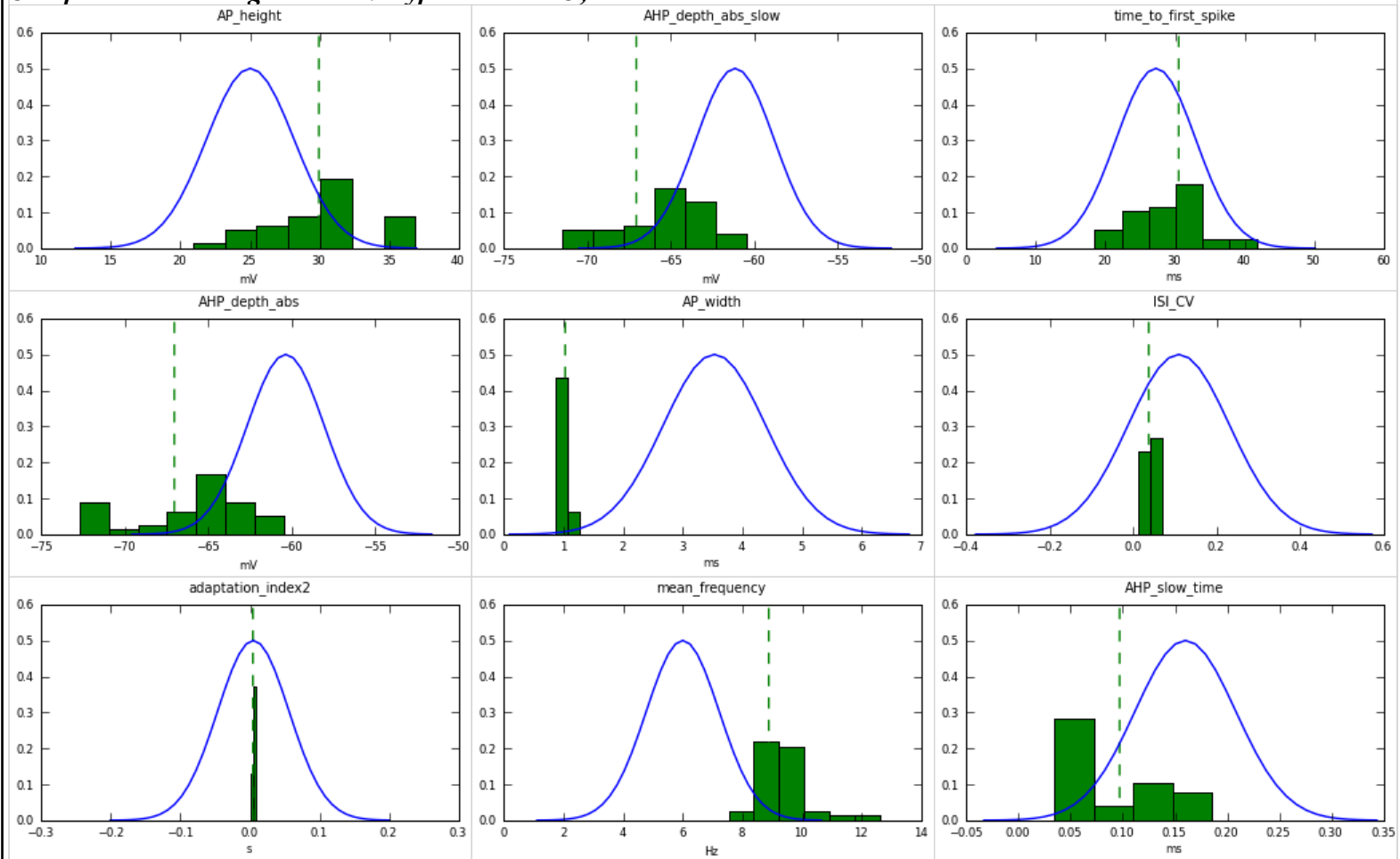
Comparison to biological data $MType = L5PC, n = 1$



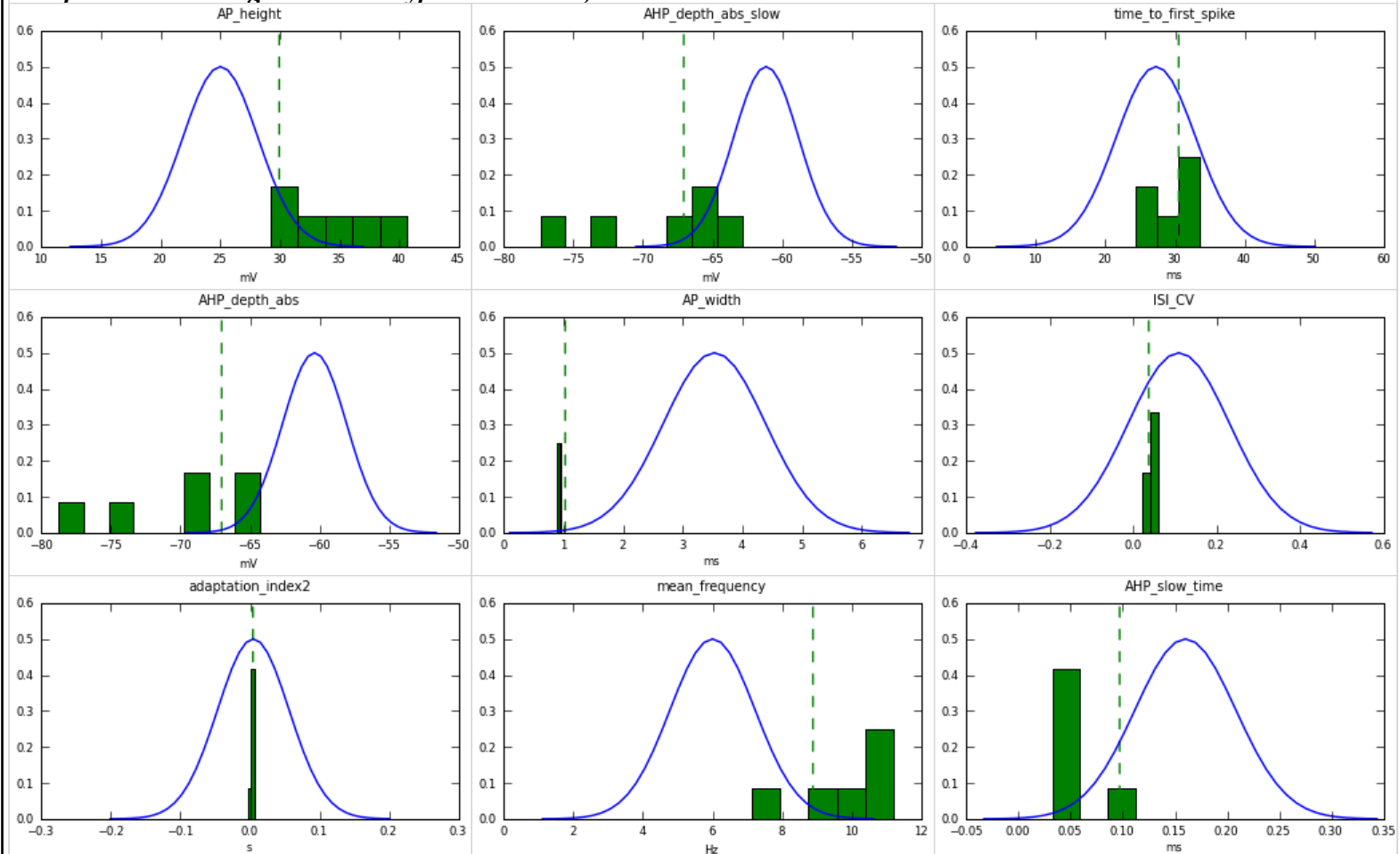
Comparison to biological data $MType = L5STPC, n = 5$



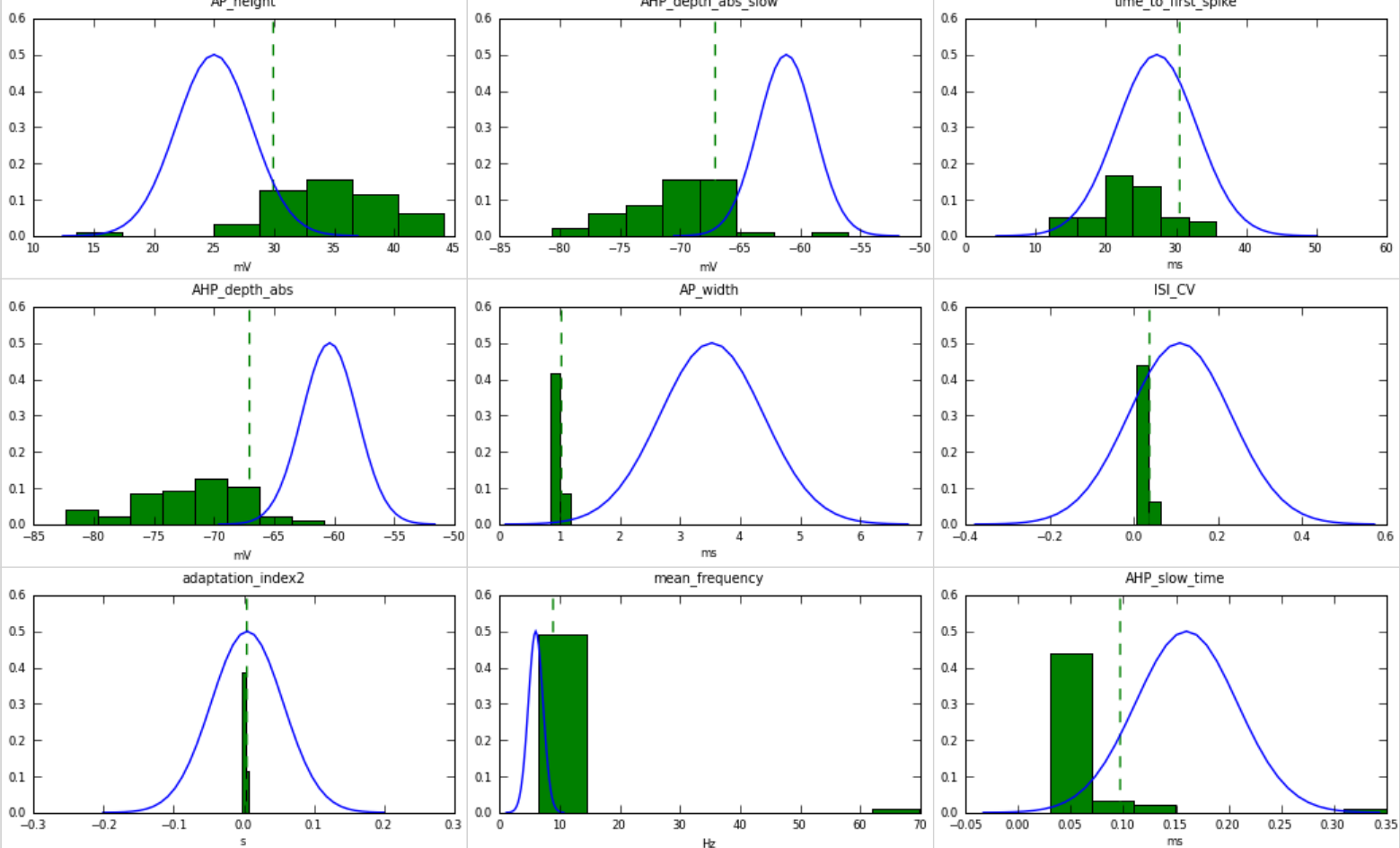
Comparison to biological data $MType = L5TTPC, n = 39$



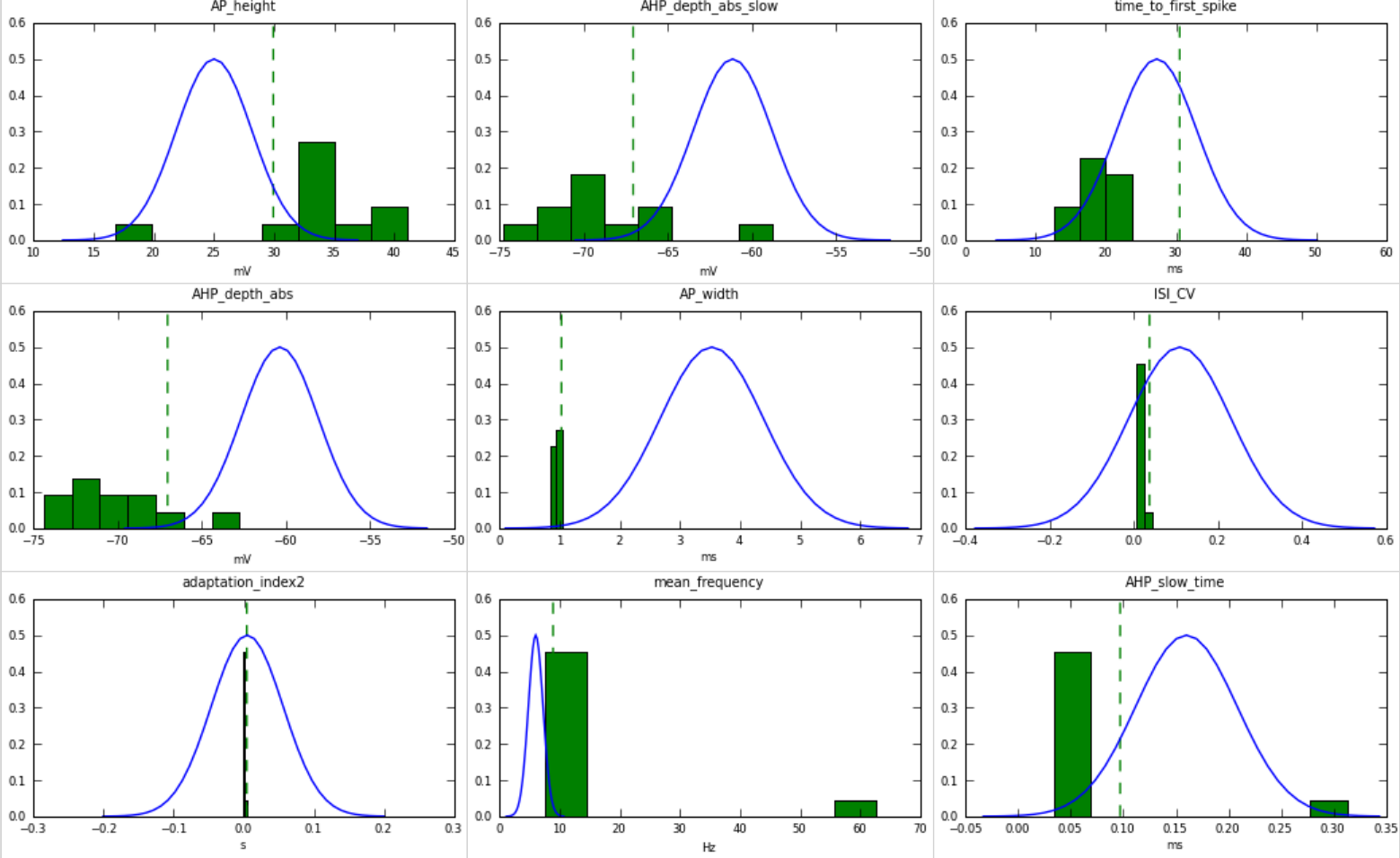
Comparison to biological data $MType = L5UTPC, n = 6$



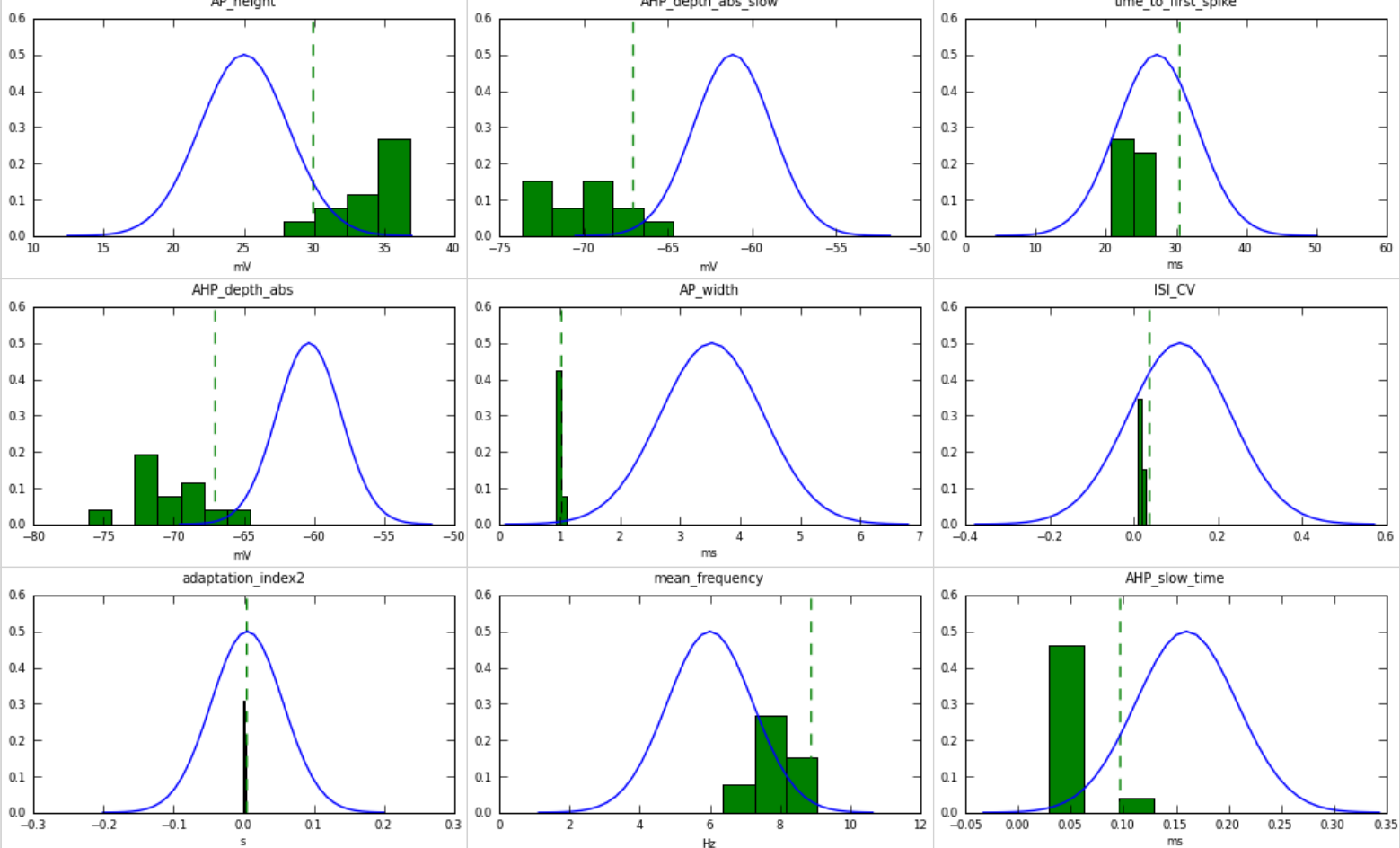
Comparison to biological data *MType = L6CCPC, n = 48*



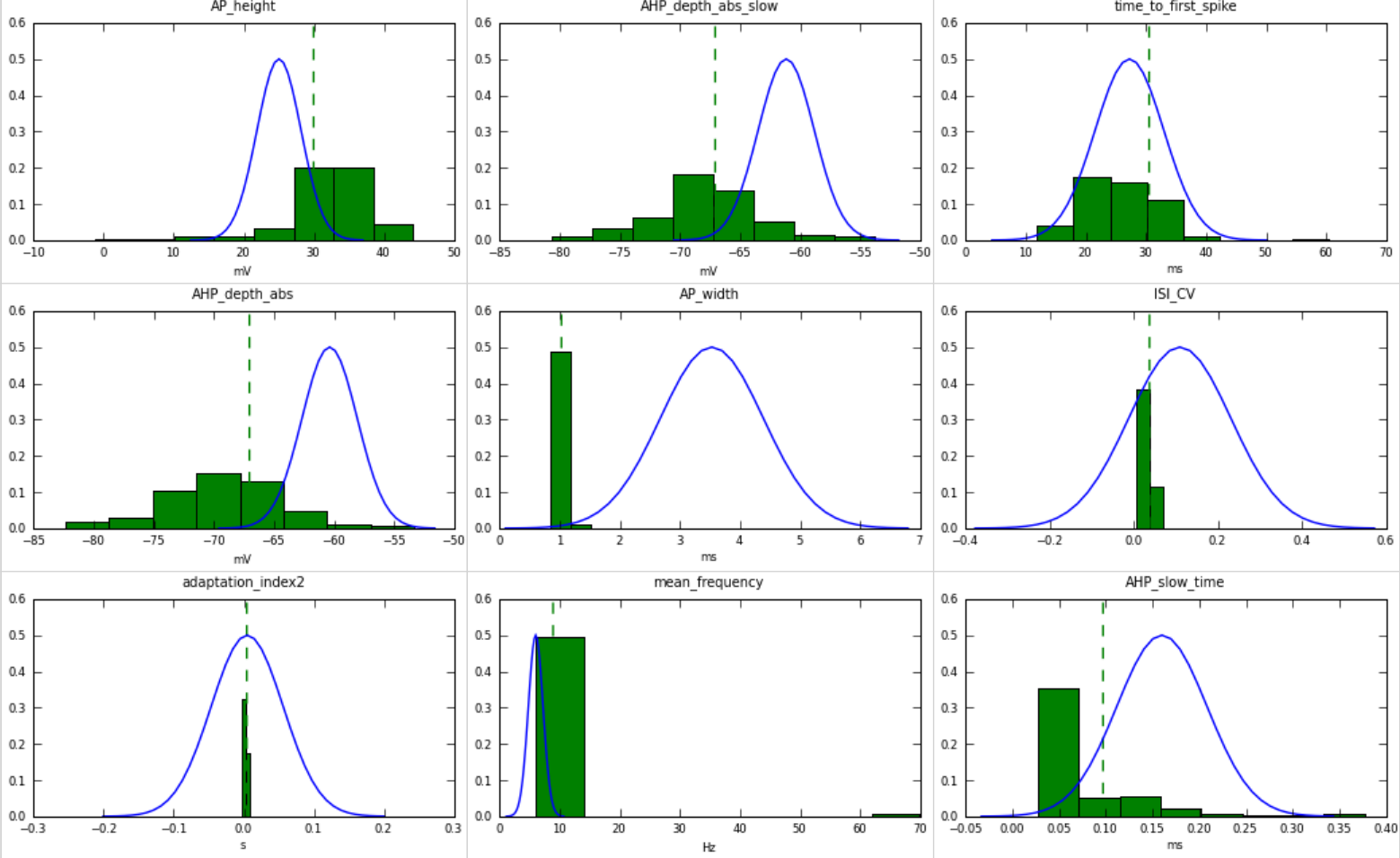
Comparison to biological data *MType = L6CLPC, n = 11*



Comparison to biological data $MType = L6CTPC, n = 13$



Comparison to biological data $n = 173$



Part VII

CURRICULUM VITAE

SRIKANTH RAMASWAMY

EDUCATION

- Ph.D. Computational Neuroscience, Swiss Federal Institute of Technology (EPFL)** **May 2006 – Present**
- Research Assistant to **Prof. Dr. Henry Markram** in the **Blue Brain Project**
 - Awarded a **full scholarship** by the Doctoral School in Neuroscience, EPFL
 - Led several **multidisciplinary projects** as part of a diverse team of 15+ nationalities. Published 10+ papers & posters
 - Awarded a full scholarship for the **Okinawa Computational Neuroscience Course 2007, Japan** (top 1% of 300 applicants)
 - Selected for the **Novartis International Biotechnology Leadership Camp, BioCamp 2011** (top 1% of 2000+ applicants)
- M.Sc. Electrical Power Engineering with Business, The University of Strathclyde, UK** **Oct. 2003 – Oct. 2004**
- Awarded a **British Chevening Open Science Scholarship** by the **UK Government** (top 0.1% of 6000+ applicants)
- B.E. Electrical and Electronics Engineering, Visweswaraiah Technological University, India** **Oct. 1998 – Jun. 2002**
- Graduated with First class honours. Received distinction for Bachelor's thesis and published results in *IEEE-TENCON '03*

PROFESSIONAL EXPERIENCE

- Co-founder, Committee member & Ph.D. student representative, The Consulting Society, EPFL** **Feb. 2011 – Present**
- Co-founded management consulting interest group on campus to educate students of consulting career options
 - Conceived & organized case study workshops and networking events with companies for 80+ student members
- Founding Advisor, EduCare – Online higher education and career consultancy** **Jan. 2009 – Present**
- Co-founded higher education consultancy. Counselling 10+ undergraduate students in career choice and selection
- Assistant Editor, www.Scholarpedia.org** **Jan. 2008 – Present**
- Copyedited scientific articles and wrote biographies of Scientists as part of an international team of 35+ editors
- Graduate Teaching Assistant, Faculty of Life Sciences, EPFL** **Oct. 2006 – May 2009**
- Trained 40+ neuroscience master's students in analyzing time series data in *Matlab* and *MS-Excel*
- Research Internship in Neurophysiology, Universidad Autónoma de Madrid** **Jan. 2005 – Apr. 2006**
- Awarded a fellowship from Fundación BBVA (top 0.5% of applicants). Published key findings in *Neurocomputing*
- Research Internship, Korea Advanced Institute of Science and Technology, Daejeon, S. Korea** **Oct. 2004 – Nov. 2004**
- Awarded a scientific exchange fellowship to learn about bio-inspired systems engineering and brain modeling
- Research Trainee, National Institute of Advanced Studies, India** **Aug. 2002 – May 2003**
- Co-developed a framework for automatic character recognition of ancient Indian scripts for translation into English

EXTRA-CURRICULAR ACTIVITIES

- President, Student Council, Doctoral School in Neuroscience, EPFL** **May 2008 – May 2010**
- Elected representative of 65+ students. Initiated a forum to facilitate interactions between the students and administration
- Committee Member, ShARE (Sharing Knowledge for Development and Social Progress), EPFL** **Oct. 2008 – Jun. 2009**
- Surveyed European carbon credit market practices. Identified areas for improved Asian practices with ShARE-China
- Volunteer, Rebelión - Amnesty Association, Madrid** **Mar. 2005 – Mar. 2006**
- Co-organized humanitarian visit to Ceuta for 60+ members. Interacted with 200+ migrant refugees on human-rights abuse
- Treasurer, Indian Students Association, The University of Strathclyde** **Nov. 2003 – Sep. 2004**
- Managed an operating budget of £1,000 in a group of 100+ members. Organized fund-raising cultural events
- Secretary, Quiz Club, Visweswaraiah Technological University** **Sep. 1999 – Jun. 2002**
- Conceived and spearheaded quizzing forum for 300+ students. Led team that won 4+ inter-university competitions
- Scout Troop Leader, Sri Vidya Mandir High School & K.L.E Society Pre-University College** **May 1994 – Jun. 1998**
- Led a group of 40+ scouts. Organized camps for social service. Received state Governor's award for community service

SKILLS

- **Languages** – Fluent in **English, French, Hindi, Kannada, Tamil**. Intermediate in **Spanish**. Beginner in **German**
- **Soft skills** – Adaptability, team player, mentorship, leadership & communication skills. Entrepreneurial and 'can do' attitude
- **IT** – Modeling and simulation, statistical methods, large scale data analysis, programming in *Matlab, C, NEURON*

INTERESTS

- **Quizzing** – Won 20+ competitions through high school, college and university
- **Music** – Avid player of the Indian percussion instrument "Mridangam". Organized and performed at concerts for 6+ years
- **Reading** – Read 35+ books last year – an assortment of Indian fiction, biographies and travelogues
- **Travel and Culture** – Well travelled across 20+ countries. Backpacked across India between Jul.–Aug. '98 & May–Aug. '03
- **Writing** – College Magazine writer during B.E. ('98–'02). Authored articles for EPFL-FLASH and www.Chevening.com

